1997

A Novel Biosensor Using Nanolithographically-Produced Submicron Optical Sources for the Study of Cell Adhesion and Chemotaxis

Alastair Sheridan Hood

PHD

A Novel Biosensor Using Nanolithographically-Produced Submicron Optical Sources for the Study of Cell Adhesion and Chemotaxis

Hood, Alastair Sheridan

Award date:
1997

Awarding institution:
University of Plymouth

A Novel Biosensor Using Nanolithographically-Produced Submicron Optical Sources for the Study of Cell Adhesion and Chemotaxis

by

Alastair Sheridan Hood

A thesis submitted to the University of Plymouth
in partial fulfilment for the degree of

Doctor of Philosophy

School of Electronic, Communication and Electronic Engineering
Faculty of Technology

Collaborating Establishments
FORCE Cancer Research Centre, Exeter
Centre for Applied Microbiology and Research, Porton Down

November 1997

A Novel Biosensor Using Nanolithographically-Produced Submicron Optical Sources for the Study of Cell Adhesion and Chemotaxis

by

Alastair Sheridan Hood

ABSTRACT

Cell adhesion and chemotaxis are two key factors determining cell behaviour and differentiation which are currently analysed by microscopic examination of the cell or membrane-associated fluorescence labels. These analyses are often slow, labour intensive and of limited informational content. This thesis describes the physical theory and experimental aspects of an optical method suitable for monitoring cell contact, adhesion to a surface and chemotaxis beyond the conventional limit of optical microscopy by means of a device that utilises both a plain bare surface and arrays of apertures nanolithographically-produced in the surface of a Surface Plasmon Resonance (SPR) sensor structure. Any minute vertical movement of the cell, within the near-field of the SPR active surface or actual cell/surface contact, creates intensity fluctuations, detectable in the far-field. This was demonstrated during experiments with non-apertured devices. (A video demonstrating the biological features of the device accompanies this thesis and may be obtained by contacting University of Plymouth's LRC.) The light scattered by each nanolithographically-produced aperture also fluctuates as a consequence of the cell approaching to within a few hundred nanometres of the aperture bearing surface and demonstrated detection of minute vertical movement on the surface of the apertured device. The combination of apertured and non-apertured detection results in a highly spatially-sensitive 3-dimensional sensor. Digitising the output from a

CCD camera allows patterns of intensity fluctuation to be correlated with the contact and adhesion of individual cells on the active surface over a short period of time (2-3 minutes).

Initial trials of an apertured device (diameter (ϕ) « wavelength of incident light (λ)) carried out by our collaborating partners Drs R. Carr and S. Al-shukri at the Centre for Applied Microbiology and Research, Porton Down demonstrated that the use of apertures etched in a SPR metal surface produced a highly sensitive dielectric monitor, i.e. sensitive to very small changes in the refractive index of the micro-environment adjacent to the aperture. This was proposed as being of potentially great value in the development of extremely sensitive probes of dielectric particulates of sub-micron dimensions, i.e. biological macromolecules and supramolecular structures. Characterisation of the associated radiative and non-radiative evanescent fields on the surface of the device was conducted in order to gain a greater knowledge of the mechanisms by which the interactions between the cells adjacent to and in direct contact with the apertures and evanescent fields produced such significant intensity fluctuations in the results at CAMR.

A combinational Scanning Probe Microscope was developed and used in Scanning Near-field Optical Microscope and Photon Scanning Tunnelling Microscope modes of operation to detect the evanescent and radiative fields respectively. Detailed mapping of the radiative pattern in the near-field of the large apertures ($\phi \gg \lambda$) demonstrated a diffraction of approximately 25% of the Surface Plasmon Wave (SPW) either side of the centre of the aperture with the remainder being contained within the metal layer. Scattering at the second aperture interface, i.e. air/metal, was shown to be of a lower magnitude as a result of non-surface plasmon enhancement within the non-resonant aperture. Characterisation of the intensity profile of small apertures ($\phi < \lambda$) was beyond the scope of this project due to its limited time and finance and was not undertaken. A section in the conclusions is dedicated to giving a possible cause of the intensity profiles

detected during the initial studies at CAMR with possible procedures required to verify and expand such work.

In order to investigate the potential of the device in the biological environment, biological trials were carried out with collaborating establishments at Salisbury and Exeter and demonstrated that this dual sensing microscopic technique had great potential in the 3-dimensional monitoring of cell movement together with the capability of extending our knowledge of cell behaviour with the view to a system of rapid screening for tumour cells. This technique has produced real-time images of cell behaviour, which to our knowledge has not been previously seen before by any other microscopy technique. The finding of these trials are documented in this thesis with possible theories as to what the biological effects responsible for these results may possibly be. Future work into the verification of these effects and more biological trials and procedures are described in the hope that after further work the device may be developed into a commercial and readily available scientific unit for use in the laboratory.

CONTENTS

TABLE OF FIGURES

NOMENCLATURE

AC	Alternating Current
ADC	Analogue-Digital-Converter
AFM	Atomic Force Microscope
ATR	Attenuated Total Reflection
CAMR	Centre for Applied Microscopy and Research
CCD	Charged Coupled Device
CHO	Chinese Hamster Ovary
CRIST	Centre for Research into Information Storage Technology
CVC	Commonwealth Vacuum Corporation
DC	Direct Current
DNA	Deoxyribonucleic Acid
ECACC	European Collection of Animal Cell Cultures
ECM	Extra Cellular Matrix
EDTA	Ethylenediaminetetraacetic Acid
FORCE	Friends of the Oncology and Radiotherapy Centre at Exeter
FTIR	Frustrated Total Internal Reflection
HP	Hewlett Packard
IBM	International Business Machines
ICAM	Intracellular Adhesion Molecules
IL3	Interleukin 3
MRC	Materials Research Company
NA	Numerical Aperture
PC	Personal Computer
PCX	Personal Computer Paintbrush
PMT	Photo Multiplier Tube
PSTM	Photon Scanning Tunnelling Microscope
RF	Radio Frequency
RGD	Rayleigh-Gans-Debeye
RIE	Reactive Ion Etching
SNOM	Scanning Near-Field Optical Microscope
SP	Surface Plasmon
SPM	Scanning Probe Microscopy
SPR	Surface Plasmon Resonance
SPW	Surface Plasmon Wave
SPWV	Surface Plasmon Wave Vector
STM	Scanning Tunnelling Microscopy
TIR	Total Internal Reflection
UV	Ultra Violet

NOMENCLATURE OF BIOLOGICAL TERMS

Apoptosis	Cell death as a result of induction of an internal 'suicide' programme.
Cancerous Cells	Cells that have undergone certain changes which enable them to divide indefinitely and invade underlying tissue.
Cell Cytosol	The cytoplasm other than the various membrane-bounded organelles.
Chemotaxis	Reaction of motile cells or micro-organisms to chemical stimuli by moving towards or away from source of chemical.
Collagen	One or all of a family of fibrous proteins found throughout vertebrates.
Cytoplasm	All the living part inside the cell membrane and excluding the nucleus.
Cytoskeleton	Internal proteinaceous framework of a cell.
Epithelial	Cells which are tightly bound together, lining any external or internal surface in multicellular organisms.
Extra Cellular Matrix	Macromolecular ground substance of connective tissue.
Filopdia	Thread-like pseudopodia of some protozoans.
Glycosaminoglycans	Any of a group of polysaccharides made up of repeating disaccharide units of amino sugar derivatives.
Haematopoietic cells	Blood forming cells.
Hormone	A substance that is produced by one tissue and transported to another tissue where it induces a specific physiological response.
In vivo	Biological processes occurring in a living organism.
Lamella	Any tiny or plate-like structure.
Ligand	Any molecule that binds to another.
Macromolecules	Very large organic molecule such as a protein.
Macrophages	Small phagocytic blood cell.
Membrane	A thin film, skin or layer.
Metabolism	Integrated network of bio-chemical reactions in living organisms.
Metastatic	A migrated cancer cell which colonise and grow in other tissues and organs.
Microvilli	Thin fingerlike infoldings of the cell surface.
Organelles	A structure within a cell in which certain functions and processes are localised.
Peptide	A compound of two or more amino acids.
Phototaxis	Movement in response to light.

Pseudopodia	Protrusion of cytoplasm put out by cell.
Receptor	Specialised tissue or cell sensitive to a specific stimuli.
Serum	Fluid component of blood after removal of cells and fibrinogen.
Squamous Epithelial Cells	A simple sheet of cells tightly bound together made up of flat nucleated cells
Stochastic	A process in which there is a an element of chance or randomness.
Supramolecular	Over and above the resolution of the eye.
Tumour	A growth resulting from the abnormal proliferation of cells.

ACKNOWLEDGEMENTS

I would like to express my gratitude to all those people and organisations who have helped in the completion of this project, in particular;

My supervisors Mr R. Neal (Director of Studies), Dr C. Reeve of the University of Plymouth and Dr R. Carr of CAMR, Porton Down, Salisbury for their constant support, invaluable discussions, encouragement and guidance throughout the project.

Dr S. Al-shukri (CAMR, Porton Down, Salisbury) for her immense optical knowledge and practical know-how without which the completion of this project would not have been possible.

All the staff at the FORCE Cancer Research facility, Exeter (especially Dr J. Garland) for their biological knowledge and assistance.

All the staff within the C.R.I.S.T. facility (University of Plymouth) especially Mr. Phil Brown and Mr Stuart Warner for their thin-film knowledge and assistance.

Mr A. Matthews (University of Plymouth) for his assistance in the manufacture of the mechanical coupling rig and subsequent modifications throughout the project.

AUTHOR'S DECLARATION

At no time during the registration for the degree of Doctor of Philosophy has the author been registered for any other University award.

This study was jointly financed with the aid of a pump primer grant from SERC, FORCE Cancer Research Unit, Exeter and a studentship from University of Plymouth, Faculty of Technology.

A programme of advanced study was undertaken, which included the extensive reading of literature relevant to the research project attendance at an EPSRC Short Course in Engineering Management and attendance at international conferences and seminars on Nanotechnology and Bio-Medical Optics.

Papers from part of the work in this thesis have been presented at the 1st UK National Synopses of Nanotechnology in Medicine and the Biosciences, Royal Postgraduate Medical School, Hammersmith Hospital, London, 1994 and the Europto-SPIE sponsored Biomedical Optics conference, Barcelona, Spain, 1995.

Alastair Hood

Date 14/4/97.

DEDICATION

To my parents
Stewart and Lorna Hood

Chapter 1

1. INTRODUCTION

Initial trials carried out by our collaborating partners Drs R. Carr and S. Al-shukri at CAMR, Porton Down demonstrated that the use of apertures etched in an otherwise plain SPR metal surface produced a highly sensitive dielectric monitor, i.e. sensitive to very small changes in the refractive index of the micro-environment adjacent to the surface. This was proposed as being of potentially great value in the development of extremely sensitive probes of dielectric particulates of sub-micron dimensions. During initial studies at Plymouth it was quickly recognised that novel images of unknown structure and significance of cell images could be produced using a similar configuration as that at CAMR. Collaboration with FORCE Cancer Research, Exeter provided further biological trials of the device in order that further study of cell adhesion and chemotaxis was possible. The content of this thesis is therefore directed towards the processes involved in the imaging of the cells under SPR conditions associated with this device and to describe the novel cell movements witnessed in biological trials and illustrate the devices' usefulness in monitoring minute cell movement. What follows in this section is a

brief description of the cell adhesion and chemotaxis followed by an introduction to Surface Plasmon Resonance.

1.1 INTRODUCTION TO BIOLOGICAL CELL ADHESION AND CHEMOTAXIS

Cell adhesion and movement are two fundamental properties determining tissue growth and differentiation. Cell adhesion is initiated by the interaction of receptor sites on the cell surface with specific intercellular matrix proteins or adhesion molecules present on other cells (ICAMS and adhesions). Intracellular matrix molecules (collagens, glycosaminoglycans) also sequester other peptide growth factors from serum or surrounding cells and present them to cells where they may stimulate or repress growth [Gordon *et al.* (1987)]. Together, such molecules and their interaction regulate cell growth, tissue formation, differentiation and position of cells within an environment.

Cell movement is a widespread property of cells. Even those apparently stationary remain in situ by virtue of their interaction with biological substrates (e.g. matrix proteins) and whose composition may vary significantly with time. Tissue regeneration relies heavily on cell movement to generate its three dimensional structure. Other cells, e.g. blood and tissue macrophages and cells of the immune system, are specialised for rapid and free movement in response to stress factors [Stossell *et al.* (1994)]. This freedom of movement in the immune system is of vital importance for the successful generation of response. Finally, tumour cells have an increased capacity for movement which is responsible for their fatal dissemination through the body. Cell movement can be considered at two levels:

a) movement of the whole cell usually along a chemo-attractant gradient and

b) movement of the cell surface membranes and components therein.

Monitoring and analysis of whole cell movement currently relies on crude, labour intensive and time consuming visual observation, albeit often assisted by time lapse video. Cells are typically placed in a microchamber connected by a capillary to another chamber containing a cell attractant and movement of the cell along the chemo-attractant gradient is monitored over long periods (several hours). However, cell movement is often stochastic and difficult to quantify objectively. Furthermore, time-lapse video can only deal with a limited number of cells at once over a long time period, cannot resolve events within the time-frame access period and cannot readily merge or process data into a manipulative (digitised/binary) form. Currently there is considerable interest in developing methods by which the movement of cells can be studied at the molecular level, i.e. as mediated by aggregation of receptor peptides, etc. No good analytical methods exist beyond labelling surfaces with antibodies and using optical microscopy to monitor gross movement of label. For instance, Fluorescence Energy Transfer (FET) between neighbouring molecules has been used with some success but the technique is highly spatially dependent and its specificity for peptides directly associated with primary ligand is uncertain [Curtis (1991)]. These techniques report on the overall change in cell contact and membrane behaviour but it is known that the contact that the cell makes with its substrate can vary with different substrate properties and under different environmental stimuli. The development of analytical techniques by which the contacting of cell surfaces with underlying biological substrates can be measured and changes in that contact (adhesion) correlated with the onset of cell movement would be of significant interest to cell biologists.

A sensor utilising Surface Plasmon Resonance (SPR) has been developed. The sensor allows direct visualisation of cell behaviour as a direct consequence of the interactions of the cell membrane with the optical evanescent field associated with SPR. Specifically those regions of the cell that either contact or approach to within the near-field of the device surface are visually detectable. This method is a dual device based on the microscopic detection of fluctuations of light scattered from the interactions of biological

cells modulating the SPR evanescent field on a plain metal surface and the scattered intensity by arrays of apertures in a thin metal film in which Surface Plasmons (SP's) are excited by an incident laser beam. The intensity fluctuations are caused by contact of the cell wall with the SPR surface and the scattering of the SPR evanescent field by the cell. The images gained from experiments with the non-apertured device demonstrated the potential of visualising cell contact points and novel cell movements. (A video demonstrating the biological features of the device accompanies this thesis and may be obtained by contacting University of Plymouth's LRC.) The size and spacing of apertures in the array are such that any given cell will cover a number of apertures, allowing high resolution studies of cell contact/adhesion to be made within individual cells. Utilising the spatial content of the evanescent field 3-dimensional monitoring of the active cell can be produced.

Surface Plasmons and Surface Plasmon Resonance has been used as an analytical tool for many years. Acute resonant characteristics provide a highly sensitive monitor for the detection of a change in dielectric constant of the medium above the SPR surface. The bulk of SPR devices monitor the reflected intensity profile and consequently deduce the optical properties of the medium above the SPR surface.

The configuration used in this project allows the active surface of the device to be studied from above with some notable results. The device utilises a regular matrix of refractive index discontinuities etched in the metal film (circular apertures) as discrete centres of scattering of the SPW providing an accurate 2-dimensional measurement of cell movement in the plane of the surface of the device. Modelling the extent of the evanescent field on the upper surface of the device and the interactions of the cell with the SP field provides additional knowledge of any cell movement within approximately the near-field of the active SPR metal surface.

In order to monitor the adhesion and chemotaxis of an animal cell on or near the surface of the device, a combinational SNOM/PSTM (Scanning Near-field Optical Microscope/Photon Scanning Tunnelling Microscope) device was developed. Working in PSTM configuration the intensity profile of the SPR non-radiative evanescent wave on the surface of the substrate was mapped and characterised. In the SNOM configuration the intensity profile of the radiative wave at the edges of the apertures and refractive index discontinuity were also characterised. The use of this combinational device provided valuable information on the field distribution from the apertures under both SPR and white light epi-illumination (conventional white light illumination). The knowledge of such fields provided additional information possibly to explain further the results gained during the biological trials of the device.

A number of test devices were produced having different physical properties. Silver (Ag) and Chromium (Cr) coated devices were used to investigate the evanescent field distribution and to carry out a number of biological trials.

1.2 HISTORY OF NON-RADIATIVE SURFACE PLASMONS

Non-radiative surface plasmon waves, i.e. waves which do not radiate away from the surface, were first described as solutions of Maxwell's equations by Sommerfeld in 1909. In 1965 Raether achieved excitation of surface plasmons by electrons. In 1968 Andreas Otto developed a method of exciting non-radiative surface plasmons on smooth conducting surfaces by light. The existence of this optical field is directly attributed to the high proportion of free electrons that are characteristic of a metal. In these experiments he utilised the optical technique of Frustrated Total Internal Reflection (FTIR). Employing FTIR, excitation of a propagating wave in a metal film occurs, when it is brought sufficiently close to the incident coupling prism thus matching the phase of the evanescent wave, on the upper surface of the prism, and the propagating wave in the metal waveguide (Figure 1.1).

In the same year as Otto's breakthrough Kretschmann and Raether (1968), applying a similar technique of excitation, were able to excite non-radiative surface plasmons on the upper surface of a metalised dielectric substrate (Figure 1.2).

A grating coupler [Raether (1988)] can be used to excite surface plasmons on the metalised surface of a coated dielectric. Working on a similar principle as the prism coupler, i.e. matching the phase of the incident wave to that of the SP's in the metal, a non-radiative SPW could be excited and used in a sensor configuration.

In this project the Kretschmann-Raether configuration was used for two reasons, namely, its ease of use in the optical and biological laboratory and its high inherent coupling efficiency. No strict control over the thickness of the air gap between the prism and metal film is necessary, as is the case in the Otto configuration, and a clear un-obstructed view of the active SPR surface is attained.

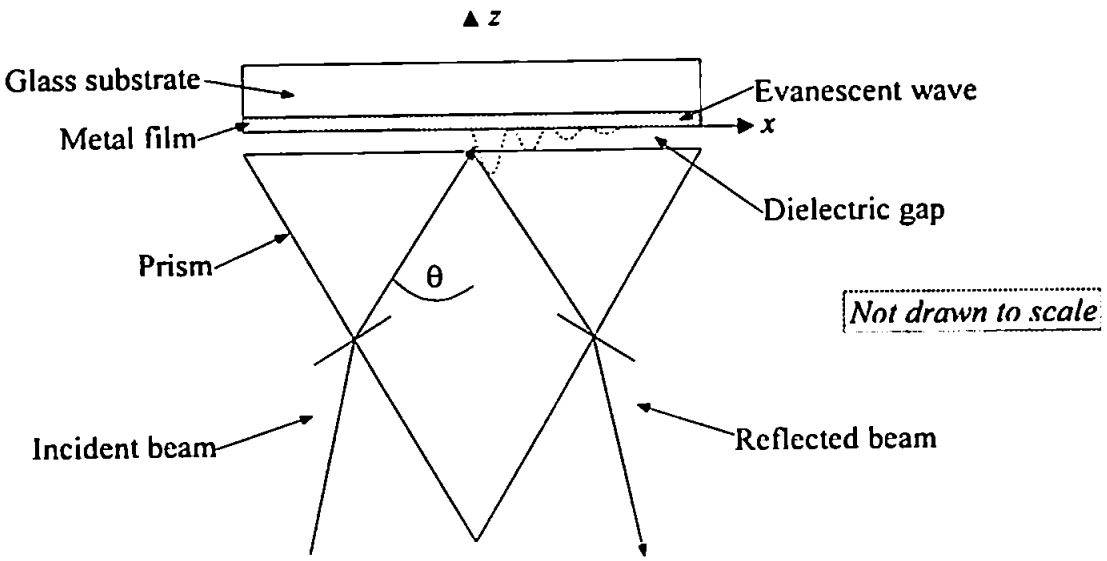

Otto configuration

Figure 1.1 - Schematic of the Otto SPR configuration.

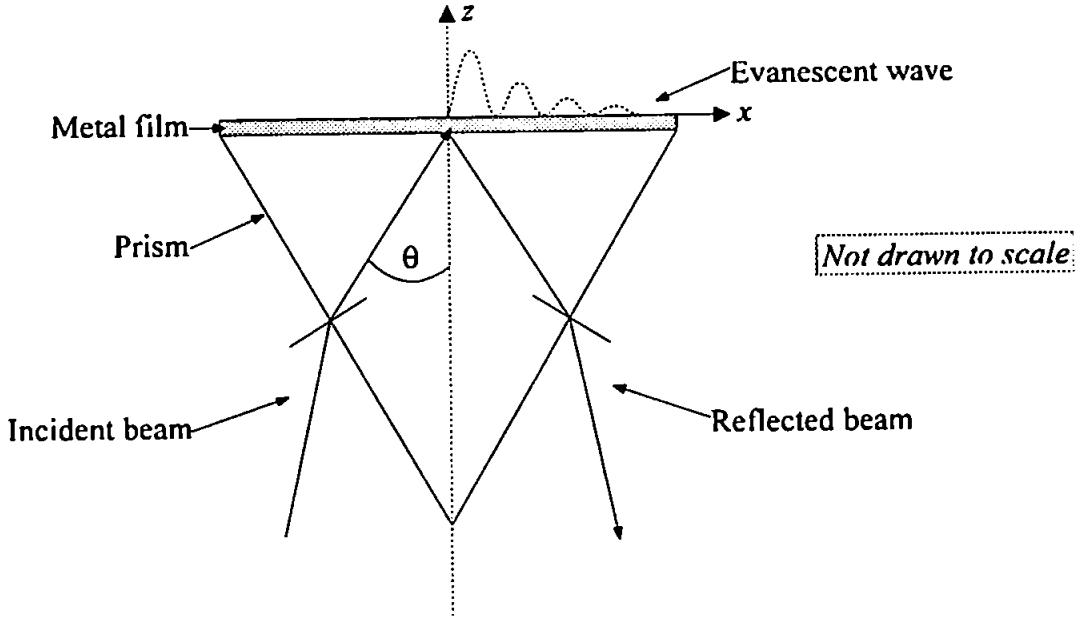

Kretschmann-Raether configuration

Figure 1.2 - Schematic of the Kretschmann-Raether SPR configuration.

1.2.1 Overview of SPR devices

1.2.1.1 Otto configuration

In the Otto configuration, Figure 1.1, a high refractive index prism is brought to within approximately one wavelength of the incident radiation of a metal coated dielectric substrate. Using the principle of Frustrated Total Internal Reflection, described in Section 3.2.2.2, the electromagnetic energy in the form of an exponentially decaying evanescent field can couple across the air gap exciting surface plasmons on the air/metal interface of the metalised substrate. The surface plasmon field is itself evanescent and decays exponentially away from the metal surface (z-direction) while propagating parallel to the interface (x-direction). Maximum coupling occurs, across the air gap, at an optimum coupling angle (θ_{SPR}) where surface plasmon resonance is at its peak. The air gap size is a very important parameter in determining SP coupling. Great care is needed to prevent re-coupling of the plasmon field back into the prism. In certain experimental configurations a half prism is used with the incident wave striking the coupling interface at the prism's edge thus preventing any re-coupling (Figure 1.3).

1.2.1.2 Kretschmann-Raether configuration

In the Kretschmann-Raether configuration, Figure 1.2, a metal film is deposited directly on to the prism's surface. Maximum coupling occurs when the incident radiation, at the optimum coupling angle (θ_{SPR}), has sufficient momentum to excite surface plasmons within the metal and thus produce a SPW. (A full explanation of SPR in the Kretschmann-Raether configuration can be found in Section 2.2.2). This device configuration is considerably easier to fabricate than the Otto configuration or grating coupler.

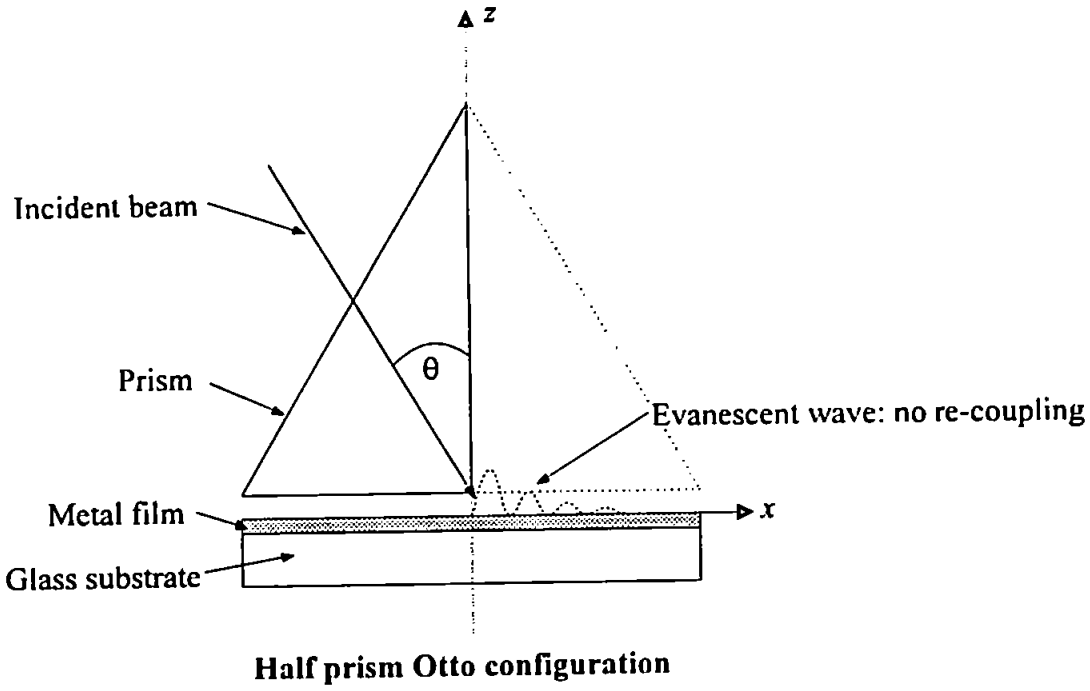

Figure 1.3 - Schematic of the Otto SPR half prism coupling configuration.

1.2.2 Commercially Available Devices

Variations to the experimental techniques discussed have been used by a number of investigators. A development of significant importance is the use of SPR to monitor the constituents of fluid flow over the excited metal surface of a SPR device. Any change in the refractive index of the medium above the excited surface will result in a change in the characteristics of the plasmon resonant peak the calibration of which can provide useful information concerning the dielectric characteristics of the medium under analysis.

Tien and Ulrich (1970) discuss the theory of the prism-metal coupler in the Otto configuration which allows for accurate measurement of the refractive indices of thin-film waveguides. A variety of SPR based chemical sensors have been developed in recent years for use in immunoassay, gas, and liquid sensing [Jorgenson *et al.* (1993)]. Commercially available SPR systems (Figure 1.4) are now produced by the Swedish manufacturer Pharmacia (Uppsala, Sweden), the British manufacturer Fisons Applied Sensor Technology (Cambridge, UK) and the Swiss manufacturer Artificial Sensor Instruments (Zurich, Switzerland). Pharmacia utilises SPR in the sensor whereas Fisons Applied Sensor Technology utilises a similar technology as the SPR device except that at the sensing surface the metal is replaced with a dielectric resonance waveguide layer producing an evanescent field. Artificial Sensor Instruments utilise a variation on the optical evanescence coupling technique, using a diffraction grating to couple the evanescent wave instead of a low refractive index layer [Lukosz *et al.* (1991)]

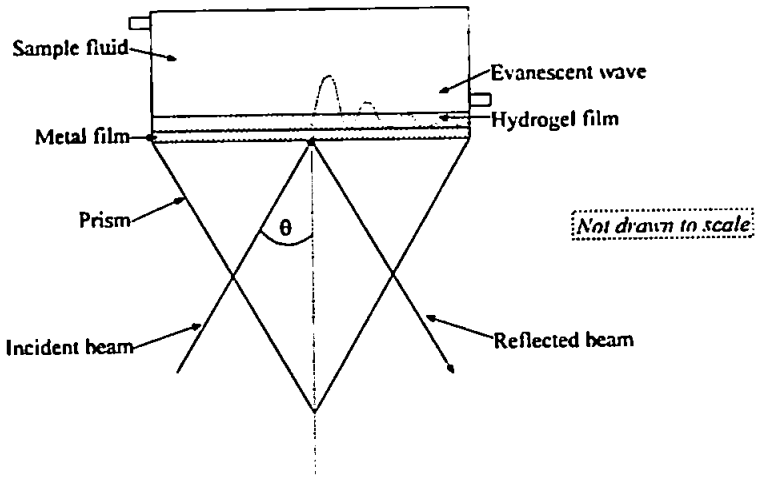

Pharmacia's SPR device

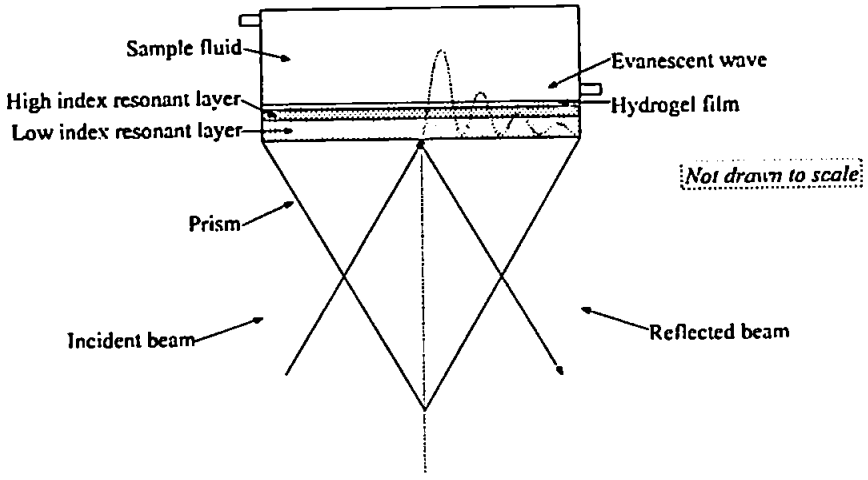

Fisons' resonant mirror device

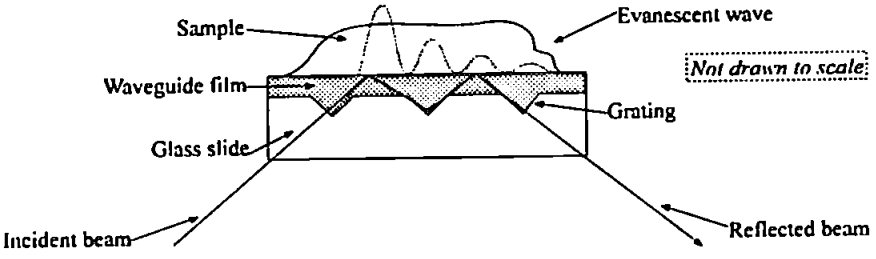

ASI's grating coupler

Figure 1.4 - Schematic of three commercially available evanescent wave bio-sensors.

Some of the most recent experimental developments in the technology utilises the SPR and evanescent qualities available in an optical fibre [Jorgenson *et al.* (1993)]. By exposing the core of an optical fibre and coating the exposed region with a metal film, excitation of the SPW can be achieved by illuminating the core with a beam of white light introduced at the end of the fibre. As the rays propagate along the fibre a SPW and associated evanescent field are excited in the metal coated core. Utilising this evanescent field and using a white light source makes for a versatile and wide dynamic range sensor (Figure 1.5).

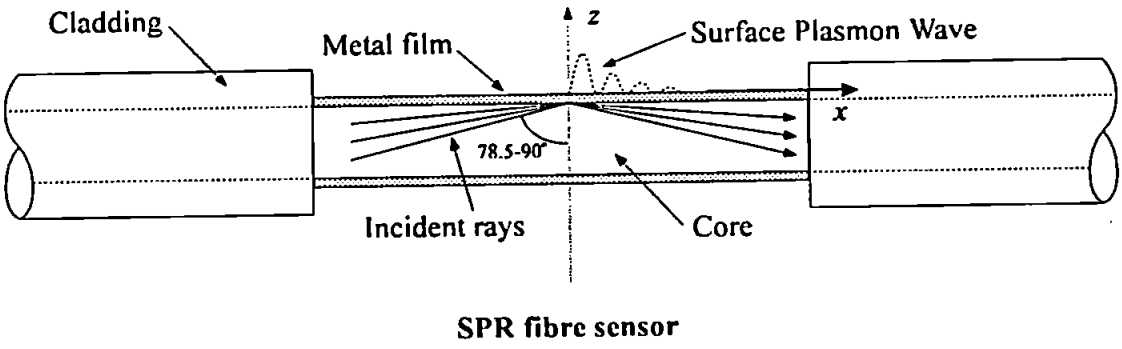

Figure 1.5 - Schematic of a SPR fibre sensor.

Chapter 2

2. FUNDAMENTALS OF THE OPTICAL SYSTEM

INTRODUCTION

In the following section the optical theories of the system used in this project are discussed. The fundamental optical theory of reflection and transmission is initially given in order that the reader may gain an insight into the theory of surface plasmon resonance. The diffraction of the surface plasmon wave by the introduction of apertures into the otherwise continuous metal film is described along with the principles of the biological cell de-coupling processes responsible for its visualisation on the otherwise dark background of the metal film.

2.1.1 Optical Properties of Metals

The optical properties of a non-absorbing medium, at a given wavelength of incident light λ, can be described by a single constant, the refractive index n, i.e. a ratio of the speed of electromagnetic radiation in a vacuum to the speed of electromagnetic radiation

in the medium. However, in the case of an absorbing medium such as a metal, a second constant must be specified to describe the strength of the radiation absorption on entering the medium. As metals contain free electrons in their structure they intrinsically have very high absorption properties, resulting in the intensity of the incident light falling to zero in a fraction of a wavelength distance within the metal layer. The refractive index is then given as a complex quantity;

$$\hat{n}_i = n_i^{'} + j\kappa_i^{''} \tag{1.}$$

where $n_i^{'}$ is the real component of the refractive index and $\kappa_i^{''}$ is the imaginary component and is sometimes referred to as the extinction coefficient of the medium.

Also

$$n_i^{'2} - \kappa_i^{''2} = \frac{\varepsilon_i^{'}}{\mu_i} \tag{2.}$$

and

$$2n_i^{'}\kappa_i^{''} = \frac{\varepsilon_i^{''}}{\mu_i} \tag{3.}$$

where $\varepsilon_i^{'}$ and $\varepsilon_i^{''}$ are the real and imaginary components of the permittivity of the material respectively (otherwise known optically as the dielectric constant) and μ_i is the magnetic permeability of the material, in this case approximately equal to unity.

The reflectance and transmittance of light at an optically flat interface are very much dependent on wavelength, refractive indices, polarisation and angle of incidence. In general metals are the best reflectors, a fact which is related to their ability to conduct electricity and their subsequent high absorption. For a thin-film layered structure, the

reflectivity is a resultant of the individual reflectivity of each of the interfaces. The phase change of the wave as it propagates and reflects within the multi-layer structure also must be considered. In the following section the theory underlying the optical properties of layered systems is outlined.

2.1.2 Reflection and Transmission at a Single Non-Absorbing Interface

In 1823 Fresnel developed the formulae for the amplitudes of reflected and transmitted waves at a single non-absorbing non-magnetic dielectric interface. The electromagnetic theory of dielectric reflection and refraction involves the application of 'boundary conditions' to Maxwell's equations. Thus they are described by the components of the electric and magnetic fields parallel to the interface in the incident medium equalling the correspondingly parallel components immediately on the other side of the boundary [Born & Wolf (1980)], i.e. the tangential components of the electric and magnetic vectors of the incident wave are continuous across the boundary. There are thus four conditions;

$$\begin{aligned} E_x^i + E_x^r &= E_x^t \qquad H_x^i + H_x^r = H_x^t \\ &\text{and} \\ E_y^i + E_y^r &= E_y^t \qquad H_y^i + H_y^r = H_y^t \end{aligned} \tag{4.}$$

where the superscripts i, r and t refer to the incident, reflected and transmitted components respectively.

Assuming a normalised plane polarised harmonic wave incident on an interface (a-b), the amplitude reflection and transmission coefficients, denoted by r and t respectively, are given by;

$$r_{//a,b} = \frac{n_b\cos(\theta_a) - n_a\cos(\theta_b)}{n_b\cos(\theta_a) + n_a\cos(\theta_b)} \qquad r_{\perp a,b} = \frac{n_a\cos(\theta_a) - n_b\cos(\theta_b)}{n_a\cos(\theta_a) + n_b\cos(\theta_b)}$$

and (5.)

$$t_{//a,b} = \frac{2n_b\cos(\theta_a)}{n_b\cos(\theta_a) + n_a\cos(\theta_b)} \qquad t_{\perp a,b} = \frac{2n_a\cos(\theta_a)}{n_a\cos(\theta_a) + n_b\cos(\theta_b)}$$

Where // and $\perp$ denote parallel (p) and perpendicular (s) polarisation respectively, n_a and n_b are the refractive indices of the respective media and θ_a and θ_b are the incident and refractive angles of the respective media.

These are known as the *Fresnel Coefficients*.

A surface plasmon can not be excited by a s-polarised wave and thus in all experimental work it was necessary to use p-polarised incident light as the electric component of the incident radiation is normal to the plane of the metal and thus excitation of surface plasmons can be achieved. Henceforth all the calculations are made for p-polarisation. Accordingly, separate notation of s and p-polarisation are unnecessary and not used.

2.1.3 Reflection and Transmission at a single Non-Absorbing Thin-Film layer

Consider a plane polarised wave at normal incidence ($\theta = 0°$, i.e. $cos(\theta) = 1$) to a single non-absorbing film (n_b) surrounded on both sides by dielectric media of refractive index n_a and n_c, as shown in Figure 2.1. The transmitted wave, back into the first medium, will traverse an optical distance of $2n_bd_b$, where d_b is the physical thickness of the dielectric layer b, relative to the first reflection at $z = 0$, with the phase difference (δ_b) given by $\frac{2\pi}{\lambda}2n_bd_b$, where λ is the wavelength of the incident radiation.

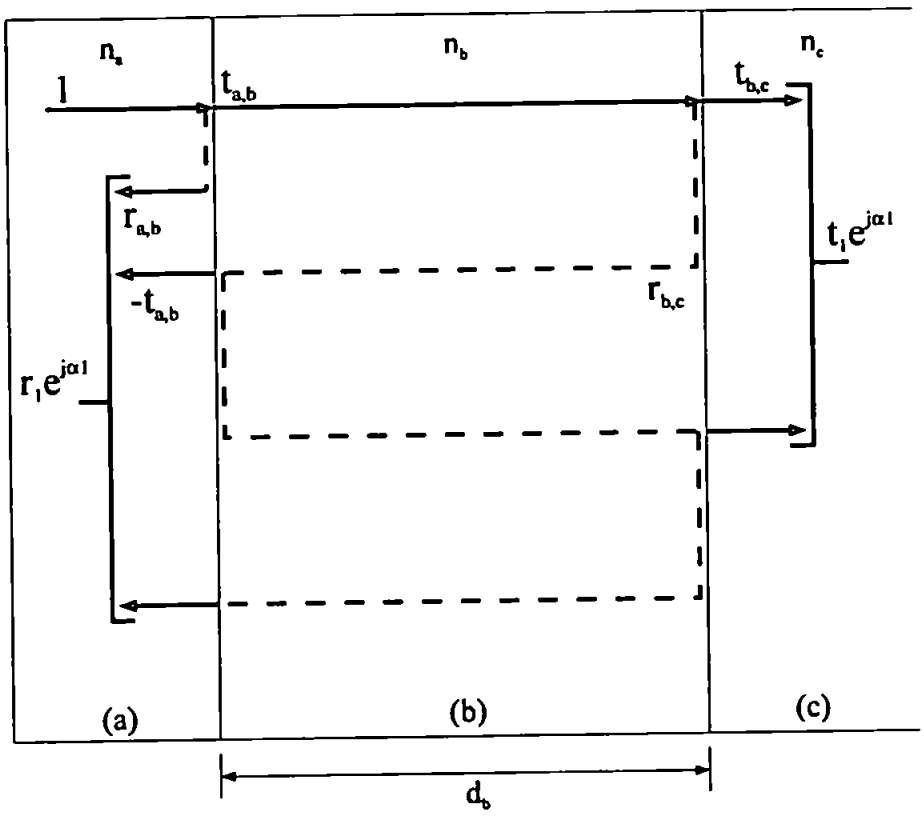

Figure 2.1 - Reflections and Transmissions at a non-absorbing layer.

The presence of the two interfaces of the thin-film layer results in the wave experiencing multiple reflections and refractions between these boundaries. The overall reflection coefficient for a single layer can be determined by the summation of all these individual reflections and is given by;

$$r_1 e^{j\alpha_1} = \frac{r_{ab} + r_{bc} e^{j\delta_b}}{1 + r_{ab} r_{bc} e^{j\delta_b}} \tag{6.}$$

where $r_{a,b}$ and $r_{b,c}$ are the Fresnel reflection coefficients for the interface between medium a - b and b - c respectively [Anders (1967)].

Similarly, as seen in Figure 2.1, the transmission coefficient for the second interface is given by;

$$t_1 e^{j\alpha_1} = \frac{t_{ab} t_{bc} e^{j\frac{\delta_b}{2}}}{1 + r_{ab} r_{bc} e^{j\delta_b}} \tag{7.}$$

where $t_{a,b}$ and $t_{b,c}$ are the Fresnel transmission coefficients for the interfaces between medium a - b and b - c respectively.

If a further layer of refractive index n_c is added to the single layer structure shown in Figure 2.1 the reflection formula for a triple interface can be readily obtained by employing equation (5.) for each of the interfaces. The reflection coefficient for a double layer system is then given by the summation of all the individual reflections;

$$r_2 e^{j\alpha_2} = \frac{r_{ab} + r_{bc} e^{j\delta_b} + r_{cd} e^{j(\delta_b+\delta_c)} + r_{ab} r_{bc} r_{cd} e^{j\delta_c}}{1 + r_{ab} r_{bc} e^{j\delta_b} + r_{ab} r_{cd} e^{j(\delta_b+\delta_c)} + r_{bc} r_{cd} e^{j\delta_c}} \tag{8.}$$

where δ_c is the phase difference due to the layer c.

Applying this same analogy to the transmission coefficient in a double layer system realises the coefficient;

$$t_2 e^{j\alpha_2} = \frac{t_{ab} t^2_{bc} t_{cd} e^{j\frac{(\delta_b+\delta_c)}{2}}}{1+r_{ab}r_{bc}e^{j\delta_b}+r_{bc}r_{cd}e^{j\delta_c}+r_{ab}r^2_{bc}r_{cd}e^{j(\delta_b+\delta_c)}} \tag{9.}$$

Similarly, extending this analysis to a triple layer assembly results in the reflection coefficient;

$$r_3 e^{j\alpha_3} = \frac{\begin{array}{l} r_{ab}+r_{bc}e^{j\delta_b}+r_{cd}e^{j(\delta_b+\delta_c)}+r_{da}e^{j(\delta_b+\delta_c+\delta_d)}+r_{ab}r_{bc}r_{cd}e^{j\delta_c} \\ +r_{ab}r_{cd}r_{da}e^{j\delta_d}+r_{ab}r_{bc}r_{da}e^{j(\delta_c+\delta_d)}+r_{bc}r_{cd}r_{da}e^{j(\delta_b+\delta_d)} \end{array}}{\begin{array}{l} 1+r_{ab}r_{bc}e^{j\delta_b}+r_{ab}r_{cd}e^{j(\delta_b+\delta_c)}+r_{ab}r_{da}e^{j(\delta_b+\delta_c+\delta_d)}+r_{bc}r_{cd}e^{j\delta_c} \\ +r_{cd}r_{da}e^{j\delta_d}+r_{bc}r_{da}e^{j(\delta_c+\delta_d)}+r_{ab}r_{bc}r_{cd}r_{da}e^{j(\delta_b+\delta_d)} \end{array}} \tag{10.}$$

2.1.4 Reflection at a Non-Absorbing Interface at an Oblique Angle

A wave incident on a thin-film layer at an oblique angle *(θ)*, will experience an optical path difference of *cos(θ)*. The overall optical path of the wave after reflection from the secondary interface will then become *2ndcos(θ)*, with a phase change relative to the initial incident wave of $\frac{4\pi}{\lambda} ndcos(\theta) = \delta^{*}$. Hence, δ in all the above equations will be replaced by δ^{*}.

In all cases the measurable quantities of the system, given by the Reflectance (R) and the Transmittance (T) are obtained by multiplying the overall reflection and transmission coefficients by their complex conjugate, i.e.

$$R = \left(re^{j\alpha}\right)\left(re^{j\alpha}\right)^{*} \text{ and } T = \left(te^{j\alpha}\right)\left(te^{j\alpha}\right)^{*} \tag{11.}$$

where * in the above equation denotes the complex conjugate.

2.1.5 Reflectance and Transmittance in Absorbing Media

In the case of an absorbing (metal) film the reflection coefficients requires slight modification when using the complex refractive index of equation (1.). All occurrence of the complex refractive indices of the corresponding metal layer in equation (5.) are therefore replaced by equation (1.).

In the previous sections the perpendicular component of the wave vector of an obliquely incident wave was simply calculated using geometric optics, i.e. *cos(θ)*. This can not be assumed the case in an absorbing medium, such as a metal. With the introduction of the complex refractive index the solutions of Maxwell's equations yield retarded dispersion relations for the surface of a semi-infinite metal and a dielectric medium. The

perpendicular component of the wave vector (k_{zi}) in each of the media is now calculated using the quadratic relation;

$$k_{z_i} = k\sqrt{\varepsilon_i - \varepsilon_a sin^2(\theta_a)} \tag{12.}$$

where k is the wave vector of the incident radiation $\left(\frac{2\pi}{\lambda}\right)$, ε_i is the dielectric constant of the secondary medium (n_i^2), ε_a is the dielectric constant of the incident medium (n_a^2) and θ_a is the angle the incident radiation makes with the normal to the interface in the incident medium.

Substituting the perpendicular components of the wave vector (k_{zi}) modifies Fresnel's reflection and transmission coefficient equations. The reflection and transmission coefficients of the incident radiation may therefore be calculated in a similar manner to that of a non-absorbing layer. Hence, $r_{a,b}$ and $t_{a,b}$ of equations (6.) and (7.) will be given by;

$$\mathrm{r}_{a,b} = \frac{n_b^2 k_{z_a} - n_a^2 k_{z_b}}{n_b^2 k_{z_a} + n_a^2 k_{z_b}} \tag{13.}$$

and

$$\mathrm{t}_{a,b} = \frac{2n_b^2 k_{z_a}}{n_b^2 k_{z_a} + n_a^2 k_{z_b}} \tag{14.}$$

with $\delta_b = 2d_b k_{zb}$

Again the reflectance and transmittance are calculated in similar manner to that for a non-absorbing layer and given by equation (11.). Figure 2.2 and Figure 2.3 show the

theoretical reflectance and transmittance for a single *Ag* film on a dielectric substrate as a function of the angle of incidence.

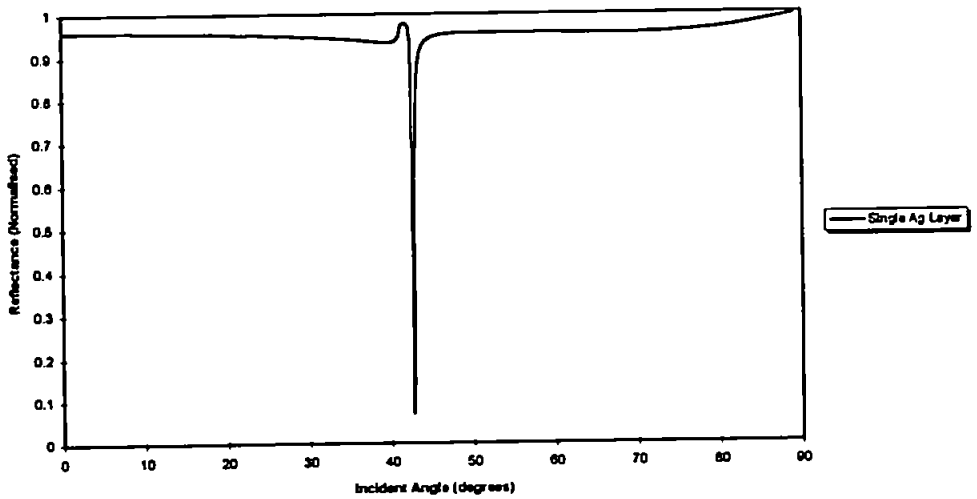

Figure 2.2 - Theoretical reflectance as a function of incident angle for a single 50nm *Ag* layer system (n_1=1.517, $\hat{n}_2 = \sqrt{-18.3 + j0.67}$ @ 632.8nm, n_3=1).

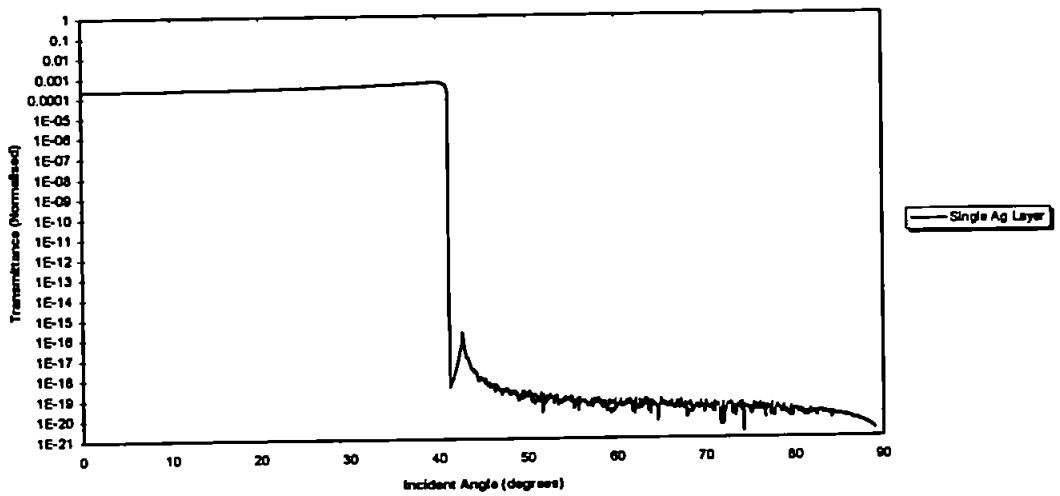

Figure 2.3 - Theoretical transmittance as a function of incident angle for a single 50nm *Ag* layer system (n_1=1.517, $\hat{n}_2 = \sqrt{-18.3 + j0.67}$ @ 632.8nm, n_3=1).

2.2 THEORY OF SURFACE PLASMONS

2.2.1 Surface Plasmons

A metal can be regarded as an array of fixed positive ions immersed in an equal number of free electrons. Under the action of an electric field, increased numbers of free electrons are drawn towards the surface layer of the metal where, in conjunction with the positive ions they constitute a plasma. Surface plasmons exist on the surface of a metal as a result of the high density of free electrons being acted on by the normal component of an oscillating external electric field creating charge oscillations plus a linked surface electromagnetic mode. Figure 2.4 shows the oscillations of the charges in the surface as the plasma wave propagates along the boundary.

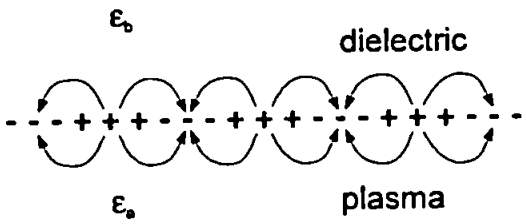

Figure 2.4 - Charge oscillations on a plasma boundary.

Maxwell's theory shows that electromagnetic waves can propagate along a metallic surface or in a metal film. A portion of this wave extends above the surface and is said to be evanescent (i.e. the extension of the field above the surface of the medium in which it is propagating) and decays exponentially orthogonal to the direction of propagation.

2.2.2 Excitation of Surface Plasmons

Non-radiative surface plasmons cannot radiate from a smooth surface directly into air or vacuum as a consequence of their momentum perpendicular to the surface being always

larger than that of light of the same frequency [Raether (1977)]. The excitation of non-radiative surface plasmons however requires light-plasmon coupling structures, such as grating or prism couplers. They both share similar characteristics; they match the wave vectors of the incident light to the wave vector of the surface plasmon.

For a normal incident wave on a metal in a vacuum the wave vector is given by;

$$k_x = \frac{\omega}{c}\sqrt{\varepsilon_o} \tag{15.}$$

where ω is the angular frequency of the radiation, c is the speed of electromagnetic radiation in a vacuum and ε_o is the relative dielectric constant of free space i.e. $\varepsilon_o = 1$.

There is insufficient momentum in the incident wave to match that of the surface plasmon in the metal and thus cannot excite non-radiative surface plasmons on the surface of a metal. Introducing the incident wave to the metal interface in a medium of dielectric constant greater than that of a vacuum increases the wave vector accordingly;

$$k_x = \frac{\omega}{c}\sqrt{\varepsilon} \tag{16.}$$

where ε=2.3 for BK7 glass @ 632.8nm.

The component parallel to the direction of propagation in the metal film of the wave vector in the dielectric at an incident angle (θ) to the normal, is then given by;

$$k_x = \frac{\omega}{c}\sqrt{\varepsilon}\sin\theta \tag{17.}$$

Comparing (15.) with (16.) it can be seen that the momentum of the incident wave has increased by the factor $\sqrt{\varepsilon}/\sqrt{\varepsilon_0}$ under the differing conditions.

2.2.3 Dispersion Relation

Raether (1988) shows that the relationship between the wave vectors of the x and z-components of the plasma wave and the dielectric constants of the two media inside and outside the plasma (metal ε_a and dielectric ε_b) link to form the dispersion relation for p-polarised oscillations of a non-radiative plasmon on a semi-infinite metal surface for all values of k_x, i.e.

$$k_x = \frac{\omega}{c}\sqrt{\frac{\varepsilon_a \varepsilon_b}{\varepsilon_a + \varepsilon_b}} \qquad (18.)$$

where ω is the angular frequency of the incident wave.

An s-polarised wave cannot excite surface plasmons due to the fact that the electric field E_y is continuous and no surface charges exist normal to the metal surface. If the wave vector (k_x) of the wave travelling in the metal has an imaginary component, i.e. jk_x, the magnitude of the field decays exponentially away from the surface, the wave is said to be non-radiative thus propagating no energy away from the surface. Alternatively the wave is said to be radiative if the wave vector (k_x) is real.

In the case of an asymmetric layer system, of glass, metal and air the dispersion relation becomes complex ($\hat{k}_x = k_x^{'} + jk_x^{''}$) with the introduction of the complex dielectric constant of the metal layer. The imaginary component relates to the damping of the wave as it propagates along the metal surface. The real and imaginary components of the dispersion relation are thus given by;

$$k_x^{'} = \frac{\omega}{c}\sqrt{\frac{\varepsilon_a^{'} \varepsilon_b}{\varepsilon_a^{'} + \varepsilon_b}} \qquad (19.)$$

$$k_x'' = \frac{\omega}{c}\left(\frac{\varepsilon_a'\varepsilon_b}{\varepsilon_a' + \varepsilon_b}\right)^{3/2} \frac{\varepsilon_a''}{2\varepsilon_a'^{2}} \qquad (20.)$$

where ε' and ε'' are the real and imaginary components of the dielectric constant and the subscripts a and b denote the respective media.

Figure 2.5 demonstrates the dispersion relation (or wave vector) for a dielectric/metal/air system as a function of angular frequency [Raether (1988)], where;

i. is the wave vector in a vacuum of the incident radiation at an angle,
ii. is the wave vector in a vacuum of the incident radiation at grazing incidence,
iii. is the wave vector in a dielectric medium of the incident radiation at an angle,
iv. is the wave vector in a dielectric medium of the incident radiation at grazing incidence and
v. is the dispersion relation of the surface plasmon.

The wave vector of incident radiation in a dielectric (17.) may excite plasmons at a certain frequency where the dispersion relation (v) intersects the plots iii. and iv. (points x' and x'' respectively). The incident radiation in a vacuum (i. and ii.) cannot excite surface plasmons as they have insufficient wave vectors, at any frequency and incident angle of incident radiation, to match the dispersion relation of the surface plasmon.

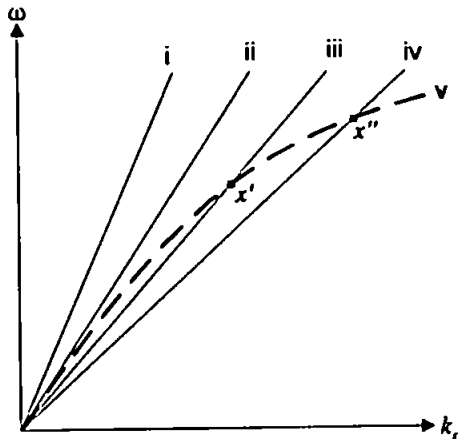

Figure 2.5 - Dispersion Relation of surface plasmons for a dielectric/metal/air system.

2.2.4 Propagation Length of Surface Plasmons

As a consequence of the lossy nature of a metal, at optical frequencies, as described in Section 2.1.1, the intensity of the surface plasmon wave as a function of propagation distance decreases exponentially, i.e. $e^{-2k_x''x}$. Subsequently, the propagation length P_L at which the intensity of the SP field falls to *1/e* of its initial value is given by;

$$P_L = \frac{1}{2k_x''} \tag{21.}$$

Figure 2.6 shows the theoretical intensity plot of a surface plasmon wave propagating in an *Ag* film as a function of the propagation distance. It is seen that at the point when the intensity has decreased to a value of *1/e* of its initial value (36.78%) the wave has travelled a distance of 46.3μm.

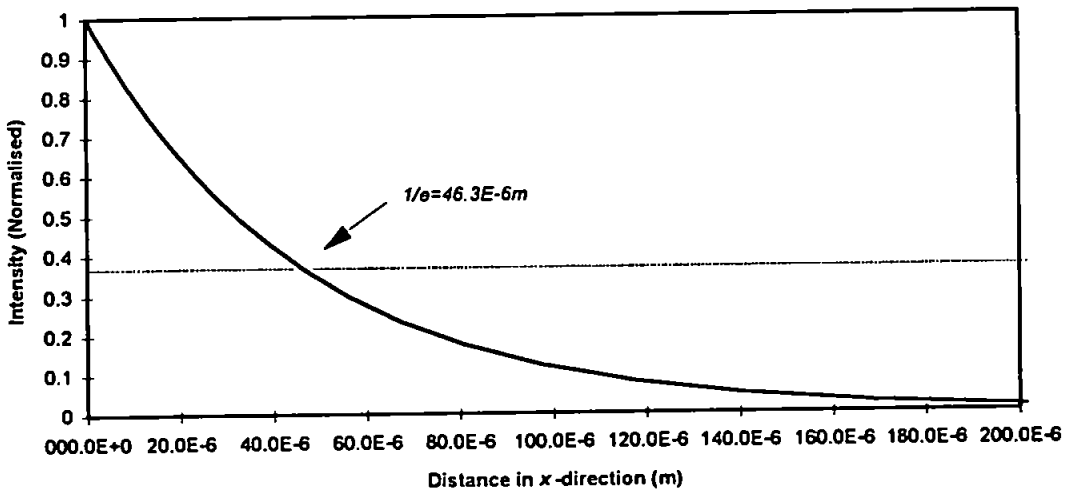

Figure 2.6 - Theoretical intensity plot of a SPW as a function of the propagation distance for an *Ag* thin-film device (n_1=1.517, $\hat{n}_2 = \sqrt{-18.3 + j0.67}$ @ 632.8nm, n_3=1).

2.2.5 Field Enhancement at Surface Plasmon Resonance

As shown in Section 2.1.5, Figure 2.2, the reflectivity as a function of incident angle goes through a minimum, the intensity of the electromagnetic field being a maximum at the surface of the metal. The ratio of the coupled field intensity at the surface of the metal to the field intensity of the incident wave is known as the '*Enhancement Factor*', and is used to indicate the efficiency of the different layer configurations and dielectric constants;

$$Enhancement = \frac{2\left|\varepsilon_b^{'}\right|^2 \sqrt{\left|\varepsilon_b^{'}\right|\left(\varepsilon_a - 1\right) - \varepsilon_a}}{\varepsilon_c \varepsilon_b^{''}\left(1 + \left|\varepsilon_b^{'}\right|\right)} \qquad (22.)$$

where ε_a, ε_b and ε_c are the dielectric constants of the media a, b and c respectively and the superscripts $'$ and $''$ denote the real and imaginary components of the complex dielectric constants of the medium [Raether (1988)].

The maximum enhancement factors for a single Ag (n_1=1.517, $\hat{n}_2 = \sqrt{-18.3 + j0.67}$, n_3=1 θ_{spr}=42.7°) and Cr (n_1=1.517, $\hat{n}_2 = \sqrt{-6.274 + j35.853}$, n_3=1 θ_{spr}=41.3°) device is 244 and 0.74 respectively. This demonstrates the excellence of Ag as a SPR metal but as seen later Cr has its own merits as a useful SPR sensor.

2.2.6 Spatial Extension of Surface Plasmons

The spatial extension of the surface plasmon field above the metal surface is perhaps the most important property of the device with regard to this application. The characterisation of the field plays a key role in identifying the behaviour of the cells on the sensor surface. The spatial extension of the surface plasmon above and below the surface of the metal is characterised by the wave vectors in the metal and in the medium above and decays exponentially. The extent at which the intensity decays to *1/e* of its initial value is given by the normal component of the surface plasmon wave vector;

$$z = \frac{1}{|k_{z_i}|} \tag{23.}$$

Figure 2.7 shows the calculated spatial extension of the surface plasmon wave normal to the surface for a dielectric/silver/air system.

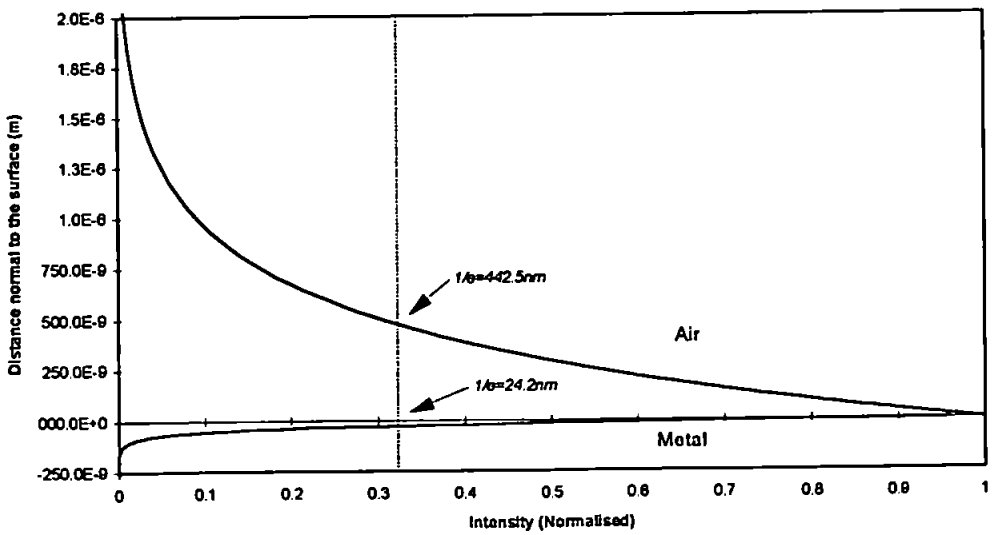

Figure 2.7 - Theoretical plots of the intensity of the SPW as a function of the spatial extension above and below the dielectric/metal interface (n_1=1.517, $\hat{n}_2 = \sqrt{-18.3 + j0.67}$ @ 632.8nm, n_3=1).

2.2.7 Optimisation of Surface Plasmon Coupling

Maximum excitation of SP's by incident radiation is dependant on several critical factors, namely.

i) The incidence angle at which maximum resonance occurs.
ii) The wavelength of the incident radiation.
iii) The metal film physical properties.
and
iv) The dielectric properties of the surrounding media.

A measure of SPR is generally recognised as the minimum reflectance from the initial interface of a metal layer.

Solutions of the reflectance equations are sought in order to find the value of the incident angle and the metal thickness at which the minimum value of reflectance occurs. Differential solutions, with respect to θ and d, of the reflectance equations in Section 2.1.5 when equated to zero, yield the minimum values of incident angle and film thickness.

As shown in Figure 2.2 the incident angle at which the reflectance has a minimum is approximately 42° for an Ag coated device (n_1=1.517, $\hat{n}_2 = \sqrt{-18.3 + j0.67}$ @ 632.8nm, n_3=1). This is confirmed with the numerical solution to the differential equations;

$$\frac{dR}{d\theta} = 0 \quad @ \quad \theta = 42.684°$$

and

$$\frac{dR}{dd} = 0 \quad @ \quad d = 51nm$$

2.3 APERTURES - DISCRETE CENTRES OF SCATTERING

This section deals with the changes to the SPW by the presence of refractive index discontinuities. If the metal waveguide is abruptly terminated, with a dielectric, the SPW will experience a dramatic change in propagating conditions, unable to sustain a non-radiative SPW the energy will de-couple and scatter in a manner described by diffraction theory (Figure 2.8). The following section describes the process by which the SPW is scattered by the circular apertures etched in the otherwise plain metal film.

2.3.1 Diffraction at the Initial Boundary of the Aperture

The metal film constitutes a waveguiding structure in which the wave propagates. It has a rectangular cross section, in the case of an *Ag* device used in these experiments, 2mm wide by 51nm thick. The scattering of a SPW may be described in a similar way to the diffraction of light through a slit, in a non-conducting screen. Both waves are travelling in a medium when acted on, at normal incidence, by a sharp edged obstacle with definite boundary conditions (Figure 2.8). There are two discrete models to describe the diffraction of light through slits. They were developed by Fresnel and Fraunhofer and are given in many quality text books [Jenkins & White (1965)]. Fresnel's theory relates to the diffraction of light when the source or the screen on which the diffraction pattern is viewed, or both, are at finite distances from the aperture. Fraunhofer's theory relates to the diffraction of the light when the source and the screen on which it is viewed are at infinite distances from the aperture, i.e. in the far-field (distance to point of viewing, $d \gg \lambda$).

The source of radiation, i.e. the SPW, is initiated anywhere between 0-46μm from the diffracting edge of an *Ag* device (46μm being the propagation length of the SPW, Section 2.2.4) and is contained within a metal waveguide and could therefore be

therefore can be effectively regarded as being initiated at an infinite distance from the aperture. The microscope lens, at a distance from the diffracting aperture of approximately 30mm, is at a considerable distance away and thus can be said to be viewed on a screen set at an infinite distance from the diffracting aperture. It is therefore reasonable to assume in this case that, a SPW meeting with a refractive index discontinuity may be described by Fraunhofer's diffraction through a slit. A brief theoretical description of Fraunhofer's diffraction theory is given in Section 2.3.2.

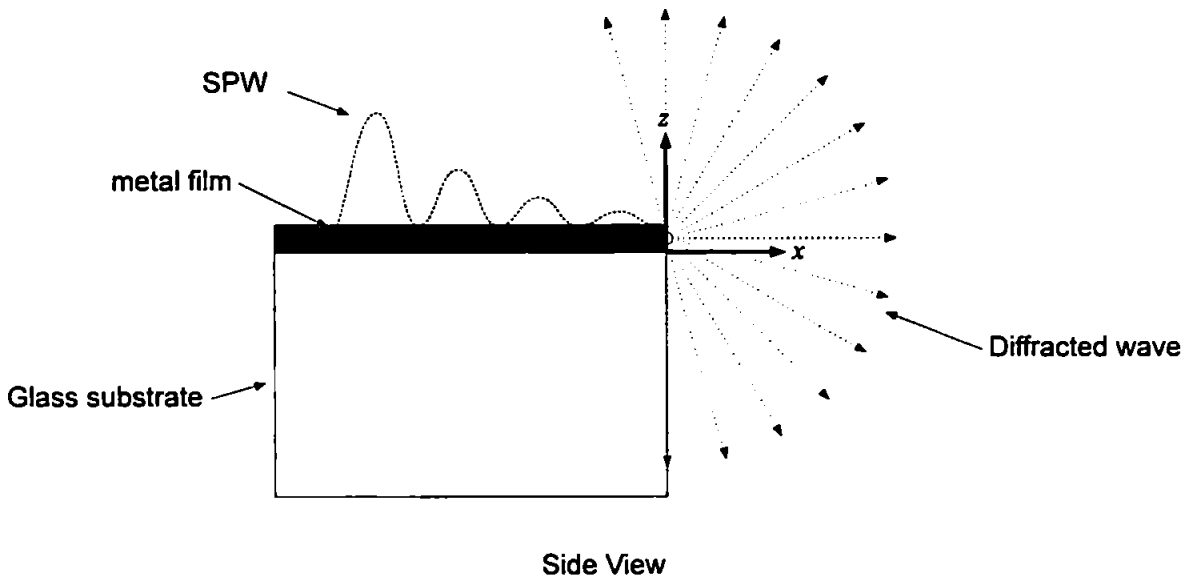

Figure 2.8- Schematic of the diffraction of a SPW by a refractive index discontinuity.

2.3.2 Fraunhofer's Diffraction Theory

The intensity function at any point on a screen from which parallel light is diffracted by a slit in a non-conducting screen is given as;

$$I = A_0^{\,2} \frac{\sin^2 \beta}{\beta^2} \tag{24.}$$

where $\beta = \left(\frac{\pi d}{\lambda}\right) \sin\theta$, d is the width of the slit and θ is the angle from the centre of the aperture to the point of observation. In practical terms β is one-half of the phase difference between the contributing diffractions from opposite edges of the slit [Jenkins & White (1965)].

The wavelength of radiation, the width and height of the slit are the predominant parameters in this case.

Diffraction theory shows that if the height of a single slit decreases, the side lobes at larger angles, as seen in the polar plots of the intensity function of the diffraction pattern, decrease and eventually vanish. Figure 2.9 illustrates this point showing a comparison between the polar diagrams for slits of different heights.

Where $d \ll \lambda$, the intensity polar diagram becomes uniform at all angles (Figure 2.9). This is comparable to the system we have employed in the thin metal film devices (*Cr* 90nm, *Ag* 50nm thick). Practically, this results in the intensity of the diffracted radiation from the end of the waveguide being of uniform intensity at all angles of observation.

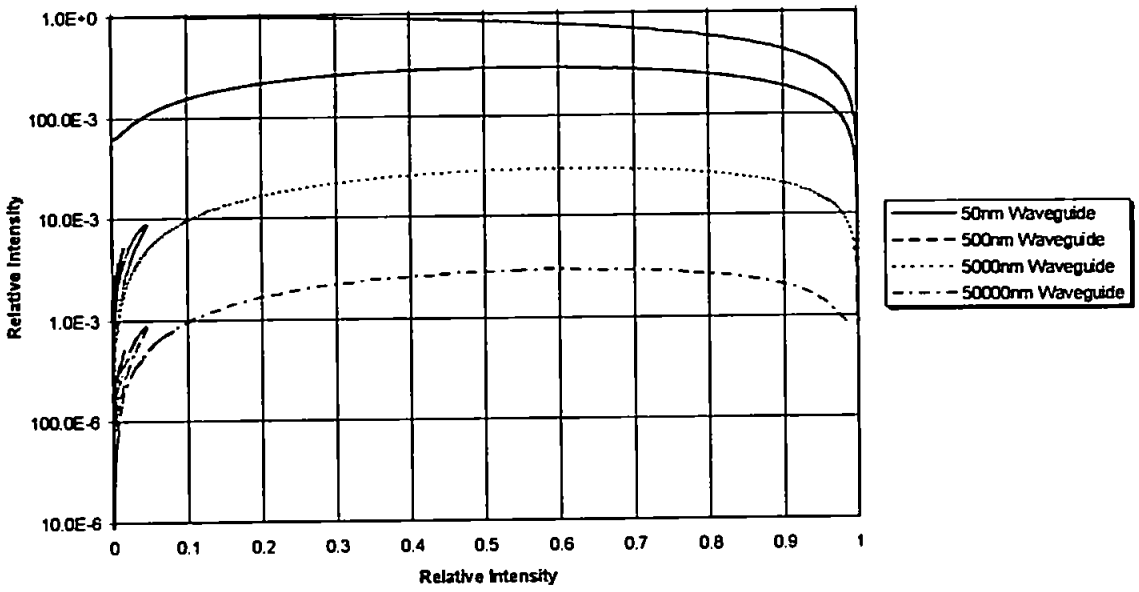

Figure 2.9 - A logarithmic theoretical comparison of the polar plot intensity profiles at the ends of abruptly terminated *Ag* films of different thickness under the influence of SPR (n_1=1.517, $\hat{n}_2 = \sqrt{-18.3 + j0.67}$ @ 632.8nm, n_3=1).

2.3.3 Diffraction at the Secondary Boundary of the Aperture

An evanescent wave exists on the upper boundary of a dielectric when a beam of light is incident on the dielectric/air interface at an angle greater than the critical angle (θ_c) of the system ($\theta_c = \sin^{-1}[n_b/n_a]$, where n_b=1 and n_a=1.517) [Syms *et al.* (1992)]. In order that a SPW may be excited on the surface of a thin metal waveguide the laser radiation must be incident on the dielectric/metal interface at the SPR angle (θ_{SPR}=42.375°, n_1=1.517, $\hat{n}_2 = \sqrt{-18.3 + j0.67}$ @ 632.8nm, n_3=1). This is an angle greater than the critical angle for a glass/air interface (θ_c=41.2°). If the evanescent wave encounters an air/metal refractive index discontinuity it will be diffracted in a similar manner to that of the SPW encountering a metal/air discontinuity, Figure 2.10. The evanescent wave on the dielectric/air interface extends to approximately 100nm above the surface of the dielectric. The extension and thus the magnitude of this evanescent wave is considerably smaller than that of the SPW. In Figure 2.10 the exponential decay of the evanescent wave is not shown as the width of the incident laser beam is considerably larger than the diameter of the aperture of which a small portion is shown.

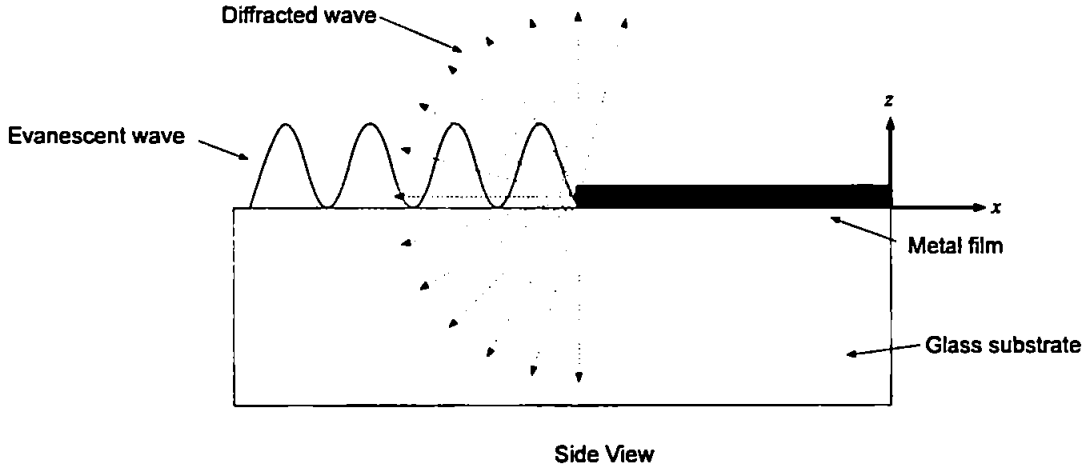

Figure 2.10 - A schematic diagram of the diffraction of the evanescent wave within an aperture by a refractive index discontinuity, the incident beam is illuminating the entire aperture.

2.4 REFRACTION AT THE APERTURE PERIPHERY

Figure 2.11 shows, using geometric optics, a schematic diagram of a SPW interacting with the boundary of a large aperture (diameter, $\phi \gg \lambda$) etched in the otherwise plain metal film. Consider a single ray of a SPW striking the centre of the aperture circumference, i.e. at normal incidence. Reflection and transmission at the interface will take place. At distances away from the centre of the circumference the angle the incident beam makes to a normal at that point on the periphery of the aperture gradually increases until total reflection, i.e. no transmission, of the incident beam occurs. The reflectance and transmittance, of the incident SPW and evanescent wave, at the boundaries of the aperture may be calculated at various positions on the circumference and is described in the following section.

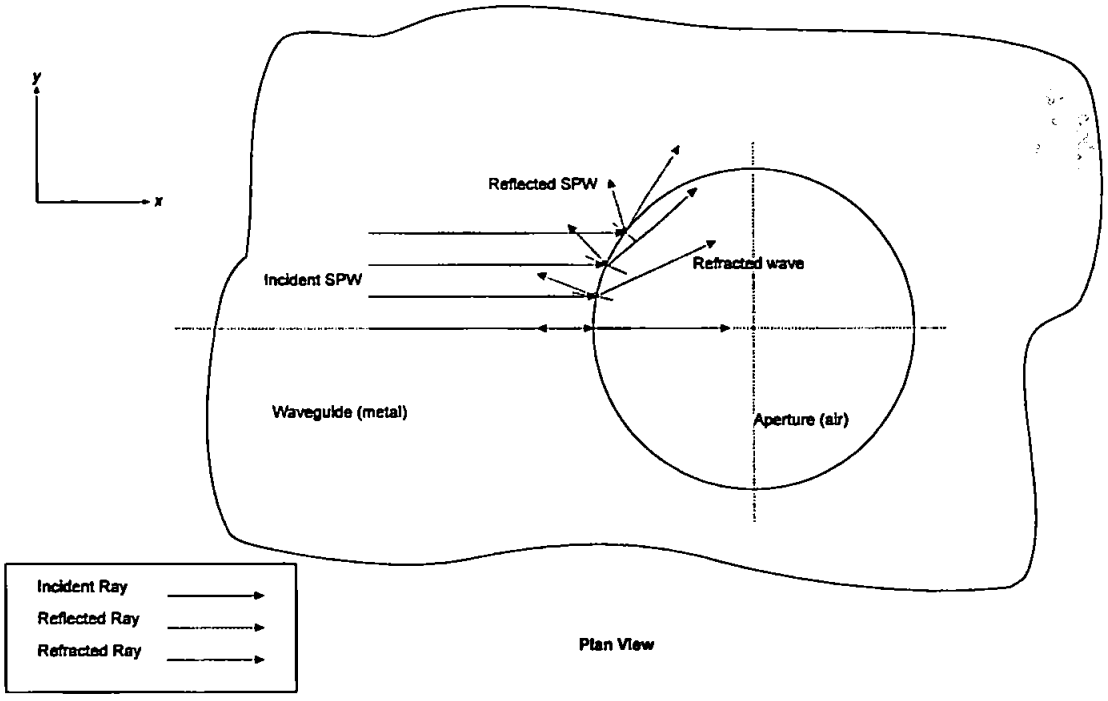

Figure 2.11 - Schematic showing the refraction of the SPW by an aperture boundary.

2.5 REFLECTION AND TRANSMISSION OF A SPW AT AN APERTURE

Fresnel's transmission and reflection coefficients at an interface, Section 2.1.2, are used to describe the portion of the incident ray reflected from and transmitted through an interface (Equation (5.));

$$r_{//a,b} = \frac{n_b \cos(\theta_a) - n_a \cos(\theta_b)}{n_b \cos(\theta_a) + n_a \cos(\theta_b)}$$

$$t_{//a,b} = \frac{2n_b \cos(\theta_a)}{n_b \cos(\theta_a) + n_a \cos(\theta_b)}$$

Using these equations the transmittance of a SPW through a metal/air interface ($\hat{n}_{Ag} = \sqrt{-18.3 + j0.67}$, $n_{air}=1$) is calculated as 20.5% of the normalised incident field. A tunnelling effect of the transmitted wave will therefore occur across the width of the aperture. At the opposite edge of the aperture the reverse configuration is present. The reflectance at normal incidence to this air/metal interface is, like any good conductor, very high, 98.4% of the wave incident on the air/metal interface will be reflected. A minute amount will be transmitted into the metal film decaying rapidly with the majority of the evanescent wave being diffracted/scattered into the medium above. At aperture diameters in the order of the wavelength of the incident wave a Fabry-Perot type resonance effect will occur due to this high reflection coefficient. Figure 2.12 shows the calculated transmittance from a metal/air interface and the reflectance from an air/metal interface as a function of incident angle.

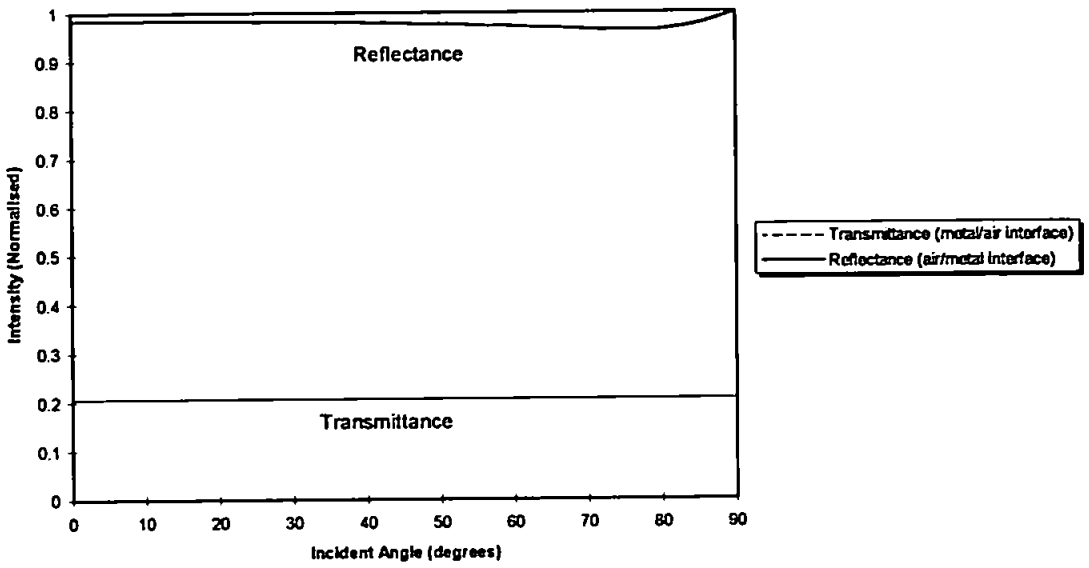

Figure 2.12 - Calculated Transmittance and Reflectance of an incident wave at a metal/air and air/metal interfaces respectively ($\hat{n}_{Ag} = \sqrt{-18.3 + j0.67}$ @ 632.8nm and n_{air}=1).

2.6 FIELD DETECTION BY OPTICAL FIBRE PROBE - THEORETICAL ASPECTS

In order to investigate the electromagnetic fields on the surface of the sensor a standard telecommunications optical fibre was used as a SPM probe. The following section describes the theory of the detection of the radiative fields by an optical fibre probe used in the SNOM configuration. The probe tip, as described in Section 3.3.1, (originally 10μm diameter core/125μm diameter cladding tapered down to 400nm/5μm) is a highly selective detector. If an optical fibre core, much smaller than the illuminating source, is scanned across a beam of light, an increasing cross sectional area of its cleaved end face will be exposed to the radiation until the complete core is illuminated. This gradual increase is depicted in Figure 2.13 with relative intensity as a function of the increase in the radius of the fibre core exposed.

If this SNOM probe is mounted perpendicularly to the terminating 50nm waveguide and scanned over a metal/air interface (Figure 2.14), having similar diffraction characteristics as shown in Figure 2.9, an intensity maxima will occur at the terminating edge, where the radiation is incident on the exposed end face at normal incidence and maximum coupling may occur. Only rays at, or very close to, the acceptance angle or mode matching conditions of the optical fibre will be accepted by and propagate along the length of the fibre to the detector. Any rays outside these conditions will not. The resultant will be a symmetrical intensity profile of that shown in Figure 2.13. If the probe is scanned at 45° to the normal over the edge of the discontinuity an increase in distance over which the probe is able to detect radiation occurs as shown in Figure 2.15. From simple geometry the overall distance (x') over which the fibre is able to detect the radiative intensity pattern is a factor of;

$$\frac{1}{\cos(\alpha)} \tag{25.}$$

where α is the angle at which the probe makes with the normal.

therefore $$x' = x\left(\frac{1}{\cos(\alpha)}\right) \tag{26.}$$

where x is the distance over which the source is detectable at normal incidence.

This increase will be similar to the symmetrical intensity profile shown in Figure 2.13 but will be expanded over a greater detectable distance, i.e. at 45° the width of the profile will have increased by a factor of 1.41 times the size of the normal profile.

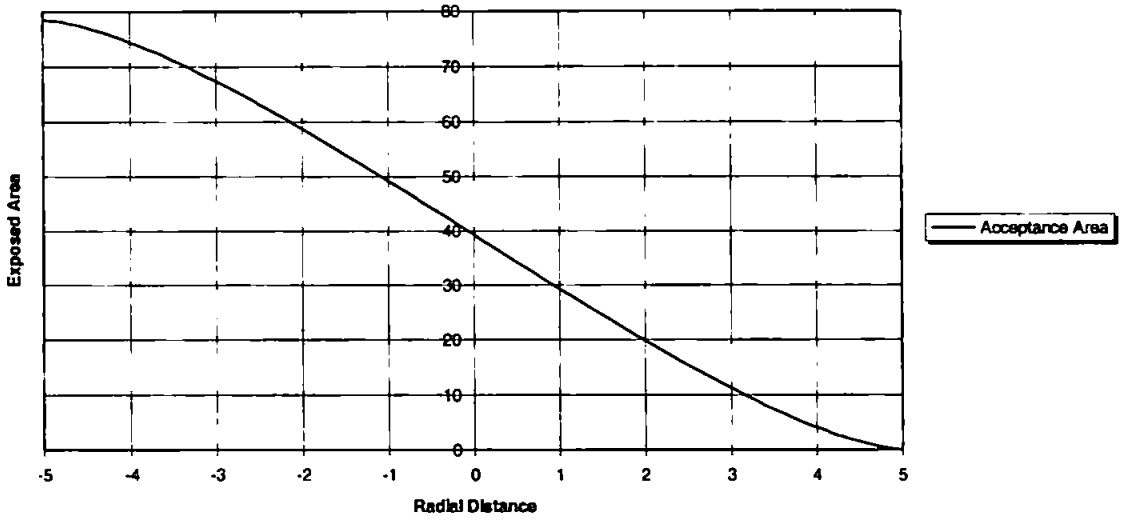

Figure 2.13 - Surface area of probe tip as a function of radial distance exposed to a beam of light.

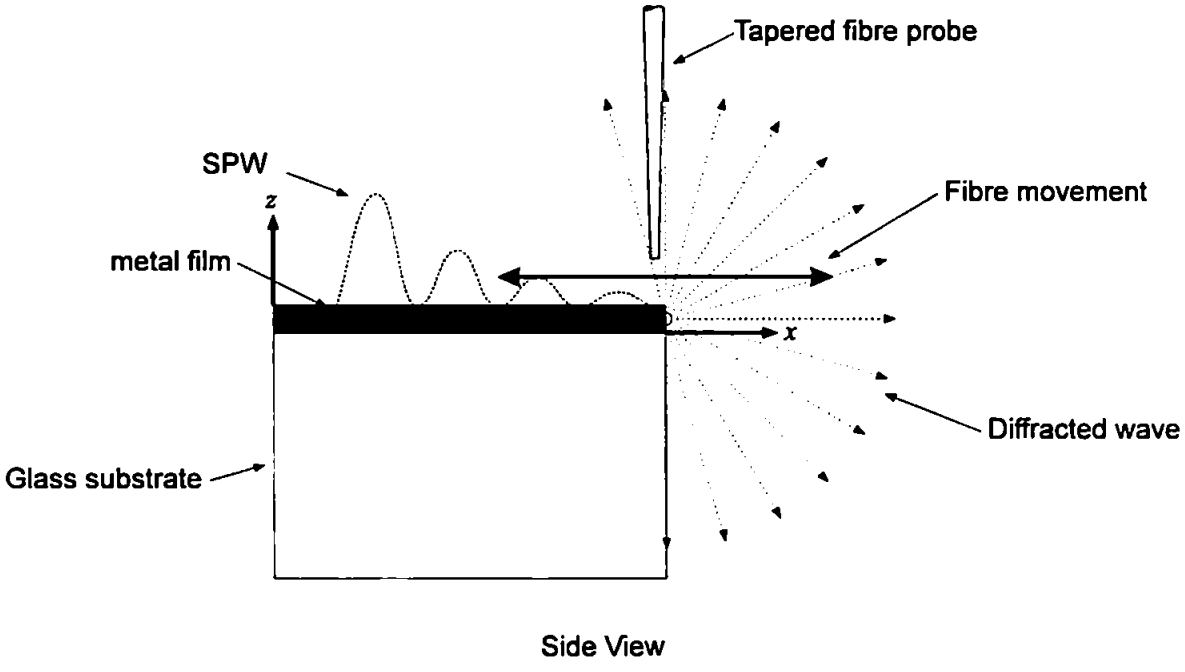

Figure 2.14 - Schematic depicting the diffraction of the SPW and the SNOM detection system at a refractive index discontinuity.

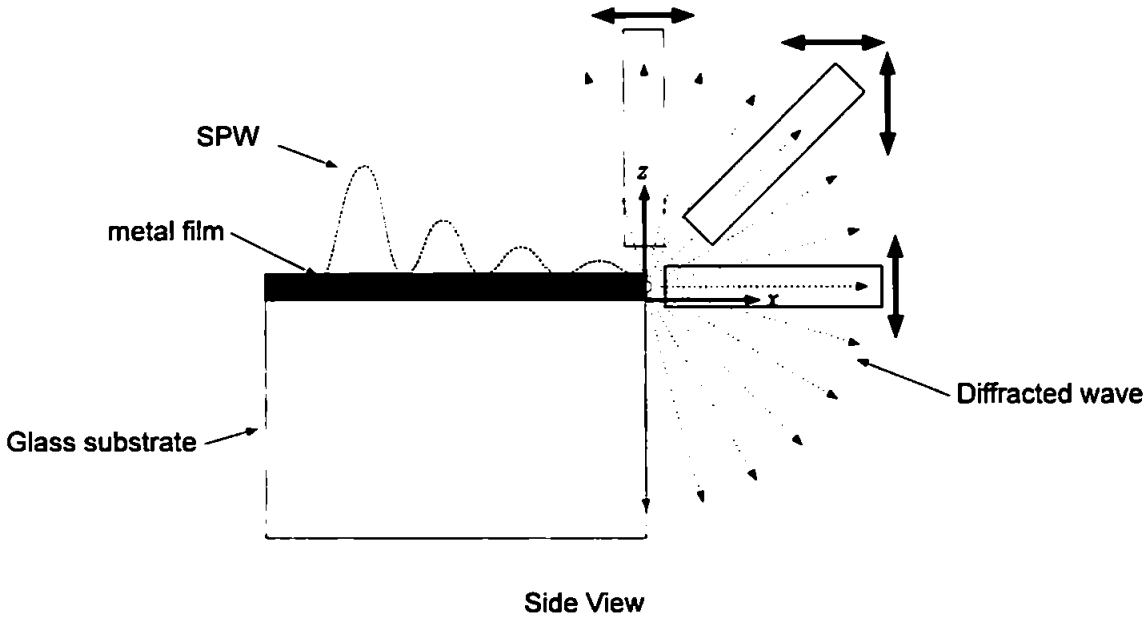

Figure 2.15 - A schematic depicting the diffraction of the SPW and the SNOM detection system at a refractive index discontinuity in different orientations with the associated detection limits.

2.7 VISUALISATION OF CELL UNDER SPR

The interactions of a dielectric structure, or part thereof, such as an isolated animal cell with the electromagnetic fields associated with a non-radiative SPW will cause scattering of the wave in all directions. In this case the detectable intensity in the far-field is orthogonal to the metal surface. There are several possible explanations describing how these processes occur.

2.7.1 De-Coupling of SPW by cell contact points

Figure 2.16 illustrates the calculated transmittance of incident laser radiation through a three layer system. The critical angle and SPR angle can be clearly identified as 61.3° and 67.3° for a glass/silver/water layered system respectively. As the cell makes contact with the active SPR metal surface the resonant conditions at the point of contact change considerably. At the point of contact the system is now a glass/silver/cell system of a considerably different dispersion relation to the former system, resulting in the point of contact becoming no longer resonant and no longer capable of sustaining a propagating SPW. The result is a de-coupling of the SPW energy from the metal waveguide and thus allowing the contact to be seen from above. The relative transmittance through the glass/silver/cell system (Figure 2.16) has now changed and at the otherwise resonant angle of the glass/silver/water system (to which the system is optimised) has increased approximately considerably. As the animal cell is essentially aqueous a substantial portion of the radiation will be further transmitted through the cell and into the medium above for visual interpretation and image analysis.

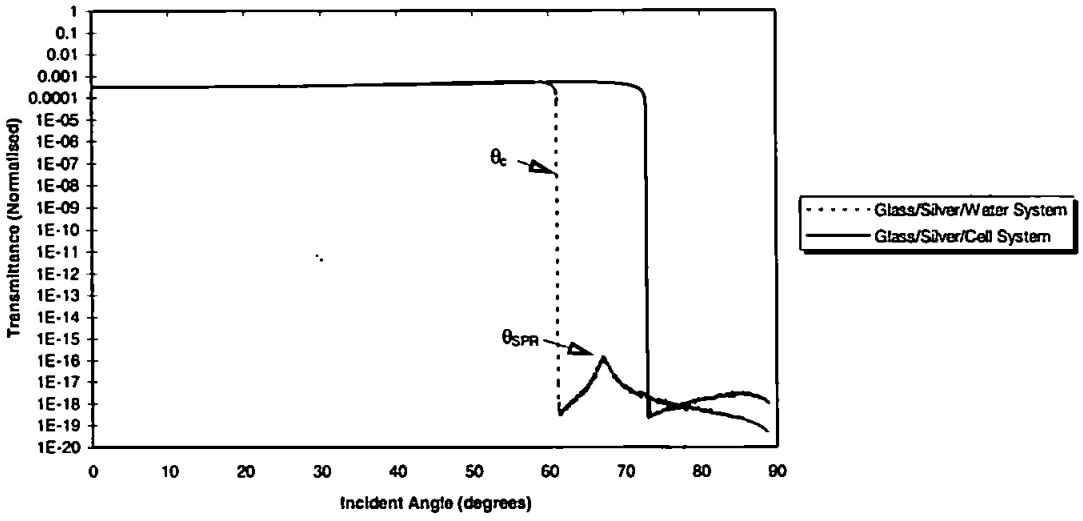

Figure 2.16 - Comparison of the calculated transmittance through a system as a function of incident angle for glass/silver/water (n_1=1.517, $\hat{n}_2 = \sqrt{-18.3 + j0.67}$ @ 632.8nm, n_3=1.33) system and a glass/silver/cell (n_1=1.517, $\hat{n}_2 = \sqrt{-18.3 + j0.67}$ @ 632.8nm, n_3=1.45) system.

As a consequence of the interaction mechanism between the cell and the SPW the outline of the cell/particle may be visualised by the distinct intensity profile it produces relative to the dark background. The following section describes in more detail the physical processes involved in the scattering of the evanescent wave, by the presence of a dielectric discontinuity, into the field of view.

2.7.2 Scattering of SPW by an Animal Cell

An electromagnetic field acting upon an animal cell of a different dielectric constant to that of the surrounding medium experiences a change in propagation conditions. The animal cell entering the SPW evanescent field will scatter the otherwise non-radiative wave which will be detected orthogonal to the metal. This accounts for the visualisation of the cell before it actually touches the active SPR metal surface.

As the evanescent wave is of an exponential nature the closer the cell is to the surface of the substrate the stronger the incident field acting upon it becomes. Thus, as the cell drifts down towards the surface of the sensor the scattered intensity produced by the presence of the cell increases. The degree of scattering and the direction of the scattered wave will be very much dependant on the refractive index difference, the size and shape of the scatterer and also the scattering elements within it.

Several mathematical models exist to described the scattering coefficients of an incident wave by an intrusive particle. The main factors contributing to these scattering effects are the physical size and shape of the scatterer and its relative dielectric constant. A method known as Rayleigh-Gans-Debye Scattering, named after the leading contributors to this area of scattering, is the most appropriate theory in this case, describing scattering of an incident electromagnetic wave by an arbitrary shaped particle of small relative refractive index [Kerker (1969)].

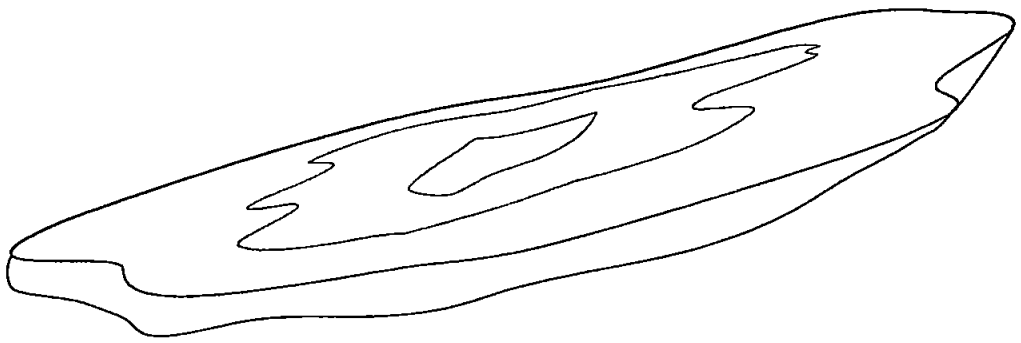

Figure 2.17 - The typical asymmetric shape of an adherent cell.

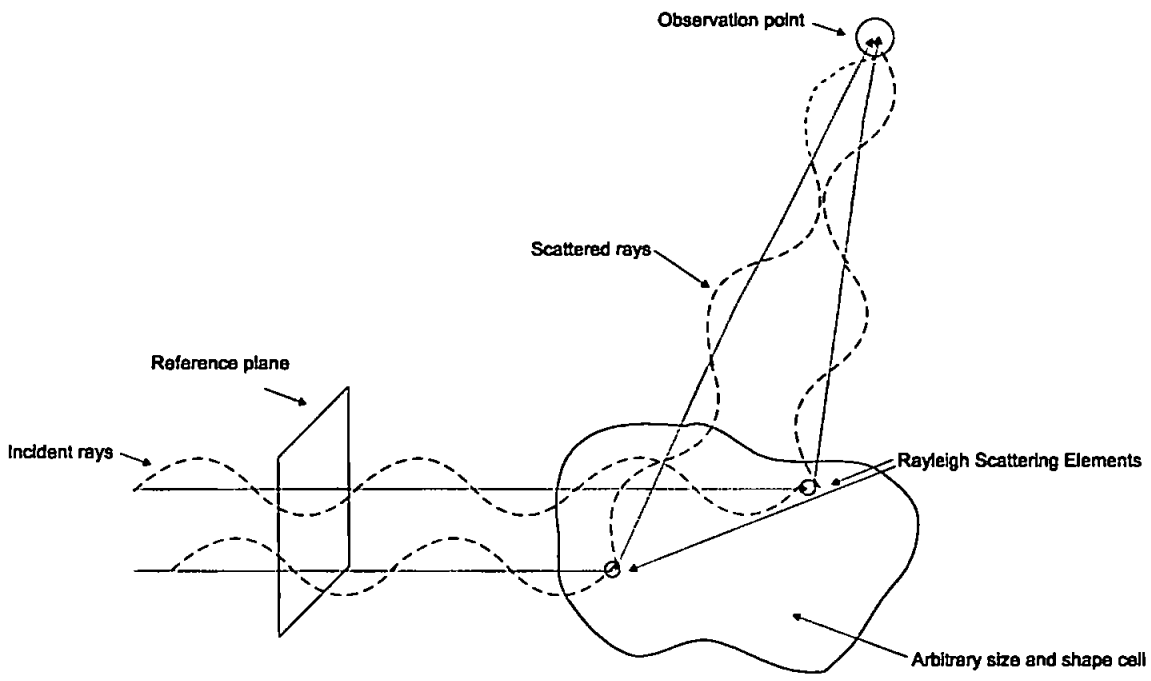

Figure 2.18 - Schematic of Rayleigh-Gans-Debye scattering.

2.7.3 Rayleigh-Gans-Debye (RGD) Scattering

RGD scattering theory uses several fundamental approximations in order to model the scattering from an irregularly shaped particle. The primary approximation being that the phase shift of the incident electromagnetic radiation corresponding to any point in the particle be negligible i.e. the overall size may not be too large and the refractive index of the particle may not be significantly different to that of the surrounding medium, i.e.

$$2ka(m-1) \ll 1 \tag{27.}$$

where k is the wave vector of the incident wave, a is the longest dimension through the particle and m is the relative refractive index of the scatterer.

It is possible in this case to use RGD theory to describe animal cells scattering a SPW. The complete cell could be imagined as being asymmetric in shape, approximately 15-20μm long, 3-5μm thick and of refractive index of 1.45 (Figure 2.17).

It is known that animal cells actually crawl over the surface of a substrate [Stossel (1994), Ambrose *et al.* (1977)]. They do not make total cell contact with the base substrate, but rather part of their cortex flows out, from the main body, to form a flat projection known as the leading lamella. Through the action of membrane-adhesion proteins the bottom of the lamella attaches itself to the base substrate providing sufficient friction for the body to propel itself forward. The lamella then detaches itself from the substrate and flows forward yet again. This continuous flowing cycle propels the cell over the surface.

The SPR evanescent field on the upper surface of an *Ag* device is known to extend, and has been verified experimentally (Section 5.1.3), to approximately 400nm above the active surface [Gourdonnet *et al.* (1993)]. The cell itself can be in the region of 4-8μm in

depth. It can therefore be said that the SPR field only acts upon a small proportion of the underside of the cell, the section in closest proximity to the active surface.

With these assumptions, i.e. relative refractive index close to unity and the portion of cell contacting the metal surface or scattering the evanescent field is not excessively large, it is possible to use RGD scattering theory to describe the visualisation of the cell in an otherwise non-radiative evanescent field. The basis of RGD scattering theory assumes that a particle of arbitrary shape can be subdivided up into numerous Rayleigh scattering elements which can be excited by an incident electromagnetic field which is unperturbed by the presence of the other elements.

The amplitude function for each of the volume elements in the whole scatterer, for incident radiation polarised perpendicular to the scattering plane is given by;

$$dS_1(\theta) = \frac{j3k^3}{4\pi}\left(\frac{m^2-1}{m^2+2}\right)e^{j\delta}dv \qquad (28.)$$

where $e^{j\delta}$ relates the phase of each elemental wavelet at the position of the observer to a common reference plane (Figure 2.18).

At an observation point the resultant amplitude function which arises from vector summation of the interference of each of the individual wavelets from the individual scatterers over its volume is given by;

$$S_1(\theta) = \frac{j3k^3}{4\pi}\left(\frac{m^2-1}{m^2+2}\right)\int e^{j\delta}dv \qquad (29.)$$

The scattered intensity at a distance r from the scattering particle is given by;

$$I_1 = \left(\frac{k^4 v^2}{4\pi^2 r^2}\right)\left(\frac{m^2-1}{m^2+2}\right)^2 F(\theta) \qquad (30.)$$

where $F(\theta) = \frac{1}{v^2}\left|\int e^{j\delta} dv\right|^2$ is the *form factor* for the complete scattering particle and represents the modification of the scattered intensity due to its arbitrary size and deviation from sphericity.

Several models have been developed for defined physical structures [Bohren *et al.* (1986)]. Rayleigh in 1881 gave the form factor for a homogeneous sphere and Neugebauer in 1943 gave the form factor for a thin rod of length L at perpendicular incidence.

Homogeneous Sphere $$F(\theta) = \left(\frac{9\pi}{2u^3}\right) J_{3/2}^2(u) \qquad (31.)$$

where $u = 2ka\sin\left(\frac{\theta}{2}\right)$ and $J_{3/2}^2$ is the three-halves order Bessel function.

Thin Rod $$F(\theta) = \frac{1}{z}\int_0^{2z} \frac{\sin(\omega)}{\omega} d\omega - \left(\frac{\sin(z)}{z}\right)^2 \qquad (32.)$$

Where $z = \left(\frac{2\pi L}{\lambda}\right)\sin\left(\frac{\theta}{2}\right)$, L is the length of the rod being acted on by the incident field.

In this particular case it is impossible to describe with confidence the specific size and shape of the section of the cell modulating the evanescent wave but by making certain assumptions it can be said that the sections of the cell making contact with the active surface is more suited to be modelled by a cylinder of finite size rather than the scattering

model of a sphere. The next section considers the scattering functions for a cylinder with worked examples.

2.7.4 Modelling the Cell as a Cylinder

The scattering model used in the case of a cell adherent to the active surface of the device is that used to model the scattering by a circular cylinder of a uniform incident electromagnetic field. The amplitude function for a cylinder is given by Montroll & Greenberg (1954) for a TM polarised incident wave;

$$I_1(\theta) = \left(\frac{\pi\alpha^2}{2}\right)(m-1)\sqrt{F(\theta)} \qquad (33.)$$

where $\alpha=ka$ and $F(\theta)$ is the *form factor* for a thin rod and is given by Equation (32.).

Figure 2.19 shows how the scattering of the incident field may be modelled by a cylinder of arbitrary size.

Figure 2.20 shows the calculated normalised scattering intensity pattern for a 400nm thin rod of length L (the depth of the SPR evanescent field) and 400nm in diameter (an estimate of the size of the section of the cell in contact with the active SPR device surface). It is shown that 27.95% of the intensity of the incident field for perpendicular polarised (TE) incident radiation is scattered orthogonal to the plane of the metal with 13.73% of the intensity of the incident field for parallel polarised (TM) incident radiation being scattered orthogonal to the plane of the metal. This theory provides a basic description of the portion of the evanescent field which accounts for the visualisation of the extremities of the cell before it actually touches the active surface of the SPR sensor.

The limit for RGD scattering theory to hold true, in this case, is when the longest dimension through the cell of relative refractive index 1.09 @ 632.8nm is approximately 500nm. That is, the size of the scattering element can become as large as 0.5μm before

phase considerations come into effect and the RGD scattering theory starts to become inapplicable.

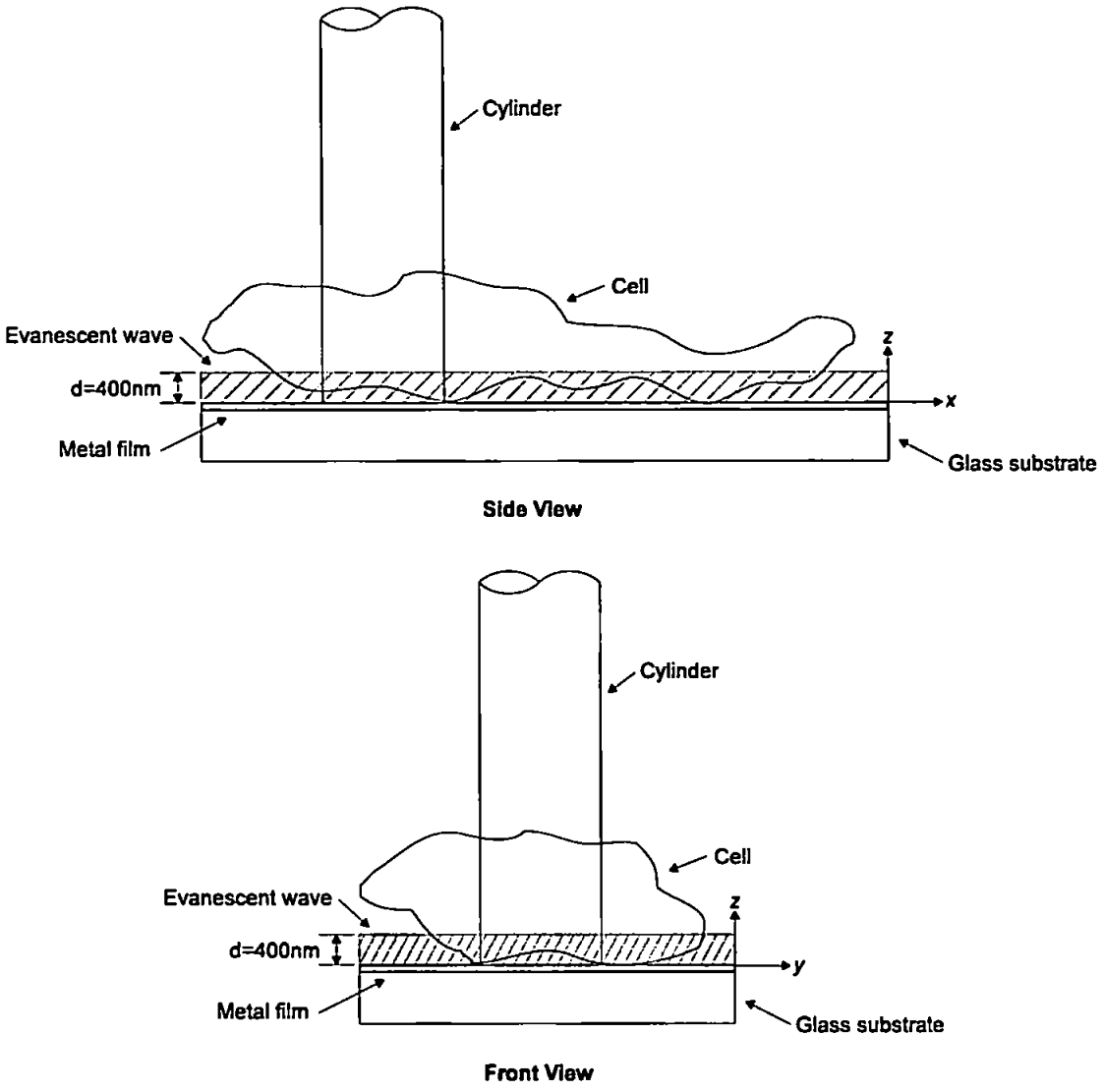

Figure 2.19 - Schematic of a cylinder representation of scattering by cell.

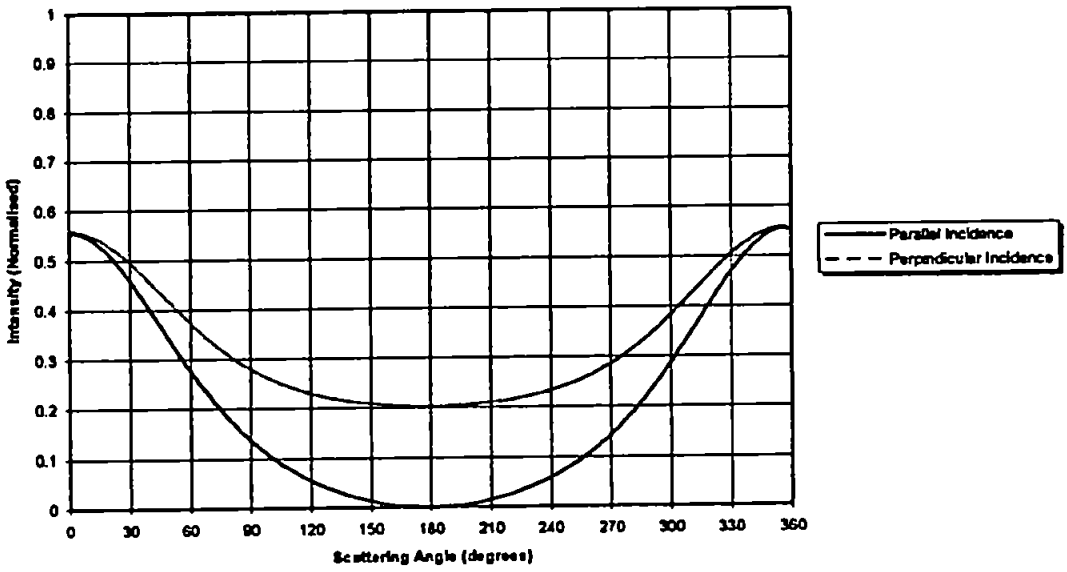

Figure 2.20 - Normalised scattering pattern for parallel and perpendicular polarised incident radiation of a cell immersed in water (n_{cell}=1.45, n_{water}=1.33).

Chapter 3

3. EXPERIMENTAL DETAILS

INTRODUCTION

This section describes the processes and equipment used to fabricate and test the devices during the different stages of the project. It also gives brief background theories and descriptions of the equipment developed to perform these tests. The methods and practical experimental procedures are discussed.

3.1 SPR DEVICE FABRICATION

During the fabrication of the SPR devices, several strictly controlled procedures were carried out in a 'clean room' environment. All sample cleaning and preparation processes apart from sputter deposition and ion milling were performed under 'class 10' conditions, i.e. in an environment containing less than 10 particles of 0.5μm in diameter

per cubic foot in the circulating air flow. The deposition and milling machines were housed in an adjacent 'class 1000' room.

3.1.1 Thin-Film Deposition Techniques

The following techniques were employed in the fabrication of the thin-film structures in the SPR devices. In our investigation glass substrates were used as the base material onto which the thin-films were deposited.

3.1.1.1 Sputtering

Sputtering is one of the vacuum deposition techniques conventionally used in the preparation of metal and dielectric thin-films on a suitable substrate. The entire process is carried out in a vacuum chamber containing two electrodes; the target (or the source of the sputtering material which forms the cathode) and the anode.

High purity inert gas is introduced into the vacuum chamber. Its particles are ionised under an applied electric field producing a plasma. A D.C. voltage is usually used when sputtering conductive materials such as metals while a R.F. voltage is required when depositing semi-conducting or insulting materials such as dielectric oxides (e.g. SiO_2). The high negative voltage at the surface of the cathode (target) attracts the ions from the plasma thus bombarding the surface of the target and freeing the surface atoms. Consequently, the vaporised target atoms are deposited uniformly over the surface of the substrate to form a thin-film coating. Figure 3.1 shows a typical sputtering system.

The quality of the deposited film is usually determined by its grain structure, thermal stress, adhesion to the substrate, step coverage, uniformity, film composition and density. These properties are controlled by the various parameters of the sputtering process. Such parameters include the sputtering pressure, temperature (cooled substrates are necessary in some cases), substrate bias voltage, field strength and the rate of deposition. There are other factors which are of equal importance in the overall quality of the film. The purity

of the target material and the inert gas, the surface quality and the cleanliness of the substrate are among the main contributing factors. Although sputtering is a versatile deposition technique, the rate of deposition is relatively slow (50Å-500Å per minute). There are several types of sputtering techniques some of which are discussed below.

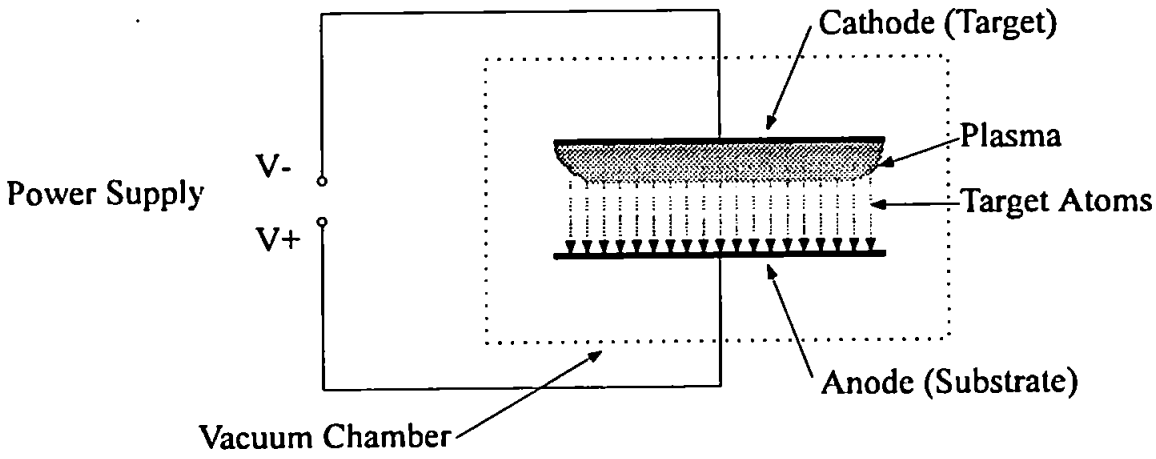

Figure 3.1 - A schematic diagram of a Sputtering System.

3.1.1.2 R.F. Sputtering

R.F. sputtering can couple through insulating materials and for this reason is used to deposit insulators.

Voltages applied at an R.F. field of 50kHz and above cause the electrons in an inert gas in the sputtering chamber to oscillate at a high frequency and hence generate ionising collisions. Sputtering from the target is achieved by producing a high positive ion flux at the target surface by placing a 'blocking' capacitor in series with the target thus presenting a high negative potential with respect to the plasma. Due to their smaller mass, the velocity of the electrons is greater for a given electric field, than that of the ions. Consequently the target surface is subject to a high energy positive ion bombardment resulting in sputtering.

An impedance matching network is required in order to optimise the coupling between the power supply and the chamber so that the generator impedance is matched to the plasma and its associated potentials, optimising power transfer and protecting the generator. A typical R.F. sputtering system is shown in Figure 3.2.

Commercial systems are restricted to operate at 13.56 MHz as allocated by the International Communications Authority so as not to interfere with terrestrial communications systems.

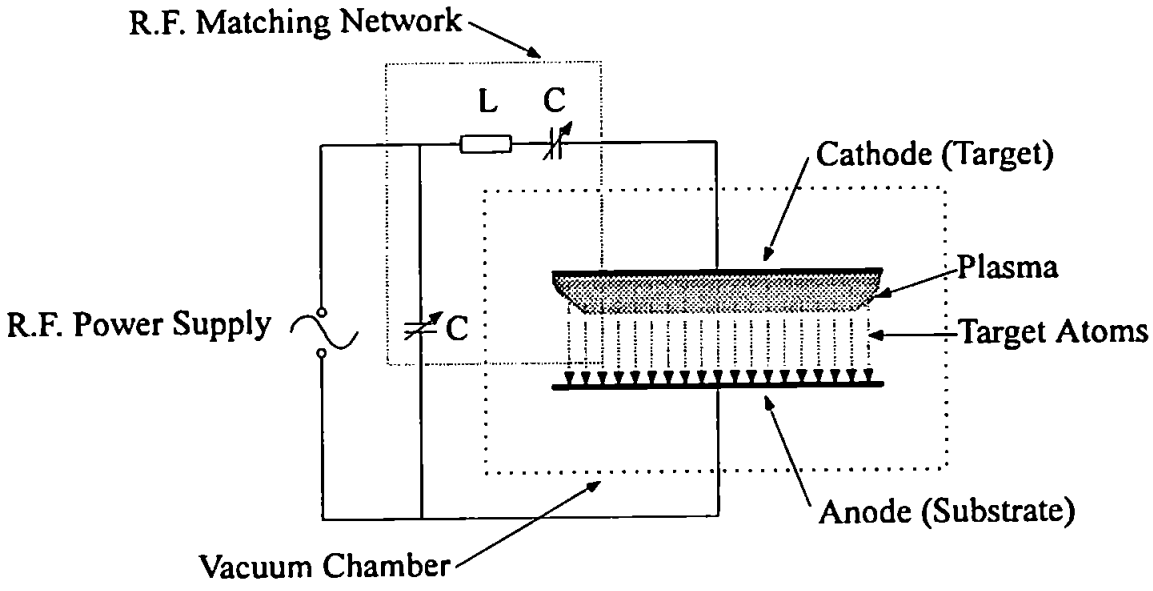

Figure 3.2 - The schematic diagram of a typical R.F. Sputtering System.

3.1.1.3 Bias Sputtering

Bias sputtering is used to give control over certain film properties such as resistivity, electrical insulation and hardness, and over the process gas incorporation into the film [Winters *et al.* (1967)]. If a negatively biased R.F. or D.C. voltage is applied to the substrate during the sputtering process it will be subjected to positive ion bombardment. This results in the preferential removal of impurities in the growing film and hence the production of a more refined film.

The most commonly used method of bias sputtering involves applying R.F. voltages to both the target and the substrate [Vossen *et al.* (1968)]. This is achieved with a single power supply in which the R.F. voltage is split between the target and the substrate by the use of a matching network.

3.1.1.4 The Target

Sputtering rate and the sputtering yield are the two key factors which determine the choice of a target. The sputtering rate is determined by the positive ion energy generated at the target surface and the sputtering yield of a particular target. The sputtering yield is defined as the number of target atoms released for every bombarding ion for a particular target material. In the overall sputtering process only a small fraction of the ionising energy is produced as the kinetic energy at the target, i.e. the energy used to dislodge the target atoms, with some 50% to 90% of the applied power needed to create the 'gas plasma' being lost as heat [Lau *et al.* (1972)]. This heating process necessitates the cooling of the target.

3.1.1.5 Thermal Deposition

This is the technique of heating a source material in a high vacuum chamber causing the source to evaporate resulting in the vaporised atoms and molecules being deposited onto the substrate. Both conductive materials and dielectric oxides can be deposited by this method. Some techniques have heating elements or crucibles, in direct contact with and

containing the source material on evaporation. This can result in contaminating the deposited films with the impurities from the crucible or the heating filament.

Thermally evaporated films are deposited at low energies and so their adhesion is inferior to sputtered films with pin-holes often forming due to the deposited atoms diffusing side ways on arrival at the substrate surface. The composition of the evaporated film can also change quite considerably from the source composition during this process.

3.1.2 Photolithography

Photolithography is the technique conventionally used to transfer a desired pattern from a mask to a suitable substrate by optical imaging and from which final thin-film electronic or opto-electronic devices are subsequently fabricated. The substrates can be glass plates, silicon wafers or single crystal wafers. In industrial mass production of devices with multi-layer structures and patterns master masks are of the highest quality to allow repeated use. Projection type of mask alignment systems are used to project the pattern image onto the substrate without making any physical contact, hence preventing any possible contact damages reducing the lifetime of the mask.

An in-contact mask aligning system, as used in our experiments and shown in Figure 3.3, is a relatively simple technique and for this reason is commonly used in research laboratories. In this technique the mask is brought into contact with the prepared substrate. The substrate is usually spin coated with photoresist (ultra-violet (UV) sensitive polymeric material) which can be referred to as positive or negative resist according to its reaction on exposure to UV light. When the masked substrate is exposed to a uniform beam of UV light for a predetermined exposure time, the mask pattern is transferred to the photoresist as a photo-modified resist pattern. The resist is then chemically developed reproducing the mask pattern and acts as a protective barrier protecting whatever lies under the resist.

The nature and complexity of the patterns and the available masks determine which type of lithography is to be used. The photoresist thickness and the UV light intensity and exposure time are monitored in order to achieve the optimum resolutions in reproducing consistent patterns for a given device.

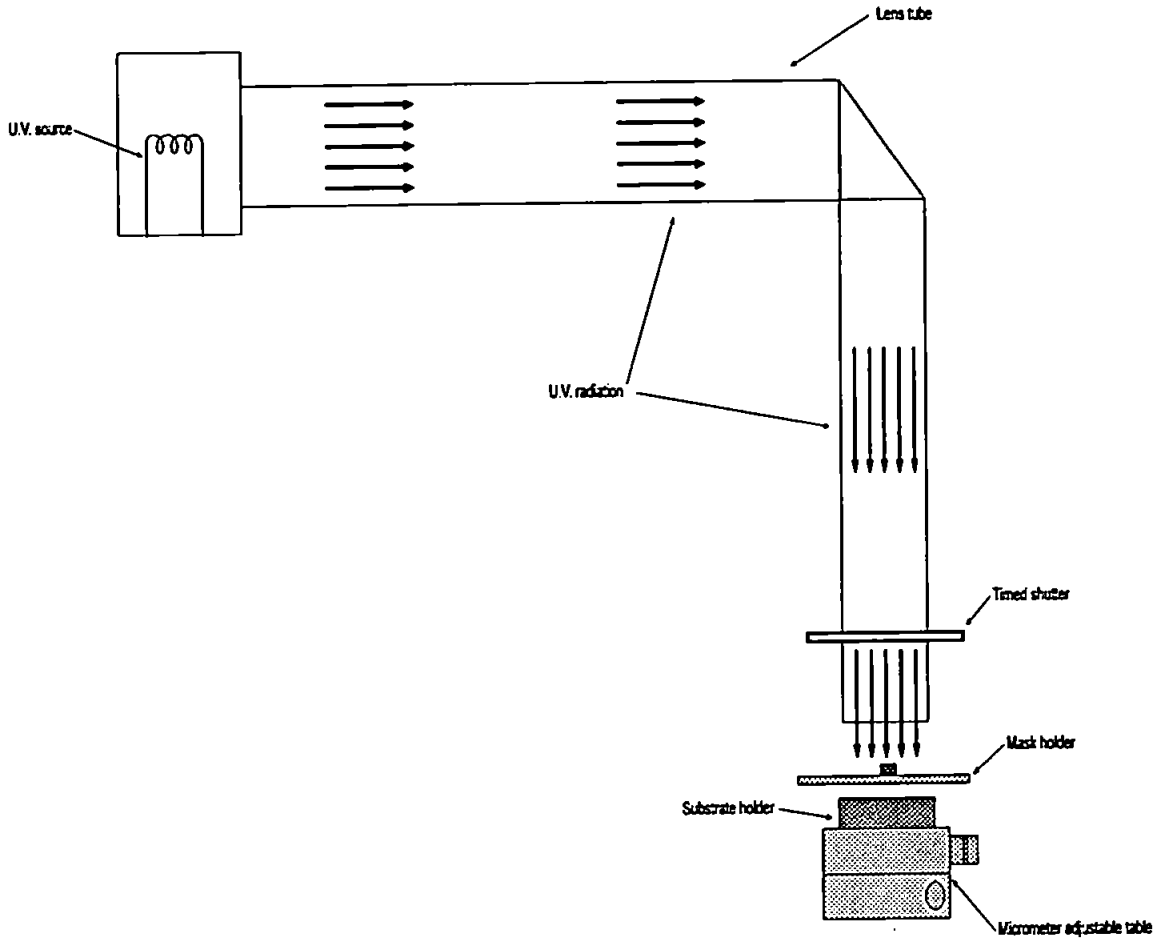

Figure 3.3 - A schematic diagram of an In-contact Mask Aligner.

3.1.3 Etching Techniques

3.1.3.1 Ion Milling

Ion beam milling is a technique used for dry etching of patterns to provide uniformly etched devices where accurate edge profiles and a minimum undercut is required. The system used during this project was a CVC Ion Beam Miller [Commonwealth Vacuum Corporation, Scientific Products Ltd, Hogwood Lane, Finchhampstead, Wokingham Berkshire, UK].

A plasma cloud is formed as a glow discharge due to the introduction of argon gas in the discharge chamber being struck by energetic electrons from the cathode. The ions generated are attracted to the high negative voltage at the accelerator grid and are formed into beamlets by passing through apertures in the screen grid. The ion beam is neutralised by thermionically-emitted electrons from the neutraliser to stop the beam from expanding due to Coulomb repulsion, and to prevent charge build up at the substrate surface when insulators are milled. The ion source and water-cooled rotating substrate stage are positioned in the vacuum chamber such that the ion beam is aimed at the substrate. The substrate stage angle is adjusted to achieve the correct etch profile (Figure 3.4).

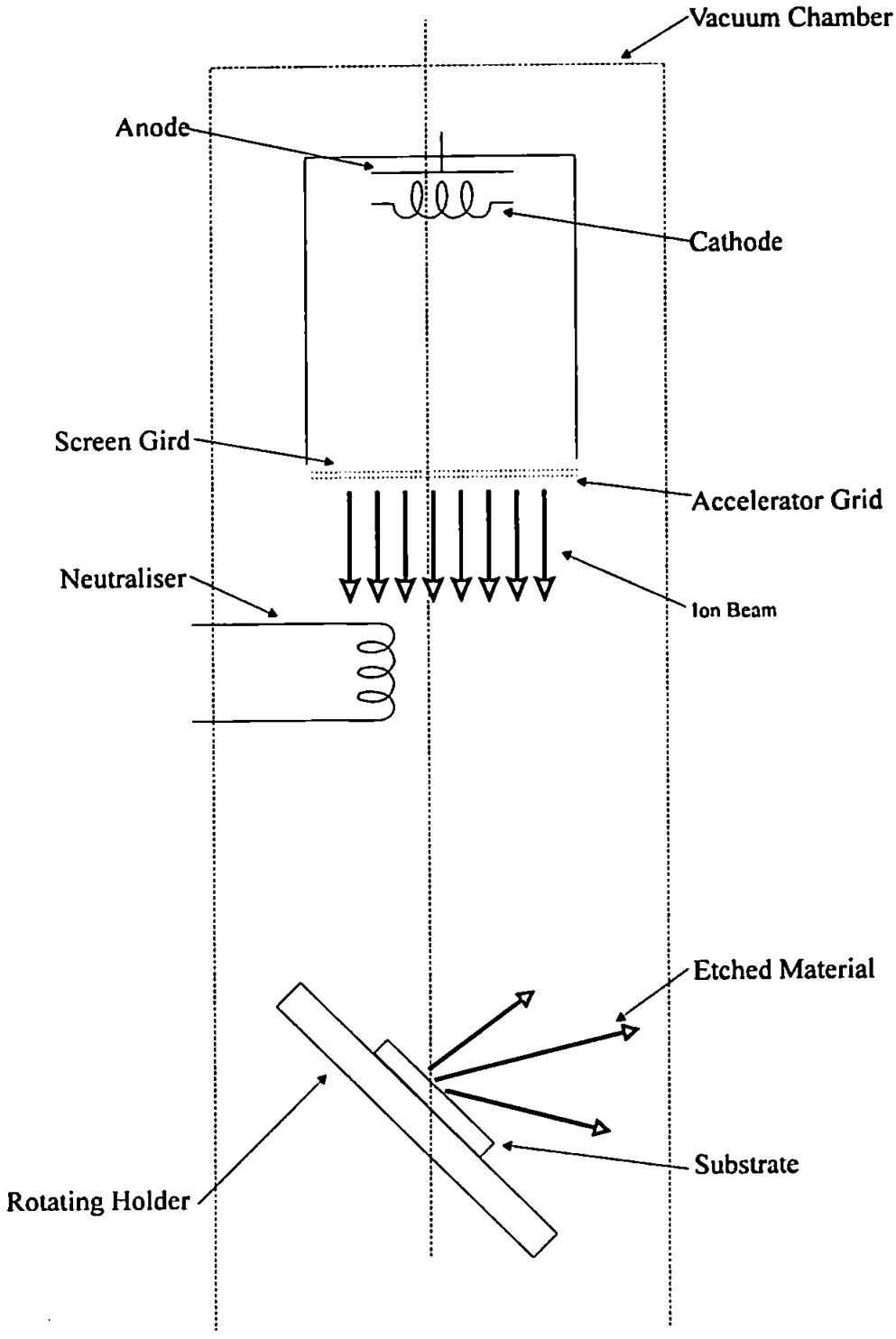

Figure 3.4 - A schematic diagram of an Ion Beam Miller.

3.1.4 Device Fabrication Procedures

3.1.4.1 Substrate Preparation

In order to ensure the quality, reproducibility and adhesion of the deposited films, substrate cleanliness is essential.

The substrates were thoroughly scrubbed with hot Neutracon detergent solution (1 part detergent : 10 parts water), [Merck Ltd, Hunter Boulevard, Magna Park, Lutterworth, Leics.], at a temperature of 65°C using a soft 'clean room' wipe. They were then dipped in de-ionised water and placed in an ultrasonic bath containing a diluted hot solution of detergent (1:10) at a temperature of 65°C where they were cleaned for a further 15 minutes. The substrates were finally rinsed with filtered de-ionised water and dried using filtered compressed Nitrogen (N_2) gas before thorough visual inspection for cleanliness. If not completely clean, the complete process was repeated. Finally, the substrates were placed in a constant air-flow oven to dry at a temperature of 135°C for 30 minutes before they were transferred to the sputtering chamber.

3.1.4.2 Coating

Silver coated devices were found to be prone to atmospheric oxidisation which caused deterioration under experimental conditions. An oxidisation preventative coating was necessary to passivate the metal surface against air-borne and biological contaminants. Silicon Dioxide (SiO_2) [Goodfellow Cambridge Ltd, Cambridge Science Park, Cambridge, UK] was used for this purpose as it offered high transparency (refractive index: n=1.46 @ 500nm, n=1.445 @ 1600nm, region of transparency: 200nm - 8000nm in thin films and 99.98% purity [Palik (1985)]), excellent adhesion properties and can be sputtered in the same chamber as the metal without effecting the system vacuum.

It was found that layered Ag films (refractive index: $\hat{n}_{Ag} = \sqrt{-18.3 + j0.67}$ @ 632.8nm and 99.9% purity [Palik (1985)]) did not adhere to glass substrates sufficiently to be used

in biological procedures. In order to rectify this problem a thin layer of Chromium (*Cr*) [Goodfellow Cambridge Ltd, Cambridge Science Park, Cambridge, UK], (thickness: 2-3nm, refractive index: $\hat{n}_{Cr} = \sqrt{-6.274 + j35.853}$ @ 632.8nm and 99.9% purity [Palik (1985)]), known to have excellent adhesion properties, was sputtered onto the glass before the *Ag* layer giving an improved foundation on which to bind. A number of alternative devices, using only a single *Cr* layer, were prepared for evaluation purposes and biological trials. Although *Cr* does not have as good SPR qualities as *Ag* it does have good adhesion qualities, mechanically robustness and its rate of oxidisation in air is slow compared to *Ag*. Given these qualities it was used in devices during the initial experimental phase of the project. A theoretical comparison of the resonant characteristics of *Ag* and *Cr* is shown in Figure 3.5.

Constant exposure of the deposition chamber to the high pressure atmospheric environment, when changing the coating material, inevitably resulted in contamination and degradation of the finished layered device. Consequently, sputtering of the *Cr*, *Ag* and SiO_2 layers in a single chamber and under the same conditions was carried out during a single sputtering run.

The experimental $Cr/Ag/SiO_2$ devices were made up of a 2nm *Cr* adhesion layer sputtered in the MRC sputter coater [Material Research Company Ltd, 303 Ballards Lane, North Finchley, London, N12.] for 1 minute at 100 watts. A 50nm *Ag* layer sputtered for 2 minutes 10 seconds at 100 watts and a 5nm thick passivation layer of SiO_2 layer sputtered for 10 minutes at 200 watts. The single *Cr* layer devices were sputtered for 24 minutes 11 seconds at 100 watts to produce a 90nm thick film device.

Figures 3.6-3.8 shows the theoretical comparison of the resonant conditions after the addition of each of these extra layers as a function of incident angle. *Ag* devices were used during studies involving non-biological/aqueous samples as the constant exposure to non-chemically clean air did not sufficiently hasten the formation of a sulphide layer on

the surface and allowed fabrication and experimental use of bare 50nm *Ag* coated devices over a short period of time.

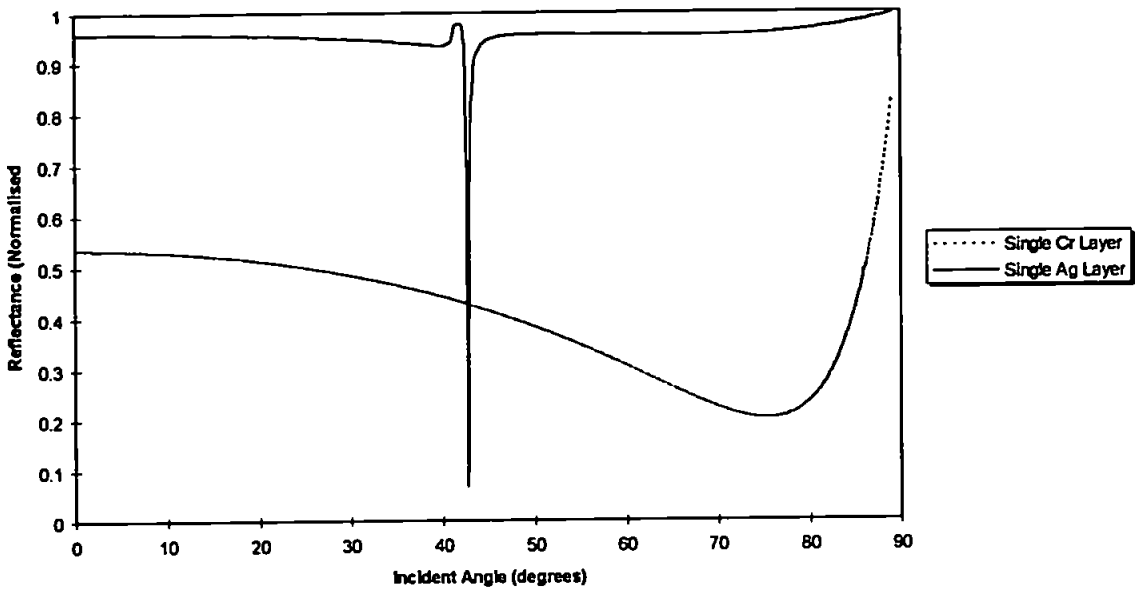

Figure 3.5 - A theoretical comparison of the reflectance of *Cr* and *Ag* coatings ($\hat{n}_{Cr} = \sqrt{-6.274 + j35.853}$ @ 632.8nm and $\hat{n}_{Ag} = \sqrt{-18.3 + j0.67}$ @ 632.8nm respectively).

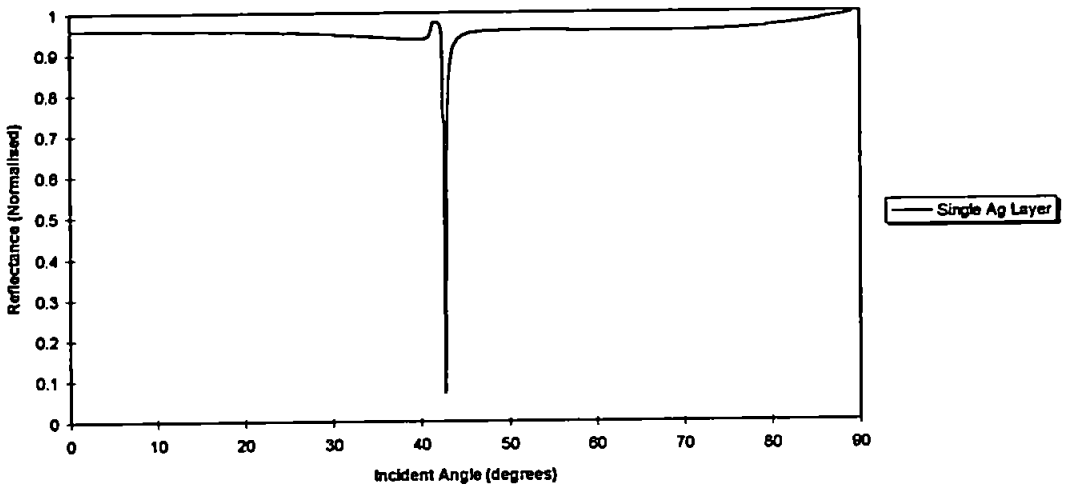

Figure 3.6 - Theoretical plot of the reflectance of an Ag device ($\hat{n}_{Ag} = \sqrt{-18.3 + j0.67}$ @ 632.8nm,).

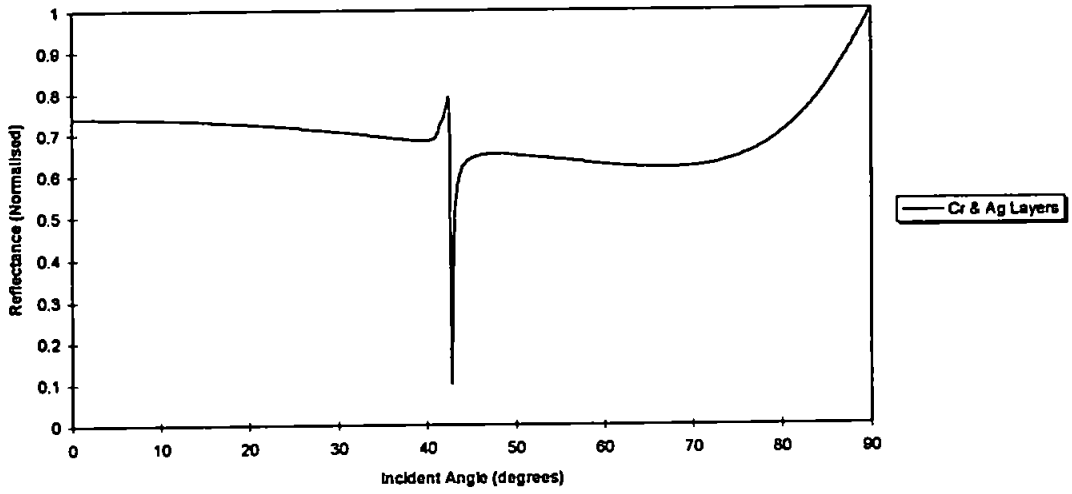

Figure 3.7 - Theoretical plot of the reflectance of the layered device with Ag and Cr ($\hat{n}_{Ag} = \sqrt{-18.3 + j0.67}$ @ 632.8nm, $\hat{n}_{Cr} = \sqrt{-6.274 + j35.853}$ @ 632.8nm respectively).

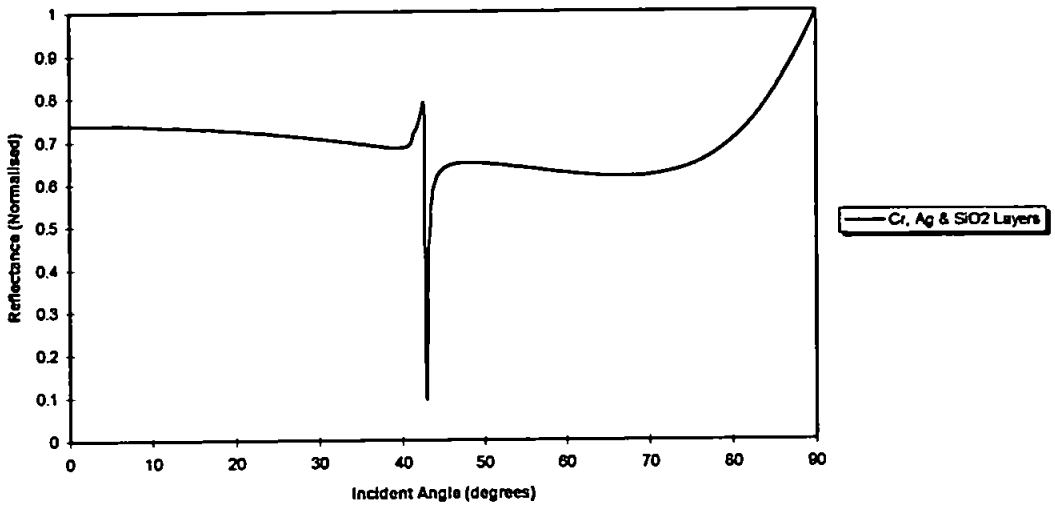

Figure 3.8 - Theoretical plot of the reflectance of the layered device with *Ag*, *Cr* and SiO_2 ($\hat{n}_{Ag} = \sqrt{-18.3 + j0.67}$ @ 632.8nm, $\hat{n}_{Cr} = \sqrt{-6.274 + j35.853}$ @ 632.8nm and n_{SiO2}=1.45 @ 632.8nm respectively).

3.1.4.3 Film Thickness

On-line monitoring or calibration is necessary in order to have accurate control over the thickness of deposited thin-films during the device fabrication process to within approximately ±5% of the desired thickness.

The Edwards thermal deposition unit, used in this project [Model No. 306, Edwards High Vacuum, Manor Royal, Crawley, Sussex, UK] is equipped with an 'in situ' crystal thickness monitor, a quick and easy on line monitoring system.

Deposition calibration curves were produced for the MRC sputter coater, used in this project by etching a step profile in several different sputtered layers with the Ion Beam Miller. The thickness of the step was then measured using a Talystep thin-film step profiler [Model No. 223-7, Rank Taylor Hobson, Guthlaxton Street, Leicester, LE2 0SP]

3.1.4.4 Mask Design

A master mask plate was prepared in order that a range of device structures of differing aperture sizes and inter-aperture spacing were readily available. The apertures ranged in size from 10μm in diameter with 20μm between centres, 7μm with 15μm centres, 5μm with 10μm centres, 3μm with 8μm centres and 1μm apertures with 5μm spacing between centres.

The master masks were fabricated externally at The Nanotechnology Unit, CAMR [Dr. S. Alshukri, Centre for Applied Microbiology and Research, Porton Down, Wiltshire, SP4 OJG]. Commercially available Hoya glass plates [Corning Glass Works, Corning, New York, USA] were used to generate the required patterns by Electron Beam Lithography [Philips EBM4, Philips Research Ltd, Redhill, Surrey.].

3.1.4.5 Photo-Resist Processes

The electron beam mask patterns were duplicated in the photoresist layer of the device. A positive photoresist [No. 1813, Shipley Europe Ltd, Herald Way, Coventry, CV3 2RQ] was used for this purpose and was applied to the substrate by spin coating at 4000rpm on a Headway Research Inc. AHT S4 series Photo-Resist Spinner [Headway Research Inc., 3713 Forrest Lane, Garland, Texas, USA] to a thickness of 1.3μm. The substrate was then baked at 120°C on a hot plate in an air flow oven for 30 minutes to release the solvent and harden the photoresist (Figure 3.9i).

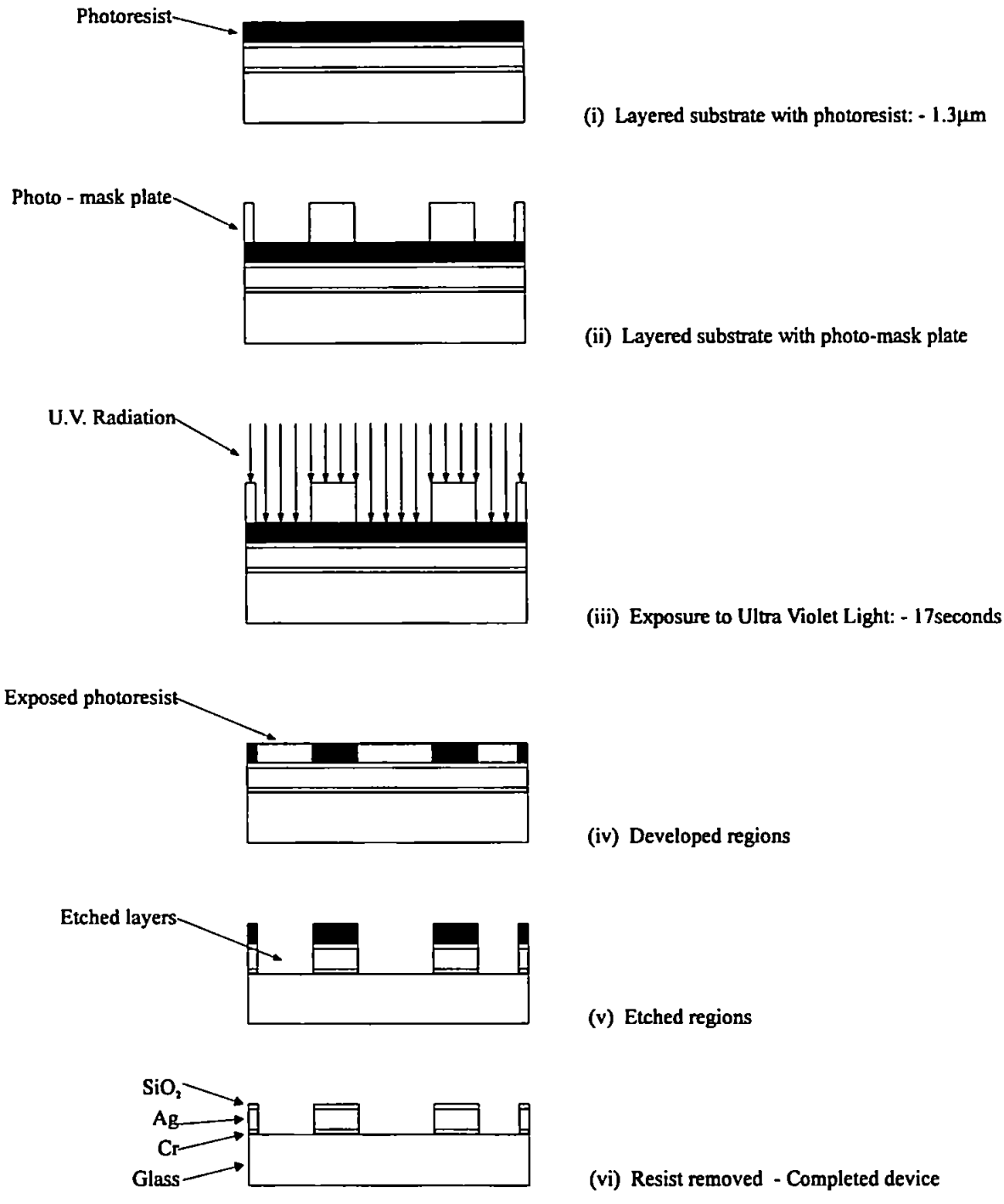

Figure 3.9 - Various stages of the photoresist procedure as described in Section 3.1.4.5.

The photo-resist coated films were exposed to U.V. light using an in-contact mask aligner fitted with a 200 watt mercury lamp and a timed shutter [Model No. MAS11/12, Cammax Percima Ltd, Hampstead Avenue, Mildenhall, Suffolk]. The substrate and mask surfaces were floated and levelled using a cushion of air. Once levelled they were separated so that the substrate holder could be moved with precision to align the mask using the adjustable stage on the optical microscope. Once aligned, the substrate and mask were held together in a vacuum clamp (Figure 3.9.ii). The UV light was then shone from above exposing any of the photoresist regions which were not shadowed by the *Cr* pattern (Figure 3.9.iii). In order to achieve an optimum line definition, the exposure time was determined experimentally as 17 seconds.

The substrate was then developed in Shipley 351 Microposit developer for 10-15 seconds to reveal the photo-resist pattern (Figure 3.9.iv). After developing, the substrate was thoroughly rinsed in de-ionised water and dried with filtered compressed nitrogen gas.

The prepared $Cr/Ag/SiO_2$ devices were etched in the Ion Beam Miller at 4.9µtorr for approximately 17 minutes at 400 volts. The *Cr* coated substrates were also etched using the Ion Beam Miller, at 4.9µtorr for approximately 5 minutes at 200 volts (Figure 3.9.v).

The photo-resist mask was then removed by gently washing in Acetone [Merck Ltd, Hunter Boulevard, Magna Park, Lutterworth, Leics.] to reveal the patterned metal film (Figure 3.9.vi). The substrate was then thoroughly rinsed and dried ready for use.

3.2 SCANNING PROBE MICROSCOPY (SPM)

A Scanning Near-Field Optical Microscope (SNOM) was designed and constructed for the purpose of probing and identifying the visible electromagnetic fields generated by the sensor. A Photon Scanning Tunnelling Microscope (PSTM) was also constructed to probe the evanescent electromagnetic field on the surface of the device and map its profile. These two detection systems were integrated into a single combinational microscopy tool. The following sections describe the background and physical principles of operation of the SNOM and PSTM as analytical tools.

3.2.1 Scanning Near-Field Optical Microscopy (SNOM)

Historically the optical limit to microscopy has been the theoretical limit identified by Lord Rayleigh (1879) governing the limit of diffraction, i.e. $x = 0.61\lambda/N.A.$, where $N.A.$ is the numerical aperture of the microscope ($N.A. = n_o \sin\theta_{max}$, n_o is the refractive index of the immersing medium and θ_{max} is the half angle of the maximum cone of light picked up by the lens). Synge (1928) discussed a scheme to overcome this diffraction limit in which he described a back illuminated small aperture ($d < \lambda$) acting as a small optical source brought sufficiently close (within the near-field ($z < \lambda$)) to a transparent sample to allow direct detection of the transmitted light obviating the need for diffraction limited lenses. The amount of light collected through the illuminated sample is representative of a very small surface area of the sample. This principle is now employed in modern SNOM systems.

Although the Scanning Near-Field Optical Microscope is a recent development, Ash and Nicholls (1972) demonstrated Synge's theory with microwaves to a resolution of 1/60th of a wavelength in one dimension. Primarily due to the mechanical advances in piezoelectric nanometre control in the early 1980's, the advent of Scanning Tunnelling

Microscopy (STM) [Binnig & Rohrer (1982)] enabled researchers to use optical near-fields as part of a viable microscopy system. These initial studies began independently in Europe and America [Pohl, IBM Zurich (1982) and Lewis *et al.*, Cornell University (1983) respectively]. Further developments in high resolution scans and full images from 'transmission' SNOMs were realised in the mid to late 1980's [Pohl *et al.*(1985); Durig *et al.* (1986) and Betzig *et al.* (1987)]. Fischer *et al.* (1988), in collaboration with the researchers at IBM Zurich developed the first 'reflection' microscope. Reddick *et al.* (1989), de Fornel *et al.* (1989) and Courjon *et al.* (1989) implemented very similar arrangements whereby a tapered optical fibre brought close to the surface ($z < \lambda$) at which an evanescent field has been established, could detect the tunnelling of photons between the evanescent field and the probe tip with a strict analogy to Scanning Tunnelling Microscopy (STM) (see Section 3.2.2).

Several variations of the SNOM device have been developed during the last few years in which different techniques have been combined. Pohl *et al.* (1995) have developed a combined aperture SNOM/PSTM. Appreciating the separate advantages of both these configurations, i.e. well defined operating conditions with high lateral resolution exhibited by SNOM and the sensitivity to the gap width variation brought about by the tunnelling of the photons between the probe tip and sample in PSTM, they have combined these devices in a novel system to create the so-called Tunnelling Near-field Optical Microscope (TNOM).

Garcia *et al.* (1994) have also developed a novel system similar to Pohls'. Utilising the tunnelling effect of the STM, the outer cladding of an optical fibre is coated with gold and used to sense the tunnelling current between the tip and the sample. The fibre acts as a conventional aperture SNOM while the simultaneous sensing of the tunnelling current offers STM control over the tip-sample separation.

Kawata *et al.* (1995) have developed a Scanning Probe Optical Microscope where by a submicron vibrating metallic probe scatters the evanescent field on the sample surface. The scattering is monitored using a lock-in detector linked to a far-field detector. Any surface profiles will thus be shown as a function of the scattered light intensity.

3.2.1.1 Theory of SNOM

There are two main techniques of Scanning Near-Field Optical Microscopy; the 'Illuminating-Mode' SNOM and the 'Collection-Mode' SNOM (Figure 3.10).

'Illuminating-Mode' SNOM involves the sample under study being illuminated by a focused spot of light from the tapered probe, usually of sub-wavelength dimensions. The probe is brought sufficiently close to the surface ($z < \lambda$) to eliminate diffraction of the incident light. The light 'transmitted' through the sample is then collected in the far-field by a conventional microscope objective.

Conversely, the 'Collection-Mode' SNOM works on the principle of the sample under study being illuminated by a spot of light from the far-field with the collection of the 'reflected' light made by a similar tapered probe in the near-field. As discussed previously no diffraction of the reflected radiation occurs. In both modes the spatial resolution obtained is far superior to that of conventional optical microscopy. The resolution being determined by the close proximity of the tapered probe tip to the surface under study and the size of the tip aperture.

Two primary factors govern the resolution of the device;

i. degree of control over the separation distance of the tip/sample, and the

ii. size of the probing tip.

Several methods have been devised to control these factors.

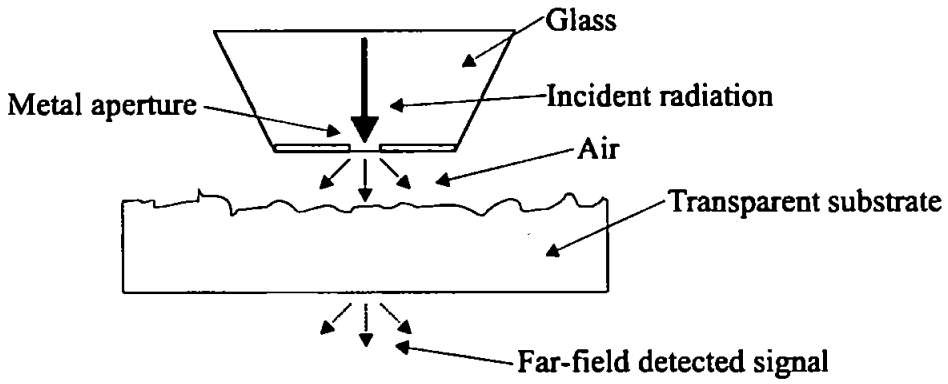

i. Transmission SNOM

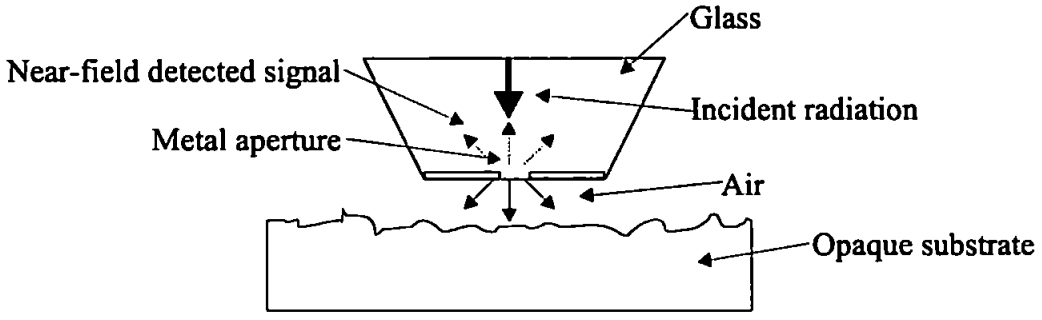

ii. Reflection SNOM

Figure 3.10 - i. A schematic diagram of a Transmission Microscope, ii. A schematic diagram of a Reflection Microscope.

3.2.1.2 Distance Control

At tip-sample distances of tens of nanometres it is important to control the separation distance accurately to within a few nanometres. There are a number of techniques available for controlling the separation distance between the probe and the sample surface.

Electron Tunnelling [Lieberman *et al.* (1993)] or Capacitance regulation [Hartmann *et al.* (1993)] is a popular method of probe/sample control. Based on Scanning Tunnelling Microscopy (STM) where the monitoring of the magnitude of the current arising from the tunnelling of electrons from the conductive sample to a conductive probe allows for a high resolution microscopy tool, the outer cladding of the probe tip is coated with a conductive material and a circuit made between the conductive metal films. Sensing of the electron tunnelling current between the tip and the conductive sample offers a highly accurate and efficient means of sample-tip separation control. This technique is limited however as it requires both a conductive probe and sample and is sometimes unreliable under ambient temperature conditions as moisture in the air and other determining factors can be detrimental on the conduction process.

Shear Force regulation [Vohnsen *et al.* (1995)] is an effective and reliable method of feedback control. The probe, usually a tapered fibre or micro-pipette, is caused to oscillate at or close to its natural resonant frequency. As the distance between the probe tip and the sample decreases to within a few tens of nanometres the interaction forces experienced between the tip and the sample decreases the resonant amplitude which can then be detected as light scatter or differential interferometry.

3.2.1.3 SNOM Probe

Unlike STM, where the dimensions of the tip determines the ultimate resolution of the device, the tip dimensions in SNOM need to be large enough to allow transmission of the detectable light, i.e. transmitted or receiving radiation.

Pohl *et al.* (1984) and Durig *et al.* (1986) used Aluminium-coated quartz tips during their initial studies of SNOM, but frequent damage to the tip prompted the development of an alternative more reliable method. One such method was the micro-pipette probe [Betzig *et al.* (1987)]. These were fabricated by pulling and consequently tapering micro-pipettes in a flame producing excellent results, although damping losses along the length of the pipette were quite high. Chemical etching of multi-mode and mono-mode optical fibres [Pangaribuan *et al.* (1992), (1994)] has produced a highly accurate and reproducible means of probe fabrication but is time consuming and the use of such chemicals is somewhat hazardous. Betzig *et al.* (1991) and Fischer *et al.* (1992) have developed a simple technique of tapering an optical fibre using a conventional fusion splicer, a technique frequently used in optical fibre research laboratories.

3.2.2 Photon Scanning Tunnelling Microscope (PSTM)

Photon Tunnelling Optical Microscopy is another variant of Scanning Tunnelling Microscopy. As its name suggest the principle of operation is the detection of photon tunnelling between the probing tip and sample surface. The use of photons instead of electrons has advantages in the study of biological samples where the samples can tolerate the use of photons as opposed to the interactive electrons in STM or the physical contact of the Atomic Force Microscopy (AFM) [Fujihira (1995)].

In 1982, Binnig *et al.* showed that imaging of the surface of metals and semiconductors was possible with a resolution of atomic dimensions by utilising the tunnelling current between the conductive sample and the metal tip of the probe (STM). He received the Nobel Prize in 1986 for further work in this area which brought about a significant advance in the analysis of nano-scale structures.

Reddick *et al.* (1989) and Courjon *et al.* (1989) developed what is now known as the Photon Tunnelling Optical Microscope. A bare tapered optical fibre brought sufficiently close to the sample was capable of coupling the energy across the gap into the optical fibre for detection. Since this work several research groups have modelled the optical interactions between the dielectric tip and the sample surface [Girard *et al.* (1990), Labani *et al.* (1990), Van Labeke *et al.* (1992) and Cites *et al.* (1992)].

Several variations based on the SNOM principle have also been developed. These include the combined SNOM/PSTM [Pohl *et al.* (1995)] and the Apertured PSTM [Tsai *et al.* (1993)]. In the APSTM a tapered fibre probe is coated with an opaque layer of metal along the taper length producing an aperture at the end face, the advantage of which is the metallic layer reduces the contamination of any stray light along the taper length. This is similar to the SNOM/PSTM in that the feedback control is provided by the sensing of the evanescent field by the tip.

Marti *et al.* (1993), Adam *et al.*. (1993) and Dawson *et al.* (1995) have directly measured the intensity profile of a surface plasmon produced on the surface of a silver film by means of a PSTM. Using a tapered optical fibre as the probing device Dawson was capable of measuring the propagation length of the surface plasmon on a *Ag* film. Choo *et al.* (1995) have been successful in probing and measuring the evanescent characteristics of the propagating modes of an optical channel waveguide using a similar device to that of Dawson.

3.2.2.1 Theory of PSTM

PSTM can be theoretically described as a double layer thin-film arrangement utilising Frustrated Total Internal Reflection (FTIR).

3.2.2.2 Frustrated Total Internal Reflection (FTIR)

The concept of photon tunnelling has been described elsewhere [Strong (1958), Hecht *et al.* (1974), Diament (1990)] but will be briefly explained here. As described previously in Section 2.1.2, a wave incident on an interface between two media of refractive index n_1 and n_2 ($n_1 > n_2$) will experience reflection and transmission. The value of the refractive indices of the respective media and the angle of incidence determine reflectance and/or transmittance across the interface (Equation (11.)). If the angle of incidence is increased to above that of the critical angle, $\theta_c = \sin^{-1}[n_b/n_a]$, assuming zero absorption, all the incident radiation is reflected from the interface and is contained in the first medium. This phenomenon is known as Total Internal Reflection (TIR), Figure 3.11.

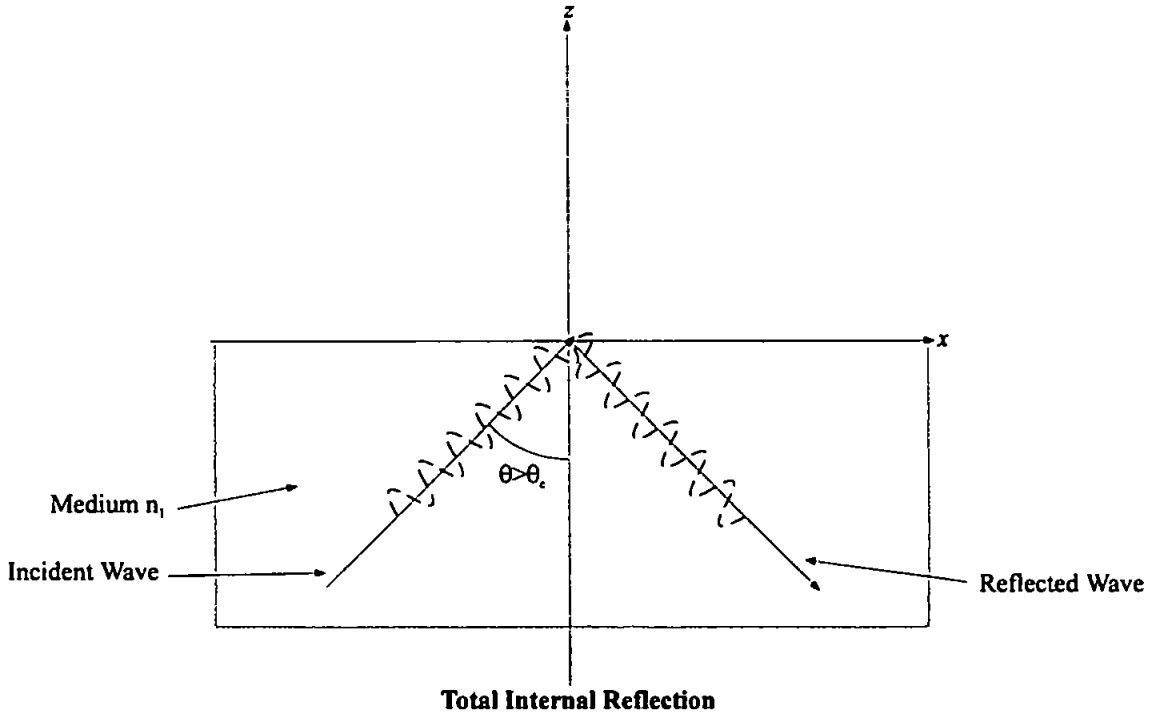

Figure 3.11 - Total Internal Reflection ($n_1 > n_2$)

At incident angles greater than the critical angle (θ_c), there is no effective transmittance into medium n_2 (Figure 3.12). A non-radiative wave is produced on the upper boundary of the interface and is said to be 'evanescent'. This evanescent field has a maximum at the surface decaying exponentially normal to the surface (Figure 3.13). If a third medium n_3 is brought sufficiently close to the interface, deliberately forming a 'thin-film layer' of medium n_2, the light is said to be "frustrated", a term coined by Leurgans and Turner in 1947 (Figure 3.14). A coupling process occurs as a consequence of phase matching across the gap with transmission of energy into medium n_3.

Figure 3.15 shows the normalised transmittance across a thin-film of air into medium n_3 as a function of incident angle for a planar configuration. In this case all three media are assumed to be transparent (zero loss) at the operating wavelength. If instead the second medium is absorbent, the term Attenuated Total Reflection (ATR) is used.

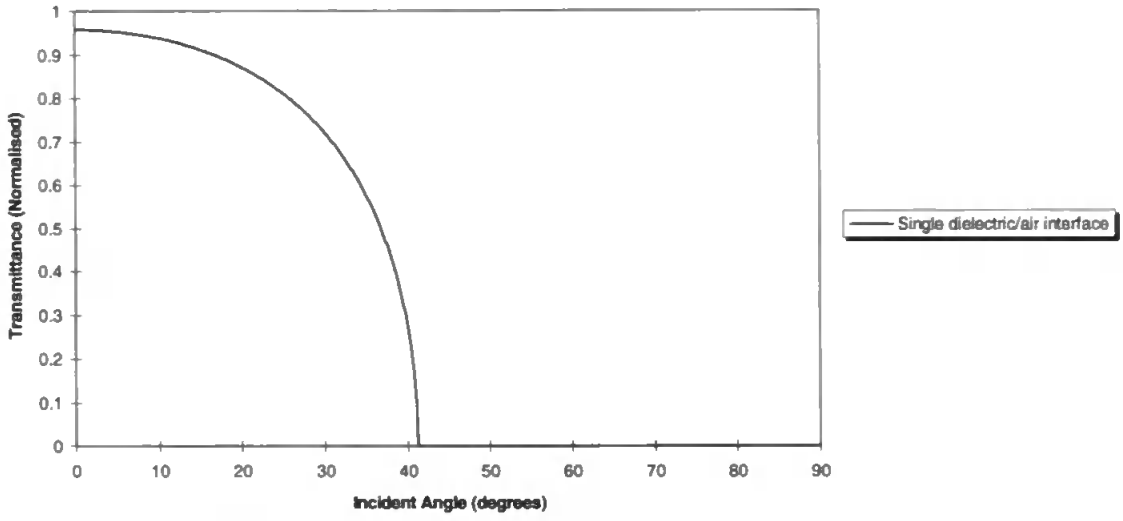

Figure 3.12 - Calculated normalised Transmittance as a function of Incident Angle for a single *dielectric/air* interface ($n_1=1.517$, $n_2=1$).

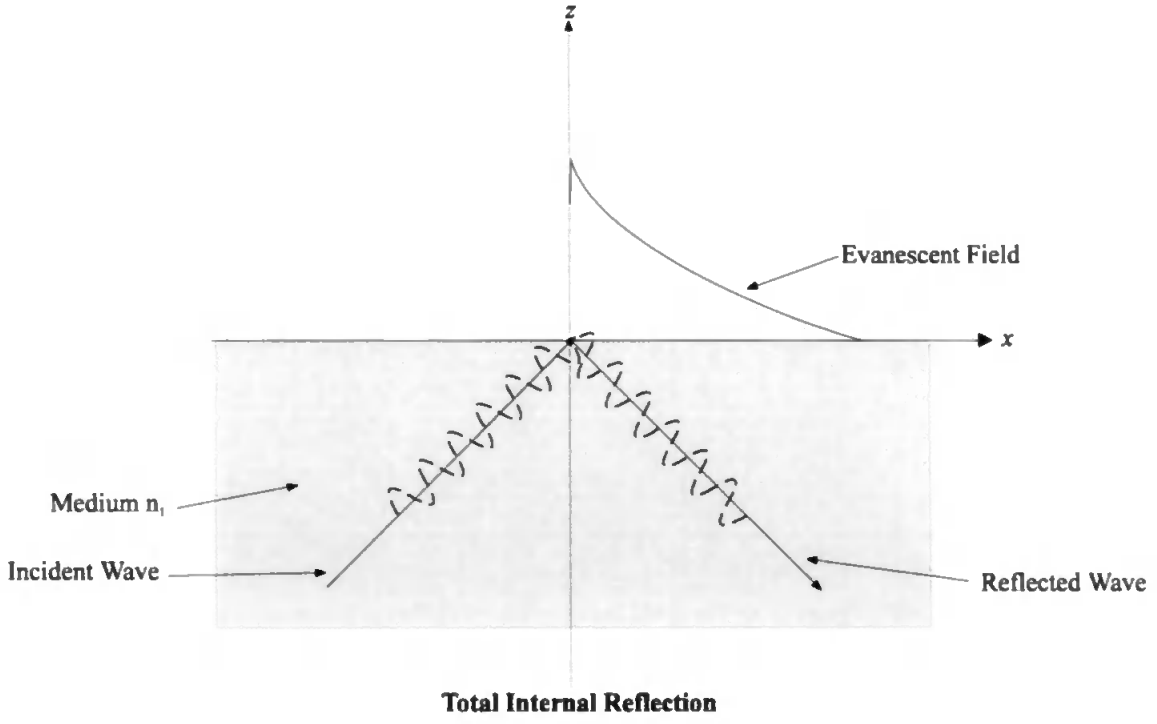

Figure 3.13 - An evanescent exponentially decaying field produced as a result of Total Internal Reflection (TIR) ($n_1>n_2$).

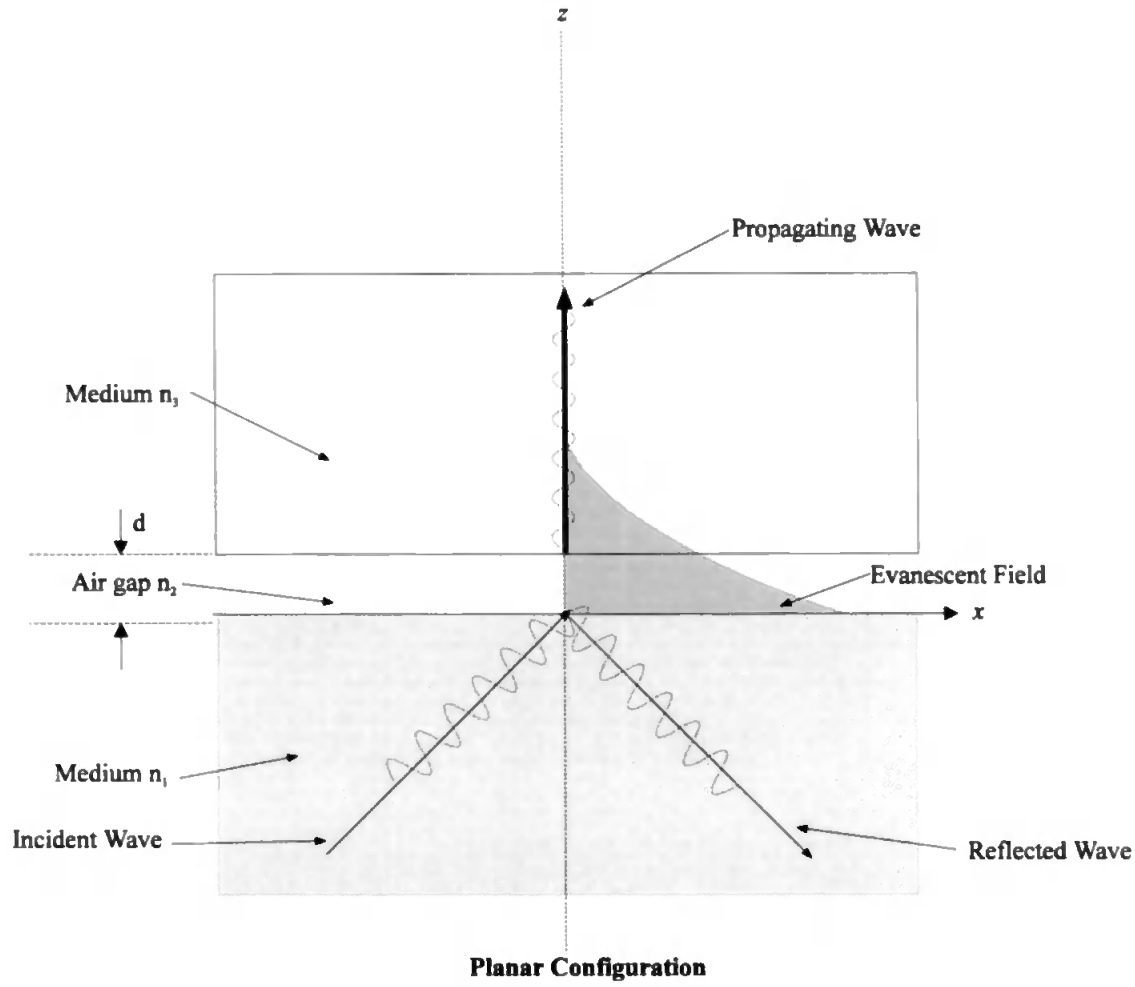

Figure 3.14 - A schematic diagram of Frustrated Total Internal Reflection (FTIR).

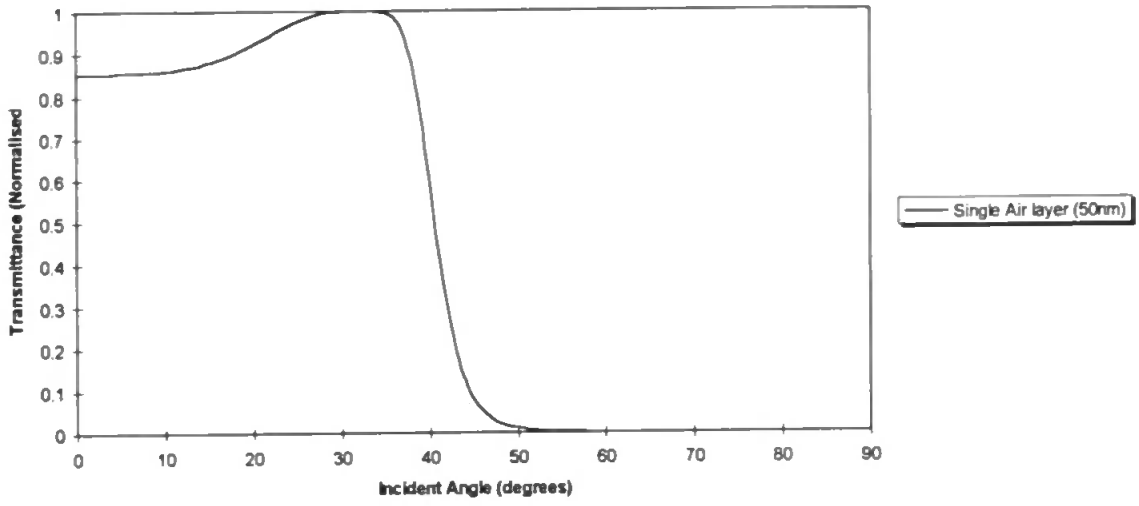

Figure 3.15 - Calculated normalised Transmittance as a function of Incident Angle for a single 50nm *Air* layer (n_1=*1.517*, n_2=*1*, n_3=*1.517*).

In order to model accurately the coupling process between the PSTM probe tip (Figure 3.16) and the evanescent field the 'effective aperture' of the tip must first be calculated. Equation (11.) is used for plane infinite boundaries. The effective transmittance or detection is a function of the tip diameter and is given by integrating the transmittance of a planar slab over the surface area of the probe tip. With a cylindrical tip tapered fibre the effective transmittance into a tip of radius 'r' is given by;

$$\textit{Effective Transmittance} = T\pi r^2 \tag{34.}$$

where T is the transmittance for an infinite planar boundary and πr^2 is the planar area of the probe tip.

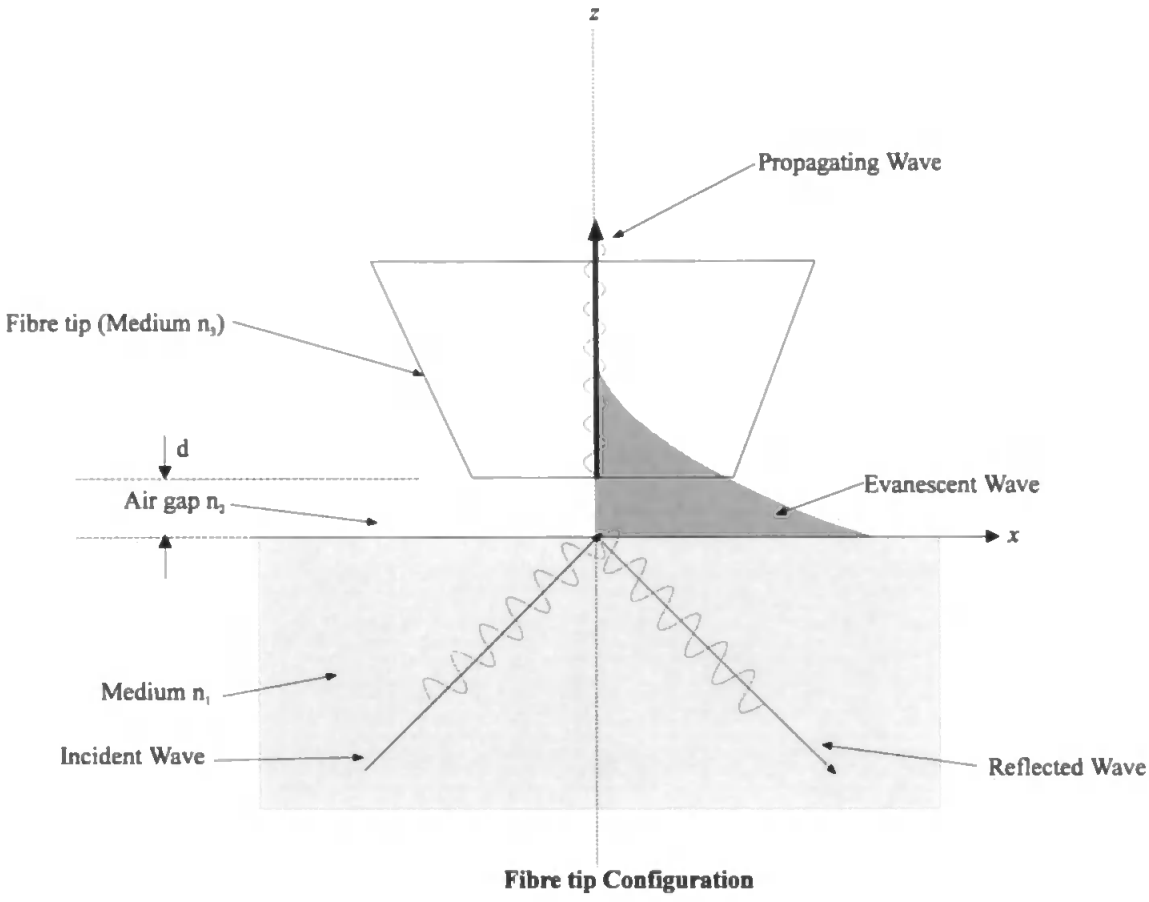

Figure 3.16 - A schematic of the principles under which a Photon Scanning Tunnelling Microscope (PSTM) operates.

This theory can now be extended for use in SPR. As described in Section 2.2, under certain critical conditions, an exponentially decaying evanescent wave extends above the surface of a metal, i.e. in the case of *Ag* to approximately 400nm. If a fourth medium n_4, of refractive index greater than that of the third medium n_3 ($n_4 > n_3$) is brought sufficiently close to medium n_2 transmission, or coupling, of the incident energy can occur across the air gap into medium n_4. This process of energy coupling into medium n_4 is shown in Figure 3.17. Figure 3.18 shows the calculated normalised transmittance through the system as a function of air gap thickness in a SPR configuration using a tapered fibre probe of 80nm ϕ. Note that the introduction of the fourth medium in the SPR system effectively modulates the evanescent field into one where the maximum coupling occurs at approximately 1μm above the active SPR surface.

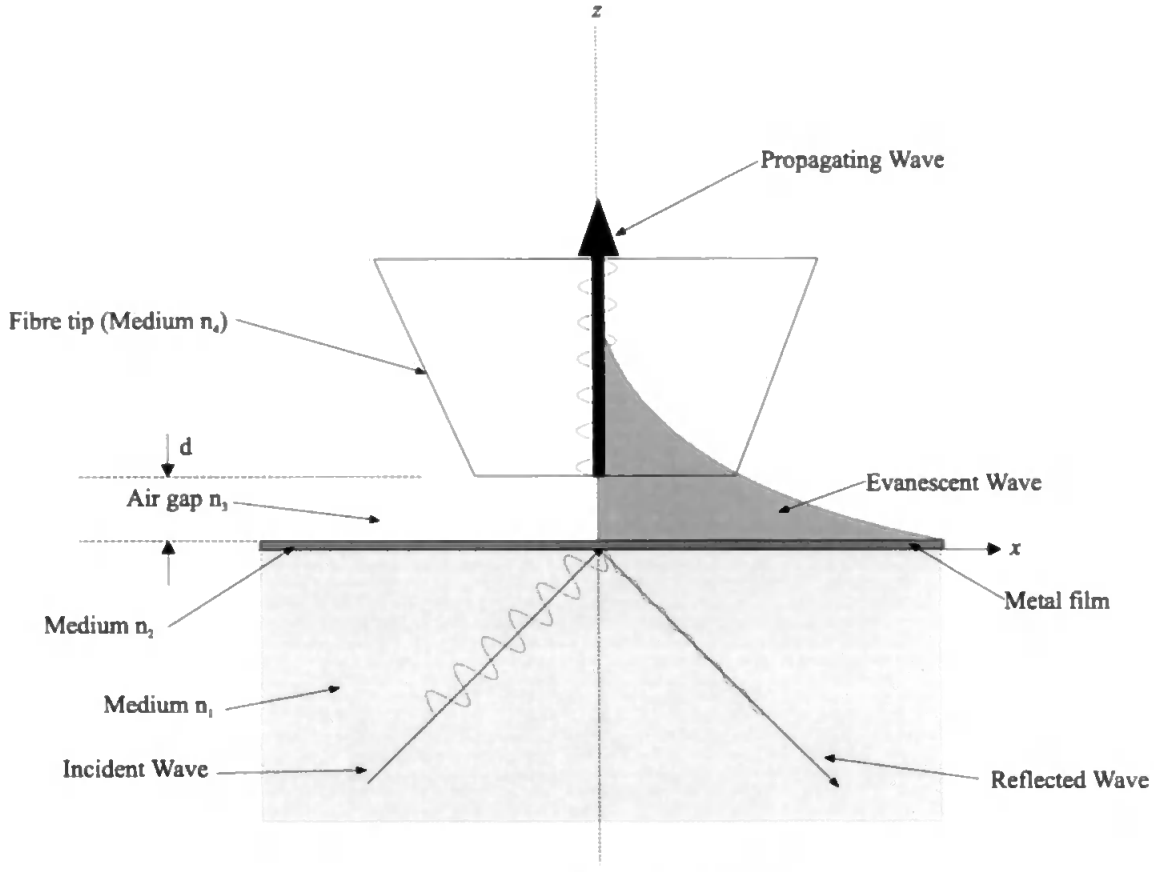

Figure 3.17 - A schematic of the principles under which a Photon Scanning Tunnelling Microscope interacts with a Surface Plasmon Wave on a metal film.

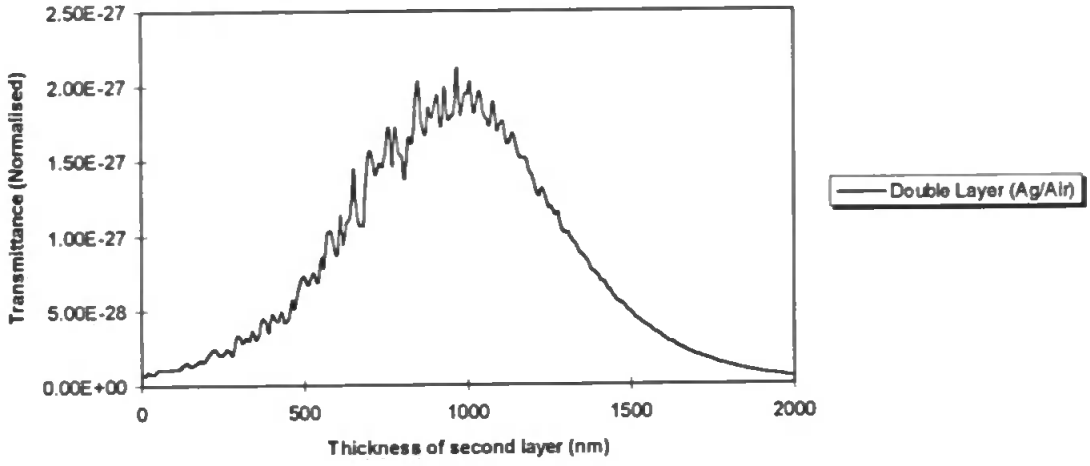

Figure 3.18 - Calculated normalised Transmittance as a function of second layer thickness for a single 50nm Ag layer (n_1=1.517, $\hat{n}_{Ag} = \sqrt{-18.3 + j0.67}$ @ 632.8nm, n_3=1) at the SPR angle integrated over the area of the probe tip (80nm ϕ, n_4=1.517).

3.3 SNOM/PSTM Experimental Procedures

3.3.1 SNOM/PSTM Probe Fabrication

As described in Section 3.2.1.3 there are several methods of fabricating SNOM/PSTM probes. For simplicity and convenience the tapered fibre technique was used in this project. Several centimetres of the plastic sheath protecting the glass optical fibre, in the middle of 1m length pieces of multi-mode and single-mode telecommunications fibre (50/10μm diameter core and 125μm diameter cladding, Optical Fibres, Second Ave, Deeside Industrial Park, Deeside, Clwyd, CH5 2NX), were stripped away with an optical fibre stripping tool [K-Tech, Optical Fibre Products, K-Tech Microprecision, 16/18 Barton Road, Bletchly, Milton Keynes, MK2 3JH.] to expose the outer cladding. These sections of fibre were placed into a conventional fusion splicer [Tritec Fase II, Tritec Development Ltd, England] with the arcing probes central to the length of stripped fibre (Figure 3.19). The splicer was turned on its side in a vertical position and a small force applied to one end of the fibre with the other end clamped in the splicer. An arc was struck and the resulting heat generated, usually used to bond two ends of a fibre together, was sufficient to melt the fibre. Due to the force being applied to each end, the fibre elongated and eventually separated leaving a parabolic tip at each end of the fibre sections (Figure 3.20and Figure 3.21). With fine adjustment of the arcing time, arcing current and elongation force applied to the end of the fibre it was possible to achieve a repeatable, low cost and easy fabrication technique for producing tapered fibre probes.

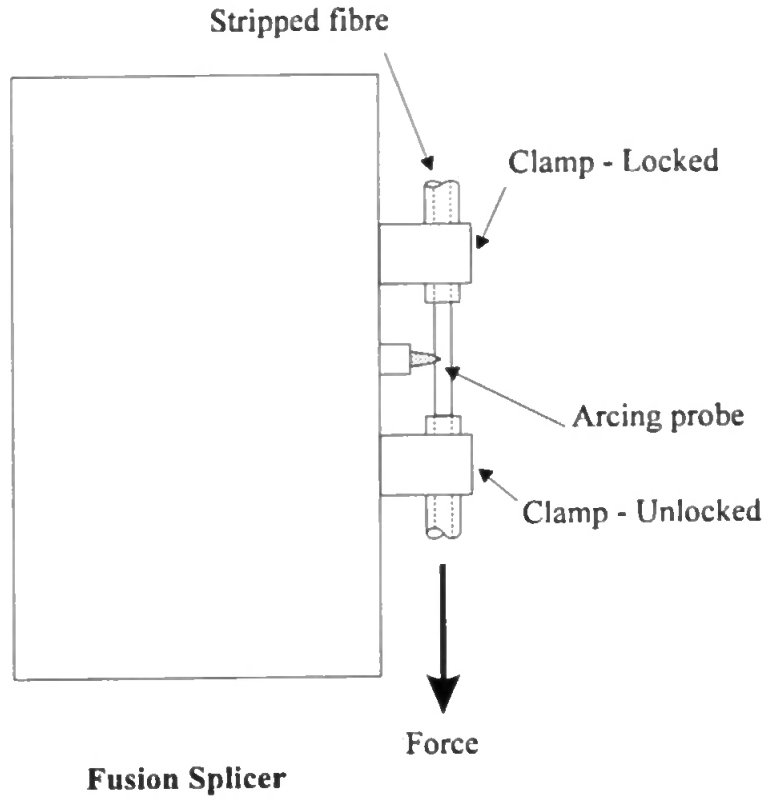

Figure 3.19 - A schematic diagram of an Optical fibre fusion splicer used as a probe tapering unit.

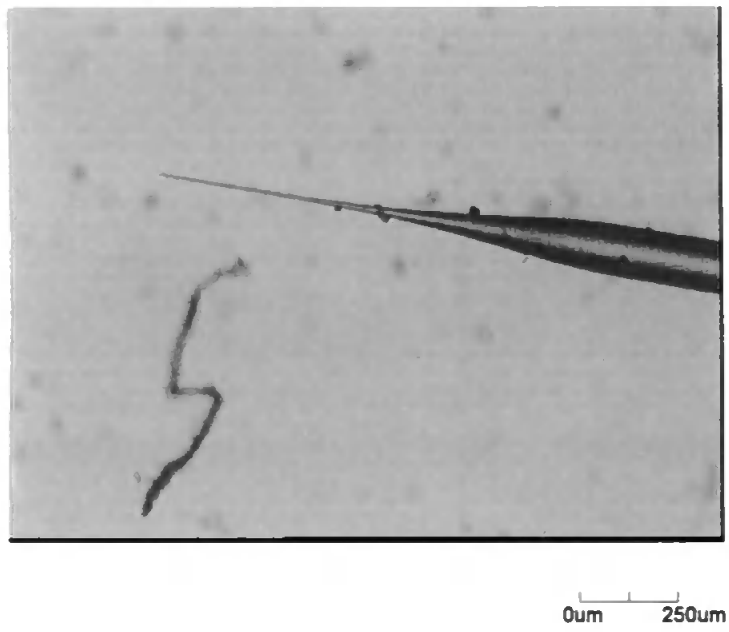

Figure 3.20 - Image of a tapered single-mode 10/125µm ϕ fibre.

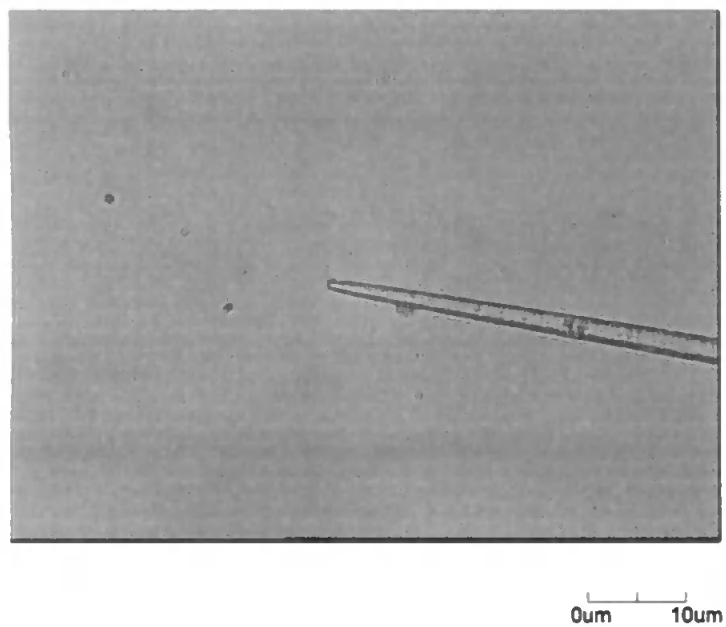

Figure 3.21 - A magnified image of the tip of the tapered single-mode 10/125µm ϕ fibre shown in Figure 3.20.

The angle of the tapered section made it possible for radiation to couple through the fibre cladding to the core and propagate to the detector. The tapered section of the fibres were therefore coated, in the vapour coater described in Section 3.1.1, with 120nm of *Al* [refractive index: $n_{Al} = \sqrt{-56.5904 + j21.267}$ @ 632.8nm] and measured with a real time crystal thickness monitor to render the outer cladding opaque. The end face of the tapered fibre was then cleaved resulting in a high resolution aperture probe. The un-tapered end was cleaved and connected to a Photo-Multiplier Tube (PMT) [Model No.H957, Hamamatsu Photonics UK Limited, Lough Point, 2 Gladbeck Way, Windmill Hill, Enfield, Middlesex.].

Utilising this technique PSTM fibre probes could be repeatably fabricated with an outer cladding diameter of 1μm ± 0.5μm.

3.3.1.1 Piezo Control Feedback

The distances necessary to achieve optical tunnelling of a SPW on an *Ag* device between two planar media is less than two microns, Figure 3.18. In order to keep the tip of the sensing probe from touching the SPR active surface a method of electrical feedback was implemented and is described below.

An evanescent field on the surface of a substrate decays exponentially normal to the surface and can be used to provide a technique of separation control. The sensing probe tip was brought into the evanescent field above the metal surface with the use of a high resolution piezo-electric actuator [Model No. 150/4/50, Pickelmann Piezomechanik, Elliot Scientific Ltd, Gladstone Place, 36-38 Upper Malborough Road, St Albans, AL1 3US]. The signal collected by the fibre probe was converted into an electrical signal with the use of a photo-multiplier tube at the end of the optical fibre. Any variation in the intensity profile of the evanescent field picked up by the probe was sensed and fed back to the piezo-electric actuator to maintain a constant detected intensity at the probe. This is known as 'Constant Intensity' mode. Another mode of operation is known as

'Constant Height' mode where by the probe is held at a constant position above the sample and scanned over the sample with no variation in the vertical axis. This method is much easier to attain but unfortunately can only be used over short horizontal distances before parallelism between the probe and the sample surface becomes an issue.

3.3.2 SNOM/PSTM Controlling Algorithm

Implementation of control over the scanning probe movement was achieved with the use of a computer program specially developed in this project in Turbo C++ programming language. A dual purpose program it was used to monitor the detected intensity by the probe tip and control of the tip in 3-dimensions. The following section describes the logic and computer program developed for these processes.

3.3.2.1 Turbo C++ Controlling Program

The purpose of the C program was to;

a) Control the movement of the piezo-electric actuators.

b) Record the relative intensity detected by the SNOM/PSTM probe.

3.3.2.2 Program Description

The control of the piezo-electric actuator and measurement of the detected signal was carried out by an Digital-to-Analogue Converter (DAC) acquisition card [Model No. PCX312, MA Instruments, Yelverton, Nr. Plymouth, U.K.] connected to a IBM compatible personal computer. The DAC was a 12 bit device with 4096 separate levels over two separate output voltage ranges, i.e. ±5v, ±10v. The smallest incremental voltage of each setting was therefore 2.441mv and 4.883mv respectively. Several input voltage ranges were acceptable, i.e. ±1.5v, ±2.5v, ±5v and ±10v. All the settings could be software triggered or selected.

3.3.2.3 Feedback Routine

As described in Section 3.3.1, the PSTM can be controlled in two modes of operation, i.e. 'constant intensity' and 'constant height' mode. This following section describes the computer program controlling the system in 'constant intensity' mode.

The translation stages and the desired intensity levels sensed by the PSTM probe were set at the initialisation of the program. The program continuously monitored the detected intensity level picked up by the probe as it scanned in the x-direction, in the plane of propagation. The sensed voltage level was compared against a pre-set voltage level and tolerance. If this sensed voltage level was outside an upper or lower pre-determined tolerance level a sub-routine was initialised to correspondingly increase or decrease the applied voltage to the z-piezo-electric actuator, thus raising or lowering the probe in the evanescent field and subsequently returning the intensity to within the pre-set tolerance levels. This resulted in keeping the intensity level detected by the sensing tip constant. The program continued by increasing the voltage to the x-piezo actuator, thus moving the probe in the horizontal direction whilst continually monitoring the intensity level. The feedback network diagram is shown in Figure 3.23.

3.3.2.4 Intensity Profile

After each incremental movement the applied voltages to the three separate piezo-electric actuators were saved in an array under a user specified file name and a plot of the intensity profile was drawn on the screen for visual interpretation. A flow diagram is shown in Figure 3.22 showing the overall logic of the software control system. Sample software algorithms for the two modes of operation are listed in Appendix B.

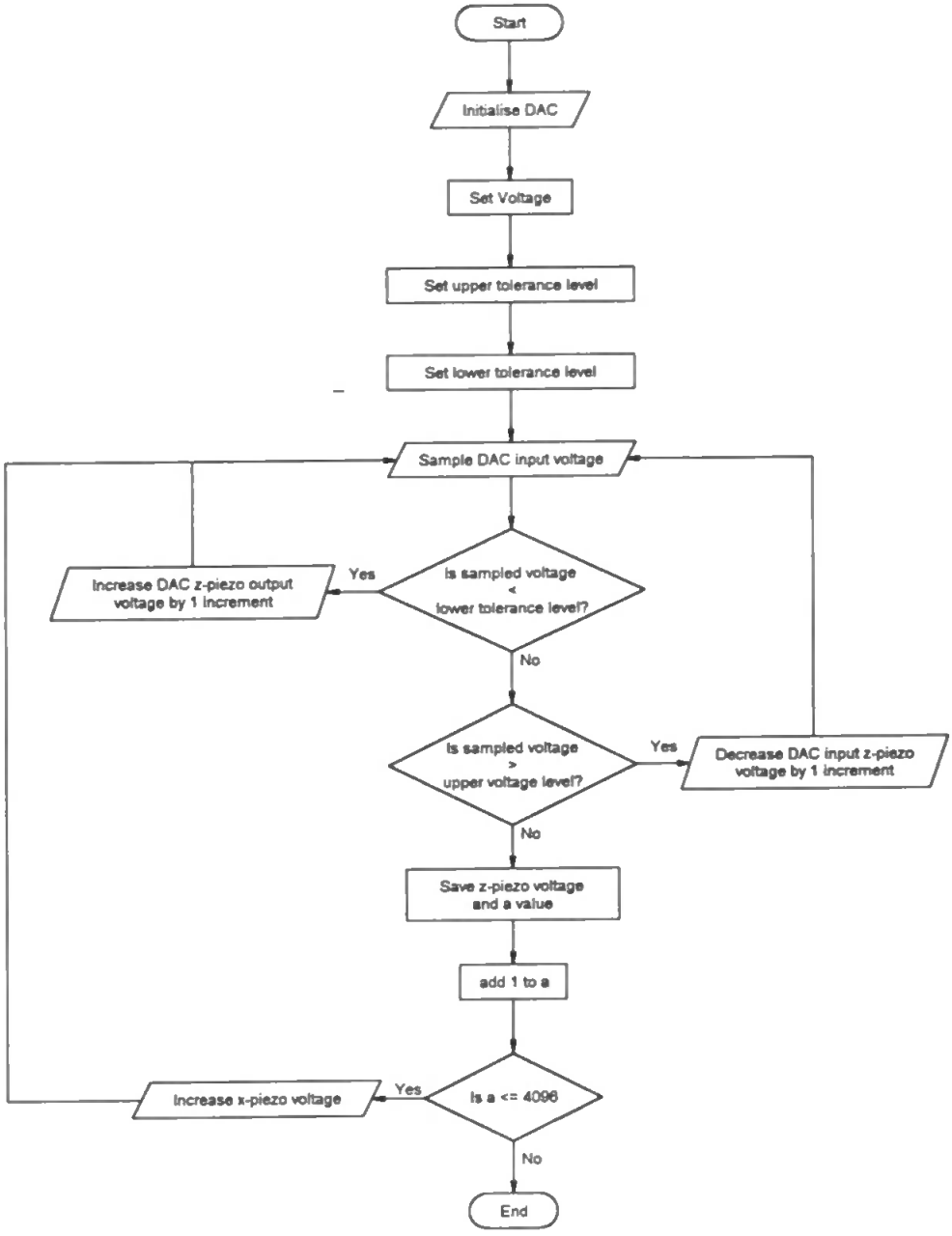

Figure 3.22 - PSTM control software flow chart.

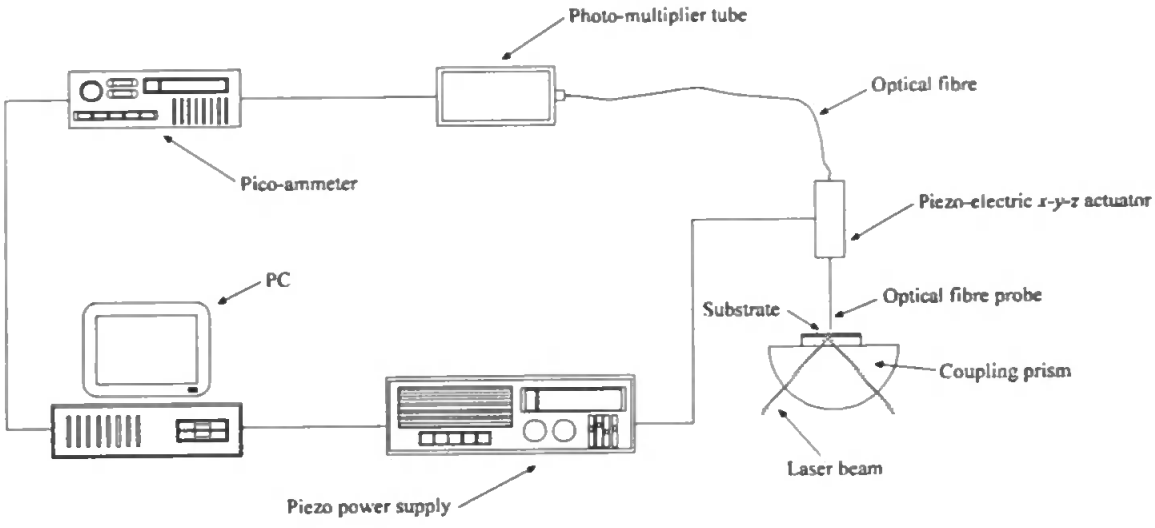

Figure 3.23 - A schematic diagram of a PSTM feedback network.

3.3.3 SPR Coupling Set-up

A description of the mechanical set-up of the SPR coupling system is given in the following section along with a description of the prism configuration, the PSTM/SNOM configuration and the procedure used to achieve SPR.

3.3.3.1 Prism/Substrate Configuration

The prepared substrates (Section 3.1) were placed on the upper surface of the coupling prism with index matching fluid used to match optically the slight refractive index difference between the prism and the substrate (Figure 3.24).

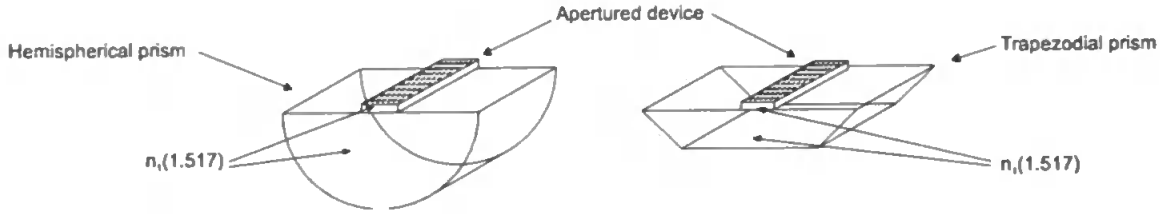

Figure 3.24 - A schematic diagram of the prism/substrate configuration.

3.3.3.2 Mechanical Coupling Device

The mechanical coupling device was designed and constructed to be easily adapted for several different configurations employed in this project. A high precision 2-dimensional mechanical translation stage was constructed to which an optical microscope with a NA of 0.28, X10 long working distance objective [Model No. 378-833, Mitutoyo, Japan] was fixed. The microscope incorporated a zoom facility on to which was fitted a Fujitsu high sensitivity CCD camera [Model No. TCZ-230 EA, Fujitsu General Ltd, Videor Technical E, Hartig GMBH] which was capable of being positioned in order that any

part of the substrate could be monitored. A second translation stage, described in Section 3.3.3.5, was developed for use with the PSTM/SNOM configuration.

Figure 3.25 illustrates the mechanical coupling device designed and constructed to achieve SPR while monitoring the upper surface of the substrate. A 4mw 632.8nm Spectra-Physics Helium Neon laser [Model No. 145-02, Spectra-Physics Inc., 1250 West Middlefield Road, Mt. View, California, 94042] was fixed to a micrometer adjustable rotating arm pivoted about a central axis. A customised coupler was constructed to hold the prism and substrate such that the laser radiation could be positioned anywhere on the lower surface of the substrate. A Photon Control 3-dimensional micrometer adjustment block [Model No. MicroBlock, Photon Control Ltd, Brookmount Court, Kirkwood Road, Cambridge, CB4 2PF] held the prism coupler and substrate such that its position could be optimised relative to the central pivoting axis of the rotating arm and consequently in line with the laser beam. Using this configuration, combined with an appropriate prism, the laser radiation could then make contact with the glass/metal interface under the correct coupling conditions.

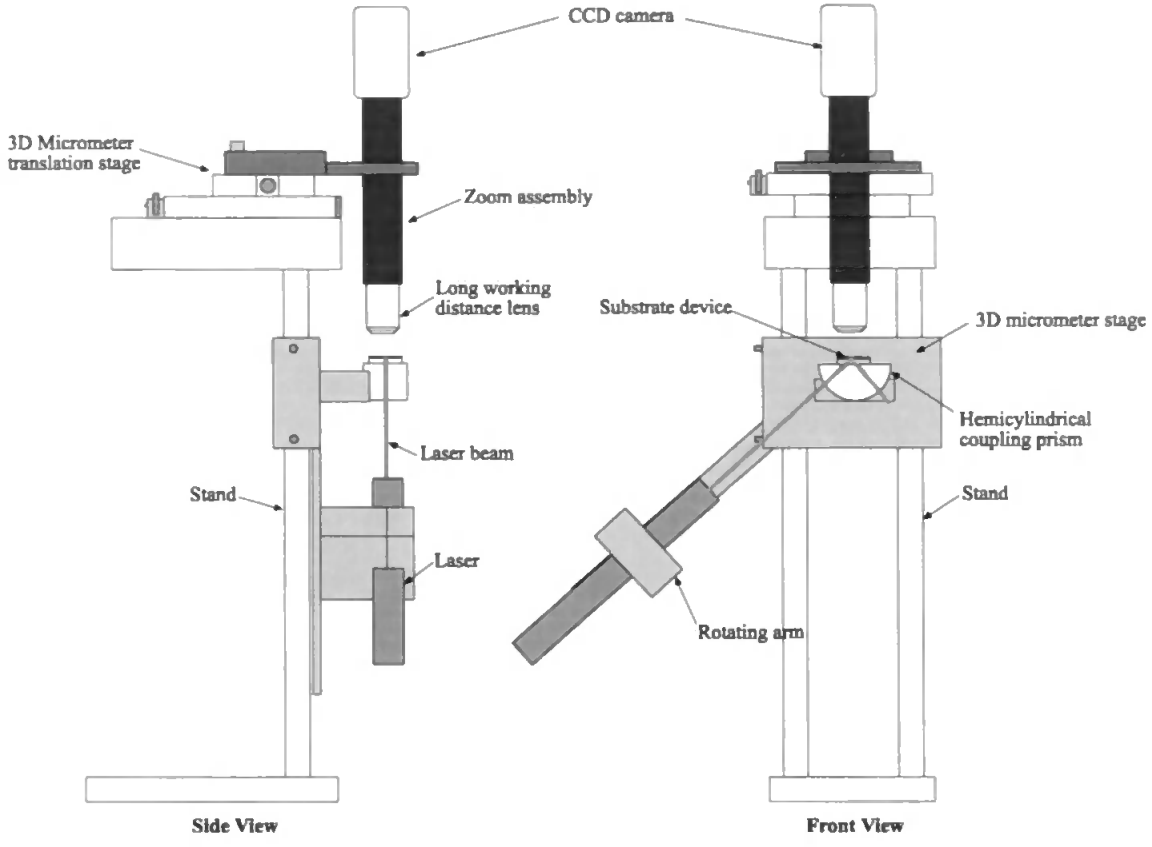

Figure 3.25 - A schematic diagram of the mechanical SPR coupling jig.

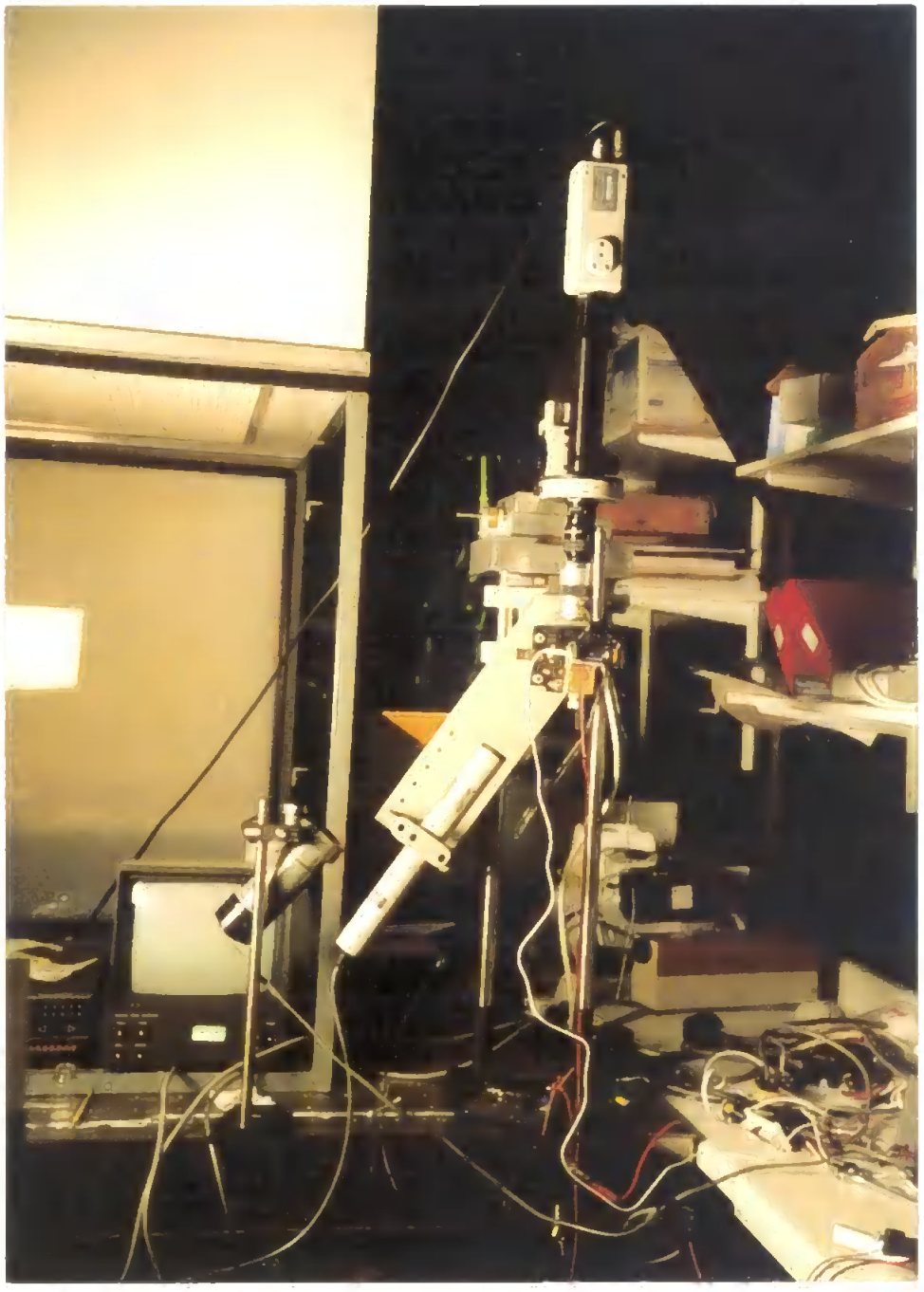

Figure 3.26 - The mechanical SPR coupling rig.

3.3.3.3 Prism Configuration

Two prisms were used in the experiments. While their optical properties were identical, i.e. commercially available BK7 glass, refractive index 1.517, their geometrical configurations were different (Figure 3.24).

The primary experimental prism was a custom made hemi-cylindrical prism of length 35mm and 26mm wide [Optical Works Ltd, Ealing Science Centre, Treloggan Lane, Newquay, TR7 1HX]. This configuration produced quick and effective alignment along the central rotational axis of the laser radiation. When optimised, the radiation was incident on the initial prism surface perpendicularly, eliminating refraction, thus the angle of incidence could be directly measured from the graduated dial on the rotating arm.

The second prism was a trapezoidal prism of length 58mm and 20mm wide [Model No. PD02, Optical Works Ltd, Ealing Science Centre, Treloggan Lane, Newquay, TR7 1HX]. Although this geometry allowed for unobstructed access to the upper and lower surfaces of the substrate this in itself created an additional problem in that refraction at the initial air/prism interface occurred, causing a deflection of the laser spot on the prism/metal interface as the laser rotating arm was moved during alignment. This small inconvenience made the initial SPR optimisation, at any given point on the substrate, more difficult.

3.3.3.4 Surface Plasmon Resonance

Surface Plasmon Resonance could be achieved through constant monitoring of the reflected laser radiation from the metal film while adjusting the incident angle. At SPR a marked decrease in the intensity of the reflected pattern was noted (a confirmation of SPR theory in Section 2.2 - Figure 2.2). A locking mechanism, on the rotating arm, was employed to secure the assembly at this angle during experimental exercises.

3.3.3.5 PSTM/SNOM Configuration

During the PSTM/SNOM experimental studies the microscope stage, described above, was replaced by a 3-dimensional piezo-electric manipulation stage and fibre holder (Figure 3.27). The microscope, attached to a moveable stand, was employed in the initial positioning of the fibre relative to the substrate surface. The height of the fibre tip above the surface was determined by sensing the electromagnetic tunnelling of the evanescent wave across the air gap until the desired height was reached.

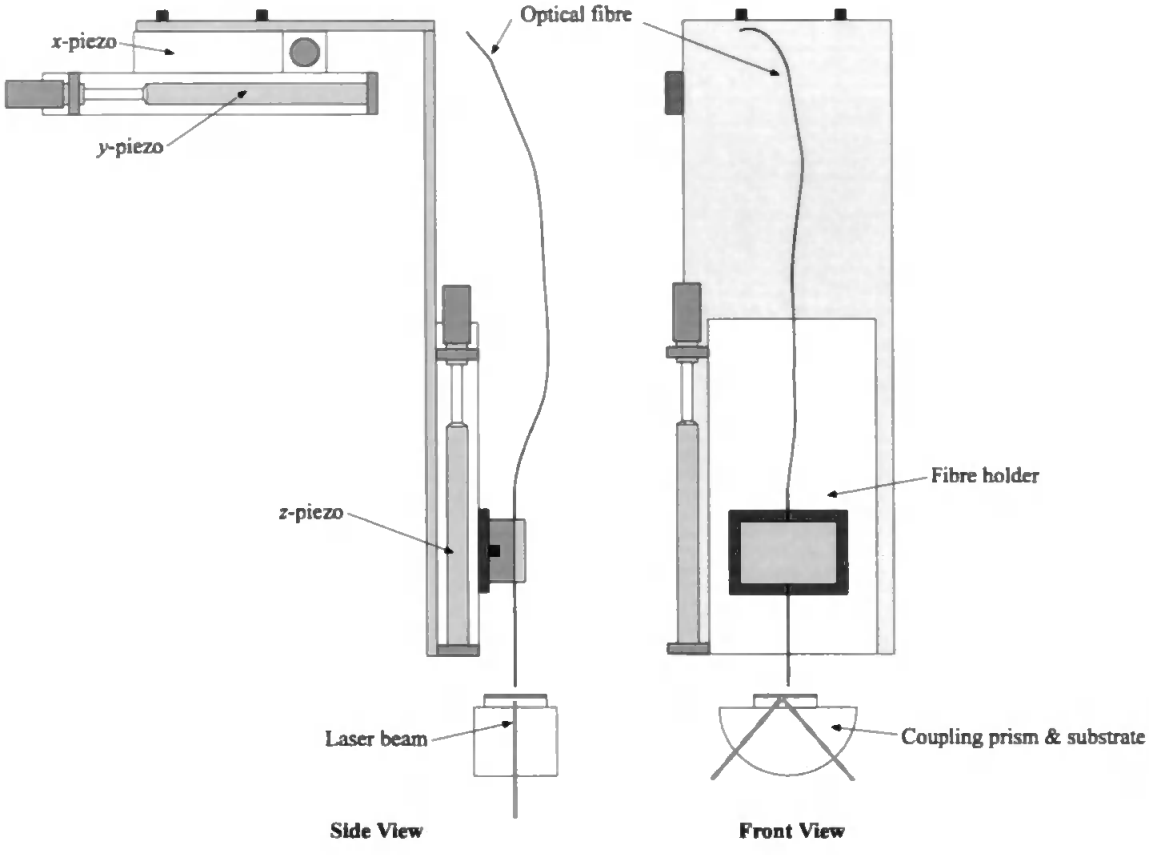

Figure 3.27 - A schematic diagram of the interchangeable top set of the PSTM probe mechanical jig.

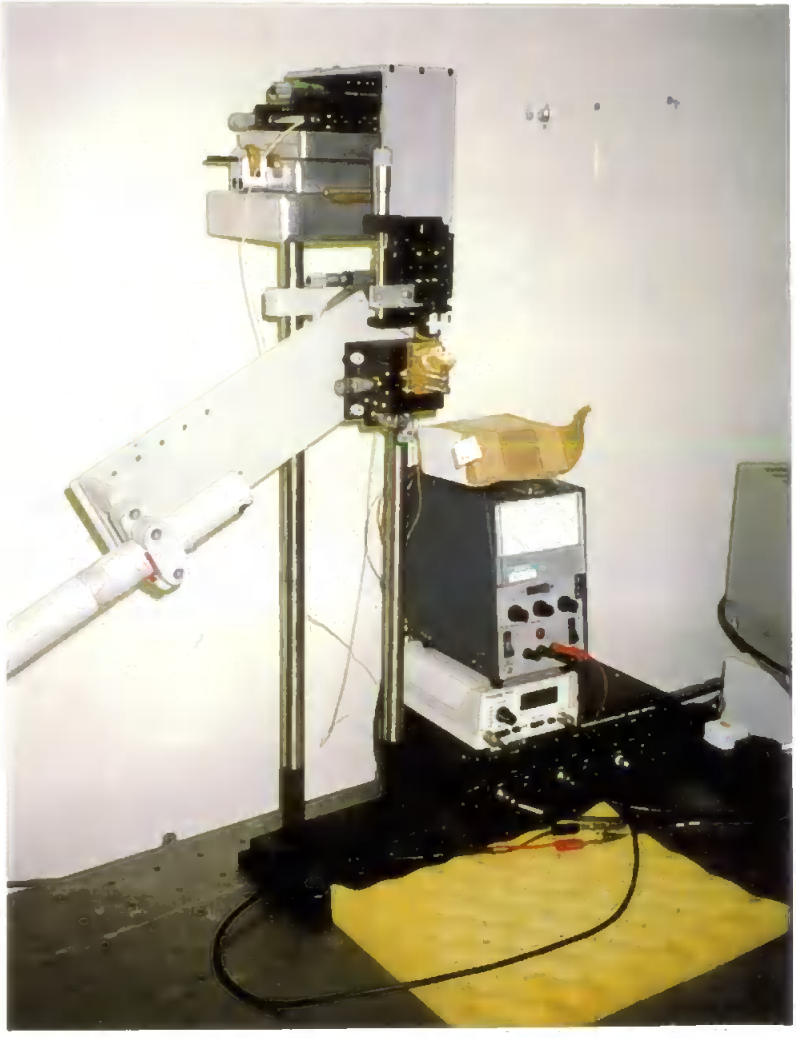

Figure 3.28 - The PSTM probe mechanical jig and feedback control.

Chapter 4

4. RESULTS & DISCUSSION - APPLICATION TO ANIMAL CELL ADHESION STUDIES

INTRODUCTION

The following sections present detailed results on the initial studies carried out at the University of Plymouth and the biological experimental trials at FORCE Cancer Research Centre, Exeter and CAMR, Porton Down. These experiments were carried out in order to quantify the nature of the SPR evanescent field, the intensity profile and biological implications of cancerous cells interacting with the electromagnetic field as seen from above the sample and the advantageous effect, if any, of apertures etched in the otherwise opaque background of the SPR device. (A video demonstrating the biological features of the device accompanies this thesis and may be obtained by contacting University of Plymouth's LRC.)

4.1 BIOLOGICAL STUDIES - PHASE I

4.1.1 Preliminary Studies - I

Initial studies at Plymouth University were conducted in order that SPR could be demonstrated on a chromium coated BK7 glass substrate. Using the trapezoidal prism and a conventional Olympus microscope [Model No. BH2, Olympus Optical Co. (U.K.) Ltd, 2-8 Honduras Street, London, EC1 Y0TX.], the devices were tested using polystyrene microspheres to investigate SPR conditions.

A suspension of polystyrene (latex) microspheres (Sigma Chemical Co. Ltd., Poole, Dorset, UK) of mean diameter 2.92μm (SD=0.012μm, Lot #92573) diluted to a concentration of 10^8/ml with demineralised 0.22μm filtered water was dropped onto the aperture-bearing surface of several *Cr* devices consisting of 2μm diameter apertures with 8μm centre separation (Figure 4.1). An 'O' ring, made from a small rubber sealing ring was used to contain a well of fluid over the apertures. A glass cover slide was placed on top of the fluid in order to present a flat optical layer through which the microscope could focus without the added optical perturbation of a curved meniscus layer. SPR was optimised by varying the incident angle of the illuminating laser beam while constantly monitoring the reflected intensity pattern until a marked reduction, indicating SPR, occurred.

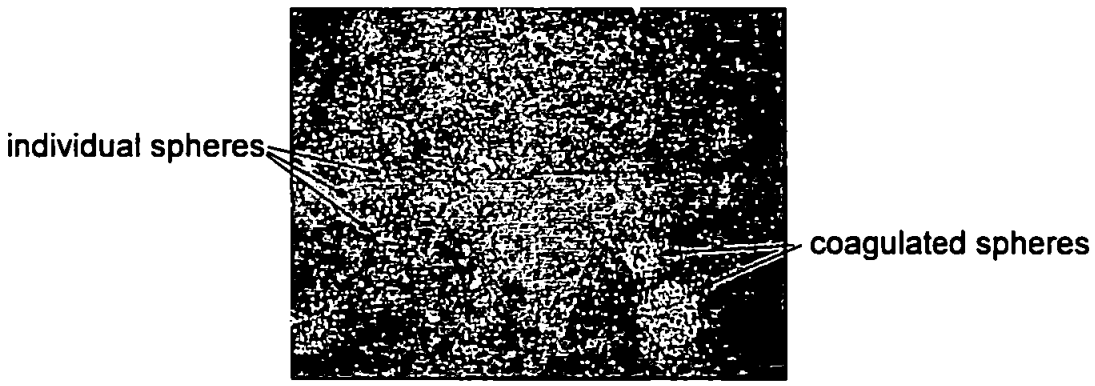

Figure 4.1 - An image of a 2μm ϕ aperture matrix with 2.92μm ϕ latex beads adherent.

4.1.2 Discussion of Experimental Results - I

Under SPR conditions the latex beads were observed moving under Brownian motion in the vicinity of and away from the apertures on the *Cr* surface. Large clusters of coagulated beads could be seen drifting en masse with minor movement of peripheral particles at the outer edges of the mass. This may have been due to thermal convection in the suspension medium or a combination of this and Brownian motion. This experiment and subsequent results confirmed the fact that the experimental coupling of the incident laser radiation to the surface plasmon mode of the metal film was successful. This was further confirmed when the laser radiation was removed and the sample lit by epi-illumination with ordinary white light. Few beads could be seen in the proximity of the apertures and none at all away from the apertures on the plain metal surface.

4.1.3 Animal Cell Studies - II

After the initial verification stages of the project were complete, further studies concentrated on live animal cell experiments. Squamous epithelial cells were obtained by spatula scraping the inside of the human cheek. These cells, suspended in demineralised 0.22µm filtered water, were placed onto the device and the microscope focused in the plane of the aperture bearing surface. These cells, of approximately 10-15µm in diameter, could be seen moving over the aperture bearing surface producing scintillations at the extremities of their mass. As the cells moved, both on and off the apertured region of the surface, an intensity profile of their movement was compiled over a short period of time, e.g. 10-20 seconds. A slowing down of the cell movement was detectable after several minutes as the temperature and appropriate living conditions deteriorated. Images of the surface were recorded for subsequent analysis at a later date. Figure 4.2 shows such an image with the regular matrix of apertures evident at the left hand side of the image and the bright spots elsewhere being animal cells. This was confirmed by observation under white light illumination.

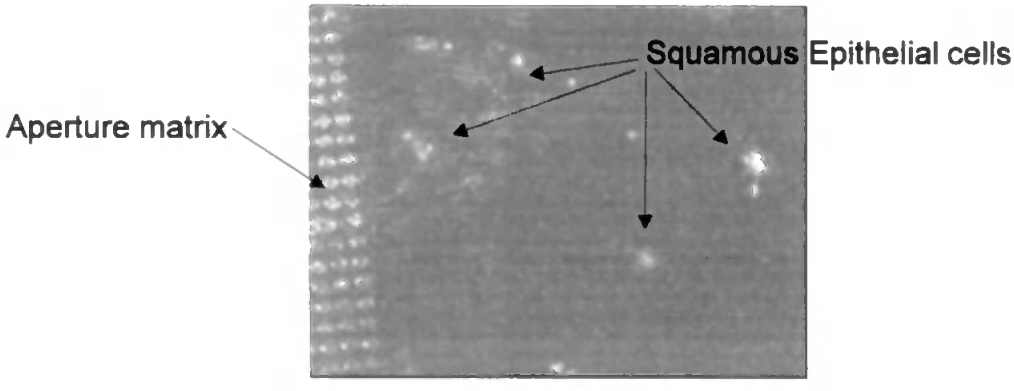

Figure 4.2 - Images of the Squamous Epithelial cells under SPR.

4.1.4 Discussion of Animal Cell Study Results - II

Utilising the regularity of the aperture matrix of the device a precise 2-dimensional calibration technique was achieved. Any movement of a cell in the vicinity of the apertures produced visible intensity fluctuations detectable in the far-field.

It is known, and shown in Section 5.1.3, that the evanescent field associated with SPR extends, in an exponential nature, vertically from the surface of the device [Adam *et al.* (1993), Dawson *et al.* (1995)]. Thus, the interactions between the cells and the non-radiative SPW, present in the metal between the individual apertures and also away from the apertures on the plain metal surface, provided additional information on the vertical content of the cell behaviour. The associated contrast in intensity fluctuations detectable in the far-field suggests differing proximity between the cell and sensor surface.

Utilising a combination of these two facets of the device i.e. detection of cell movement on the aperture matrix and away from the aperture matrix, created a 3-dimensional highly sensitive method of cell visualisation. Similar images may be obtained with the use of Phase Contrast Microscopy [Pluta (1989)] and Interference Reflection Microscopy [Curtis (1988) & Curtis *et al.* (1991)] but these devices are limited by the wavelength of light and thus have limited lateral resolution capabilities and therefore lack the significant contrast available between the otherwise opaque background of the metal surface and the cell de-coupling points available with this device.

4.1.5 Secondary Studies - I

Preliminary studies at CAMR proved useful in identifying future research strategies. A temperature controlling device was developed and used during this experimental analysis. This consisted of a Peltier heat pump using thermal conduction to transfer heat to a well of solution. The well was made from a small rubber 'O' ring placed on top of the

metalised substrate surrounding the aperture matrix. This was filled with the cell incubation solution and a glass cover slide placed on top.

4.1.6 Animal cell lines and sample preparation - I

For these animal cell studies, suspensions of Chinese Hamster Ovary (CHO) cells were obtained from the European Collection of Animal Cell Cultures (Accession No. 85050302 - ECACC, CAMR, Porton Down, Wilts.). These cells were chosen for their relative robustness, suitable size (10μm diameter) and known adherence properties. The cells were cultured in a conventional cell culture medium (Hams S12 containing 10% fetal calf serum; PAA Gmbh, Austria) at 37°C. Suspensions of cells adhering to culture bottles were prepared by treatment with trypsin/EDTA (Ethylenediaminetetraacetic Acid, Gibco Ltd., Paisley, Scotland) prior to mixing in fresh medium to a concentration of 10^5 cells/ml. To minimise bacterial contamination the suspending medium contained aliquots of a solution of Penicillin and Streptomycin (50,000 units/ml - Gibco Ltd.) diluted to a final solution of 5,000 units/ml. Cell concentrations were confirmed microscopically by haemocytometer count with Trypan Blue visualising dye.

Aliquots of cell suspensions were placed onto aperture arrays comprising 1.4μm diameter apertures at 5μm centre spacing. The diameter of the cells (approx. 10μm ϕ spheres) meant that, on adhesion to the surface (with a concomitant slight increase in diameter to typically 15μm), each cell would cover at least 3 apertures at any given time. The overall cell concentration was selected such that surface coverage of the aperture array would approach 10% when all cells had settled onto the surface and subsequently adhered.

Cells were incubated in the aperture array illumination system for up to 24 hours, initial signs of sedimentation and adhesion being apparent after the first 3-4 hours. Images of the surface were recorded at suitable intervals (e.g. for 5 minutes every 2-3 hours) for

subsequent analysis. The data obtained from the experiments using CHO cells was analysed using a personal computer imaging package [PCX Systems, Brian Reece Ltd, Newbury, Berkshire, U.K.]. Particular areas of interest, i.e. points at which cells contacted the surface, were monitored and intensity plots of scanned areas were recorded. Individual frames were digitally frozen and stored for visual interpretations and analysis at a later date.

4.1.7 Discussion of Secondary Studies - I

After approximately twelve hours under experimental examination the cells had 'out gassed' to such an extent that the view of the lower well surface was obscured by gas bubbles. Once these gas bubbles were removed by extraction with a syringe, an inspection of the grid using conventional white light microscopy showed that a number of cells had adhered to the aperture bearing surface. Further confirmation of the presence of the adherent cells was made with Trypan Blue visualising dye after initial experiments. Minute fluctuations could be seen in the intensity pattern of the aperture matrix as the cell entered the otherwise radiative field altering its characteristics and thus its intensity profile.

Figure 4.3 is a plot of the intensity pattern of the matrix being modulated by an individual cell in the near-field of an aperture grid under three different illumination conditions.

- Combined laser and white light illumination, (2-10sec) showed a high mean intensity level with moderate amplitude fluctuations: - Low Signal-Noise (S/N) ratio.

- White light illumination, (10-29sec) showed a low mean intensity level and low amplitude fluctuations: - Very Low S/N ratio.

- Laser illumination, (29-55sec) showed a high mean intensity level and large amplitude fluctuations: - High S/N ratio.

Figure 4.4 demonstrates the three states of Figure 4.3. it can be seen that the contrast of the laser illumination technique produces a sharper image than the other forms of illumination. To confirm the presence of cell adhesion during these experiments the grids were 'blue stained' after rinsing and dried before being visualised with a conventional white light microscope.

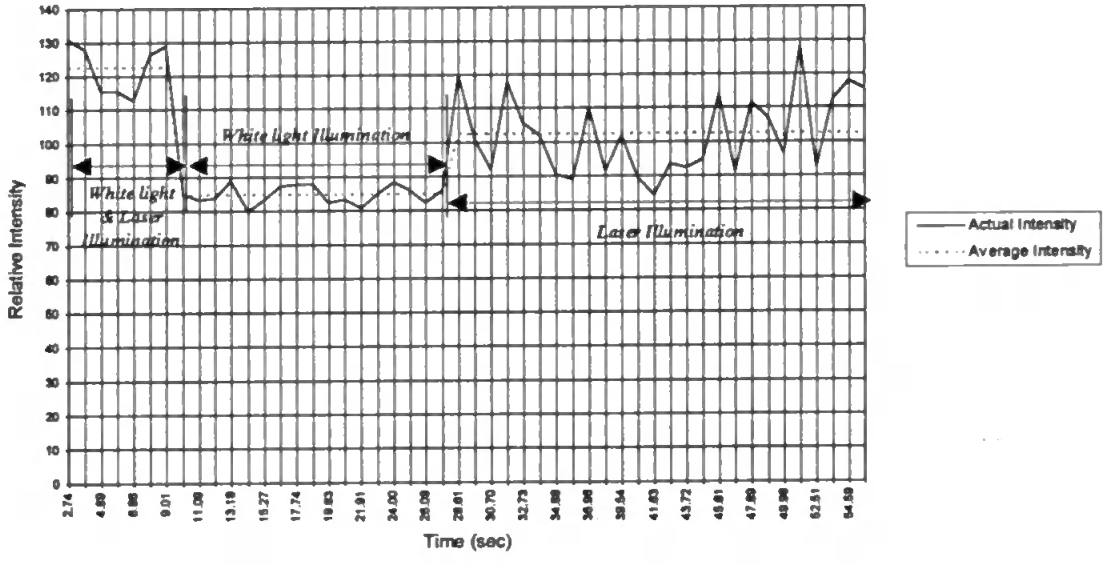

Figure 4.3 - The relative intensity plot of visible radiation from an individual 1.4μm ϕ aperture being modulated by a CHO cell after 18 hours under white light and laser illumination (2-10sec), white light illumination (10-29sec) and laser illumination (29-55sec).

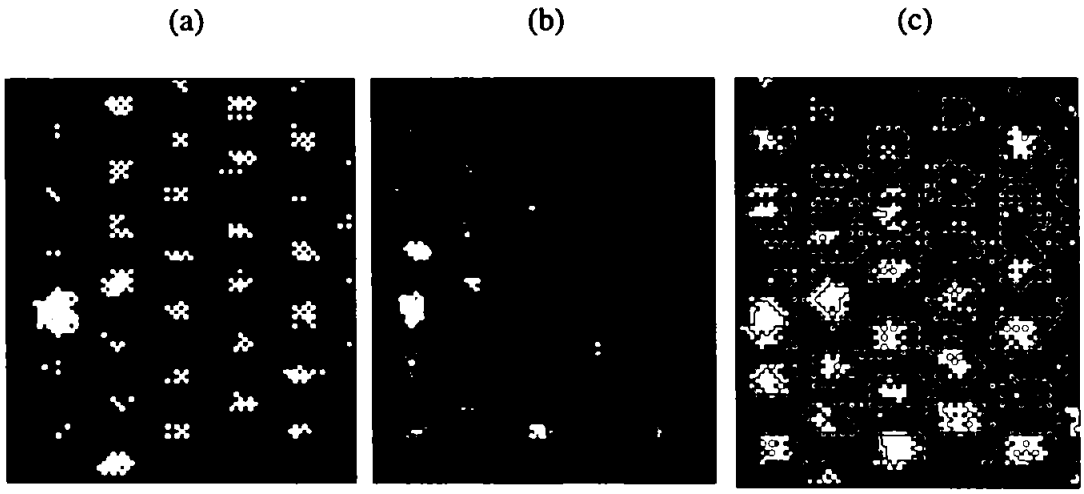

Figure 4.4 - A visual comparison of the differing illumination conditions in the SPR coupler.

Shown in the rectangular box, Figure 4.6, is a large section of stained animal cells adherent to the aperture bearing surface of the sensor (illuminated under conventional white light microscopy). A magnified section, Figure 4.8, shows a significant reduction in the magnitude of light radiating through the apertures. As the cells were chosen for their suitable size (≈10μm) and known adherence qualities they covered numerous apertures once adherent. It was observed, that under SPR, as opposed to white light illumination, the apertures acted as very sensitive lateral movement sensors resulting from the edges of the cell disrupting the radiative fields within the apertures, as discussed earlier in Section 4.1.7. This disruption could be monitored as intensity fluctuations in the far-field.

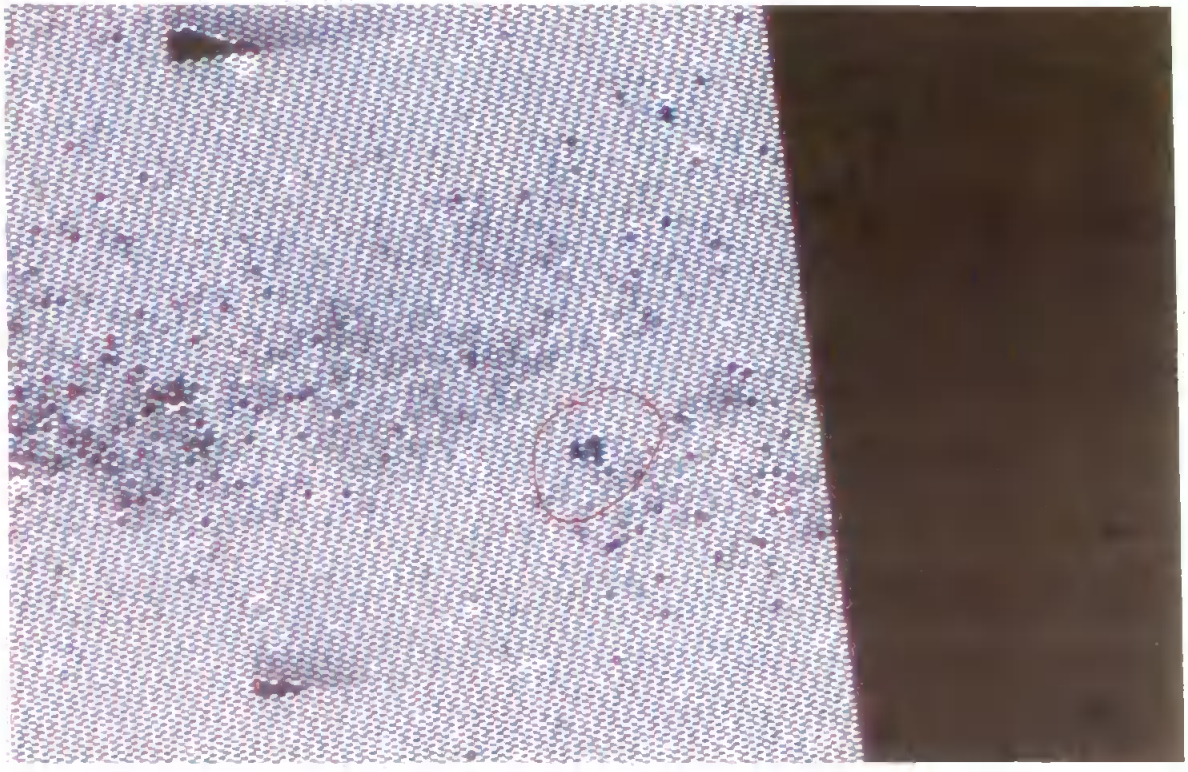

Figure 4.5 - Colour photograph of a section of a 1.4µm aperture grid with Chinese Hamster Ovary cells adherent.

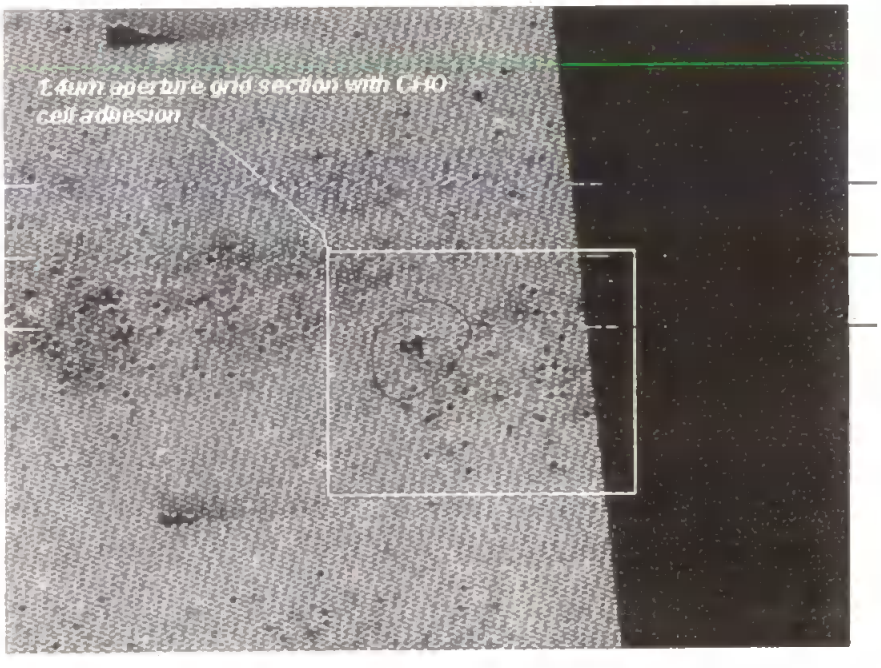

Figure 4.6 - A computer captured section of a 1.4µm aperture grid showing Chinese Hamster Ovary cells adherent within the rectangular box.

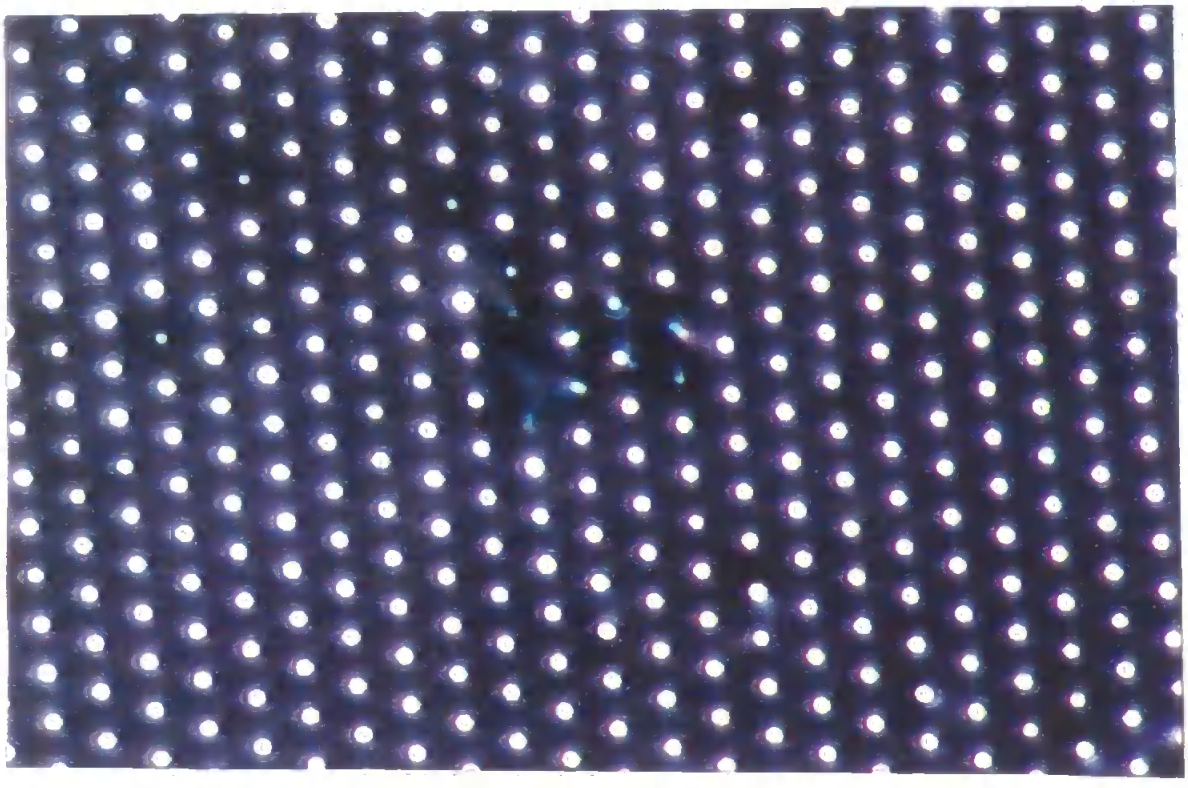

Figure 4.7 - A colour photograph of a magnified section of a 1.4µm aperture grid with Chinese Hamster Ovary cells adherent.

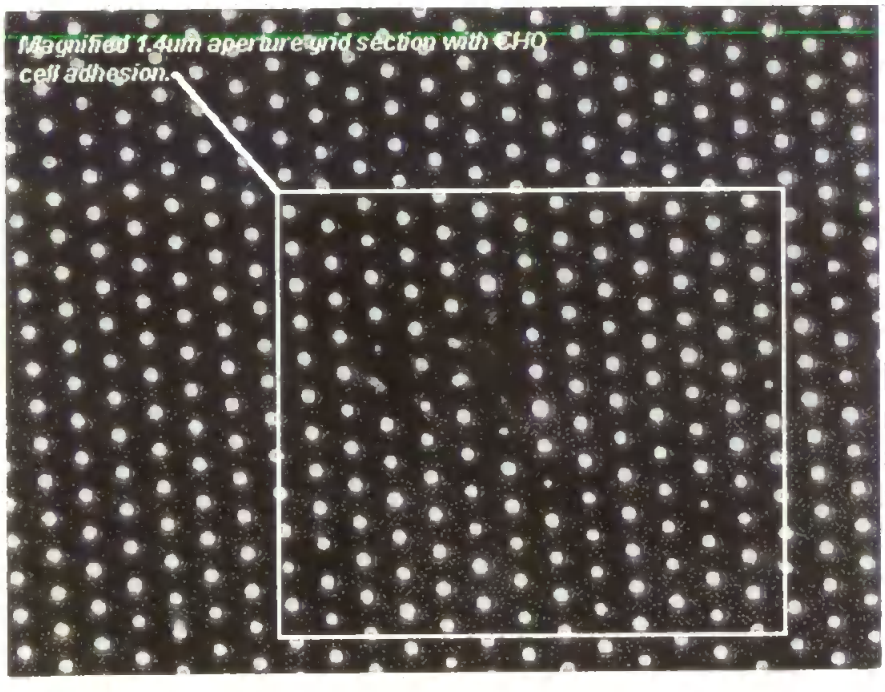

Figure 4.8 - A magnified section of the same section of the 1.4µm aperture grid with Chinese Hamster Ovary cells adherent.

4.2 BIOLOGICAL STUDIES - PHASE II

4.2.1 Preliminary Studies - II

These studies were carried out at the FORCE Cancer Research Centre, Exeter on prepared *Cr* and *Ag* devices. The initial investigation was to ascertain the suitability of various metal films when exposed to tissue culture medium. The *Ag* films were immediately stripped by the medium whereas the *Cr* coated devices remained stable and therefore were used in all subsequent experiments. Devices were immersed in tissue culture medium and left for a period of between 12 and 24 hours. When viewed under SPR conditions, the device exhibited a uniform dark granular background devoid of Brownian movement. However, debris entering the SPR field were evident as rapidly fluctuating points of light exhibiting Brownian movement.

The next stage was to examine murine haematopoietic cell lines, derived from bone marrow and dependent on a growth factor Interlukin 3 (IL3) for survival and growth [Garland *et al.* (1993)]. Such cells grow as suspension cultures but readily settle onto surfaces but do not adhere. Cells in active growth were settled onto metallised substrate sensors for 30 minutes before examination. Under epi-illumination there was no evident movement within individual cells although over a period of several minutes cell migration over small distances was detected. Under SPR conditions cells were individually identifiable by between 10 and 20 clusters of bright spots of light. It was apparent that cells were actively moving over the device surface in random directions, shown by spot clusters of light migrating over the surface of the sensor. To confirm overall cell migration, the positions of individual cells were visually marked and were seen to move slowly over the device surface. A period of at least 2 minutes was required to establish changes in relative position.

4.2.2 Secondary Studies - II

It is known that animal cell adhesion to surfaces is initiated by Extra Cellular Matrix (ECM) components. In order to investigate the adhesion of cells onto surfaces pre-coated with ECM's, it was necessary to demonstrate that the ECM layers themselves did not result in adversely effecting subsequent cell studies. Metallised substrates were coated with ECM components by placing them individually into ECM solutions for a predetermined time prior to testing on the SPR coupling rig. It was found that the absorption of ECM protein did not significantly affect the position of the SPR reflection dip from that of a glass/metal/water layered system, suggesting that a molecular film of hydrated ECM protein did not alter the effective dielectric constant at the metal/water interface significantly. SPR was optimised for each of the experiments and layering configurations.

In order to explore how SPR conditions in metallised substrates would reveal differences in cell movement dependent on different biological substrates, human breast cancer cell lines and a selection of collagens known to constitute ECM, namely collagen I, II and IV were chosen. Also included was poly-L-lysine, a peptide frequently used to increase in-vitro adherence. Metallised strips were pre-coated with the various ECM proteins, as described earlier and placed together in a single culture dish, ensuring that all strips were under identical culture conditions. Cells were added and allowed to adhere to the device surface overnight.

These results are given for the human breast tumour line MDA-MB-231 [European Collection of Animal Cell Cultures, Porton Down, Wiltshire (Accession number 92020424)]. Cells adhered to poly-L-lysine or collagen I or II films appeared to be immobile under direct epi-illumination. Under SPR conditions, an intensity profile similar to that of haematopoietic cells was seen for each cell, consisting of a cluster of bright spots of light within the bounds of the cell's outer periphery. Unlike those of the haematopoietic cells, these spots remained stationary and did not migrate over the

surface of the substrate. No movements in the clusters were detected over a period of several minutes. However, cells adherent to collagen IV films exhibited remarkably different behaviour. Although these cells also remained stationary, i.e. did not undergo lateral movement, and showed similar spot patterns to those from the other cultures, the spot patterns underwent extremely regular, pulsatile oscillations. These pulsations displayed a periodicity of less than 4 seconds. Continuation of this regular alternation was observed over long periods of time (up to 30 minutes), giving the impression of regular pulsations. In any individual cell the spot patterns gradually changed, but their periodicity remained constant. Importantly this pulsatile behaviour was dependent on metabolism as cooling the stage caused their cessation. All cells in the culture displayed similar pulsations with the same periodicity, but were not synchronised. To ensure that failure to observe such behaviour on other substrates might be due to different times of sampling, strips were randomised before viewing, with the same result. Figure 4.9 shows these breast tumour cells over a time period of 9 seconds with 1 second intervals (the brighter the image the closer the cell is to the device surface and the greater the scattered intensity, as shown in Section 5.1.3).

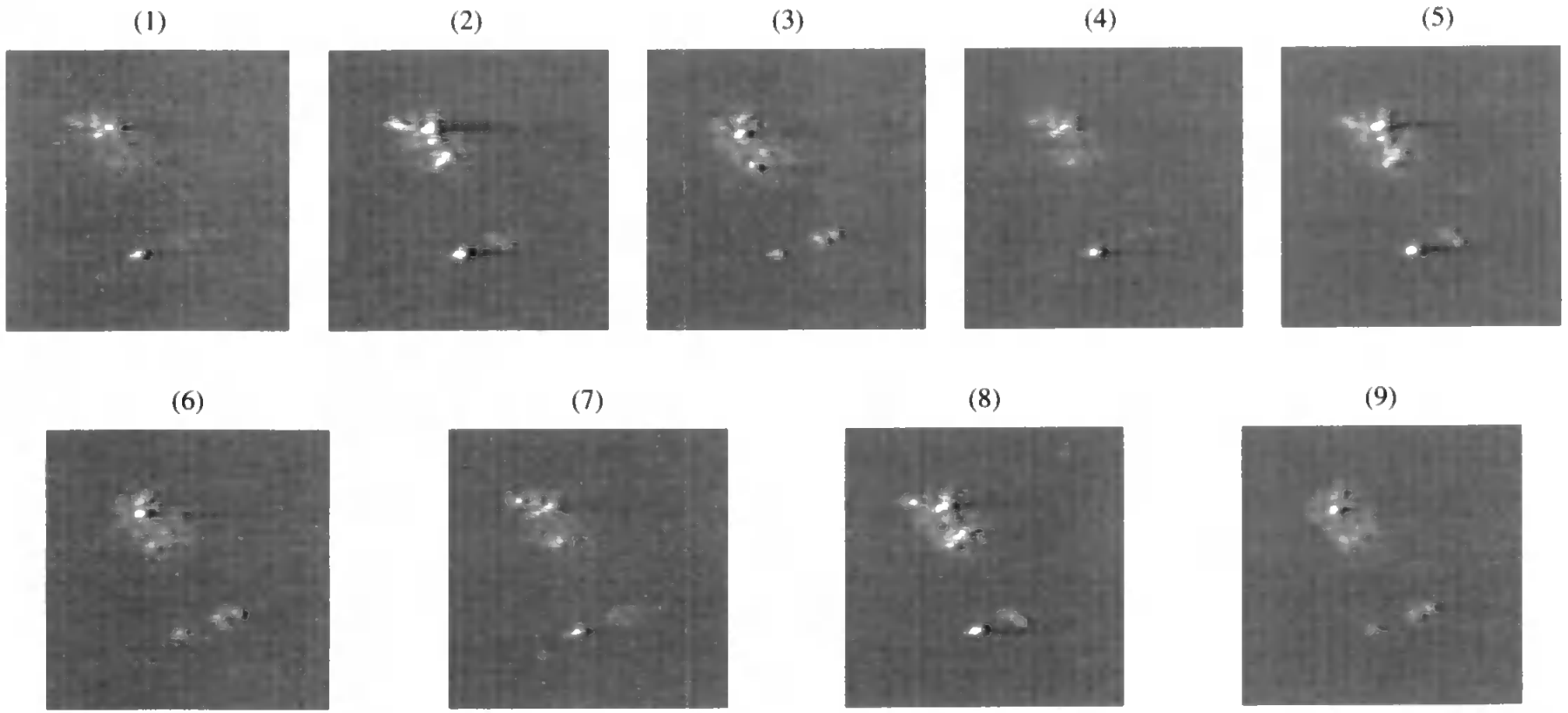

Figure 4.9 - Captured images of a cell line (157 on collagen 8 chemical substrate) waxing and waning with a regular periodicity of approximately 1½ - 2 seconds (each picture +1 second).

4.2.3 Analysis of Secondary Study Results - II

It is known that in order to migrate, cells extend structures from their leading edges which adhere to the undersurface thus presenting the cell with a frictional force with which to 'roll or fold' a secondary edge over the initial extension presenting a mechanism by which the cell can move [Alt *et al.* (1995), Cheng *et al.* (1992)]. Cheng proposes a model by which cells move by their so-called 'minipodia' extending from the underside of the lamella at the edges of the cell where they attached to the substrate producing adhesion foci from which movement may be initiated.

It has been shown in this thesis that initial studies with latex beads exhibiting Brownian movement, Section 4.1.1, and the evanescent field profiling, Section 5.1.3, revealed that the intensity fluctuations are representative of material entering the vertical extension of the SPR field. It is known that the undersurface of adherent cells does not completely contact the surface but rather specific points of contact are made with the underlying surface. Physically, the oscillatory behaviour, shown in Figure 4.9 is due to the cell extensions alternately entering into and retracting from the SPR field. Due to the exponential nature of the evanescent field, Section 5.1.3, the brightest points are the sections of the cell in direct contact with the substrate. In the case of haematopoietic cells, these extensions are associated with rapid (at the cellular level) cell translocation and could represent a mechanism of cell 'walking'. The studies with adherent human breast tumour cells and the effect of various ECM proteins also suggest that the clusters of scattered light represent points of cell membrane interacting with a substrate. Thus, they do not move when cells are stationary on certain substrates but undergo rapid, pulsatile movements in the presence of one particular type of ECM protein, collagen IV. Oberleithner *et al.* (1993) has successfully imaged the lamellipodium of migrating epithelial cells in vivo by atomic force microscopy and found that the points of contact exhibits numerous microvilli and dimples approximately 30nm wide and 8nm high. It is

possible therefore, but has yet to be firmly established, that the points of contact visualised by this device are therefore these microvilli and dimples modulating the SPW.

Significantly, collagen IV is a basement membrane protein which specifically regulates apoptosis (programmed cell suicide) and hormone signalling in normal breast cells [Goberdhan *et al.* (1996)]. It thus appears that the breast tumour cells are responding to a natural ligand normally controlling growth and cell integrity. Whilst other cells are known to exhibit some periodic pulsations, these are measured in many minutes [Beloussov *et al.* (1972) (14min), Grebecki *et al.* (1978), Fleischer *et al.* (1975) (1-3min)], and to our knowledge such rapid (in seconds) regular and reciprocal pulsations have not been described in any mammalian cells before. Some results may suggest that the periodic fluctuations may be due to scattering centres in the cell interior. These may be of the time scale observed here and would certainly slow down with a drop in temperature but the observed rhythmic movement was of such a regular periodicity and pulsatile nature that a whole cell movement mechanism is more probable in this instance. Although Alt *et al.* (1995), observed extension waves rotating around the periphery of the cell with regular alternating pulsations of the lamella (outer cell extension edges) protrusions, they were of a period of 25-60 minutes and not of the time scale observed here. The observed periodicity of the findings in this thesis have yet to be explained fully and we have no ready explanation for this phenomenon, except that it is clearly dependent on interaction with matrix proteins and metabolism.

We have shown that novel movements of cells can be revealed by a simple SPR device capable of installation with standard laboratory equipment. The device itself allows cells to be monitored for long periods of time in tissue culture conditions under very low intensity laser illumination and effectively images cell-substrate interactions not readily visible by other means. Utilising this method of illumination an improvement in sensitivity over conventional white light microscopy is achieved.

Chapter 5

5. Results & Discussion - Physical Characterisation of Optical Discontinuities

Introduction

The results from a detailed study and characterisation of the SPR field on both a plain metal surface and a refractive index discontinuity, in the form of an aperture, are given and discussed. This is necessary in order to confirm the validity of the observations gained during the experimental biological trials at our collaborating establishments in Exeter and Salisbury.

5.1 SNOM/PSTM SYSTEM

5.1.1 Calibration of SNOM/PSTM System

Calibration of the SNOM/PSTM system was required before any accurate measurements of the radiative and non-radiative fields associated with the device could be made. The calibration procedure consisted of multiple scans over the surface of a known substrate configuration. Using the system in 'constant height' mode the probe was scanned over a *Cr* coated glass substrate containing apertures of size ranging in diameter from 10μm down to 1μm. Figure 5.1 is an image of 1μm ϕ matrix with a 30μm wide outer border captured by a computer video frame grabber [Model No. E2531A, Hewlett Packard Vidjet Pro, Video Communications Division, 5301 Stevens Creek Boulevard, Santa Clara, California, USA]. The apertures are not visible in this image under this magnification. The tip of the fibre probe was cleaved using a Fujikura CT-07 precision optical fibre cleaver [Fujikura Instruments, Japan] and brought to within a few microns of the surface under piezo-electric control. The intensity of light picked up by the probe was continuously monitored and shown in 2 dimensions on a personal computer. Detailed 3-dimensional analysis of the intensity profile was shown on a commercially available computer graphics package [Cantata - Khoral Research Inc., 6001 Indian School Road, NE Suite 200, Albuquerque, NM 87110, USA.] on a Hewlett Packard Workstation [Model No. 715/100, 5301 Stevens Creek Boulevard, Santa Clara, California, USA].

Several scans over each of the calibrated substrates were made with different sized probes in order to achieve maximum calibration profiles for each configuration of fibre tip, the results of which are given and discussed in the following section. The intensity readings in all the following PSTM/SNOM experiments are arbitrary levels produced by the DAC with a level of 2000 representing a lower detected intensity reading than the 0 level recorded. Figure 5.2 is the intensity profile of a horizontal scan with an un-tapered

50/125μm multi-mode fibre across the 30μm square rim shown in Figure 5.1 back illuminated with white light. A similar horizontal scan with an un-tapered 10/125μm single-mode fibre across the same 30μm square rim back illuminated with white light is shown in Figure 5.3.

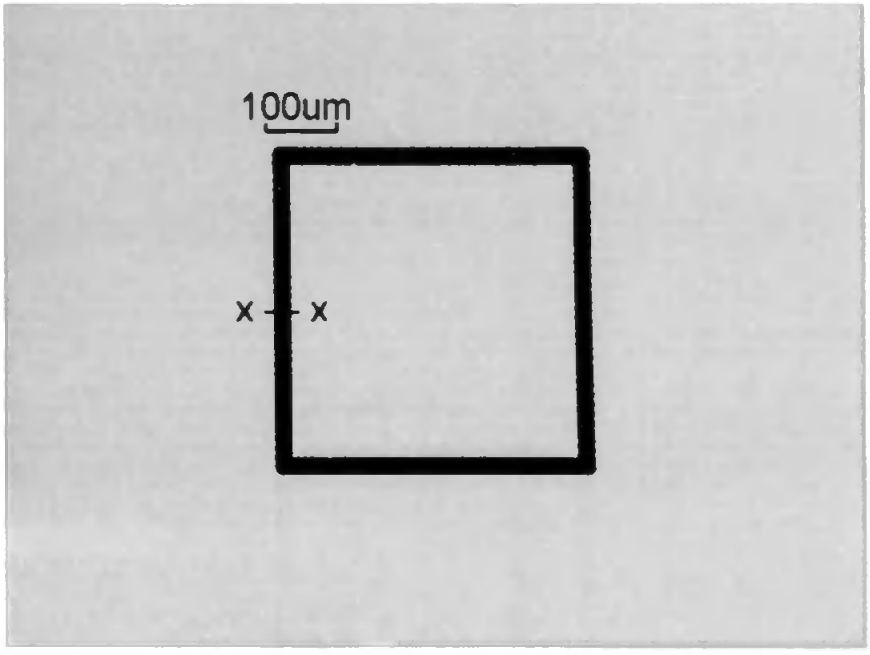

Figure 5.1- An image of a *Cr* coated device. The dark band is an etched rim of 30μm wide enclosing an array of 1μm ϕ apertures (not visible under this magnification).

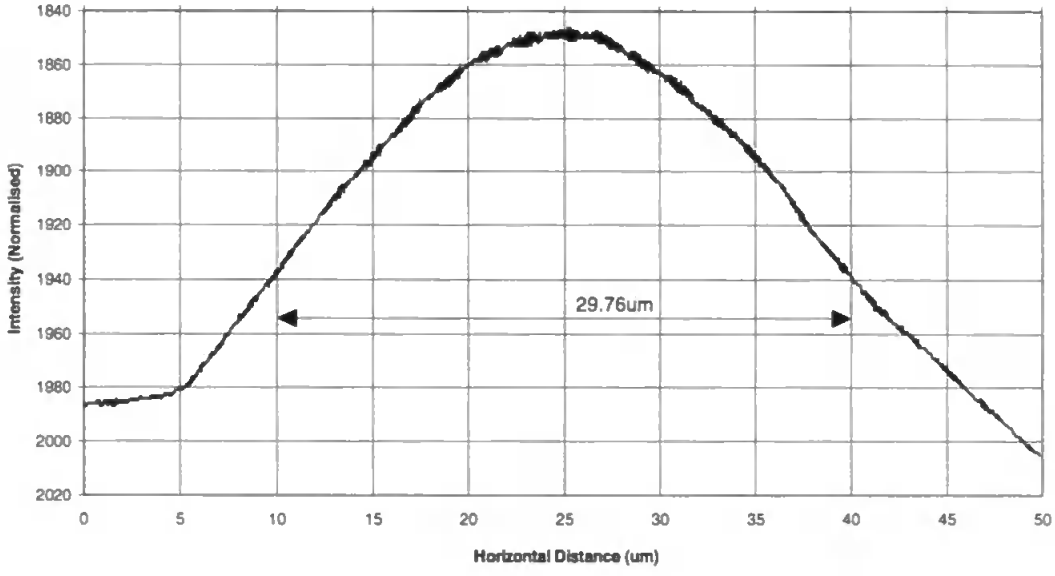

Figure 5.2 - Horizontal intensity scan with an un-tapered 50/125μm multi-mode fibre across a 30μm square rim back illuminated with white light (section x-x in Figure 5.1).

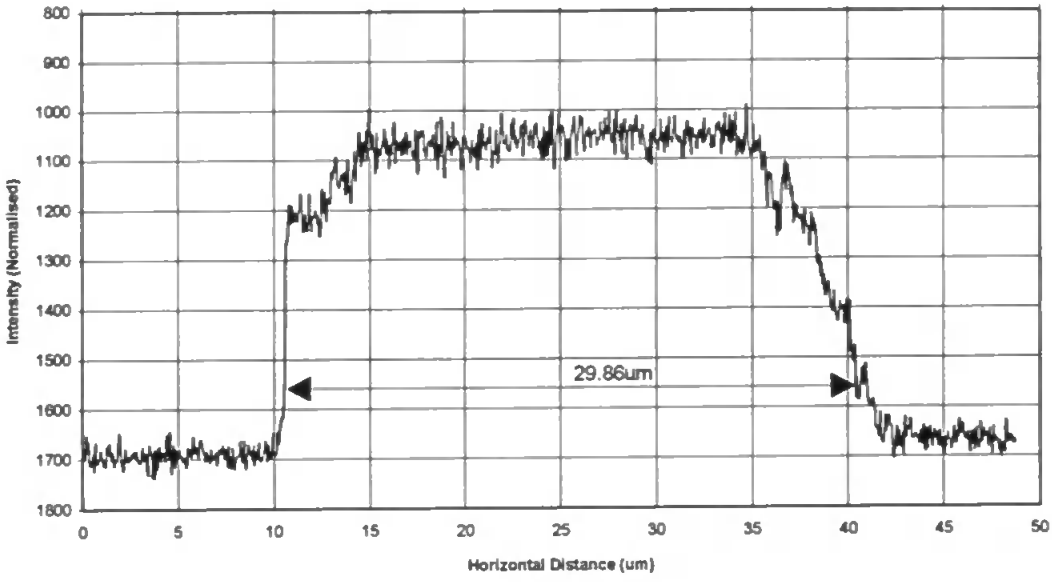

Figure 5.3 - Horizontal intensity scan with an un-tapered 10/125μm single-mode fibre across a 30μm square rim back illuminated with white light (section x-x in Figure 5.1).

Figure 5.4 is a conventional microscope image of a 10μm ϕ aperture matrix with 20μm between centres. Scans across the aperture with an AFM and SNOM (back illuminated with white light), are shown in Figure 5.5 and Figure 5.6 respectively with a raster scan of several apertures under white light illumination in Figure 5.7.

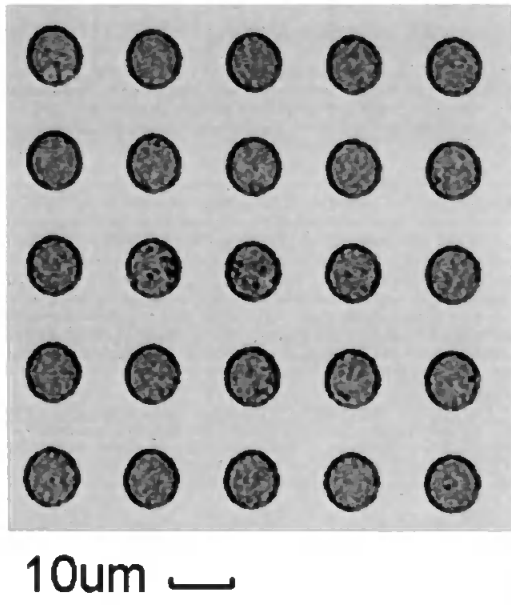

Figure 5.4 - A section of a 10µm ϕ aperture matrix with 20µm between centres.

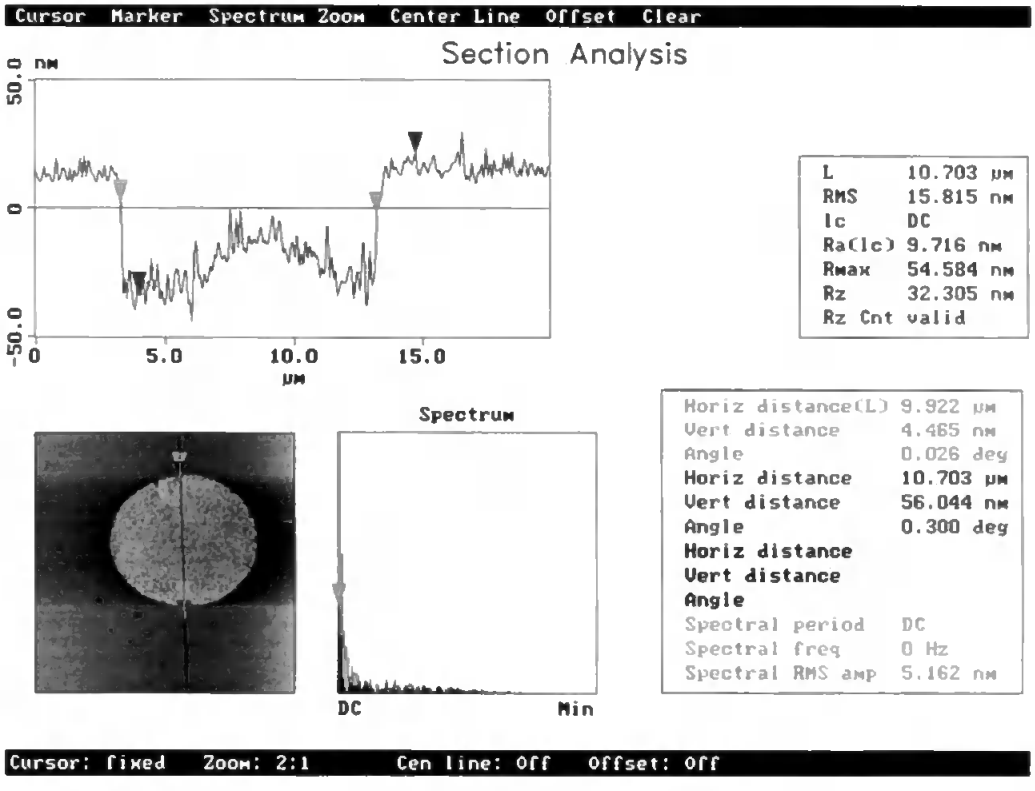

Figure 5.5 - An Atomic Force Microscope sectional analysis of a 10µm ϕ aperture shown above.

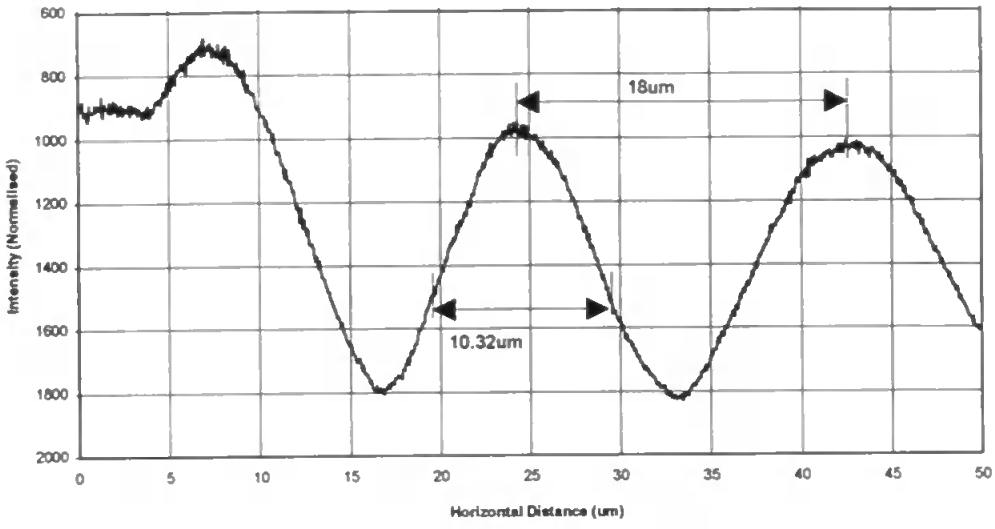

Figure 5.6 - Horizontal intensity scan with an un-tapered 10/125μm single-mode fibre across several 10μm ϕ apertures back illuminated with white light (the centre of the apertures corresponds to the peaks of the intensity plots).

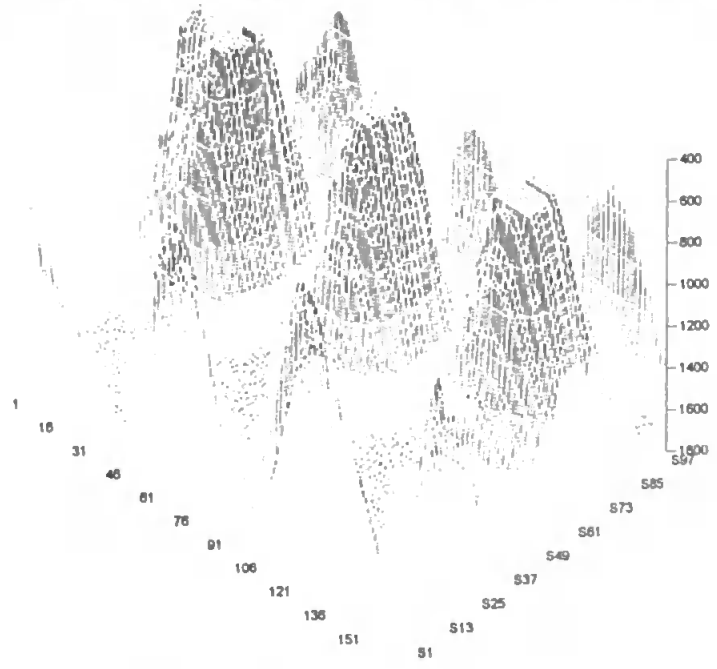

Figure 5.7 - A 3-dimensional horizontal intensity plot of a 2-dimensional scan with an un-tapered 10/125μm single-mode fibre across 10μm ϕ apertures back illuminated with white light (the centre of the apertures corresponds to the peaks of the intensity plots).

5.1.2 Discussion of SNOM/PSTM calibration procedure

The shape of the profile shown in Figure 5.2 is a combination of several factors. As described in Section 2.6 the end face of an optical fibre when scanned normal to an illuminating source will be exposed to a gradual increase in detectable light as the tip is gradually exposed to the illuminating source (Figure 2.14). In this particular case the fibre probe core is larger than the actual illuminating source (the square rim) and as a result will gradually detect the emitted light until a maximum is reached when the probe is central to the line source, before decreasing as it moves across to the opposite edge.

At the *1/e* point of maximum intensity the line width is 29.76μm (Figure 5.2). A similar scan with a smaller un-tapered 10/125μm single-mode fibre (Figure 5.3) produced a more pronounced square pulse effect and width of 29.86μm. The tip diameter used to scan the outer rim in Figure 5.3 is considerably smaller than the width of the illuminating source thus tending to decrease the dispersive effect associated with the large core fibre probe over such a small core.

The sectional analysis of the aperture in Figure 5.4 with an AFM (Figure 5.5) not only shows the width of an individual 10μm aperture as 9.922μm but also the metal and glass substrate have quite pronounced surface roughness.

The width of the nominal 10μm aperture in Figure 5.6 was measured graphically as 10.32μm @ *1/e* of the peak value with the inter-aperture spacing of 18μm. The dispersive square pulse effect of Figure 5.6 is similar in shape as Figure 5.2 This is due to the comparable size of the probe tip and the illuminating source (an individual aperture) as mentioned previously. A 3-dimensional plot of the aperture bearing surface is shown in Figure 5.7 of a raster scan of 30μm by 30μm.

Having established that the piezo-electric actuator 3-dimensional stage was accurate to within approximately ±1%, the experimental stages of the project could be undertaken with confidence.

5.1.3 Evanescent Field Measurements - I

Using the SNOM/PSTM system in the PSTM configuration, detection and confirmation of the evanescent field on the surface of the metal associated with SPR was investigated. The following section discusses the procedures used to detect and verify the presence of the SPW.

As shown mathematically in Section 3.2.2.2 and Figure 3.18, the introduction of the fibre probe into the SPR evanescent field modulates the exponential field in such a way that the maximum intensity occurs several hundred nanometers above the metal surface.

Evanescent field measurements were carried out on a number of non-apertured *Ag* devices. SPR was optimised for each of the individual metal devices. The fibre probe tip was centred on the illuminating spot of incident radiation and brought into contact with the surface of the device. The distance between the probe tip and the metal surface was increased incrementally and the resultant intensity recorded and displayed on a personal computer. Figure 5.8 shows the intensity profile on the surface of an *Ag* device under SPR as a function of vertical distance between the probe tip and the metal surface. Several scans of the same point on the substrate were made at different incident angles of the laser radiation. Figure 5.9 shows an experimental comparison between the intensity profile at SPR on a plain *Ag* surface and 1° > SPR as a function of the distance between the probe tip and the metal surface.

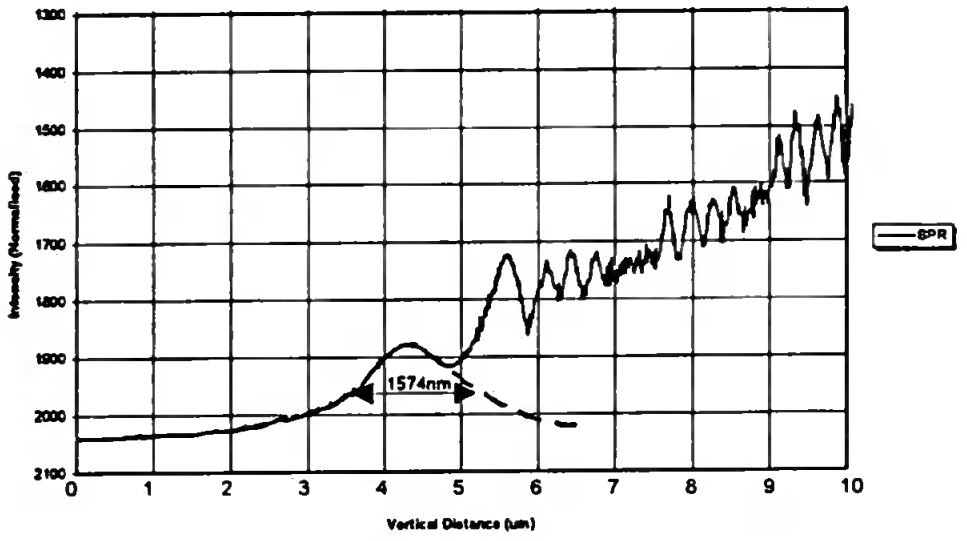

Figure 5.8 - Vertical scan of the evanescent field intensity normal to the active surface of an *Ag* coated device (n_1=1.517, $\hat{n}_2 = \sqrt{-18.3 + j0.67}$ @ 632.8nm, n_3=1) with a 10/125μm un-tapered single-mode fibre under SPR.

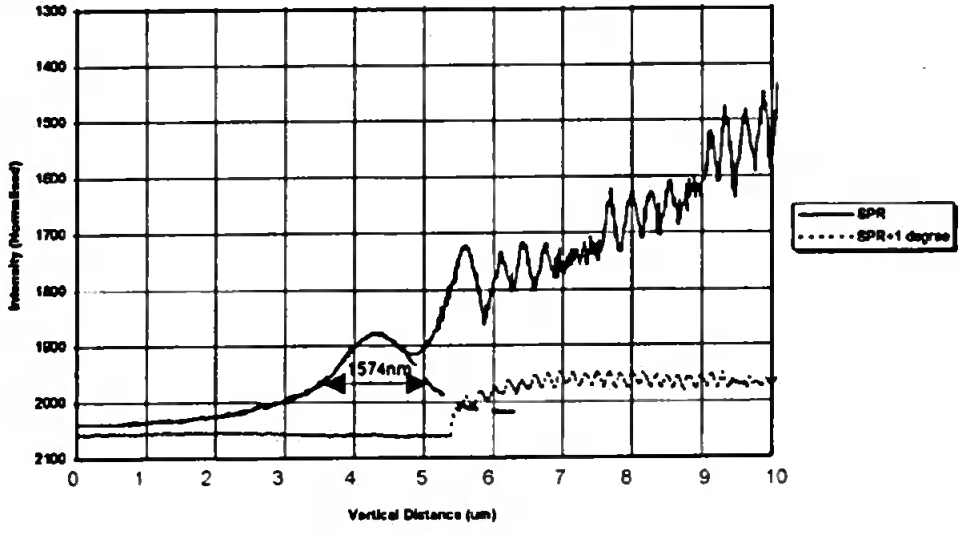

Figure 5.9 - Comparison between vertical scans of the evanescent field intensity normal to the active surface of an *Ag* coated device (n_1=1.517, $\hat{n}_2 = \sqrt{-18.3 + j0.67}$ @ 632.8nm, n_3=1) using a 10/125μm un-tapered single-mode fibre at SPR and 1° > SPR.

5.1.4 Discussion of Evanescent Field Measurements - I

If the profile of the initial peak in Figure 5.8 (within the near-field of the surface) is made symmetrical its width is approximately 1600nm, similar to the calculated profile shown in Section 3.2.2.2, Figure 3.18.

The intensity fluctuations at heights above that of the initial evanescent extension, it is thought, are due to interference from the dipole (fibre probe) and its mirror image in the ideal conducting metal surface of the sample. Work carried out by Strutt (1929), Sommerfeld and Renner (1942), Morawitz (1969), Change *et al.* (1975) and Lukosz *et al.* (1977) all report this effect in the far-field especially if the sample is an ideal conductor and the dipole is vertical. The periodicity of these oscillations are approximately 600nm (approximately the wavelength of the incident radiation), suggesting that they are indeed the resultant of interference fringes generated from probe/sample interactions. The slight noise intrusive on the fringes may be due to surface roughness resulting in surface scatter of the SPW.

Although separated by only 1° the secondary plot in Figure 5.9 shows no resonant peak characteristic of a SPR evanescent field in Figure 5.8. At angles greater than the SPR angle ($\theta > \theta_{SPR}$) total internal reflection occurs producing an evanescent wave at the interface. Again the intensity fluctuations seen in Figure 5.9 have a period of approximately 600nm suggesting interference fringes generated from probe/sample interactions.

Note that the magnitude of the interference fringes is much smaller than the SPR scatter pattern, confirmation of acute surface plasmon resonance.

5.1.5 SPW's at Refractive Index Discontinuities

INTRODUCTION

The investigation into the effects of a SPW at a refractive index discontinuity was carried out in order to understand further the results of the studies carried out by Dr. Al-shukri and Dr. Carr at CAMR. During these initial studies at CAMR it was demonstrated that the 100nm diameter apertures etched in the surface of a SPR sensor acted as points of scatter of the SPW which were very sensitive to local perturbations of the refractive index. These experiments involved the use of a crude SPR configuration whereby surface plasmons could be excited in the metal surface of a device, similar to the ones used in this project. Using a conventional optical microscope and visualising the resonant surface from above, the presence of antibodies (20nm ϕ) attached to a gold label (70nm ϕ) entering an aperture could be visualised. This posed the question of why apertures etched in an otherwise opaque resonant layer were so sensitive to local perturbations. These initial results were the basis for the investigation of SPW's at refractive index discontinuities as possible detectors of minute local refractive index disturbance.

Maradudin *et al.* (1983), Jamid *et al.* (1995), Stegeman *et al.* (1981) all describe the reflection and transmission of a SP encountering a dielectric barrier between two surface active dielectric media, i.e. a surface active medium is one whose dielectric constant is negative. It was hoped that further consideration of this aspect would be of value in explaining results obtained during initial studies at CAMR in which an antibody of approximately 20nm attached to a 70nm gold particle on entering the aperture caused an increase in intensity radiating from the aperture, detectable in the far-field.

This next section describes the experimental analysis carried out in order to quantify these conditions. The process employed was experimentally to characterise and establish theoretically the intensity profile of a series of large apertures (10-1μm in diameter) with

the use of the SNOM/PSTM. Unfortunately, due to time constraints and resources it was not possible to proceed beyond the point of 1μm diameter apertures.

Initial studies of the aperture bearing surface of the metalised substrate were carried out using an un-tapered 10/125μm optical fibre in 'constant height' mode. The sensing of the evanescent field in the PSTM configuration provided a mechanism by which the height of the probe above the metalised substrate could be monitored. The fibre was then brought to within the near-field of the active surface with the use of piezo-electric actuators. The SPW propagating within the metal, when interrupted by an abrupt refractive index discontinuity such as an aperture etched in the metal film could no longer sustain a non-radiative surface plasmons and consequently coupled energy back into radiation detectable in the far-field (Figure 5.10).

In each of the following intensity profiles the probe was scanned from right to left. In Section 2.3 the process by which the SPW is diffracted by the refractive index discontinuity is described. In order that the intensity polar plot of the diffracted wave at the refractive index discontinuity could be obtained a fibre probe was initially scanned over the trailing edge of a device in several different orientations, i.e. normal to the plane of propagation, at 45° to the plane of propagation and also in the plane of propagation of the SPW, as shown in Figure 5.11.

Figure 5.12-15 are scans across an *Ag*/air refractive index discontinuity at normal incidence, at 45° to the normal, in the plane of propagating and at normal incidence to an air/*Ag* refractive index discontinuity respectively. Figure 5.16 also is a horizontal scan of a 30μm wide outer rim of the *Cr* device previously described in experimental Section 5.1.1, under SPR. With a measurement of 30.87μm between the centres of the intensity peaks.

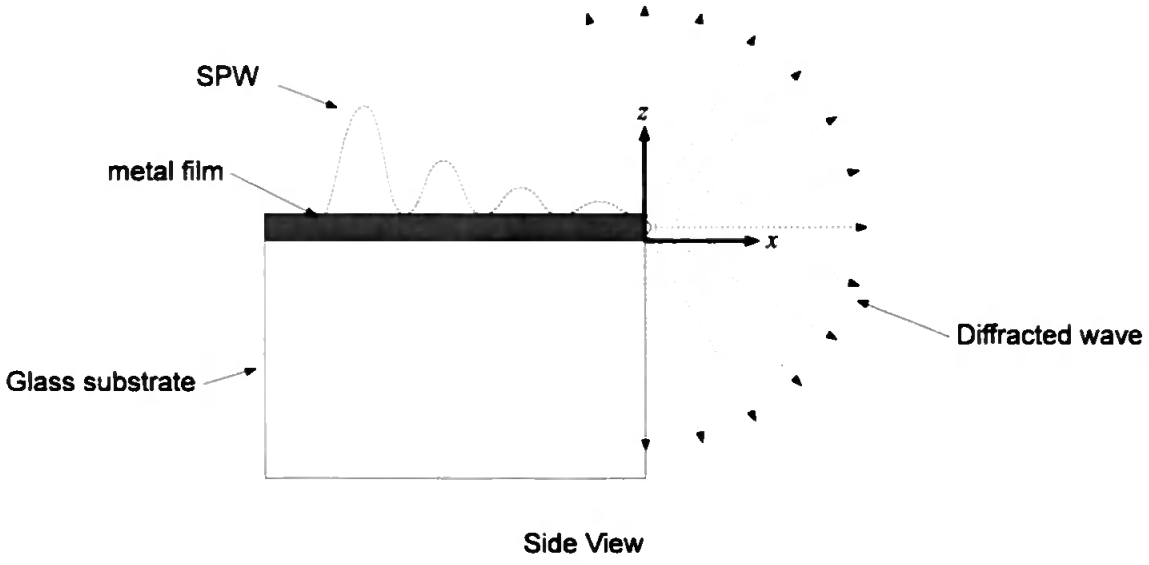

Figure 5.10 - Schematic of a SPW incident on a metal/air refractive index discontinuity.

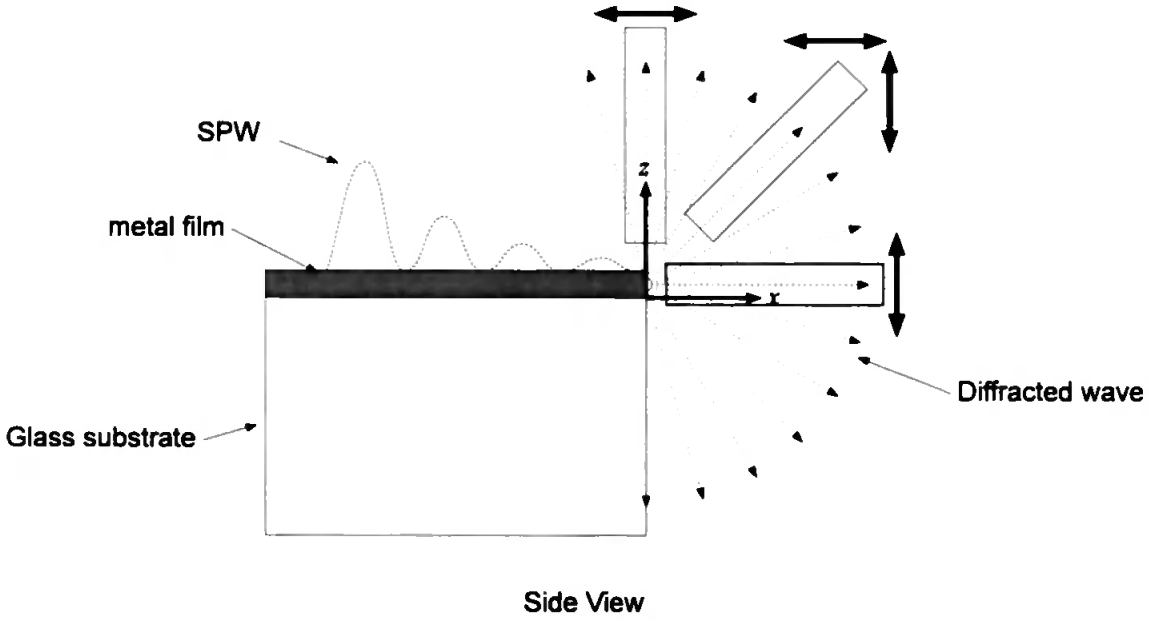

Figure 5.11 - Schematic of probe orientation during various scans of a SPW incident on a metal/air refractive index discontinuity.

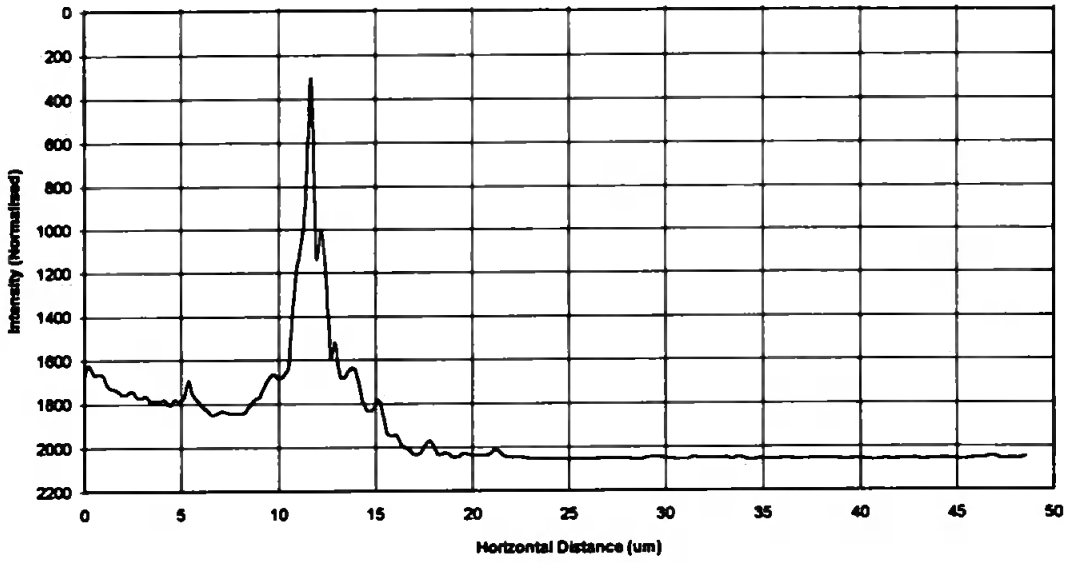

Figure 5.12 - Horizontal scan normal to a SPW incident on an *Ag*/air refractive index discontinuity ($\hat{n}_{Ag} = \sqrt{-18.3 + j0.67}$, n_{air}=1) *(SPW propagation from right to left).*

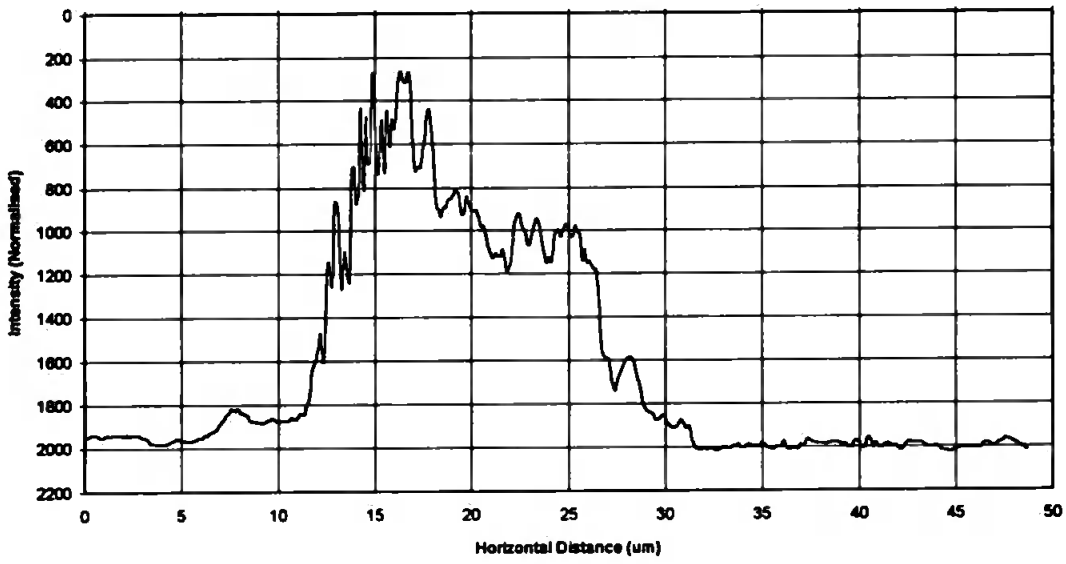

Figure 5.13 - Horizontal scan at 45° to a SPW incident on an *Ag*/air refractive index discontinuity ($\hat{n}_{Ag} = \sqrt{-18.3 + j0.67}$, n_{air}=1) *(SPW propagation from right to left).*

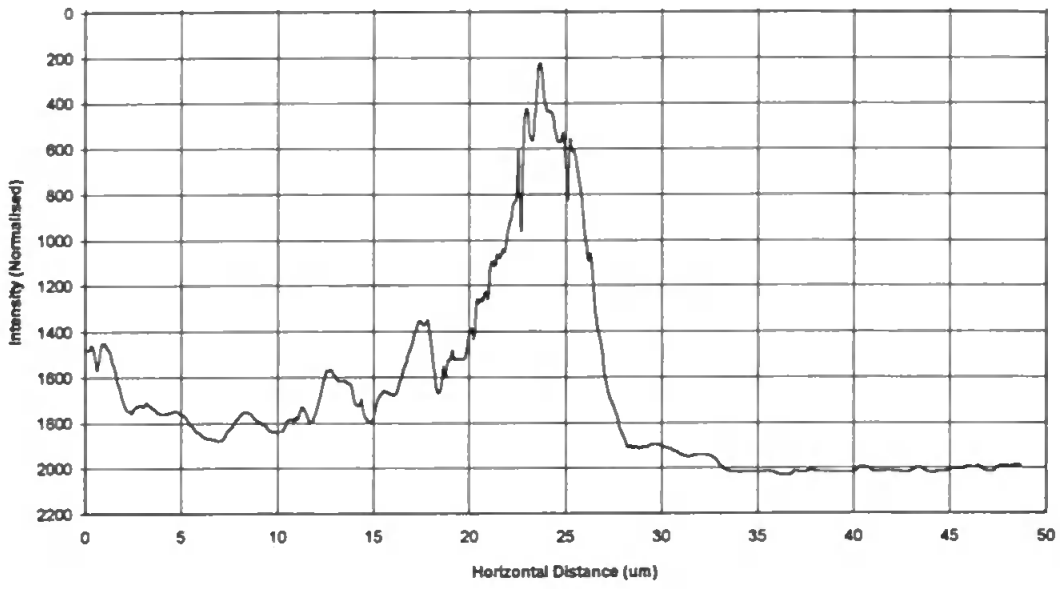

Figure 5.14 - Vertical scan in the plane of propagation of the SPW incident on an *Ag*/air refractive index discontinuity ($\hat{n}_{Ag} = \sqrt{-18.3 + j0.67}$, n_{air}=1) *(SPW propagation from right to left).*

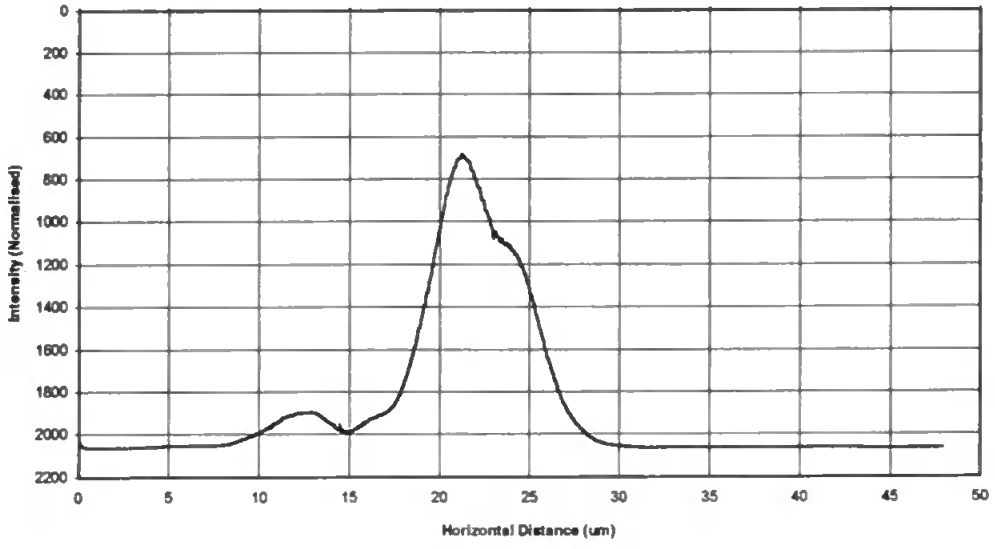

Figure 5.15- Horizontal scan normal to a SPW incident on an air/*Ag* refractive index discontinuity (n_{air}=1, $\hat{n}_{Ag} = \sqrt{-18.3 + j0.67}$) *(SPW propagation from right to left).*

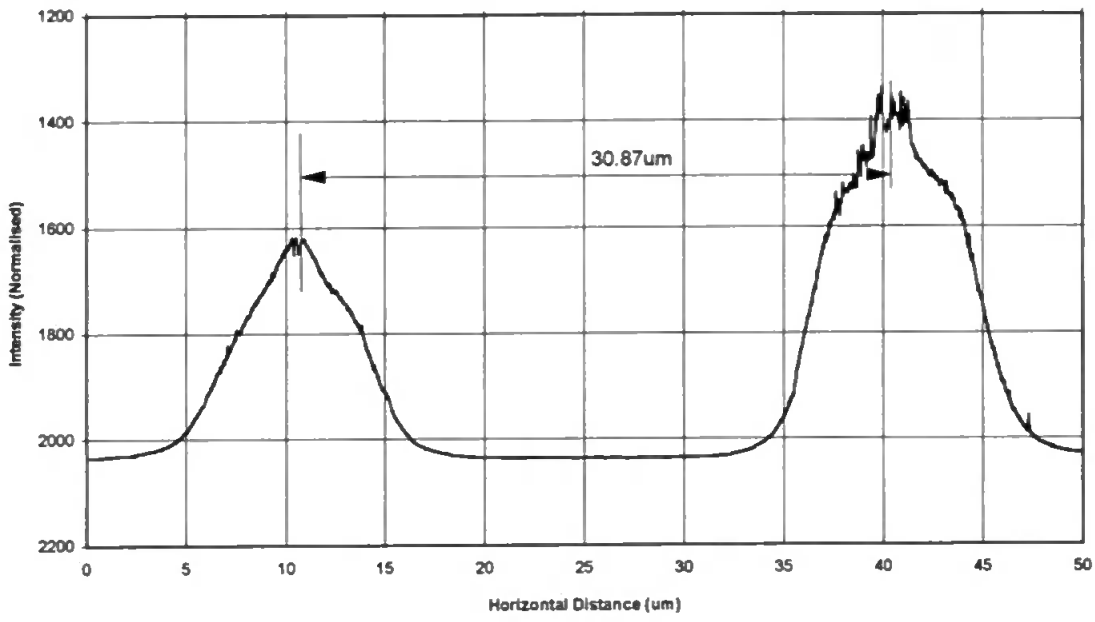

Figure 5.16 - Intensity scan with un-tapered 10/125μm single-mode fibre of the *Cr* device over the 30μm etched square ring under SPR illumination (n_1=1.517, $\hat{n}_2 = \sqrt{-6.274 + j35.853}$, n_3=1) *(SPW propagation from right to left).*

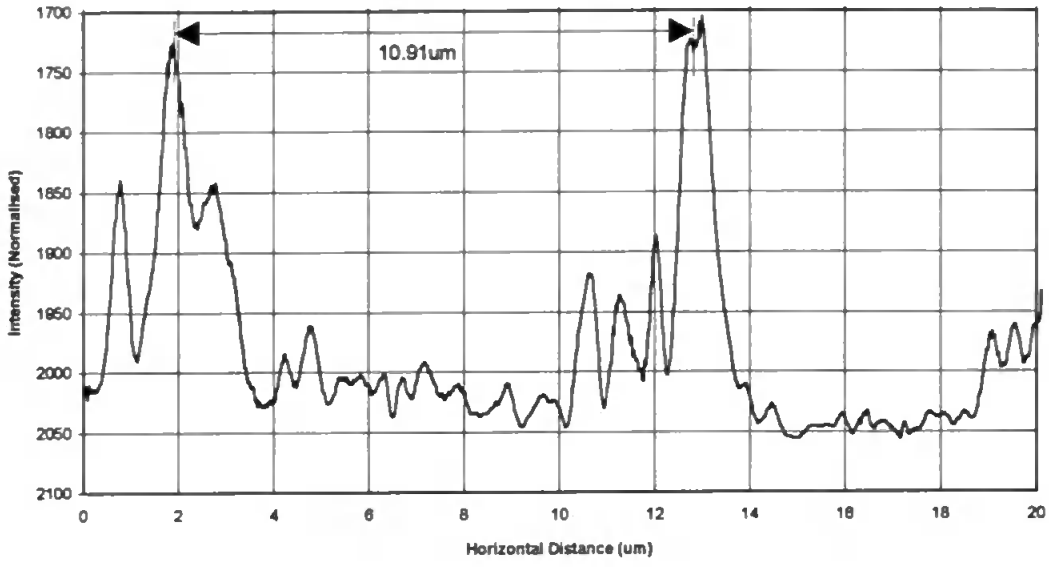

Figure 5.17 - Horizontal scan of a 10μm diameter aperture of a *Cr* device under SPR (n_1=1.517, $\hat{n}_2 = \sqrt{-6.274 + j35.853}$, n_3=1) *(SPW propagation from right to left).*

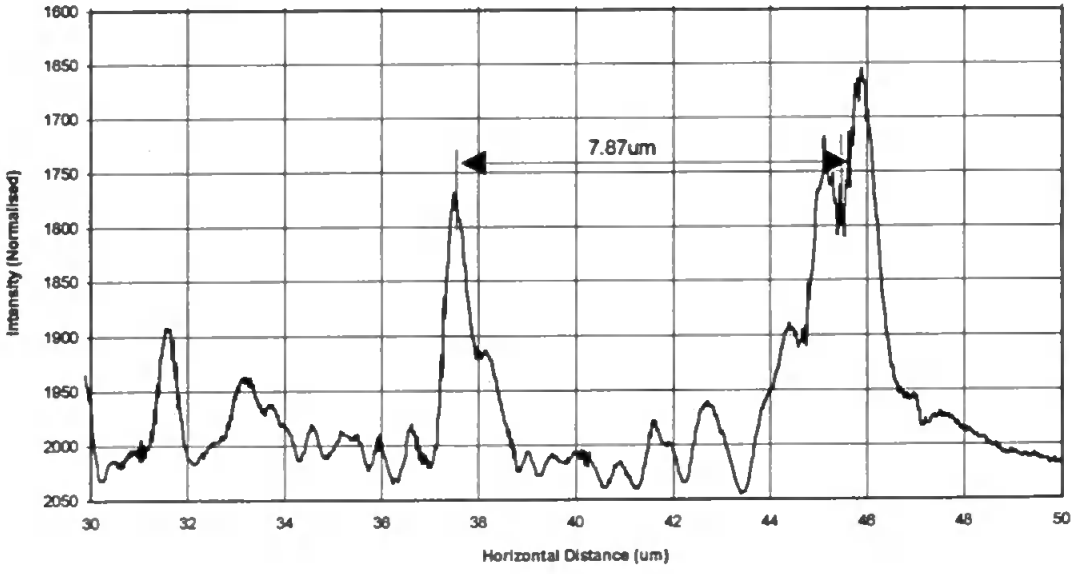

Figure 5.18 - Horizontal scan of a 7μm diameter aperture of a *Cr* device under SPR (n_1=1.517, $\hat{n}_2 = \sqrt{-6.274 + j35.853}$, n_3=1) *(SPW propagation from right to left).*

The fine detailed behaviour of the optical field around the edge of and within the apertures necessitated the use of a small diameter sensing probe. A 10/125μm single-mode fibre was tapered down by the procedure described in Section 3.3.1, to a outer cladding diameter of 11μm (core diameter 880nm) and coated with an external opaque cladding of 125nm of *Al*. This formed a highly selective detector. Horizontal scans across the centre of 10μm, 7μm, 3μm and 1μm diameter apertures respectively were made under SPR generated conditions and are shown in Figure 5.17-20. Prominent intensity peaks are visible at the metal/air refractive index discontinuities with slightly smaller peaks at the opposite air/metal interface. As the apertures decrease in size the distance between the discontinuity intensity peaks at each side of the apertures also decreases with the intensity levels remaining relatively stable. Figure 5.21-24 are raster scans of 1μm, 3μm and 7μm diameter apertures respectively under SPR conditions using the tapered probe described earlier.

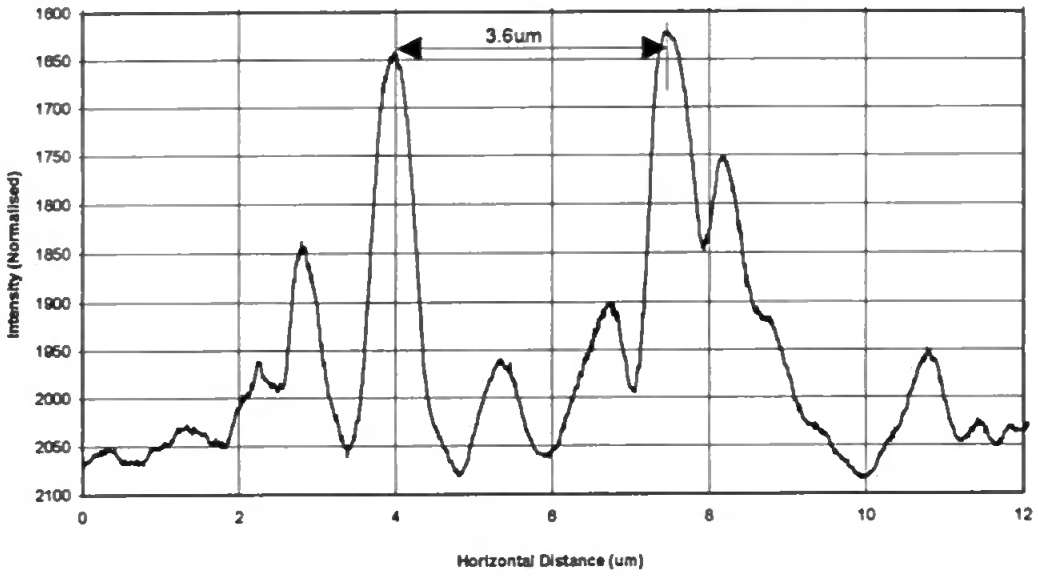

Figure 5.19 - Horizontal scan of a 3μm diameter aperture of a *Cr* device under SPR (n_1=1.517, $\hat{n}_2 = \sqrt{-6.274 + j35.853}$, n_3=1) *(SPW propagation from right to left).*

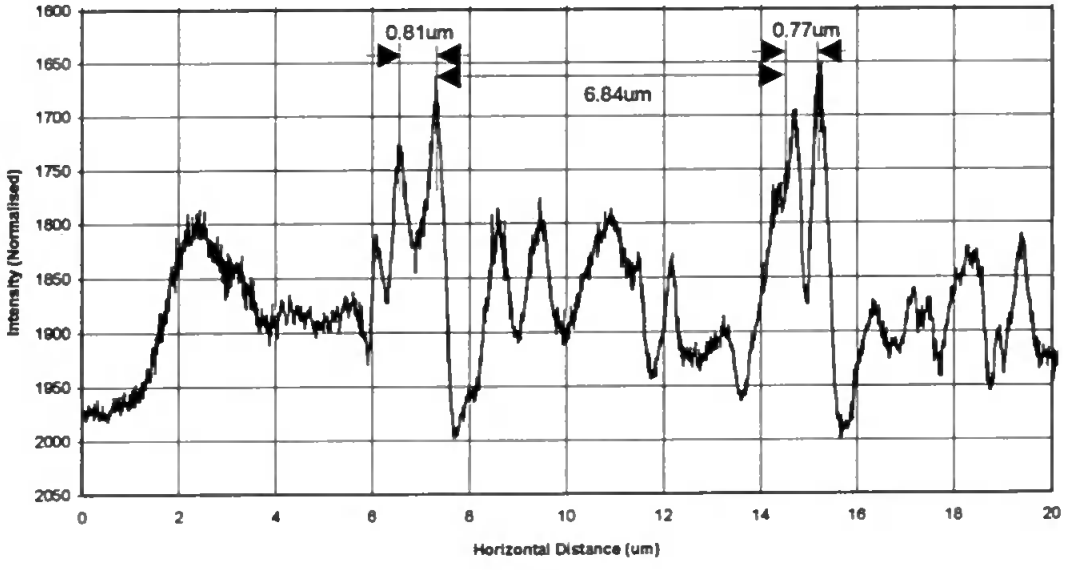

Figure 5.20 - Horizontal scan of a 1μm diameter aperture of a *Cr* device under SPR (n_1=1.517, $\hat{n}_2 = \sqrt{-6.274 + j35.853}$, n_3=1) *(SPW propagation from right to left).*

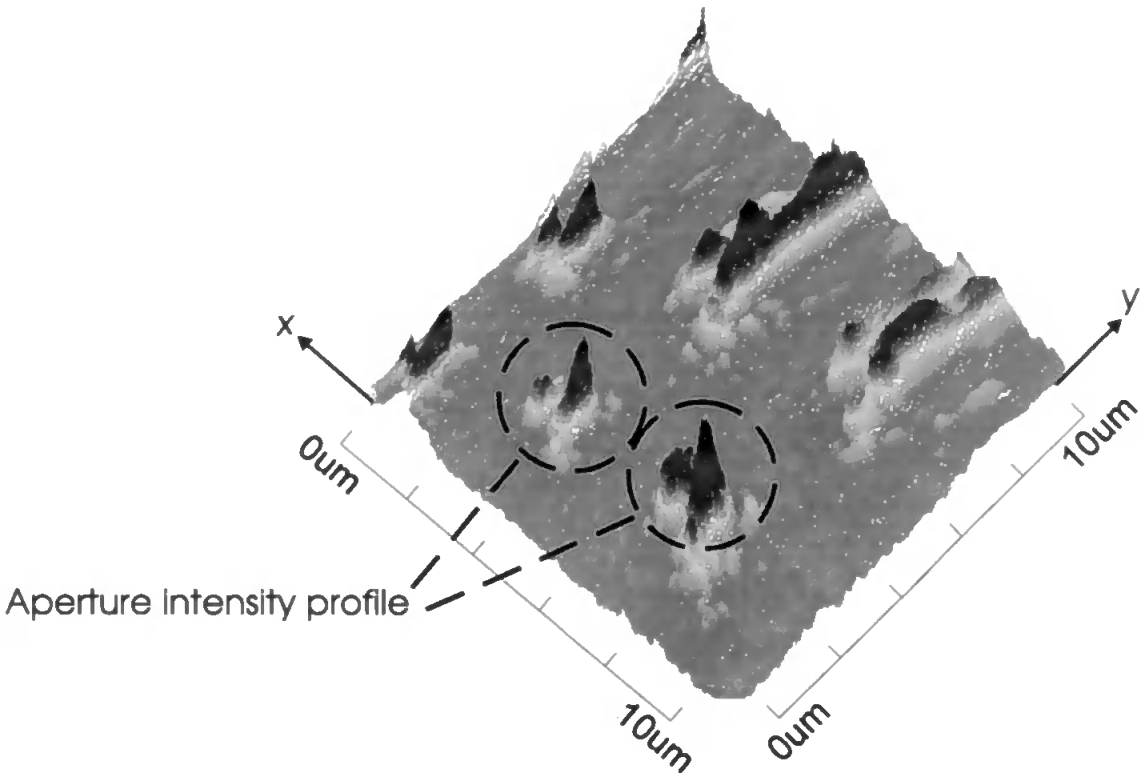

Figure 5.21 - A 400 x 400 point raster scan of a 1μm diameter *Cr* device matrix under SPR (n_1=1.517, $\hat{n}_2 = \sqrt{-6.274 + j35.853}$, n_3=1) *(SPW propagation in x-direction).*

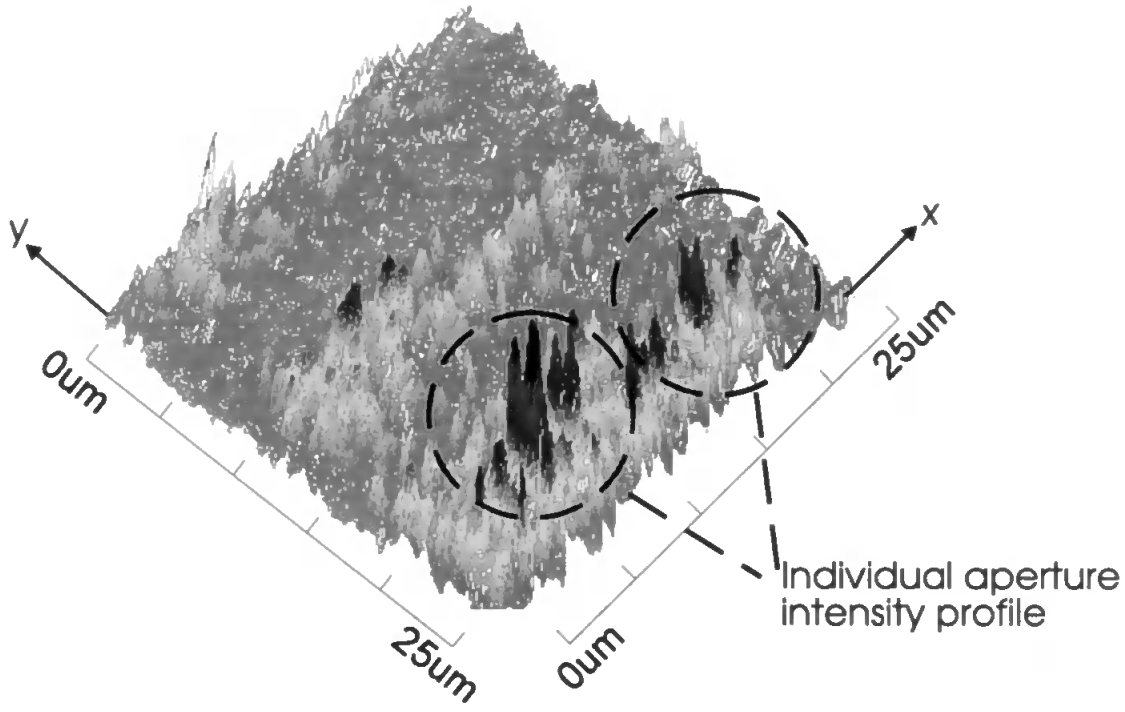

Figure 5.22 - A 400 x 400 point raster scan of a 3μm diameter matrix under SPR (n_1=1.517, $\hat{n}_2 = \sqrt{-6.274 + j35.853}$, n_3=1) *(SPW propagation in x-direction).*

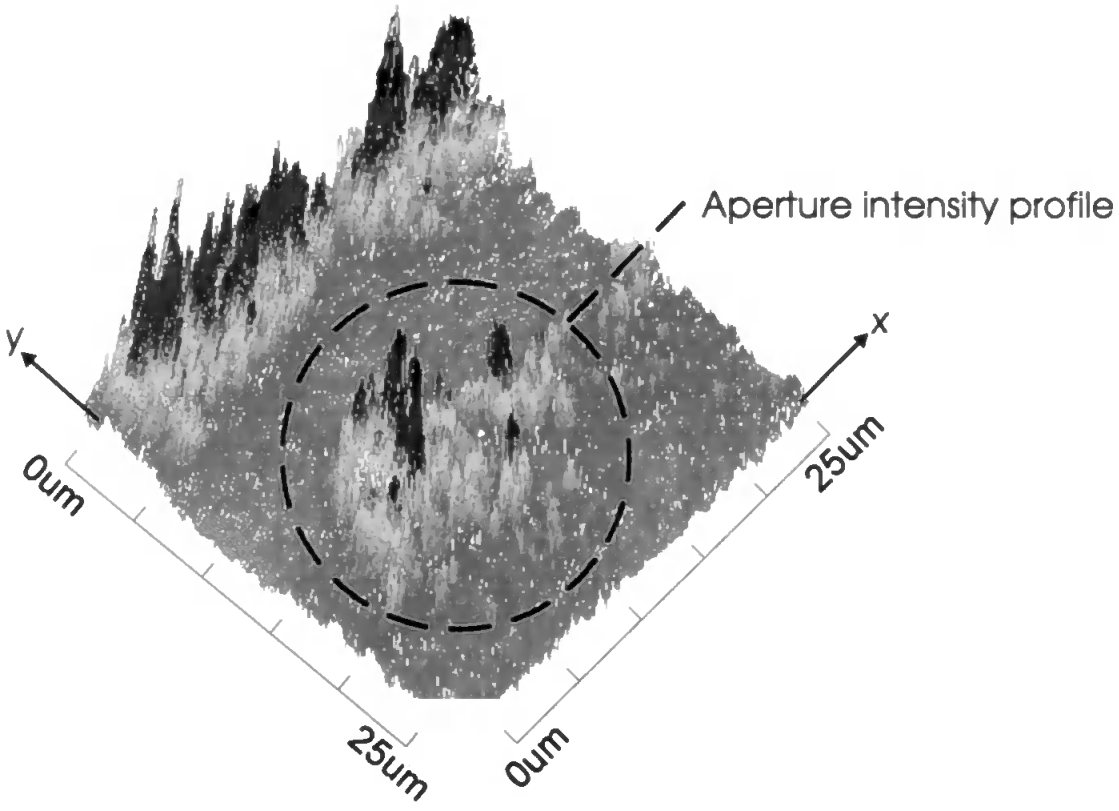

Figure 5.23 - A 400 x 400 point raster scan of a 7μm diameter matrix under SPR (n_1=1.517, $\hat{n}_2 = \sqrt{-6.274 + j35.853}$, n_3=1) *(SPW propagation in x-direction).*

5.1.6 Discussion of SPW's at Refractive Index Discontinuities

Stegeman *et al.* (1981) and Agranovich *et al.* (1981) describe methods of calculating the reflection and transmission of the SP's at an interface. Agranovich *et al.* describe the coefficients as modifications on Fresnel's formulae whereas Stegeman *et al.* use the term normal-mode analysis to describe their analysis of the system. None of these papers however, address the problem of the polar diagram of the diffraction of the wave as it is transformed into a bulk radiative wave at the metal/air interface.

Although the magnitude of the polar diagram may be calculated the experimental verification is somewhat more difficult. The polar plots can only give a relative description of the magnitudes associated with the diffraction as it is extremely difficult to ascertain with any certainty the actual coupling efficiency of the SPR system due to the processes involved in the transformation of incident laser light into SP's and its associated losses. Maradudin *et al.* (1983) calculated the reflection and transmission of a SP at an interface assuming that the geometrical and material discontinuities are of a finite extent in the direction of propagation. Stegeman *et al.* (1981) and Agranovich *et al.* (1981) assume the geometrical and material discontinuities are of a infinite extent. Jamid *et al.* (1995) have calculated the diffraction of the surface plasmon in an abruptly terminated dielectric-metal interface by the mathematically intensive Method of Lines. However they do not attempt to verify their theories by actual experimental analysis.

Here the relative polar diagrams have been mapped and compared to that of the Fraunhofer diffraction of a wave through a slit of similar dimensions as the metal film. Figure 5.12-14 shows that the intensity profiles of the diffracted SPW at an abrupt interface are all of similar relative magnitude. Figure 5.13, the diffracted wave at 45° to the normal, is wider than that detected normal to and in the plane of propagation, Figure 5.12 and Figure 5.14 respectively. This closely matches the predicted shape discussed in Section 2.3.1. This experimental analysis of the diffraction profile demonstrates that,

similar to Fraunhofer's diffraction theory, as discussed in Section 2.3, the intensity polar diagram of the diffracted SPW at a metal/air refractive index discontinuity is of a uniform nature further reinforcing the description of the diffraction model of Fraunhofer's diffraction theory of light through a thin slit in a non-conducting screen. The size and shape of the tip of the probe is the determining factor of the resolution of the scanning device. In this instance with an inner core diameter of 880nm and an outer cladding diameter of 11mm it is debatable whether or not the core/cladding refractive index difference is sufficient to produce a guiding mode in the fiber while using 632.8nm wavelength light. It is thought that as the outer cladding surface of the taper was coated with 125nm of *Al* the fibre probe was still able to guide light within the taper length of the fibre where upon it could be contained within the fibre core and propagate in a conventional manner to the detector.

As described by the theory in Section 2.3.1 the magnitude of the evanescent wave set up on the bare glass surface of the prism is approximately a quarter that of the SPW in the metal film. Shown in Figure 5.15 the normalised intensity detected at the air/metal interface is much smaller in magnitude than that of the SPW diffraction at the metal/air interface discontinuity. Although the comparisons between the refractive index discontinuities shows that the magnitude of the detected intensity of the metal/air discontinuity is not a factor of 4 larger than that of the air/metal discontinuity the air/metal detected intensity is substantially smaller. Figure 5.16 demonstrates this result further showing the intensity plot across the square rim of the *Cr* coated device in Figure 5.1 with the magnitude at the air/metal interface (left hand peak) less than the metal/air interface. The separation of the peaks in Figure 5.16 occur at 30.87μm with no direct indication of the interference between the two edges. It is to be expected therefore, that diffraction at each edge of the apertures act independently at large separations ($d \gg \lambda$).

It can be seen in Figure 5.17-20 that although definite intensity peaks exist at the edges of the aperture there are also intensity fluctuations from the metal surface and the prism

surface within the apertures. These, are assumed to be due to roughness variations in the associated surfaces scattering the evanescent fields. As seen in Figure 5.5 the surface roughness is quite substantial at the nano-scale level with large roughness variations on the surface of the substrate, i.e. within the aperture.

As can be seen from Figure 5.17-20 as the diameter of the apertures decrease, the distance between the intensity peaks, associated with the separate refractive index discontinuities at each edge of the apertures, converge. In the intensity profiles associated with apertures of 10μm, 7μm and 3μm, two distinct intensity peaks are evident without actually combining. It can be seen for a 1μm diameter aperture, Figure 5.20, that the individual peaks becomes increasingly more difficult to separate. It is therefore assumed that the individual peaks at the edges of apertures less than 1μm diameter will effectively merge under SPR conditions. Maradudin *et al.* (1983) suggests that the maximum in the transmission coefficient occurs for gap lengths, between the active media, that are integer multiples of half the wavelength of the bulk waves in the gap region, suggesting similarities between these effects and those in Fabry-Perot interferometers and thin film interference filters. It is probable therefore, that the situation at CAMR, which produced these initial results, may have met the criterion for such an oscillatory effect resulting in a resonant cavity effect.

In Section 2.4 the refraction associated with a SPW incident on a circular refractive index discontinuity (aperture) is described in a similar fashion as Agranovich *et al.* (1982). It is can be seen using this theory that total internal reflection of the incident radiation takes place at a distance approximately one quarter of the radial distance from the centre of the circumference, i.e. literally all the incident radiation is reflected at the interface and contained within the incident metal film. Only a small section of the aperture (25% either side of the central section) is therefore capable of producing diffraction of the incident radiation with the remainder of the radiation being reflected from the interface. Figure 5.21-23 shows 3-dimensional intensity raster scans of

individual aperture matrices under SPR conditions. Although it is hard to visualise an individual aperture in any of the plots, individual intensity peaks associated with the edges of the apertures are evident. The distances between these peaks show good correlation to Figure 5.20, Figure 5.19 and Figure 5.18 respectively. An intensity peak occurs at the centre of the circumference of the aperture where the SPW is effectively at normal incidence to the aperture circumference. As shown in the 2-dimensional plots of Figure 5.17-20 the secondary intensity peak, occurring at air/metal interface of the aperture, is slightly smaller than the primary peak at the metal/air interface. This aspect of the diffraction intensity profile also appears in the 3-dimensional plots (Figure 5.21-23). The magnitude of the secondary peak is noticeably smaller than that of the initial peak, but nevertheless is still visible.

At these dimensions, i.e. > 1 micron, the radiative effect of the apertures, although they look circular in the far-field, are actually a 'ring fire' effect occurring at the central section of the apertures in the direction of propagation. Only the leading and trailing edges of the apertures produce this effect and thus are responsible for the fluctuating light scatter from the interactions of the cells and the radiative apertures. The outer sections of the circumference of the apertures (beyond 25% of the radial distance) do not radiate the energy and thus only produce intensity fluctuations associated with non-radiative evanescent field/cell interactions. These fluctuations are much smaller than the radiative field/cell fluctuations and it is probable therefore that the 2-dimensional aspect of a large apertured device is much more sensitive in the direction of propagation of the SPW as orthogonal to the direction of propagation in the plane of the metal.

Chapter 6

6. CONCLUSIONS

6.1 BIOLOGICAL STUDIES

Initial experiments, carried out by our collaborators Drs R. Carr and S. Al-shukri at CAMR, Porton Down, appeared to show that the use of apertures etched in a SPR metal surface produced a highly sensitive dielectric monitor, i.e. sensitive to very small changes in the refractive index of the micro-environment adjacent to the aperture. This was proposed as being of potential value in the development of very sensitive probes of dielectric particulates of sub-micron dimensions, i.e. biological macromolecules and supramolecular structures. This initially lead us concentrate our resources on the development of a device consisting of a surface matrix of apertures 10μm and 1μm in diameter, easily fabricated at the University of Plymouth. The use of aperture arrays, to achieve the required 2-dimensional spatial sensitivity initially provided very encouraging results as described in Section 4.1.

Although recognised for their spatial sensitivity the resultant illumination effect of these relatively large apertures created a high 'D.C.' noise level much larger than that of the SPW/cell interaction signal. Although the resultant noise effectively suppressed any information on the vertical aspects of the sensor, provided by the evanescent field, the regularity of the aperture matrix and the sensitivity to dielectric change of the region adjacent to the apertures provided valuable information, in the plane of the sensor surface, of cell movement in real time. The protrusion of the membrane lamellipodia or filopodia at the edges of the cell extremities, used to produce a mechanism whereby it can adhere and translocate, disturbs the optical characteristics of the area in the immediate vicinity of the aperture as it traverses the sensor surface. This is shown as intensity fluctuations due to the disturbance of the SPW. The density of the aperture matrix and the dimensions of the individual apertures produce a highly accurate record of a cell's lateral movement which can be assembled over a short period of time (2-3 minutes) with a conventional CCD camera and video recorder. A considerable improvement over traditional microscopy techniques [Curtis (1988)].

Detection of minute cell movement on the plain metal film was similarly accomplished utilising the Kretschmann/Raether SPR configuration and viewing the sample from directly above. Employing the dark background of the virtually opaque plain metal film and the evanescent field associated with SPR, it was possible to visualise minute movement within the cell cytosol or membrane ruffling as intensity fluctuations detectable in the far-field. Confirmation of the extent of this effect was shown to occur within the near-field ($z < \lambda$) of the active metal surface for an Ag device (Section 5.1.3) where the SPW extended exponentially to approximately 450nm. This is less than the wavelength of the incident radiation and it is reasonable to assume therefore, that this minute cell movement is beyond the optical limit of conventional microscopy [Rayleigh (1879)], (Section 3.2.1). Understanding cell migration and movement is vitally important to being able to discover how cancer cells are able to continue dividing and why they abnormally migrate. Therefore an understanding of the mechanism by which cell

attachment to matrix proteins occurs is of fundamental benefit to the understanding of cancerous cell migration throughout the human body [Hood *et. al.* (1995)]. The ability to visualise movement of these dimensions will provide an additional increase to the understanding of cell biology and chemotaxis to stimuli.

Visualisation of the cell contact points from above the sample, through the medium, demonstrated whole cell movement and precise points of contact with the active surface of the device. It is known that the attachment points of livings cells do protrude from the underside of the cells producing points of adhesion from which the cell can produce forward movement [Cheng (1992), Goldmann *et al.* (1995), Alt *et al.* (1995)]. It is unlikely that these fluctuations are the cause of intra-cellular movement of cell cytosol or cell organelles as the regularity of the movements suggest a rhythmical pulsation of cell tissue entering and exiting the evanescent field. Supramolecular structures of cell organelles at these dimensions would move with Brownian motion, i.e. random movement with a half life of less than 0.1 second, and would not produce rhythmical pulsations as witnessed in these experiments. It is thought that the points of contact between the cell and active SPR surface, seen as explicit points of intensity maxima, were caused by the cell's minapodia actually touching the active SPR surface. Although no confirmation of the cells actual points of contact was achieved, overall confirmation of the presence of the these adherent cells was obtained by washing and 'blue staining' adherent cells for visualisation under conventional white light microscopy. Epi-illumination of the cells while actually under SPR illumination, demonstrated their presence, although not their discrete attachment points. As discussed in Section 4.2.3 the intensity fluctuations may be the result of the cell's microvilli and dimples touching the SPR surface. Oberleithner *et al.* (1993) has confirmed the presence of these structures with the use of an AFM. If it is these particular structures responsible for these images the resolution of this device is much beyond the wavelength of light and thus conventional light microscopy.

It is therefore concluded that this device is capable of visualising rapid real-time movements of living cells. Images obtained suggest that the under-surface of cells interacts with the SPR field through cell extensions. The rhythmical and alternating movement of the secondary emission foci suggest that this is an active cell-controlled movement involving the cytoskeleton. The precise nature of the cytoplasmic extensions is not as yet known. Nevertheless, the device has revealed novel patterns of cell movement which, to our knowledge through review of the relevant literature, have not been described before.

6.2 SURFACE PLASMON RESONANCE CONCLUSIONS

It was confirmed experimentally that the properties of the surface plasmon field on the surface of the devices did behave as described by the theory of the transmission of radiation through a multi layer system, Section 2.1. With the use of a combinational SNOM/PSTM this was validated experimentally to extend to approximately 400nm above the SPR surface of an *Ag* device - in direct agreement with that calculated in theory.

It could therefore be assumed that any visualisation of a cell above the active SPR surface was a direct result of the cell interacting with the otherwise non-radiative SPW field. It was confirmed that the SPW extended in an exponential nature above the surface of the device, Section 5.1.3. Thus, it is reasonable to presume that observations of increases in intensity fluctuations were a direct result of the biological cell moving closer to the active surface of the device. The visualisation of the cell in the otherwise evanescent field was modelled by a method called Rayleigh-Gans-Debye (RGD) Scattering, Section 2.7.3. Knowing that the cell actually projects leading lamella from its cortex to attach onto the surface [Stossel (1994), Ambrose *et al.* (1977)] assumptions were made that these leading lamella are similar in profile to a known pre-modelled physical structure, a cylinder, Figure 2.20. Mathematically modelling the situation with a 400nm diameter thin rod of 400nm length, the depth of the evanescent field, the intensity of the orthogonally scattered field is 13.73% of the incident evanescent field for TM polarised radiation.

Intensity maxima occurred as the cell made contact with the active SPR surface thus altering the coupling characteristics at that particular point, Section 2.7.1. This section describes the processes involved in the visualisation of the cell as it firstly interacts with the evanescent field and the visualisation of the actual contact points the cell makes with

the active SPR surface. As the cell actually touches the surface it alters the coupling conditions at that point and the incident laser radiation is de-coupled through the metal film and detected in the far field. An increase of approximately 400^9 times the detectable intensity is indicated.

While several researchers have calculated the reflection and transmission of SP at refractive index discontinuities, they do not attempt to verify their theories by actual experimental analysis. Maradudin *et al.* (1983) calculated the reflection and transmission of a SP at an interface assuming that the geometrical and material discontinuities are of a finite extent in the direction of propagation. Stegeman *et al.* (1981) and Agranovich *et al.* (1981) assume the geometrical and material discontinuities are of an infinite extent. Jamid *et al.* (1995) have calculated the diffraction of the surface plasmon in an abruptly terminated dielectric-metal interface by the mathematically-intensive Method of Lines. It was the intention of this research to demonstrate experimentally the near-field characterisation of the radiative and non-radiative fields on this device. Experimental characterisation of the aperture-bearing surface, by means of a SNOM/PSTM device showed that the edges of the larger apertures ($\phi \gg \lambda$) acted as discrete refractive index discontinuities to the incident SPW, Section 5.1.5. This abrupt discontinuity produced diffraction of the incident SPW which was experimentally demonstrated and shown to be similar in profile to that suggest by Fraunhofer's diffraction theory of incident light through a thin slit in a non-conducting screen, Section 2.3.2. As the criteria of Fraunhofer's diffraction theory of incident light through a thin slit in a non-conducting screen are fulfilled in this instance a comparison between this theory and a SPW propagating in a metal thin film can be drawn [Jenkins & White (1965)]. With the use of a metal coated tapered fibre producing a highly spatially selective SNOM, scanning of the edge of the aperture, in several orientations, revealed an intensity profile at the metal/air interface in agreement with that suggested by Fraunhofer's diffraction theory, i.e. a uniform diffraction polar diagram, Figure 2.9.

With the use of a metal coated tapered fibre to produce a highly spatially selective SNOM, scanning of the trailing edge of the aperture (air/metal interface), in several orientations, revealed an intensity profile in agreement with that suggested by Fraunhofer's diffraction theory. It was shown that a slightly smaller intensity evanescent wave is produced between the leading and trailing edges of the aperture when the laser radiation, at the SPR angle (θ_{SPR}), at the glass/air interface was incident at an angle greater than the critical angle (θ_c) for such a system due to the fact that no evanescent wave enhancement is resultant from surface plasmon resonance within the aperture. The refractive index discontinuity of the air/metal interface resulted in diffracting/scattering the evanescent wave at this point. The diffraction characteristic of this discontinuity were shown to behave similarly to the metal/air interface discontinuity but with a smaller detectable intensity peak, Section 5.1.5.

As it was the intention of these experiments to characterise the intensity profile associated with apertures, as refractive index discontinuities, and thus attempt to formulate a description of the events taking place when a SPW is incident on very small apertures ($\phi \ll \lambda$) the characterisation of the diffraction of the SPW at the individual discontinuities of the large apertures presented a valuable insight into the phenomena responsible for the effect first seen at CAMR, Section 5.1.5. Due to the investigation of numerous apertures it was shown experimentally that as the diameter of the apertures decreased, the magnitude of the individual intensity peaks at the edges of the apertures remained constant but merged into one single peak at approximately 1μm, Section 5.1.5. Unfortunately we were unable to characterise apertures of dimensions less than 1μm due to time and budget constraints.

A SPW incident on a refractive index discontinuity of an aperture was shown to experience reflection at the curved interface, Section 5.1.5 Figures 5.21-5.23. It was suggested in Section 2.4 and shown experimentally in Section 5.1.5 that approximately 50% of the incident circumference at the centre section of the aperture caused diffraction

of the SPW. The remainder of the incident wave across the diameter of the aperture was incident on the discontinuity interface at angles greater than the critical angle for such a metal/air system and is thus contained within the incident medium. This was shown to be correct when a raster scan of several apertures revealed intensity peaks at the central sections in the direction of the incident SPW of the aperture. As shown in Section 5.1.5 a smaller peak was indeed evident at the air/metal interface when compared to the diffracted intensity caused by the metal/air interface.

The effect seen during the studies at CAMR may be due to several factors although no definite reason can be given at this stage. As seen in Section 5.1.5 when the diameter of the apertures approach 1μm the intensity peaks associated with the opposite edges of the apertures combine into a single spike. Maradudin *et al.* (1983) describe a resonant cavity effect when a SPW encounters a gap in its propagation path in the order of multiples of half a wavelength of bulk waves in the gap. They describe an effect of the barrier region (refractive index discontinuity in the metal film) supporting propagating modes similar to those found in thin film interferometer filters and Fabry-Perot interferometers. Similar to this a circular aperture, of the dimensions first used in CAMR (≈100nm), may have been appropriate to produce resonant cavity effects extremely sensitive to any dielectric change in the resonant conditions. Any dielectric change associated with a foreign object entering the cavity would produce bulk radiating modes which may help explain interesting results during initial studies at CAMR but has yet to be confirmed.

Chapter 7

7. FUTURE WORK

It has been shown that apertures etched in a SPR excited plain metal surface act as discrete centres of scattering of the SPW. The specific nature of this scattering is yet to be precisely determined. Small apertures ($\phi \ll \lambda$) etched in a plain metal surface are thought to behave as Rayleigh scatterers of the SPW. This phenomenon has yet to be identified. Therefore, future work is required to establish firmly the mechanism by which the small apertures scatter the SPW. The ability to probe the apertures with the SNOM/PSTM may improve the understanding of the scattering centres and from this we may be capable of determining the mechanism by which the effect, first seen at CAMR, occurred. This will involve a significant reduction in the dimensions of the SNOM/PSTM probe tip in order to gain the resolution necessary to detect minute intensity profiles associated with these dimensions. This reduction in overall tip dimension may involve the use of a specialised technique, e.g. chemical etching [Pangaribuan *et al.* (1992,1994)], to produce probe tips at these dimensions. Further improvements in the mechanical design of the SNOM/PSTM microscope in order to eliminate erroneous error and linearity effects when probing at these dimensions should be implemented.

It was shown in Section 5., using the combinational SNOM/PSTM, that the circular apertures radiated energy in the form of light from approximately 50% of their central aperture periphery at the leading and trailing edges of the aperture. At grazing angles the SPW's experienced TIR. At sub-micron dimensions where the apertures may be multiples of half the wavelength of the incident energy, they may act as resonant cavities and it may therefore be more efficient, in terms of a radiative wave to develop sensor configurations in which rectangular apertures in the sensor surface use their complete leading and trailing edges to couple energy out of the SPW in the form of visible radiation. If the separation between the leading and trailing edges of the apertures is an integer number of half wavelengths it may produce a resonant cavity effect extremely sensitive to dielectric constant and spacing considerations similar to the effect witnessed by Maradudin *et al.* (1983).

It has become apparent during the experimental investigation of this project that further development of the distance control system is required in order that the separation between the investigative probe and sample during detection of the radiative fields around the aperture or future geometrically different refractive index discontinuities may be pursued. Although the tunnelling between the probe tip and the active SPR surface of the evanescent field present on the opaque metal surface immediately prior to the refractive index discontinuity can be used as a probe/sample separation mechanism (PSTM mode of operation), the radiative field associated with the discontinuity renders this mechanism useless. Several other probe/sample separation control mechanisms exist; vibration of sample [Karrai *et al.* (1995), Kawata *et al.* (1995)] or electron tunnelling of metal coated tip, [Garcia *et al.* (1994] as described in Section 3.2 may be appropriate. A full investigation into the experimental implementation of such schemes should be undertaken in order to allow the further development of a useable microscopic system for actively probing radiative and non-radiative fields in a simultaneous scan.

Visualisation of intensity fluctuations associated with antibodies (20nm ϕ) attached to gold labels (70nm ϕ) entering an aperture, was achieved in initial CAMR studies though the mechanism by which this occurred is unknown. Repetition of these studies should be undertaken. Variation in laser frequency and thus SPR incident angles may produce interesting results and possible verification of minute behaviour in the vicinity of the apertures. Additional experimental analysis with a fixed frequency and varying of the incident angle of the laser radiation either side of the SPR angle may also provide additional information on the likely cause of this effect. The results of such experiments, it is thought, would be crucial in determining the mechanism responsible for causing these highly sensitive intensity fluctuations. The knowledge of such mechanisms may prove fundamental in the development of a possible sensor for particles smaller than the conventional optical microscopy limit.

The fact that the use of this device produce unique results during the biological experimental trials at FORCE and CAMR suggests that further development should be directed towards the medical science and research fields. Future biological studies should concentrate around the fact that it is possible to operate the device in a dual mode, that is, using both the apertured section and the non-apertured section in order to investigate different aspects of cell behaviour. It has been described in the context of this thesis that a decrease in the diameter of the apertures and subsequent reduction in the background noise level, associated with the large apertures, provides valuable information of the lateral 2-dimensional chemotaxis behaviour of the cells. A further biological investigation into the effect of a reduction in the size of the apertures, i.e. $\phi \ll \lambda$, is necessary in order to achieve greater resolution and detection of minute behaviour of cell minipodia causing change in the dielectric constant immediately adjacent to and within small apertures. Due to the apertures producing specific points of visible radiation further investigation may centre around the process of phototaxis, whereby the propagating light may produce a stimuli. Similarly, further studies should be carried out on the non-apertured section of the device where greater spatial resolution of the cell movement has been shown to be

achievable. Attention should be drawn to studies into other active SPR metals. Possible passivating materials which are necessary to protect some SPR metals from reaction with biological media should be investigated in order that these metals may be actively used in formal biological trials possibly providing additional useful experimental data.

In order to complete successfully more comprehensive biological studies the cell incubation system should be developed further to incorporate an efficient constant temperature stage, maintenance of suitable gas balance and the ability to accept a prepared SPR device under tissue culture conditions. This would enable controlled experiments to be carried out under constant environmental conditions.

Although visualisation of the points of contact that the underside of the cell makes with the active SPR surface is made from above the cell, the scattered light associated with these contact points passes through the cell and culture medium. This process in itself produces secondary scatter reducing further the important spatial information. Direct viewing of the underside would ensure secondary scatter was kept to a minimum. Therefore, the mechanical coupling unit should be modified such that unobstructed examination of the underside of the device is possible. The use of a hemicylindrical prism similar to the one described in Section 3.3.3 but with a flat face ground parallel to the diameter would still enable the user ease of coupling to the metalised upper surface of a device, in the same manner as described in Section 3.3.3.2 but also enable visualisation of the undersurface of the cell and present a possible enhancement of the scattered SPW.

Development of an image analysis system is essential for the analysis and understanding of the cell movement over short periods of time. This will enable recognition of specific intensity patterns of cell movement and unwanted noise. As discussed in Section 4.2.3 it may be possible to visualise cell microvilli and dimples approximately 30nm wide and 8nm high. Greater analysis of the image gained from the experiments with the use of digital signal processing routines may provide greater differentiation between contrast points on the images.

Further experimental systems using known cell lines should be made. These experiments might fall into three categories;

i. Identification of innate cell behaviour on different biological substrates: These experiments will therefore include various adherent cells to determine how their interactions with biological substrate is affected by extracellular matrix proteins.

ii. The interactions of tumour cells with established monolayers. In these experiments the integrity and movement of the adherent layer as modulated by interactions with known tumour cells should be studied. This system will model metastatic behaviour of tumour cell on, for example, vascular endothelial cells and fibrocytes.

iii. Dynamic response of cells to growth factors. Detection of changes in the cell movement or interaction with matrices according to responses with growth factors should be studied. These growth factors should include ones to stimulate growth or programmed cell death

All these biological studies will be correlated with other biological cell parameters such as proliferation and stimulation to protein synthesis, and the secretion and involvement of specific molecules such as extracellular proteases and ICAMs and their receptors.

REFERENCES

[1] Adam P.M., Salomon L., de Fornel F., Goudonnet J.P., "Determination of the spatial resolution of the surface plasmon evanescent field of a silver film with a photon scanning tunnelling microscope", Phys. Rev. B., Vol. 48 No. 4, pp. 2680-2683, 1993.

[2] Agranovich V.M., Kravtsov V.E., Leskova T.A., "Thin film on metal: Resonance effects in light diffraction at the edge.", Solid State Commun, Vol. 40, pp. 687-692, 1981.

[3] Alt W., Brosteanu O., Hinz B., Kaiser H.W., "Patterns of spontaneous motility in videomicrographs of human epidermal keratinocytes (HEK)", Biochem. Cell. Biol., Vol. 73 pp. 441-459, 1995.

[4] Ambrose E.J., Easty D.M., "Cell Biology", Second Edition, Thomas Nelson & Sons Ltd. 1977.

[5] Anders H., "Thin Films in Optics", The Focal Press, 1967.

[6] Anderson G.S., Mayer W.S., Wehner G.K., "Sputtering of Dielectrics by High Frequency Fields", J. Appl. Phys. Vol. 33 (10), pp. 2991-2992, 1962.

[7] Ash E.A., Nicholls G., "Super resolution aperture microscope", Nature, Vol. 237, pp. 510-512, 1972 .

[8] Beloussov L.V., Badenko L.A., Katchurin A.L., Kurilo L.F., "Cell movement in morphogenesis of hydroid polyps", J. Embryol. Exp. Morph., Vol. 27, pp. 317-337, 1972.

[9] Betzig E., Lewis A., Harootunian A., Isaacson M., Kratschmer E., "Near field scanning optical microscopy", Biophysics Journal, Vol. 49, pp. 269-279, 1986.

[10] Betzig E., Isaacson M., Lewis A., "Collection mode near field scanning optical microscopy", Applied Physics Letters, Vol. 51 No. 25, pp. 2088-2090, 1987.

[11] Betzig E., Trautman J.K., Harris T.D., Weiner J.S., Kostelak R.L., "Breaking the Diffraction Barrier: Optical Microscopy on a NanoMetric Scale", Science, Vol. 251, pp. 1468-1470, 1991.

[12] Binnig G., Rohrer H., "Scanning tunnelling microscopy", Helv. Phys. Acta., Vol. 55, pp. 726-735, 1982.

[13] Bohren C.F., Huffman D.R., "Absorption and Scattering of Light by Small Particles", John Wiley & Sons.

[14] Born M., Wolf E., "Principles of Optics", Electromagnetic Theory of Propagation Interference and Diffraction of Light", Sixth Edition, Pergamon Press, 1980.

[15] Cheng T.P.O., "Minipodia, Novel structures for extension of the lamella: A high-spatial-resolution video microscopic study", Experimental Cell Research, Vol. 203, pp. 25-31, 1992.

[16] Chirstensen O., "Characteristics and Application of Bias Sputtering", Solid State Technol. Vol. 13 (12) , pp. 39-45, 1970.

[17] Choo A.G., Chudgar H., Jackson E., De Brabander G.N., Kumar M., Boyd J.T., "Photon scanning tunnelling microscopy of optical channel waveguides", Ultramicroscopy, Vol. 57, pp. 124-129, 1995.

[18] Cites J., Sanghadasa M.F.M., Sung C.C., "Analysis of photon scanning tunnelling microscope images", Applied Physics Vol. 71 No. 1, pp. 7-10, 1992.

[19] Coburn J.W., Kay E., "Positive-ion Bombardment of Substrates in R.F. Glow Discharge Sputtering", J. Appl. Phys, Vol. 43, pp. 4965-4971, 1972.

[20] Comas J., Wolicki E.A., "Argon Content in (111) Silicon for Sputtering Energies below 200eV ", J. Electrochem. Soc. Vol. 117, pp. 1197-1198, 1970

[21] Courjon D., Sarayeddine K., Spajer M., "Scanning tunnelling optical microscopy", Opt. Commun., Vol. 71 No. 1,2, pp. 23-28, 1989.

[22] Curtis A.S.G., " Light Microscopy in Biology. A Practical Approach (ed. Lacey, A.J.), IRL Press: Oxford, 1988.

[23] Curtis A.S.G., Lackie J.M., "Measuring Cell Adhesion", John Wiley & Sons Ltd, 1991.

[24] Cush R., Cronin J.M., Stewart W.J., Maule C.H., Molloy J., Goddard N.J.,"The resonant mirror - a novel optical sensor for direct sensing of biomolecular interactions. 1.Principle of operations", Biosensors & Bioelectronics, Vol. 8 No.7-8, pp. 347-353, 1993.

[25] Davidse P.D., "Theory and Practice of R.F. Sputtering In Microelectronic Technology", ed. S. L. Marshall. Boston Technical Publishers Inc., Cambridge, Mass.

[26] Dawson P., Smith K.W., de Fornel F., Goudonnet J.P., "Imaging of surface plasmon launch and propagation using a photon scanning tunnelling microscope", Ultramicroscopy, Vol. 57, pp. 287-292, 1995.

[27] de Fornel F., Goudonnet J.P., Salomon L., Lesniewska E., "An evanescent field optical microscope", Proc. SPIE, Vol. 1139, pp. 77-84, 1989.

[28] Diament P., "Wave Transmission and Fibre Optics", Macmillan Publishing Company (NY), pp. 247, 1990.

[29] Drabenstedt A., Wrachtrup J., von Borczyskowski C., "A distance regulation scheme for scanning near-field optical microscopy", Appl. Phys. Lett., Vol. 68 No. 24, pp. 3497-3499, 1996.

[30] Durig U., Pohl D.W., Rohner F., "Near field optical scanning microscopy", J Appl Phys, Vol. 59 No. 10, pp. 3318-3327, 1986.

[31] Fischer U., Zapletal M., "The concept of a coaxial tip as a probe for scanning near field optical microscopy and steps towards a realisation", Ultramicroscopy, Vol. 42-44, pp. 393-398, 1992.

[32] Fischer U.C., Durig U.I., Pohl D.W., "Near field optical scanning microscopy in reflection", Appl. Phys. Let., Vol. 52 No. 4, pp. 249-251, 1988.

[33] Fleischer M., Wohlfarth-Bottermann K.E., "Correlation between tension force generation, fibrillogenesis and ultrastructure of cytoplasmic actomyosin during isometric and isotonic contrations of protoplasmic strands", Cytobiologie, Vol. 10, pp. 339-365, 1975.

[34] Fujihira M., Monobe H., Yamamoto N., Muramatsu H., Chiba N., Nakajima K., Ataka T., "Scanning near-field optical microscopy of fluorescent polystyrene spheres with a combined SNOM andAFM", Ultramicroscopy, Vol. 61, pp. 271-277, 1995.

[35] Garcia-Parajo M., Rosiu J., Yong C., "On the way to multitask near-field optical microscope - simultaneous STM/SNOM and PSTM imaging", Microsc. Microanal. Microstruct., Vol. 5 No. 4-6, pp. 399-407, 1994.

[36] Girard C., Courjon D., "Model for scanning tunnelling optical microscopy: a microscopic self consistent approach", Phys. Rev. B., Vol. 42 No. 15, pp. 9340-9349, 1990.

[37] Goberdhan N., Dive C., Streuli C.H., "The role of the extracellular matrix and lactogenic hormones in mammary gland apoptosis", Biochemical Society Transactions, Vol. 24, p. 348s, 1996.

[38] Gordon M.Y., Riley G.P., Watt S.M., Greaves M.F., "Compartmentalization of a haematopoietic growth factor (GM-CSF) by glycosaminoglycans in the marrow microenvironment", Nature, Vol. 326, pp. 403-405, 1987.

[39] Goudonnet J.P., de Fornel F., Salomon L., Adam P.M., Bourillot E., "Photon Scanning Tunnling Microscopy and Spectroscopy Applications", Inst. Phys. Conf. Ser. No. 135: Chap. 7, pp. 229-238, 1993.

[40] Grebecki A., Cieslawska M., "Plasmodium of Physarum polycephalum as a synchronous contractile system", Cytobiologie, Vol. 17, pp. 335-342, 1978.

[41] Oberleithner H., Gerhard G., Geibel J., "Imaging the lamellipodium of migrating epithelial cells in vivo by atomic force microscopy", Pflugers Arch, Vol. 425, pp.506-510, 1993.

[42] Harootunian A., Betzig E., Isaacson M., Lewis A., "Super resolution fluorescence near filed scanning optical microscope", Appl Phys Lett, Vol. 49 No. 11, pp. 674-676, 1986.

[43] Hartmann T., Gatz R., Wiegrabe W., Kramer A., Hillebrand A., Lieberman K., Baumeister W., Guckenberger R., "A scanning near-field optical microscope (SNOM) for biological applications", Near Field Optics - NATO ASI Series E Vol. 242, pp. 35-44, 1993.

[44] Hecht B., Heinzelmann H., Pohl D.W., "Combined aperture SNOM/PSTM: best of both worlds", Ultramicroscopy, Vol. 57, pp. 228-234, 1995.

[45] Hecht E., Zajac A., "Optics", Addison-Wesley Publishing Company, 1982.

[46] Hood A.S., Neal R., Garland J., Al-shukri S., Carr R., "A Novel Biosensor for the Real Time Study of Cell Movement", Proceeding of Medical and Fiber Optic Sensors and Delivery Systems, Vol. 2631, pp. 46-53, 1995.

[47] Jamid H.A., Al-Bader S.J., "Diffraction of Surface Plasmon-Polaritons in an Abruptly Terminated Dielectric-Metal Interface", IEEE Photonics Technology Letters, Vol. 7 No. 3, pp. 321-323,1995.

[48] Jenkins F.A., White H.E., "Fundamentals of Optics", McGraw Hill Book Company, Fourth Edition, 1965.

[49] Jorgenson R.C., Yee S.S., "A fibre-optic chemical sensor based on surface plasmon resonance", Sensors and Actuators B, Vol. 12, pp. 213-220, 1993.

[50] Karrai K., Grober R.D., "Piezo-electric tuning fork tip-sample distance control for near field optical microscopes", Ultramicroscopy, Vol. 61, pp. 197-205, 1995.

[51] Kawata S., Inouye Y., "Scanning probe optical microscopy using a metallic probe tip", Ultramicroscopy, Vol. 57, pp. 313-317, 1995.

[52] Keh-su Chang, Chien Chou, Chin-hwa Lin, "Focused-beam Attenuated Total-Reflection technique on absorptive film in Kretschmann's configuration", Applied Optics, 3229-3257, 1993.

[53] Kerker M., "The Scattering of Light and other Electromagnetic Radiation", Academic Press, 1969.

[54] Koenig, Maissel L.I., "Application of R.F. Discharges to Sputtering", IBM J. Res. Dev. Vol. 14 (2), pp. 168-171, 1970.

[55] Kramer A., Hartmann T., Stadler S.M., Guckenberger R., "An optical tip-sample distance control for a scanning near-field optical microscope", Ultramicroscopy, Vol. 61, pp. 191-195, 1995.

[56] Kretschmann E., Raether H., "Radiative Decay of the Non Radiative Surface Plasmons Excited by Light", Z. Naturforsch, Vol. 23a, pp. 2135-2136, 1968.

[57] Labani B., Girard C., Courjon D., Van Labeke D., "Optical interaction between a dielectric tip and a nanometric lattice: implications for near field microscopy", J. Opt. Soc. Am. B., Vol. 7 No. 6, pp. 936-943, 1990.

[58] Lau S.S., Mills R.S., Muth D.G., "Temperature Rise During Film Deposition by R.F. and D.C. Sputtering", J. Sci. Technol. Vol. 9, pp. 1196-1202., 1972.

[59] Leung P.T., Pollard-Knight D., Malan G.P., Finlan M.F., "Modelling of particle-enhanced sensitivity of the surface-plasmon-resonance biosensor", Sensors and Actuators B, Vol. 22, pp. 175-180, 1994.

[60] Leurgans P.J., Turner A.F., "Frustrated total reflection interference filters", J. Opt. Soc. Am., Vol. 37 A, p. 983, 1947.

[61] Lewis A., Isaacson M., Murray A., Harootunian A., "Scanning optical spectral microscopy with 500A spatial resolution", Biophys J. Vol. 41, p. 405a, 1983.

[62] Lieberman K., Lewis A., "Simultaneous scanning tunnelling and optical near-field imaging with a micropipette", Appl. Phys. Lett., Vol. 62 No. 12, pp. 1335-1337, 1993.

[63] Liedberg B., Lundstrom I., Stenberg E., "Principles of biosensing with an extended coupling matrix and surface plasmon resonance", Sensors and Actuators B, Vol. 11 pp. 63-72, 1993.

[64] Lofas S., Malmqvist M., Ronnberg I., Stenberg E., Liedberg B., Lundstrom I., "Bioanalysis with surface plasmon resonance", Sensors and Actuators B, Vol. 5, pp. 79-84, 1991.

[65] Lukosz W., Clerc D., Nellen Ph.M., Stamm Ch., Weiss P., "Output grating couplers on planar optical waveguides as direct immumosensors", Biosensors Bioelectronics, Vol. 6, pp. 227-232, 1991.

[66] Macleod H.A., "Thin-Film Optical Filters", Adam Hilger Ltd, London. 1969

[67] Maradudin A.A., Wallis R.F., Stegman G.I., "Surface Polariton Reflection and Transmission at a Barrier", Solid State Communications, Vol. 46 No. 6, pp. 481-485, 1983.

[68] Marti O., Bielefeldt H., Hecht B., Herminghaus S., Leiderer P., Mlynek J., "Near-field optical measurement of the surface plasmon field", Opt. Commun., Vol. 96, pp. 225-228, 1993.

[69] Montroll E.W., Greenberg J.M., "On the theory of scattering of plane waves by soft particles", Proc. Symp. Appl. Math., Vol. 5, pp. 103, 1954

[70] Morawitz, Phys. Rev., Vol. 187, pp. 1792-1799, 1969.

[71] Neugebauer T., Ann. Phys., Vol. 42, p 509, 1943.

[72] Novotny, Pohl, Regli, "Near filed, far field and imaging properties of the 2D aperture SNOM", Ultramicroscopy, Vol. 57, pp. 180-, 1995.

[73] Otto A., "Excitation of Nonradiative Surface Plasma Waves in Silver by the Method of Frustrated Total Reflection", Zeitschrift fur Physik, Vol. 216, pp. 398-410, 1968.

[74] Palik E.D., "Handbook of Optical Constant of Solids", Naval Research Laboratory, Washington D.C., Academic Press Inc., 1985.

[75] Pangaribuan T., Jiang S., Ohtsu M., "Highly controllable fabrication of fibre probe for Photon Scanning Tunnelling Microscope", Scanning, Vol. 16 No. 6, pp. 362-367, 1994.

[76] Pangaribuan T., Yamada K., Jiang S., Ohsawa H., Ohtsu M., "Reproducible fabrication technique of nanometric tip diameter fibre probe for the photon tunnelling microscope", Jpn J Appl Phys, Vol. 31, pp. L1302-L1304, 1992.

[77] Pluta M., "Advanced Light Microscopy - Specialised Methods", Vol. 2, Section 5.5.2., Figure XII, Elsevier, PWN-Polish Scientific Publishers, 1989.

[78] Pohl D.W., European Patent Application, No. 0112401, Filed 27 December 1982, US Patent 4604520, Filed 20 December 1983.

[79] Pohl D.W., Denk W., Lanz M., "Optical stethoscopy: image recording with resolution λ\20", Appl Phys Lett Vol. 44 No. 7, pp. 651-653 1984.

[80] Pohl D.W., Denk W., Durig U., "Optical stethoscopy: imaging with λ\20", Proc. SPIE, Vol. 565, pp. 56-61, 1985.

[81] Raether H., "Surface Plasma Oscillations and their applications", Physics of Thin Films, Vol. 9, 1977.

[82] Raether H., "Surface Plasmons on Smooth and Rough Surfaces and on Gratings", Springer-Verlag, 1988.

[83] Raether H., Springer Tracts of Modern Physics, Vol. 38, pp. 171, 1965.

[84] Rayleigh Lord, Phil. Mag. (5), Vol. 8, pp. 261, 1879.

[85] Rayleigh Lord, Phil. Mag., Vol. 12, p 81, 1881.

[86] Reddick R.C., Warmack R.J., Ferrell T.L., "New form of scanning optical microscopy", Phys. Rev. B, Vol. 39 No. 1, pp. 767-770, 1989.

[87] Sommerfeld A., Ann. Physik.,Vol. 28, p 665, 1909.

[88] Sommerfeld A., Renner, Ann. D. Physik. V.,Vol. 41, p 1, 1942.

[89] Stegeman G.I., Maradudin A.A., Rahman T.S., "Refraction of a surface polariton by an interface", Phys. Rev. B., Vol. 23, pp. 2576-2585, 1981.

[90] Stirland J.S., "Electron-Bombardment-Induced changes in the growth and Epitaxy of Evaporated Gold films", J. Appl. Phys. Let Vol. 8 No. 12, pp. 326-328, 1966.

[91] Stossel T.P., "The Machinery of Cell Crawling", Scientific American Vol. 271, pp. 40-47, 1994.

[92] Strong J., "Concepts of Classical Optics", W.H. Freeman & Company (San Francisco and London), pp. 124, 1958.

[93] Strutt M.J.O., Ann. D. Physik. V., Vol. 1, p. 721, 1929.

[94] Syms R., Cozens J., "Optical Guided Waves and Devices", McGraw Hill Book Company, London, p. 110, 1992.

[95] Synge E.H., "A suggested method for extending microscope resolution into the ultra-microscopic region", Phil. Mag., Vol. 6, pp. 356-362 1928.

[96] Tien P.K., Ulrich R., "Theory of Prism-Film Coupler and Thin-Film Light Guides", J. Opt. Soc. Am., Vol. 60 No. 10, pp. 1325-1337, 1970.

[97] Tsai D.P., Kovacs J., Moskovits M., "Applications of apertured photon scanning tunnelling microscopy", Ultramicroscopy, Vol. 57, pp. 130-140, 1995.

[98] Van Labeke D., Barchiesi D., "Scanning tunnelling optical microscopy - a theoretical macroscopic approach", J. Opt. Soc. Am. A-Optics, Image Science & Vision, Vol. 9 No. 5, pp. 732-739, 1992.

[99] Vohnsen B., Bozhevolnyi S., Olesen R., "Study of shear force technique for near-field microscopy with an uncoated fibre tip", Ultramicroscopy, Vol. 61, pp. 207-213, 1995.

[100] Vossen J.L., O'Neil J.J., "D.C. Sputtering with R.F. Induced Substrate Bias", RCA Review, Vol. 29 (4), pp. 566-581, 1968.

[101] Winters H.F., Kay E., "Gas Incorporation into Sputtered films", J. Appl. Phys., Vol. 38 No. 10, pp. 3928-3934, 1967.

Appendix A

Published Papers

PROGRESS IN BIOMEDICAL OPTICS

EUROPTO SERIES

Proceedings of

Medical and Fiber Optic Sensors and Delivery Systems

Nathan I. Croitoru
Mitsunobu Miyagi
Guillermo Orellana
Annamaria V. Scheggi
Henricus J. M. C. Sterenborg
Chairs/Editors

Abraham Katzir
Biomedical Optics Series Editor

12–13 September 1995
Barcelona, Spain

Sponsored by
ELA–The European Laser Association
Sociedad Española de Laser Médico Quirúrgico
Essilor International
International Biomedical Optics Society
EOS—The European Optical Society
SPIE—The International Society for Optical Engineering
The Commission of the European Communities, Directorate General for Science, Research, and Development

SPIE P

Volume 2631

A Novel Biosensor for the Real-Time Study of Cell Movement

A.S.. Hood[1], R. Neal [1], J. Garland [2], S. Al-shukri [3] & R. Carr [3]

1. University of Plymouth, School of Electronic, Communication and Electrical Engineering, Drake Circus, Plymouth, Devon, PL4 8AA, UK.
2. FORCE Cancer Research Centre, Noy Scott House, Haldon View Terrace, Wonford, Exeter, Devon, EX2 5DW, UK.
3. Centre for Applied Microbiology and Research, Porton Down, Salisbury, Wiltshire, SP4 0JG, UK.

ABSTRACT

Cell movement is vital to normal tissue growth and regulation. Although not often realised, cells are continually moving relative to each other, and many physically migrating from their original site. Blood and immune cells rely on migrating through other tissues to perform their function. Cell division also needs physical separation of daughter cells, and other cells e.g. muscle cells have developed their mechanical machinery to perfection. Substrate interactions are complicated. The ability to migrate and stop migrating when needed is a vital part of tissue regeneration. Understanding cell migration and movement is very important to being able to discover how cancer cells are able to continue dividing and why they abnormally migrate. Much other work has established that cells contact substrates through specific attachment points, but it is almost impossible to visualise these in three dimensions since cell cytoplasm is translucent and resolution limited by wavelength of light.

We have developed a small sensor device of a metallised glass substrate on which we have electron beam lithographically produced arrays of sub-micron circular apertures. A Surface Plasmon Resonance (SPR) wave is set up in the metal by excitation with an incident laser beam. The circular apertures act as discrete centres of optical scattering of the SPR wave and the associated light emanating from these points can be detected and studied using an associated image analysis system. The intensity of the light scattered from each of these apertures is a strong (exponential) function of the changes of local refractive index close to (within 250nm) the aperture. The contact of the underside of the cell with the aperture bearing surface modulates the intensity pattern of the aperture matrix allowing high resolution of the spatial distribution of the contact points between the cell and the metalised surface.

Key words - Surface Plasmon Resonance (SPR), Evanescent wave, Complex Dielectric constant.

I. INTRODUCTION

Cell adhesion and movement are two fundamental properties determining tissue growth and differentiation.

Cell adhesion is mediated by the interaction of receptor sites on the cell surface with specific intercellular matrix proteins or intracellular adhesion molecules present on other cells (ICAMS and Adhesions). Intracellular matrix molecules (collagens, pi-glycosaminoglycans) also sequester other peptide growth factors from serum or surrounding cells[1]. Together, such molecules and their interaction regulate cell growth, tissue formation, differentiation and position of cells within an environment.

Cell movement is virtually a ubiquitous property of cells. Those apparently stationary cells remain in situ by virtue of their interaction with substrates (e.g. matrix proteins). Changes in these substrates will ultimately alter the cell's behavioural characteristics. Tissue regeneration relies heavily on cell movement to regenerate tissue three dimensional structure. Other cells, e.g. blood and tissue macrophages and cells of the immune system are specialised for rapid and free movement in response to stress factors. This freedom of movement is vitally important for the successful generation of an immune response. Finally, tumour cells have[2] an increased capacity for movement which is responsible for their fatal dissemination through the body. Cell movement can be considered at two levels:

a) movement of the whole cell usually along a chemo-attractant gradient and
b) movement of the cell surface membranes and components therein.

Monitoring and analysis of whole cell movement currently relies on crude, labour intensive and time consuming visual observation, albeit often assisted by time lapse video. Cells are typically placed in a micro-chamber connected by a

 0-8194-1995-8/96/$6.00

apillary to another chamber containing a cell attractant and movement of the cell along the chemo-attractant gradient is nonitored over long periods (several hours). However, cell movement is often stochastic and difficult to quantify objectively. Furthermore, time-lapse video can only deal with a limited number of cells at once over a long time period, cannot resolve events within the time-frame access period and cannot readily merge or process data into a manipulative digitised/binary) form. Currently there is considerable interest in developing methods by which the movement of cells can be studied at the molecular level, i.e. as mediated by aggregation of receptor peptides, etc. No good analytical methods exist beyond labelling surfaces with antibodies and using optical microscopy to monitor gross movement of label; e.g. Fluorescence Energy Transfer (FET) between neighbouring molecules has been used with some success but the technique is highly spatially dependent and its specificity for peptides directly associated with primary ligand is uncertain. These techniques report on the overall change in cell contact and membrane behaviour but it is known that the contact that the cell makes with its substrate can vary with different substrate properties and under different environmental stimuli. The development of analytical techniques by which the contacting of cell surfaces with underlying substrates can be measured and changes in that contact (adhesion) correlated with the onset of cell movement would be of significant interest to cell biologists.

We have developed a method of monitoring the interaction of the cell membrane with the substrate which reports only on those regions of the cell that either contact, or approach to within ca. 250nm of the surface. The method is based on the microscopic detection of fluctuations in the intensity of light scattered by arrays of apertures in a thin metal film in which Surface Plasmons (SP's) were excited with an incident laser beam. The intensity fluctuations are caused by contact of the cell wall with the aperture surface and the size and spacing of apertures in the array are such that any given cell will cover a number of apertures, allowing high sensitivity studies of cell contact/adhesion to be made within individual cells.

II. SURFACE PLASMONS

Surface Plasmon waves or Surface Plasmons (SPs), can exist in the boundary region of a metal-dielectric interface resulting from the oscillatory behaviour of free electrons in the metal by the action of an incident optical electromagnetic field. These charge fluctuations, which are localised in the x direction are accompanied by a mixed transversal and longitudinal magnetic field disappearing at $z \rightarrow \infty$ and having a maximum at the surface $z=0$. Figure 1 gives a graphical representation of the magnetic component of the field at the metal-dielectric interface.

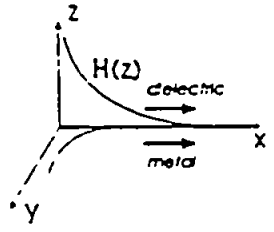

Figure 1 Magnetic field distribution at the metal-dielectric interface.

It can be shown that the field exists only for Transverse Magnetic (TM) polarisation, i.e. the magnetic field is transverse to the direction of propagation. In the z-direction the field is stationary (evanescent), thus power flow occurs only in the x-direction. The field maximum at the metal-dielectric interface explains the sensitivity of the field to changes in physical properties and disturbances at the metal surface.

III. FUNDAMENTAL PROPERTIES

A full description of surface plasmons is obtained from Maxwell's equations[8] with appropriate boundary conditions in conjunction with the properties of the interface materials. In its simplest form, the solution to the wave equation for a lossy dielectric can be expressed as:

$$H = H_{(z)} \exp^{(-z/L_z)} \exp^{j(-\omega x)} \qquad \textit{Equation 1}$$

which describes a decaying magnetic field travelling in the x-direction.
At optical frequencies, a metal can be treated as a dielectric with a complex permittivity with the real part large and negative and the imaginary part small and positive accounting for the decay of the field i.e.

$$\varepsilon_m = \varepsilon_m' - j\varepsilon_m'' \qquad \textit{Equation 2}$$

The permittivity ε_m and the wave vector $k_{(x)}$ are related as shown in equation 3,

$$k_{(x)} = \frac{\omega}{c}\sqrt{\left(\frac{\varepsilon_m \varepsilon_o}{\varepsilon_m + \varepsilon_o}\right)} \qquad \textit{Equation3}$$

where ε_o is the dielectric constant of the medium above the metal, ω is the radian frequency and c is the speed of electromagnetic radiation in a vacuum.

A necessary condition for the excitation of the SP wave, is that of phase matching the SP wave with that of the laser beam i.e.

$$k_{(x)SPW} = k_{(x)Laser} \qquad \textit{Equation 4}$$

The sine of the angle of incidence of the input laser beam is proportional to $k_{(x)SPW}$ and therefore dictates the phase matching conditions. The angle at which the excitation occurs is known as the Surface Plasmon Resonance (SPR) angle. To realise this angle it is necessary that the incident laser beam is introduced to the metal film by means of a coupling prism of refractive index n_p, where $n_p > n_m$ and n_m is the effective refractive index of the metal i.e. $(\varepsilon = n^2)$

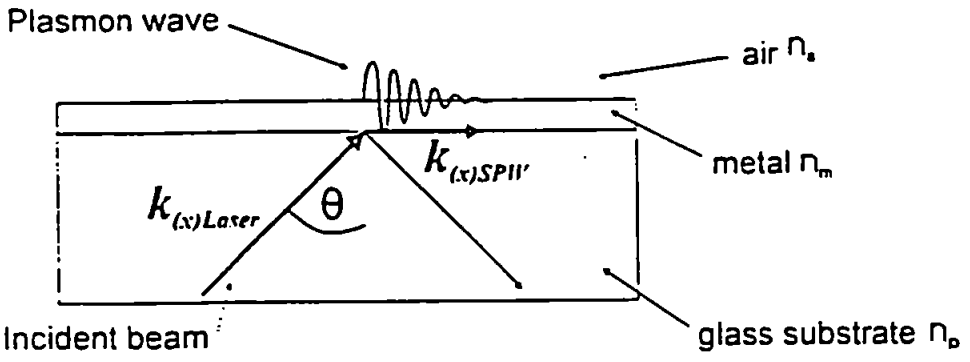

Figure 2 A schematic of a surface plasmon coupler showing the incident beam exciting the SPs.

The key properties of the SPWs are that it is a travelling wave in the x-direction and evanescent in the z-direction. The field extends above and below the metal surface. Decay is much more rapid in the metal than in air and thus SP waves will exponentially decay ($\exp^{-(k_z z)}$) with z, where k_z is the imaginary wave vectors in the medium. The *skin depth* of the SP at which its intensity falls to 1/e is given by;

$$Z = \frac{1}{|k_z|} \qquad \textit{Equation 5}$$

this exponential decay is shown in Figure 3.

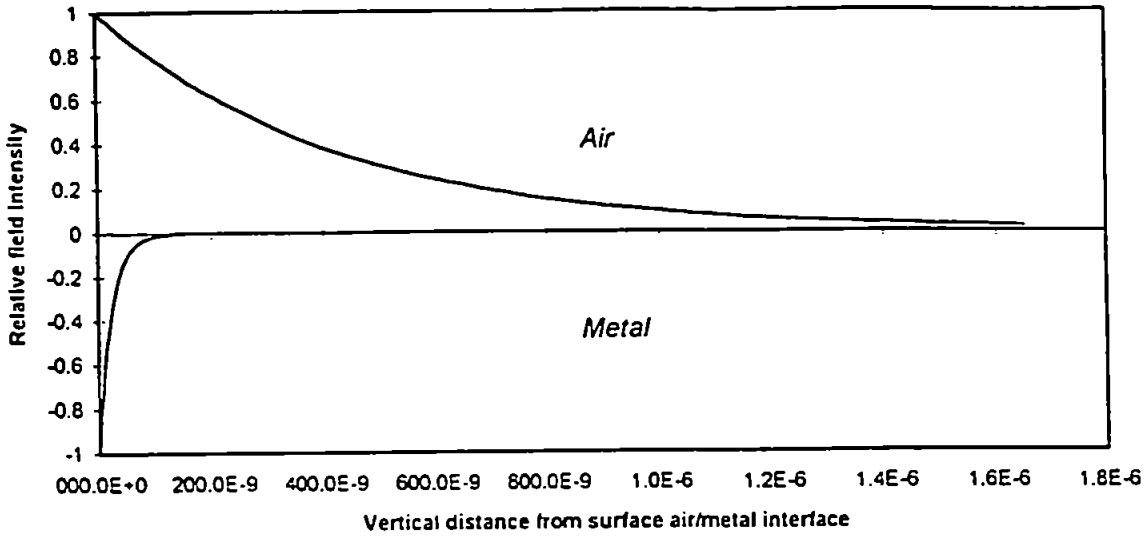

Figure 3 A plot of relative field intensity versus distance in z-direction from air/metal interface.

IV. SUBSTRATE FABRICATION

Hoya LT substrates with a refractive index of 1.53 were used to fabricate the matrix. With the availability of Electron beam written mask plates, prepared at CAMR - Porton Down, several varying sized matrixes were fabricated together in the C.R.I.S.T. facility at the University of Plymouth using photolithography techniques.

The substrates were initially ultrasonically cleaned and rinsed with Acetone and Isopropanol before being finally rinsed with de-ionised water and dried in an oven at 110°C for 20 minutes. The substrates were then metalised using a sputter coater (Materials Research Company Ltd. St. Johns Estate, Penn, Bucks, UK) depositing Chromium and/or Silver to a pre-determined optimum thickness. UCB Photoresist was spun to a thickness of 1.3μm on to the metalised surface at 5000rpm for 45 seconds and baked in the oven for 25 minutes at 125°C. The metalised substrates were then exposed to ultraviolet light through the mask plate on a Pricema International photolithography unit for 17 seconds. Again the substrates were baked in the oven at 125°C for 10 minutes and developed in Shipley 351 Microposit developer for 10-15 seconds before being etched in a Ion beam miller (CVC. Scientific Products Ltd. Hogwood Lane, Finchampstead, Wokingham, Berkshire, UK)

Utilising this method a resolution of approximately 1μm diameter aperture was repeatably achievable. The completed substrates were then diced up into individual samples with aperture matrix sections used in the coupling process. Where greater resolution, i.e. to approximately 1micron diameter and less is required, directly written substrates were fabricated at CAMR and used in the device. Several different aperture sizes and inter-aperture spacing matrices were fabricated and tested under SPR conditions. By experimental analysis it was found that the best resolvable optical results were obtained from apertures with an inter-aperture spacing of no less than 5μm when using apertures of approximately 1μm. Depending on the physical size of the cells under test different matrices were used in order that the cell would cover a range of apertures at any one time.

V. EXPERIMENTAL SET-UP

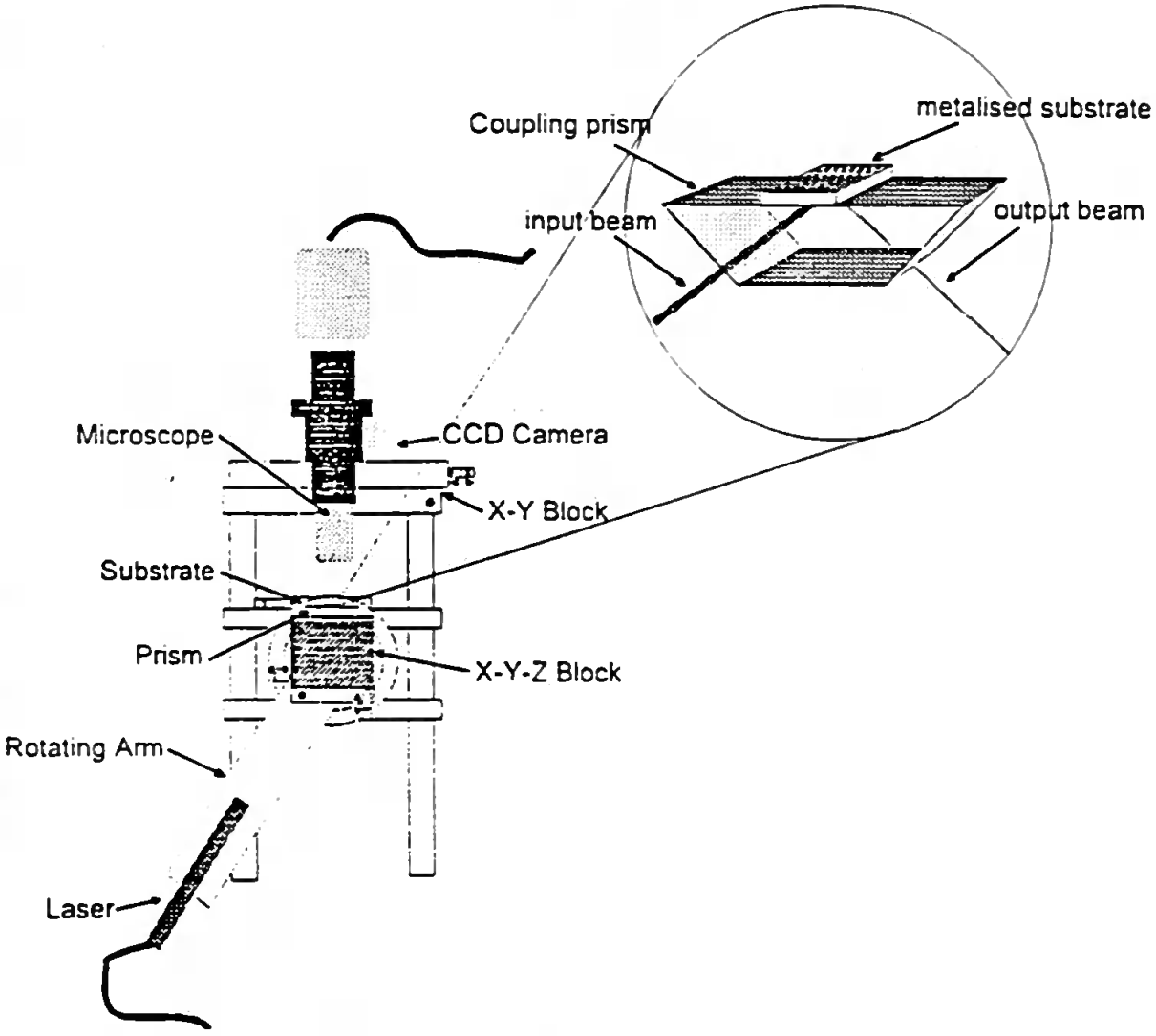

Figure 4 A diagram of the coupling rig used in the experimental analysis.

The coupling prism was mounted on a Photon Control X-Y-Z micrometer adjustment block with the substrate placed on the upper surface. A 5mW Helium Neon laser was fixed to a micrometer adjustment rotating arm such that the beam remained central relative to a point on the substrate. Surface plasmon resonance could be repeatedly attained by adjustment of the angle at which the incident laser light fell on the metal film surface and the X-Y-Z block.

An optical microscope fitted with a high sensitivity CCD camera was mounted above the X-Y-Z block such that it could be moved, in three dimensions, relative to the surface of the substrate. A long working distance x10 objective with zoom made the substrate face accessible.

The cells were kept at a constant 37°C ± 0.5°C by means of a heating unit consisting of a 2 Amp 15 volt Peltier heating device linked to a thermometer and feedback loop. With the prepared metalised substrate placed on the top surface of the dove tail prism light could be coupled into the metal surface from the underside to excite surface plasmons on the top side of the substrate. A glass cover slide was placed on top of the substrate in order to present the microscope with a flat optical surface through which the metalised surface could be viewed without the distortion of the curved meniscus of the fluid. As cells settle on to the substrate surface changing the dielectric constant in the near field of the metalised surface, an energy transformation takes place and changes in the scattering of light can be visually monitored and an intensity profile can be made.

VI. ANIMAL CELL LINES AND SAMPLE PREPARATION

Prior to animal cell studies the system described above was optically calibrated using polystyrene (latex) microspheres (Sigma Chemical Co. Ltd., Poole, Dorset, UK) of mean diameter 2.92μm (SD=0.012μm, Lot #92573) suspended to a concentration of 10^5/ml in demineralised 0.22μm filtered water. The diameter of the apertures in the array used was 2μm allowing the interaction of the 3μm beads to be clearly visualised. The intensity fluctuation associated with the approach, under Brownian motion, of the calibrant latex microspheres was recorded using a conventional video recorder and analysed using a PC based image analysis system (PCX system, Brian Reece Ltd., Newbury, Berks.) linked to the CCD camera.

For the initial animal cell studies Chinese Hamster ovary (CHO) cells were obtained from the European Collection of Animal Cell Cultures, Porton Down, Wiltshire (Accession number 85050302). These cells were chosen for their relative robustness, suitable size (10μm diameter) and adherence properties. The cells were cultured in a conventional cell culture medium (Hams S12 containing 10% fetal calf serum; PAA Gmbh, Austria) at 37°C. Suspensions of cells adhering to culture bottles were prepared by treatment with trypsin/EDTA (Gibco Ltd., Paisley, Scotland) prior to mixing in fresh medium to a concentration of 10^5 cells/ml. To minimise bacterial contamination the suspending medium contained aliquots of a solution of Penicillin and Streptomycin (50,000 units/ml - Gibco Ltd.) diluted to a final solution of 5,000 units/ml. Cell concentrations were confirmed microscopically by haemocytometer count with Trypan Blue visualising dye.

Human breast tumour cell line MDA-MB231 was obtained from the European Collection of Animal Cell Cultures, Porton Down, Wiltshire (Accession number 92020424) and grown in Leibovitz medium supplemented with 15% FBS and antibodies. Cells were released by Trypsin/EDTA treatment (Gibco Ltd., Paisley, Scotland) of established cultures and seeded into petri-dishes at 10^5/ml containing substrate grids and grown overnight. In some experiments, the aperture arrays (prepared as in Section IV.) comprising 1.4μm apertures at 5μm centre spacing were coated with Poly-L-Lysine of various collagens by pre-incubation for 30 minutes at room temperature in a solution of 1mg/ml matrix protein followed by washing in medium. The arrays were washed by gentle agitation in fresh medium and transferred directly to the stage. The diameter of the cells (approx. 15μm spheres) meant that, on adhesion to the surface (with a concomitant slight increase in diameter to typically 20μm) each cell would cover at least 3 apertures at any given time. To prevent drying, the arrays were covered with a cover-slip enclosing a capillary film of medium. The overall cell concentration was selected such that surface coverage of the aperture array would approach 10% when all cells had settled onto the surface and subsequently adhered. Images of the surface were recorded at suitable intervals (e.g. for 5 minutes every 20 minutes) for subsequent analysis. Murine IL3-dependent non-adherent B_o cells were cultured in RPMI/10%FBS supplemented with 10% WEHI conditioned medium as a source of IL3, and deposited directly on the grids as above for immediate viewing.

VII. ANALYSIS OF EXPERIMENTAL RESULTS

The data obtained from the experiments using CHO cells was analysed using the PCX personal computer package. Particular areas of interest i.e. points at which cell contact on the surface, were monitored and intensity plots of scanned areas were recorded. Individual frames were digitally frozen and stored for visual interpretations and analysis.

When cells were directly over an aperture array, the array image was clearly distorted and within each aperture intense, rapid and small scintillations were seen. Resolution of the image depended on the size of the aperture and separation distance. In addition to imaging cells over the aperture arrays, those on the adjacent plain substrate were also examined.

When B_o non-adherent cells were viewed, translocation of cells across the grid was easily visualised, marked by fluctuating punctate pattern of bright spots which moved en masse. These light patterns corresponding to positions of cell visualised by direct epi-illumination, and appear to be areas of the lower cell surface which enter the evanescent field, thus creating conditions for secondary light emission. It was noted that the whole cell movement was not random, also the intrinsic pattern of spots from an individual cell changed suggesting that either cells rotated during gross movement or that the different areas of cells transiently entered the field relating to the mechanism by which the cells translocate.

When breast tumour adherent cells were examined, similar light profiles were seen, i.e. discrete points of light distributed over the whole-cell outline. The behaviour of these points of light depended on the substrate to coat the grids. Thus, on Poly-L-Lysine and native grids these did not fluctuate significantly and the cells were immobile. However, on collagen

VIII, they fluctuated with a regular periodicity of about 2 seconds. Such fluctuations are unusual, and to our knowledge have not been reported before. Further, the fluctuations reciprocally alternated with each others. This suggests that there was rhythmical entry and exit of cell components into and from the evanescent field. i.e. that the device is recording sub-cell pulsatile behaviour in addition to overall movement.

The nature of origin and dimensions of the point secondary emissions from cells remains to be established, but appears likely to be cytoplasmic extensions into the near field. Their dynamic but regular behaviour indicates they are controlled by cell physiological mechanisms. in particular those related to the cytoskeleton, but are unlikely to derive from pseudopodia since these organelles remodel relatively slowly (minutes). Similarly, filipodia would not have the rapid regular movements seen here. The most likely candidate is membrane ruffles, although the almost exact reciprocity of the fluctuations would need explanation.

VIII. DISCUSSION

Utilising this method of illumination an improvement in sensitivity over conventional white light microscopy is achieved. It can be seen that intensity fluctuations are associated only within the immediate vicinity of a aperture however the nature of the cell movement responsible for causing the observed intensity fluctuations has yet to be identified. However it is unlikely that movement of the whole cell through Brownian motion is responsible indicating that motion at the sub-cellular level (membrane fluctuations. cytosol flow) is responsible.

Several different metals exist that could be used in SPR. We have primarily used chromium films for the initial stages of testing due to the fact that silver coated substrates are difficult to fabricate and after coating with a preventative oxidation layer, cell adhesion to the aperture bearing surface was extremely difficult.

Progressive improvement in optical coupling and control will improve the process and should allow greater resolution of the fluctuations. Similarly, increases in array density will lead to improved resolution in the analysis of cell behaviour though it must be borne in mind that the apertures can not be resolved if aperture to aperture separation is smaller than the resolution of the microscope being used. Other metals and optical configurations will be investigated in order that other cell types and adhesion processes can be studied e.g. microbial biofilms. biofouling etc.

Present and future investigations of the surface plasmons with the use of a Photon Scanning Tunnelling Microscope (PSTM) has. at present. revealed interesting field profiles on the bare metal surface extending above the metal surface and decaying exponentially. as predicted. Further studies into the surface plasmons in and around the apertures may reveal an increasing amount of detail of the interactions of the biological cells with the surface plasmons.

From the progressive improvements and investigations a mathematical model of the interactions of the surface plasmons and the biological cells will be developed and used to identify the reactions of cells to stimuli.

IX. ACKNOWLEDGEMENTS

The authors would like to thank Dr G Stacey (ECACC. CAMR) and Dr R Moore (CAMR) for their invaluable assistance in the preparation and microscopy of animal cell cultures.

Mr A Matthews (University of Plymouth) for his assistance in the manufacture of the optical coupling rig.

All the technical staff within the C.R.I.S.T. facility (University of Plymouth) for all their thin-film knowledge and assistance.

All the staff within FORCE Cancer Research for all their biological knowledge and assistance.

X. REFERENCES:

[1] Gordon M. Riley G.P. and Greaves M.F. *Nat. 326 P403-407 1987*

[2] Stossel. T.P (1994) The Machinery of Cell Crawling. *Scientific American, Sept. 1994., p 40-47*

[3] Raether H.. 'Surface plasma oscillations and their applications'. *Physics of Thin Films, Vol. 9, 1977.*

[4] Sambles R. 'Photons excitation of surface plasmons on real surfaces'.. *Surface plasmon-polaritons - IOP short meetings, Vol. 9, 1987*

[5] Pockrand I.. 'Surface plasma oscillations at silver surfaces with thin transparent and absorbing coatings'. *Surface Science, Vol. 72, 1987*

[6] Macleod H.A.. 'Thin Film Optical Filters'. *2nd Edition, 1986*

[7] Kretschmann E and Raether H. *Z Naturforsch, Teil A, 23, P2135 1968.*

[8] Born M. and Wolf E.. 'Principles of Optics'. *Pergamon, New York, 1970*

Nanobiology, 1996, Vol. 04, pp. 17-24
Reprints available directly from the publisher
Photocopying permitted by license only

A Study of Cell Adhesion and Chemotaxis Using Nanolithographically Produced Arrays of Submicron Optical Sources

A. S. HOOD[a], R. NEAL[a], J. GARLAND[b], S. AL-SHUKRI[c] and R. CARR[c]

[a]*University of Plymouth, School of Electronic, Communication and Electrical Engineering, Drake Circus, Plymouth PL4 8AA, UK;*
[b]*FORCE Cancer Research Centre, Noy Scott House, Haldon View Terrace, Wonford, Exeter, Devon EX2 5DW, UK;*
[c]*Centre for Applied Microbiology and Research, Porton Down, Salisbury, Wiltshire SP4 0JG, UK*

Cell adhesion and chemotaxis are two key factors determining cell behaviour and differentiation which are currently analyzed by microscopic examination of the cell or membrane associated fluorescence labels. These analyses are often slow, labour intensive and of limited information content. We describe an optical method suitable for monitoring cell contact and adhesion to surfaces that uses arrays of apertures nanolithographically reproduced in the surface of a surface plasmon resonance (SPR) sensor structure. The light scattered by each aperture fluctuates as cell surfaces approach to within a few hundred nanometers of the aperture surface. Digitizing the output from a CCD camera imaging the aperture array allows patterns of fluctuations to be correlated with the contact and adhesion of individual cells on the surface. Initial results with model animal (CHO) cell lines are described and future developments discussed.

Keywords: Cell Adhesion, Chemotaxis

INTRODUCTION

Cell adhesion and movement are two fundamental properties determining tissue growth and differentiation.

Cell adhesion is mediated by the interaction of receptor sites on the cell surface with specific intercellular matrix proteins or intracellular adhesion molecules present on other cells (ICAMS and Adhesions). Intracellular matrix molecules (collagens, pi-glycosaminoglycans) also sequester other peptide growth factors from serum or surrounding cells (Gordon *et al.*, 1987). Together, such molecules and their interaction regulate cell growth, tissue formation, differentiation and position of cells within an environment.

Cell movement is virtually a ubiquitous property of cells. Those apparently stationary cells remain in situ by virtue of their interaction with substrates (e.g. matrix proteins). Changes in these substrates will ultimately alter the cell's behavioural characteristics. Tissue regeneration relies heavily on cell movement to regenerate tissue three dimensional structure. Other cells, for example blood and tissue macrophages and cells of the immune system, are specialized for rapid and free movement in response to stress factors. This freedom of movement is vitally important for the successful generation of an immune response. Finally, tumour cells have (Stossel, 1994) an increased capacity for movement which is responsible for their fatal dis-

semination through the body. Cell movement can be considered at two levels:

- movement of the whole cell usually along a chemo-attractant gradient;
- movement of the cell surface membranes and components therein.

Monitoring and analysis of whole cell movement currently relies on crude, labour intensive and time consuming visual observation, albeit often assisted by time-lapse video. Cells are typically placed in a microchamber connected by a capillary to another chamber containing a cell attractant and movement of the cell along the chemo-attractant gradient is monitored over long periods (several hours). However, cell movement is often stochastic and difficult to quantify objectively. Furthermore, time-lapse video can only deal with a limited number of cells at once over a long time period, cannot resolve events within the time-frame access period and cannot readily merge or process data into a manipulative (digitised/binary) form. Currently, there is considerable interest in developing methods by which the movement of cells can be studied at the molecular level, i.e. as mediated by aggregation of receptor peptides, etc. No good analytical methods exist beyond labelling surfaces with antibodies and using optical microscopy to monitor gross movement of label; e.g. fluorescence energy transfer (FET) between neighbouring molecules has been used with some success but the technique is highly spatially dependent and its specificity for peptides directly associated with primary ligand is uncertain. These techniques report on the overall change in cell contact and membrane behaviour but it is known that the contact that the cell makes with its substrate can vary with different substrate properties and under different environmental stimuli. The development of analytical techniques by which the contacting of cell surfaces with underlying substrates can be measured and changes in that contact (adhesion) correlated with the onset of cell movement would be of significant interest to cell biologists.

We have developed a method of monitoring the interaction of the cell membrane with the substrate which reports only on those regions of the cell that either contact, or approach to within about 250 nm of the surface. The method is based on the microscopic detection of fluctuations in the intensity of light scattered by arrays of apertures in a thin metal film in which surface plasmons (SPs) were excited by frustrated total internal reflection (FTIR) with a laser beam. The intensity fluctuations are caused by contact of the cell wall with the aperture surface and the size and spacings of apertures in the array are such that any given cell will cover a number of apertures, allowing high resolution studies of cell contact/adhesion to be made within individual cells.

SURFACE PLASMONS

Surface plasmon waves (or SPs), can exist in the boundary region of a metal–dielectric interface. These propagating waves have the property of being evanescent on both sides of the interface. Surface plasmons result from the oscillatory behaviour of free electrons in the metal by the action of an incident optical electromagnetic field. Their frequency (ω) is a function of their wave vectors ($k_{(z)}$) which is given by the dispersion relation $\omega(k_{(z)})$. These charge fluctuations, which are localized in the z direction are accompanied by a mixed transversal and longitudinal magnetic field disappearing at $|x| \rightarrow \infty$ and having a maximum at the surface $x=0$.

The field maximum at the metal-dielectric interface explains the sensitivity of the field to changes in physical properties and disturbances at the metal surface and exists only for TM polarisation, i.e. the magnetic field is transverse to the direction of propagation. It can be shown by Maxwell's theory that electromagnetic surface waves can propagate along a metallic surface or on metallic films with a broad spectrum of eigen frequen-

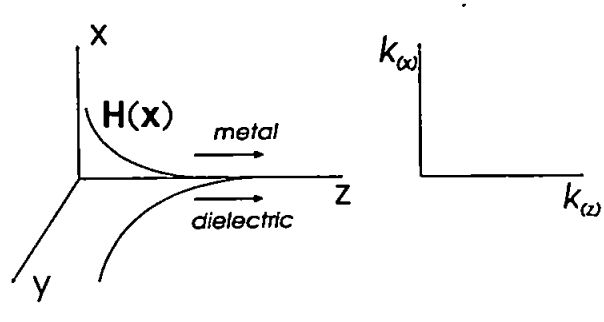

FIGURE 1 A graph of the magnetic field versus the vertical distance from the surface.

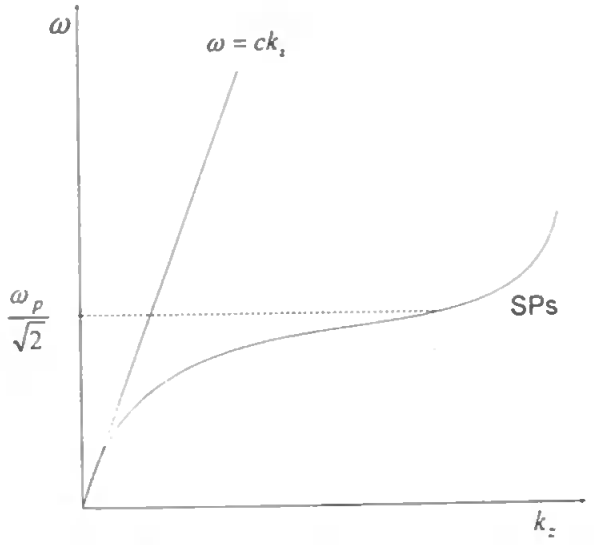

FIGURE 2 A graph of dispersion relation versus frequency showing that the dispersion relation of the surface plasmon lies to the right of the light line ($\omega = ck_{(z)}$).

cies from $\omega=0$ up to $\omega=\omega_p/\sqrt{2}$ depending on the wave vector **k** as can be seen in Figure 2.

FUNDAMENTAL PROPERTIES

A full description of SPs is obtained from Maxwell's equations using appropriate boundary conditions. At optical frequencies, a metal can be treated as a dielectric with a complex permittivity with the real part large and negative i.e. $\varepsilon_m = \varepsilon'_m - j\varepsilon''_m$.
The magnetic field is described by the equation

$$H = H(x)\exp(-k''_{(z)}z)\exp(-jk'_{(z)}z) \quad (1)$$

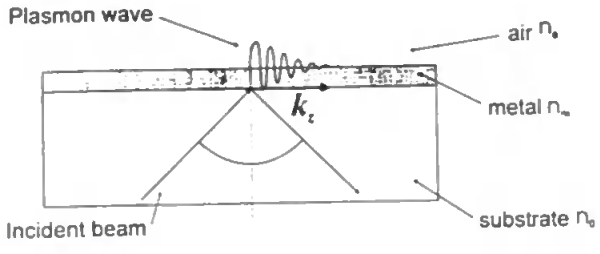

FIGURE 3 A schematic of a surface plasmon coupler.

The wave vector $k_{(z)}$ lies parallel to the z direction; $k_{(z)} = 2\pi/\lambda_p$ where λ_p is the wavelength of the plasma oscillations (Figure 3). As the wave vector $k_{(z)}$ is continuous through the interface the dispersion relation can be written as

$$k_{(z)} = \sqrt{\left(\frac{\varepsilon_m \varepsilon_a}{\varepsilon_m + \varepsilon_a}\right)} \quad (2)$$

where ε_a is the dielectric constant of the medium above the metal ($\varepsilon_a = n_a^2$) and c is the speed of electromagnetic radiation in a vacuum.

EXCITATION OF SURFACE PLASMONS BY LIGHT

Optical power can be transferred across a dielectric gap by means of an evanescent field providing the gap is small ($\cong 1\mu m$), a mechanism termed optical tunnelling. This was accomplished in this work by means of an Attenuated Total Reflection (ATR) prism coupler, the principle of which is shown in Figure 4. Photons can

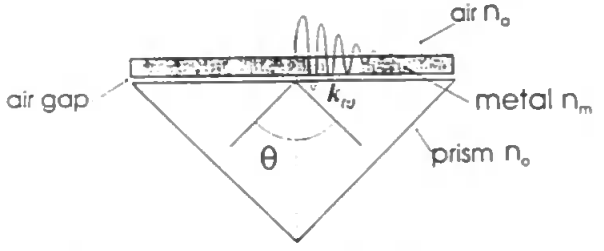

FIGURE 4 The Attenuated Total Reflection coupler.

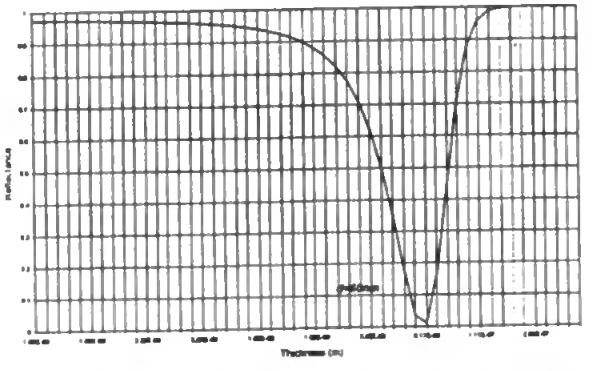

FIGURE 5 A theoretical graph of Thickness versus Reflectivity, at the SPR angle, for a Silver film using the ATR configuration.

only excite surface plasmons if $k_{(z)} \leq \omega/c$. By varying θ until the propagation vector k of the decaying evanescent wave matches the wave vector $k_{(z)}$ of the plasmon wave and plasmons are excited.

At the surface plasmon resonance (SPR) angle, the dispersion relation ($k_{(z)}$) becomes;

$$k_{(z)} = n_0 \frac{\omega}{c} \sin\theta \qquad (3)$$

where n_0 is the refractive index of the prism.

The thickness *(d)* of the metal film is a determining factor in the SPR angle and thus reflectivity (Figure 5). Changing the metal and metal thickness will determine the enhancement characteristics of the coupling process. At the wavelength in question (632.8nm) the enhancement factor of silver is considerably greater than that of chrome.

The SPR wave will exponentially decay ($e^{-k_z'' z}$) with z, where k_z'' is the imaginary value of the complex dispersion relation and is also known as the absorption factor. The Propagation Length of the surface plasmon at which its intensity falls to 1/e is given by;

$$Li = \frac{1}{k''_{(z)}} \qquad (4)$$

and is shown graphically in Figure 6.

SUBSTRATE FABRICATION

Hoya LT substrates with a refractive index of 1.53 were used to fabricate the matrix. With the availability of Electron beam written mask plates, prepared at CAMR–Porton Down, several varying sized matrixes were fabricated together in the CRIST facility at the University of Plymouth using photolithography techniques.

The substrates were initially ultrasonically cleaned and rinsed with Acetone and Isopropanol before being finally rinsed with de-ionised water and dried in an oven at 110°C for 20 minutes. The substrates were then metalised using a sputter coater (Materials Research Company Ltd, St Johns Estate, Penn, Bucks, UK) depositing Chromium and/or Silver to a pre-determined optimum thickness.

UCB Photoresist was spun to a thickness of 1.3 µm on to the metalised surface at 5000 rpm for 45 seconds and baked in the oven for 25 min at 125°C. The metalised substrate was then exposed to ultraviolet light through the mask plate on a Pricema International photolithography unit for 17 seconds. Again the substrate was baked in the oven at 125°C for 10 minutes and developed in Shipley 351 Microposit developer for 10–15 s before being etched in a Ion beam miller (CVC, Scientific Products Ltd, Hogwood Lane, Finchampstead, Wokingham, Berkshire, UK).

Utilising this method a resolution of approximately 1µm diameter aperture was repeatably achievable. The completed substrate was then diced up into individual

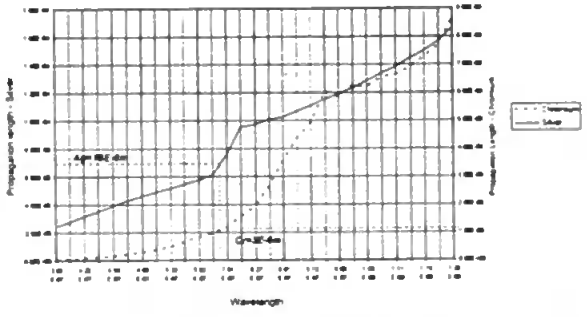

FIGURE 6 A comparison of the Propagation Length of Silver and Chromium films.

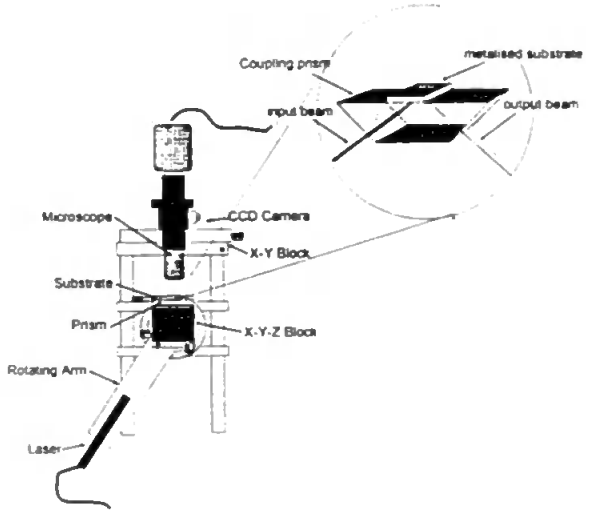

FIGURE 7 A diagram of the coupling rig used in the experimental analysis.

samples with aperture matrix sections used in the coupling process.

Where greater resolution, i.e. to approximately 1 micron diameter and less is required, directly written substrates were fabricated at CAMR and used in the ATR coupler.

Several different aperture sizes and inter-aperture spacing matrices were fabricated and tested under SPR conditions. By experimental analysis it was found that the best resolvable optical results were obtained from apertures with an inter-aperture spacing of no less than 5 µm when using apertures of approximately 1µm. Depending on the physical size of the cells under test different matrices were used in order that the cell would cover a range of apertures at any one time.

EXPERIMENTAL SET-UP

The coupling prism was mounted on a Photon Control X-Y-Z micrometer adjustment block with the substrate placed on the upper surface. A 5mW Helium Neon laser was fixed to a micrometer adjustment rotating arm such that the beam remained central relative to a point on the substrate. Surface plasmon resonance could be repeatedly attained by adjustment of the angle at which the incident laser light fell on the metal film surface and the X-Y-Z block.

An optical microscope fitted with a high sensitivity CCD camera was mounted above the X-Y-Z block such that it could be moved, in three dimensions, relative to the surface of the substrate. A long working distance ×10 objective with zoom made the substrate face accessible.

The cells were kept at a constant 37°C ± 0.5°C by means of a heating unit consisting of a 2 Amp 15 volt Peltier heating device linked to a thermometer and feedback loop. With the prepared metalised substrate placed on the top surface of the dove tail prism light could be coupled into the metal surface from the underside to excite surface plasmons on the top side of the substrate. A well, consisting of a rubber 'O' ring, was placed over the matrix of the substrate.

The well was filled with the cell mixture and a glass cover slide placed on the upper side of the 'O' ring in order to present the microscope with a flat optical surface through which the metalised surface could be viewed without the distortion of the curved meniscus of the fluid.

As cells settle on to the substrate surface changing the dielectric constant in the near field of the metalised surface, an energy transformation takes place and changes in the scattering of light can be visually monitored and an intensity profile can be made.

ANIMAL CELL LINES AND SAMPLE PREPARATION

Prior to animal cell studies the system described above was optically calibrated using polystyrene (latex) microspheres (Sigma Chemical Co. Ltd., Poole, Dorset, UK) of mean diameter 2.92µm (SD=0.012µm, Lot #92573) suspended to a concentration of 10^8/ml in demineralised 0.22µm filtered water. The diameter of the apertures in the array used was 2µm allowing the interaction of the 3µm beads to be clearly visualised. The intensity fluctuation associated with the approach, under Brownian motion, of the calibrant latex microspheres was recorded using a conventional video recorder and analysed using a PC based image analysis system (PCX system, Brian Reece Ltd., Newbury, Berks.) linked to the CCD camera.

For animal cell studies, suspensions of Chinese Hamster ovary (CHO) cells were obtained from the European Collection of Animal Cell Cultures (Accession No. 85050302 - ECACC, CAMR, Porton Down, Wilts.). These cells were chosen for their relative robustness, suitable size (10µm diameter) and adherence properties. The cells were cultured in a conventional cell culture medium (Hams S12 containing 10% fetal calf serum; PAA Gmbh, Austria) at 37°C. Suspensions of cells adhering to culture bottles were prepared by treatment with trypsin/EDTA (Gibco Ltd., Paisley, Scotland) prior to mixing in fresh medium to a concentration of 10^5 cells/ml. To minimise bacterial contamination the suspending medium contained aliquots of a solution of Penicillin and Streptomycin (50,000 units/ml - Gibco Ltd.) diluted to a final solution of 5,000 units/ml. Cell concentrations were confirmed

microscopically by haemocytometer count with Trypan Blue visualising dye.

Aliquots of cell suspensions were placed onto aperture arrays (prepared as in Section V.) comprising 1.4μm apertures at 5μm centre spacing. The diameter of the cells (approx. 10μm spheres) meant that, on adhesion to the surface (with a concomitant slight increase in diameter to typically 15μm) each cell would cover at least 3 apertures at any given time. The overall cell concentration was selected such that surface coverage of the aperture array would approach 10% when all cells had settled onto the surface and subsequently adhered.

Cells were incubated in the aperture array illumination system for up to 24 hours, initial signs of sedimentation and adhesion being apparent after the first 3–4 hours. Images of the surface were recorded at suitable intervals (e.g. for 5 minutes every 2–3 hours) for subsequent analysis.

ANALYSIS OF EXPERIMENTAL RESULTS

The data obtained from the experiments using CHO cells was analyzed using the PCX personal computer package. Particular areas of interest i.e. points at which cell contact on the surface, were monitored and intensity plots of scanned areas were recorded. Individual frames were digitally frozen and stored for visual interpretations and analysis.

Figure 8 refers to an individual cell modulating the near field of a 2μm diameter aperture grid with 5μm spacing between apertures. Thus, with the average size of the CHO cell line being approximately 10μm in diameter, the cell is centred on one aperture only. With a smaller aperture size and inter aperture spacing a greater number would be covered at any one time by a given cell, resulting in an improved interpretation.

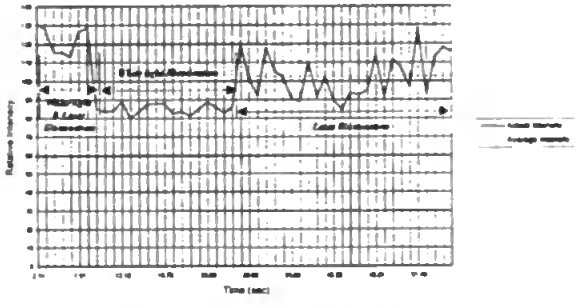

FIGURE 8 The Relative Intensity plot of the light from an individual aperture being modulated by a CHO cell after 18 hours.

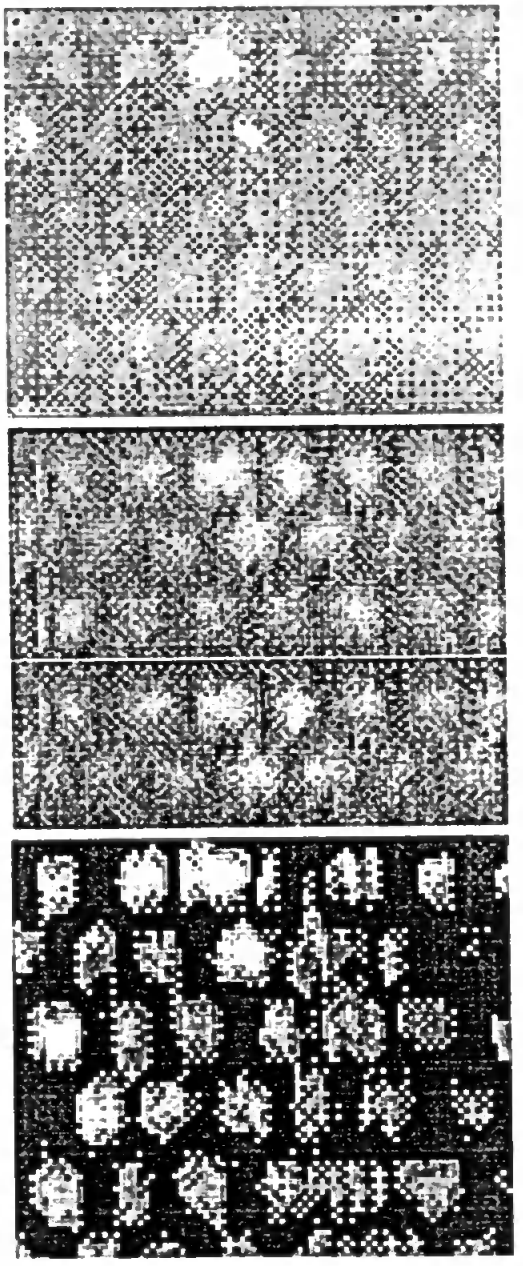

FIGURE 9 A visual comparison of the differing illumination set-ups in the ATR coupler. (a) White & Laser light illuminated. (b) White light illuminated. (c) Laser illuminated.

through higher resolution, of cell behaviour. As can be seen in Figure 8 the change in relative intensity is a result of the surface plasma in the near field surrounding the aperture being modulated by the presence of the CHO cell. Visual examination of the particular cell positioned over the aperture in this instance did not show any gross (whole cell) movement that could be considered responsible for the intensity fluctuations observed. It is probable, therefore, that the observed fluctuations are indicative of either minute movement in the cell membrane relative to the aperture or Brownian motion of cell oranelles e.g. endoplasmic reticulum, mitochondria etc. within the cell cytosol.

Figure 8 shows the aperture matrix under three states of different illumination conditions. As can be clearly seen the amplitude of the observed intensity fluctuations is greater when the device is illuminated with laser illumination as opposed to being illuminated by white light. Combined illumination of the device with laser and white light resulted in a greater overall intensity but with reduced amplitude in fluctuation intensity compared with laser illumination alone. The marked increase in the amplitude of the fluctuations during the laser illuminated period is due to the cells interrupting the surface plasmons in the near field of the metal surface by altering the dielectric constant of the medium significantly such that energy transformation occurs resulting in visual intensity changes. Figure 9 shows these three states with a marked visual contrast between the white light and laser illumination, white light illumination and laser illumination respectively.

DISCUSSION

Utilising this method of illumination an improvement in sensitivity over conventional white light microscopy is achieved. As seen in Figures 8 and 9 illumination with the laser generated a greater contrast in fluctuation amplitude as well as a higher average light intensity level. It can be seen that intensity fluctuations are associated only within the immediate vicinity of a aperture however the nature of the cell movement responsible for causing the observed intensity fluctuations has yet to be identified. However it is unlikely that movement of the whole cell through Brownian motion is responsible indicating that motion as the sub-cellular level (membrane fluctuations, cytosol flow) is responsible.

Several different metals exist that could be used in SPR. A comparison of two have been shown in this paper, Silver and Chromium. As discussed in chapter IV and shown in Figure 6 silver has a much better enhancement factor and a longer propagation length at resonance but has a much sharper and therefore a more exact resonance coupling angle. We have primarily used a chromium films for the initial stages of testing due to the fact that silver coated substrates are difficult to fabricate and after coating with a preventative oxidation layer, cell adhesion to the aperture bearing surface was extremely difficult.

Progressive improvement in optical coupling and control will improve the process and should allow greater resolution of the fluctuations. Similarly, increases in array density will lead to improved resolution in the analysis of cell behaviour though it must be borne in mind that the apertures can not be resolved if aperture to aperture separation is smaller than the resolution of the microscope being used. Other metals and optical configurations will be investigated in order that other cell types and adhesion processes can be studied e.g. microbial biofilms, biofouling etc.

Acknowledgements

This project was funded by a pump primer grant from the Science and Engineering Research Council

The authors would like to thank Dr G Stacey (ECACC, CAMR) and Dr R Moore (CAMR) for their invaluable assistance in the preparation and microscopy of animal cell cultures.

Mr A Matthews (University of Plymouth) for his assistance in the manufacture of the optical coupling rig.

All the technical staff within the C.R.I.S.T. facility (University of Plymouth) for all their thin-film knowledge and assistance.

References

[1] Gordon M, Riley G.P. and Greaves M.F. Nat. 326 P 403–407 1987
[2] Stossel, T.P (1994) The Machinery of Cell Crawling. Scientific American, Sept. 1994., p 40–47
[3] Raether H., 'Surface plasma oscillations and their applications', Physics of Thin Films, Vol. 9, 1977.
[4] Sambles R, 'Photons excitation of surface plasmons on real surfaces',. Surface plasmon-polaritons-IOP short meetings, Vol. 9, 1987
[5] Pockrand I., 'Surface plasma oscillations at silver surfaces with thin transparent and absorbing coatings', Surface Science, Vol. 72, 1987.
[6] H.A. Macleod, 'Thin Film Optical Filters', 2nd Edition, 1986

Appendix B

Scanning Probe Microscopy Software Control Algorithms

```
//* Single Horizontal Line Scan *//

#include <stdio.h>
#include <dos.h>
#include <process.h>
#include <string.h>
#include <time.h>
#include <conio.h>
#include <graphics.h>
#include <dir.h>
#include <stdlib.h>
#include <math.h>
#include <iostream.h>

/*initiating graphics drivers*/
void far detectgraph(int far *graphdriver, int far *graphmode);

/* DAC base address */
#define PCXBASE 0x220

/* Initialising adc board*/
void InitADC(void)
        {

/* select software trigger at base+12 */
        outportb(PCXBASE+11,1);

/* adc gain x1 \=/- 1.25v fsd */
        outportb(PCXBASE+9,3);

/* input channel select */
        outportb(PCXBASE+10,0);
        }

/* Digitise ADC & store result */
unsigned int digit(int channel)
        {
        unsigned int i,hibyte,lobyte,sample;

/* select channel */
        outportb(PCXBASE+10,channel);

/* digitise */
```

```
        outportb(PCXBASE+12,0);
        hibyte= inp(PCXBASE+5);
        lobyte= inp(PCXBASE+4);
        return (hibyte*256)+lobyte;
        }

/*main part of program*/
int main(void)
        {
                int a=0,c=0,j,k;
                char buffer[100];
                outport(PCXBASE+4,c);
                outport(PCXBASE+6,a);
                float e,g;
        long int totala,totalb,zero,one,upper,lower,xgrid,ygrid,oldx=0,oldy=2000;
                FILE *f;
                InitADC();

/* request auto detection */
        int gdriver = DETECT, gmode, errorcode;

/* initialise graphics mode */
        initgraph(&gdriver, &gmode, "C:\\END");
        setlinestyle(0,1,14);

/*open file and prepare to write*/
                        f=fopen("11x_001","w");
                        if (!f) return 1;

/*set limits of scan*/
                        while ((a<4000) && (!kbhit()))
                                {

/*set scan resolution*/
                                        a=a+10;
                                        outpw(PCXBASE+6,a);
                                        totala=0;totalb=0;zero=0;

/*averaging factor*/
                                        for(j=0;j<10000;j++)
                                                {
                                                totala=totala+digit(0);
                                                }
```

```
                                zero=totala/10000;

/*print to file*/
                                fprintf(f,"%u %ld\n",c,zero);

/*display results*/
                                setfillstyle(SOLID_FILL,BLACK);
                                bar(0,436,500,454);
                                sprintf(buffer,"X=%4.0u",a);
                                outtextxy(10,442,buffer);
                                sprintf(buffer,"Y=%4.0u",c);
                                outtextxy(100,442,buffer);
                                sprintf(buffer,"I=%4.0u",zero);
                                outtextxy(200,442,buffer);
                                line(oldx/8,oldy/10,a/8,zero/10);
                                oldx=a;oldy=zero;
                        }

/*return probe to initial position*/
                        for (k=a;k>0;k--)
                                {
                                outpw(PCXBASE+6,a);
                                a=k;
                                delay(2);
                                }
        fclose(f);
        return 0;
}
```

```
//* Multiple Horizontal Line Scan *//

#include <stdio.h>
#include <dos.h>
#include <process.h>
#include <string.h>
#include <time.h>
#include <conio.h>
#include <graphics.h>
#include <dir.h>
#include <stdlib.h>
#include <math.h>
#include <iostream.h>

/*initiating graphics drivers*/
void far detectgraph(int far *graphdriver, int far *graphmode);

/* DAC base address */
#define PCXBASE 0x220

/* Initialising adc board*/
void InitADC(void)
        {

/* select software trigger at base+12 */
        outportb(PCXBASE+11,1);

/* adc gain x1 \=/- 1.25v fsd */
        outportb(PCXBASE+9,3);

/* input channel select */
        outportb(PCXBASE+10,0);
        }

/* Digitise ADC & store result */
unsigned int digit(int channel)
        {
        unsigned int i,hibyte,lobyte,sample;

/* select channel */
        outportb(PCXBASE+10,channel);

/* digitise */
```

```
        outportb(PCXBASE+12,0);
        hibyte= inp(PCXBASE+5);
        lobyte= inp(PCXBASE+4);
        return (hibyte*256)+lobyte;
        }

/*main part of program*/
int main(void)
        {
                int a=0,c=0,j,k;
                char buffer[100];
                outport(PCXBASE+4,c);
                outport(PCXBASE+6,a);
                float e,g;
        long int totala,totalb,zero,one,upper,lower,xgrid,ygrid,oldx=0,oldy=2000;
                FILE *f;
                InitADC();

/* request auto detection */
        int gdriver = DETECT, gmode, errorcode;

/* initialise graphics mode */
        initgraph(&gdriver, &gmode, "C:\\END");
        setlinestyle(0,1,14);

/*open file and prepare to write*/
                        f=fopen("11x_001","w");
                        if (!f) return 1;

/*set limits of scan*/
                        while ((c<2000) && (!kbhit()))
                                {

                        while ((a<2000) && (!kbhit()))
                                {

/*set scan resolution*/
                                        a=a+5;
                                        outpw(PCXBASE+6,a);
                                        totala=0;zero=0;

/* averaging factor*/
                                        for(j=0;j<5000;j++)
```

```
                                        {
                                        totala=totala+digit(0);
                                        }
                                        zero=totala/5000;

/*print to file*/
                                fprintf(f," %ld ",zero);
                                setfillstyle(SOLID_FILL,BLACK);
                                bar(0,436,700,454);
                                sprintf(buffer,"X=%4.0u",a);
                                outtextxy(10,442,buffer);
                                sprintf(buffer,"Y=%4.0u",c);
                                outtextxy(100,442,buffer);
                                sprintf(buffer,"I=%4.0u",zero);
                                outtextxy(200,442,buffer);
                                sprintf(buffer,"SCAN No.=%4.0u",totalb);
                                outtextxy(300,442,buffer);
                                line(oldx/4,oldy/10,a/4,zero/10);
                                oldx=a;oldy=zero;
                        }

                        fprintf(f,"\n");

/*return probe to initial position*/
                        for (k=a;k>0;k--)
                                {
                                outpw(PCXBASE+6,a);
                                a=k;
                                delay(1);
                                }
                        a=0;
                        oldx=0;oldy=3000;
                        c=c+5;
                        outport(PCXBASE+4,c);
                        totalb=totalb+1;
                        }

                fclose(f);
                return 0;
        }
```

```
//* Multiple Horizontal Line Scan With 2-Dimensional Colour Contour Plot*//

#include <stdio.h>
#include <dos.h>
#include <process.h>
#include <string.h>
#include <time.h>
#include <conio.h>
#include <graphics.h>
#include <dir.h>
#include <stdlib.h>
#include <math.h>
#include <iostream.h>

/*initiating graphics drivers*/
void far detectgraph(int far *graphdriver, int far *graphmode);

/* DAC base address */
#define PCXBASE 0x220

/* Initialising adc board*/
void InitADC(void)
        {

/* select software trigger at base+12 */
        outportb(PCXBASE+11,1);

/* adc gain x1 \=/- 1.25v fsd */
        outportb(PCXBASE+9,3);

/* input channel select */
        outportb(PCXBASE+10,0);
        }

/* Digitise ADC & store result */
unsigned int digit(int channel)
        {
        unsigned int i,hibyte,lobyte,sample;

/* select channel */
        outportb(PCXBASE+10,channel);

/* digitise */
```

```
        outportb(PCXBASE+12,0);
        hibyte= inp(PCXBASE+5);
        lobyte= inp(PCXBASE+4);
        return (hibyte*256)+lobyte;
        }

/*main part of program*/
int main(void)
        {
                int a=0,c=0,j,k;
                char buffer[100];
                outport(PCXBASE+4,c);
                outport(PCXBASE+6,a);
                float e,g;
        long int totala,totalb,zero,one,upper,lower,xgrid,ygrid,oldx=0,oldy=2000;
                FILE *f;
                InitADC();

/* request auto detection */
        int gdriver = DETECT, gmode, errorcode;

/* initialise graphics mode */
        initgraph(&gdriver, &gmode, "C:\\END");
        setlinestyle(0,1,14);

/*open file and prepare to write*/
                        f=fopen("11x_001","w");
                        if (!f) return 1;

/*set limits of scan*/
                        while ((c<2000) && (!kbhit()))
                                {

                        while ((a<2000) && (!kbhit()))
                                {

/*set scan resolution*/
                                        a=a+5;
                                        outpw(PCXBASE+6,a);
                                        totala=0;zero=0;

/* averaging factor*/
                                        for(j=0;j<5000;j++)
```

```
                                        {
                                        totala=totala+digit(0);
                                        }
                                        zero=totala/5000;

/*print to file*/
                                fprintf(f," %ld ",zero);
                                setfillstyle(SOLID_FILL,BLACK);
                                bar(0,436,700,454);
                                sprintf(buffer,"X=%4.0u",a);
                                outtextxy(10,442,buffer);
                                sprintf(buffer,"Y=%4.0u",c);
                                outtextxy(100,442,buffer);
                                sprintf(buffer,"I=%4.0u",zero);
                                outtextxy(200,442,buffer);
                                sprintf(buffer,"SCAN No.=%4.0u",totalb);
                                outtextxy(300,442,buffer);
                                line(oldx/6,y,a/6,y);
                                oldx=a;
/*set colour tolerance level*/
                                lower=1300;
                                toler=100;

/*determining detected limits*/
        if((zero>lower) && (zero<(lower+(1*toler)))) setcolor(1);
        if((zero>(lower+(1*toler)) && (zero<(lower+(2*toler))))) setcolor(2);
        if((zero>(lower+(2*toler)) && (zero<(lower+(3*toler))))) setcolor(3);
        if((zero>(lower+(3*toler)) && (zero<(lower+(4*toler))))) setcolor(4);
        if((zero>(lower+(4*toler)) && (zero<(lower+(5*toler))))) setcolor(5);
        if((zero>(lower+(5*toler)) && (zero<(lower+(6*toler))))) setcolor(6);
        if((zero>(lower+(6*toler)) && (zero<(lower+(7*toler))))) setcolor(7);
        if((zero>(lower+(7*toler)) && (zero<(lower+(8*toler))))) setcolor(8);
        if((zero>(lower+(8*toler)) && (zero<(lower+(9*toler))))) setcolor(9);
        if((zero>(lower+(9*toler)) && (zero<(lower+(10*toler))))) setcolor(10);
        if((zero>(lower+(10*toler)) && (zero<(lower+(11*toler))))) setcolor(11);
        if((zero>(lower+(11*toler)) && (zero<(lower+(12*toler))))) setcolor(12);
        if((zero>(lower+(12*toler)) && (zero<(lower+(13*toler))))) setcolor(13);
        if((zero>(lower+(13*toler)) && (zero<(lower+(14*toler))))) setcolor(14);
        if((zero>(lower+(14*toler)) && (zero<(lower+(15*toler))))) setcolor(15);

                                }

                                fprintf(f,"\n");
```

```
/*return probe to initial position*/
                                for (k=a;k>0;k--)
                                        {
                                        outpw(PCXBASE+6,a);
                                        a=k;
                                        delay(1);
                                        }
                                a=0;
                                oldx=0;oldy=3000;
                                c=c+5;
                                y=y++;
                                outport(PCXBASE+4,c);
                                totalb=totalb+1;
                                }

                fclose(f);
                return 0;
        }
```

```
//* Constant Intensity Mode - Single Horizontal Line Scan *//

#include <stdio.h>
#include <dos.h>
#include <process.h>
#include <string.h>
#include <time.h>
#include <conio.h>
#include <graphics.h>
#include <dir.h>
#include <stdlib.h>
#include <math.h>
#include <iostream.h>

/*initiating graphics drivers*/
void far detectgraph(int far *graphdriver, int far *graphmode);

/* DAC base address */
#define PCXBASE 0x220

/* Initialising adc board*/
void InitADC(void)
        {

/* select software trigger at base+12 */
        outportb(PCXBASE+11,1);

/* adc gain x1 \=/- 1.25v fsd */
        outportb(PCXBASE+9,3);

/* input channel select */
        outportb(PCXBASE+10,0);
        }

/* Digitise ADC & store result */
unsigned int digit(int channel)
        {
        unsigned int i,hibyte,lobyte,sample;

/* select channel */
        outportb(PCXBASE+10,channel);

/* digitise */
```

```
        outportb(PCXBASE+12,0);
        hibyte= inp(PCXBASE+5);
        lobyte= inp(PCXBASE+4);
        return (hibyte*256)+lobyte;
        }

/*main part of program*/
int main(void)
        {
                int a=0,c=0,j,k;
                char buffer[100];
                outport(PCXBASE+4,c);
                outport(PCXBASE+6,a);
                float e,g;
        long int totala,totalb,zero,one,upper,lower,xgrid,ygrid,oldx=0,oldy=2000;
                FILE *f;
                InitADC();

/* request auto detection */
        int gdriver = DETECT, gmode, errorcode;

/* initialise graphics mode */
        initgraph(&gdriver, &gmode, "C:\\END");
        setlinestyle(0,1,14);

/*open file and prepare to write*/
                        f=fopen("11x_001","w");
                        if (!f) return 1;

/*set limits of scan*/
                        while ((a<4000) && (!kbhit()))
                                {

/*set scan resolution*/
                                        a=a+2;
                                        outpw(PCXBASE+6,a);
                                        totala=0;zero=0;
/*averaging factor*/
                                        for(j=0;j<1000;j++)
                                                {
                                                totala=totala+digit(0);
                                                }
                                                zero=totala/1000;
```

```
/* vertical control within limits*/
                        while(((zero<=lower) || (zero>=upper)) && (!kbhit()))
                                {

                                while((zero>=upper) && (!kbhit()))
                                        {
                                                c=c-2;
                                                outpw(PCXBASE+4,c);
                                                totala=0;zero=0;

                                                for(j=0;j<1000;j++)
                                                        {
                                                        totala=totala+digit(0);
                                                        }
                                                        zero=totala/1000;

                                        }

                                while((zero<=lower) && (!kbhit()))
                                        {
                                                c=c+2;
                                                outport(PCXBASE+4,c);
                                                totala=0;zero=0;

                                                for(j=0;j<1000;j++)
                                                        {
                                                        totala=totala+digit(0);
                                                        }
                                                        zero=totala/1000;

                                        }

                                }

                                totala=0;totalb=0;

/*print to file*/
                                fprintf(f,"%u %ld %u\n",a,zero,c);
                                setfillstyle(SOLID_FILL,BLACK);
                                bar(0,436,500,454);
                                sprintf(buffer,"X=%4.0u",a);
                                outtextxy(10,442,buffer);
```

```
                        sprintf(buffer,"z=%4.0u",c);
                        outtextxy(100,442,buffer);
                        sprintf(buffer,"I=%4.0u",zero);
                        outtextxy(200,442,buffer);
                        line(oldx/7,oldy/10,a/7,c/10);
                        oldx=a;oldy=c;

                }

        fclose(f);
        return 0;
}
```

```
//* Constant Intensity Mode - Multiple Horizontal Line Scan *//

#include <stdio.h>
#include <dos.h>
#include <process.h>
#include <string.h>
#include <time.h>
#include <conio.h>
#include <graphics.h>
#include <dir.h>
#include <stdlib.h>
#include <math.h>
#include <iostream.h>

/*initiating graphics drivers*/
void far detectgraph(int far *graphdriver, int far *graphmode);

/* DAC base address */
#define PCXBASE 0x220

/* Initialising adc board*/
void InitADC(void)
        {

/* select software trigger at base+12 */
        outportb(PCXBASE+11,1);

/* adc gain x1 \=/- 1.25v fsd */
        outportb(PCXBASE+9,3);

/* input channel select */
        outportb(PCXBASE+10,0);
        }

/* Digitise ADC & store result */
unsigned int digit(int channel)
        {
        unsigned int i,hibyte,lobyte,sample;

/* select channel */
        outportb(PCXBASE+10,channel);

/* digitise */
```

```
        outportb(PCXBASE+12,0);
        hibyte= inp(PCXBASE+5);
        lobyte= inp(PCXBASE+4);
        return (hibyte*256)+lobyte;
        }

/*main part of program*/
int main(void)
        {

/*initialising two separate adc boards*/
#define PCXBASE 0x210
                int d=0;
                outport(PCXBASE+4,d);
#define PCXBASE 0x220
                int a=0,c=1000,j,k,l;
                char buffer[100];
                outport(PCXBASE+4,c);
                outport(PCXBASE+6,a);
                float e,g;
        long int totala,totalb,zero,one,upper,lower,xgrid,ygrid,oldx=0,oldy=2000;
                FILE *f;
                InitADC();

/*set tolerance level*/
                printf("Input the pre-set intensity level\n");
                scanf("%f",&e);
                printf("Input the % tolerance required\n");
                scanf("%f",&g);
                upper=(long int)(e+(e*(g/100)));lower=(long int)(e-(e*(g/100)));

/* request auto detection */
        int gdriver = DETECT, gmode, errorcode;

/* initialize graphics mode */
        initgraph(&gdriver, &gmode, "C:\\END");
        setlinestyle(0,1,14);

/*open file and prepare to write*/
                        f=fopen("24xyz001","w");
                        if (!f) return 1;

/*set limits of scan*/
```

```
                while ((d<500) && (!kbhit()))
                        {

                while ((a<500) && ((c<=3995) && (c>=5)) && (!kbhit()))
                        {

/*set scan resolution*/
                                        a=a++;
                                        outpw(PCXBASE+6,a);
                                        totala=0;zero=0;

/*averaging factor*/
                                        for(j=0;j<5000;j++)
                                                {
                                                totala=totala+digit(0);
                                                }
                                                zero=totala/5000;

/*vertical control within set limits*/
while(((zero<=lower) || (zero>=upper)) && ((c<=3995) && (c>=5)) && (!kbhit()))
                                        {

while((zero>=upper) && ((c<=3995) && (c>=5)) && (!kbhit()))
                                        {
                                        c=c-2;
                                        outpw(PCXBASE+4,c);
                                        totala=0;zero=0;

                                        for(j=0;j<5000;j++)
                                                {
                                                totala=totala+digit(0);
                                                }
                                                zero=totala/5000;

                                        }

while((zero<=lower) && ((c<=3995) && (c>=5)) && (!kbhit()))
                                        {
                                        c=c+2;
                                        outport(PCXBASE+4,c);
                                        totala=0;zero=0;

                                        for(j=0;j<5000;j++)
```

```
                                        {
                                        totala=totala+digit(0);
                                        }
                                        zero=totala/5000;

                                }

                                }
                                totala=0;totalb=0;

/*print to file*/
                                fprintf(f," %u ",c);
                                setfillstyle(SOLID_FILL,BLACK);
                                bar(0,436,500,454);
                                sprintf(buffer,"X=%4.0u",a);
                                outtextxy(10,442,buffer);
                                sprintf(buffer,"Y=%4.0u",d);
                                outtextxy(100,442,buffer);
                                sprintf(buffer,"z=%4.0u",c);
                                outtextxy(200,442,buffer);
                                sprintf(buffer,"I=%4.0u",zero);
                                outtextxy(300,442,buffer);
                                line(oldx/7,oldy/10,a/7,c/10);
                                oldx=a;oldy=c;

                        }
                        fprintf(f,"\n");

/*return probe to initial position*/
                        for (l=c;l<4000;l++)
                                {
                                outpw(PCXBASE+4,l);
                                delay(1);
                                }
                                c=l;

                        for (k=a;k>0;k--)
                                {
                                outpw(PCXBASE+6,a);
                                a=k;
                                delay(1);
                                }
```

```
                        for (l=c;l>1000;l--)
                                {
                                outpw(PCXBASE+4,l);
                                delay(1);
                                }
                                c=l;
                                oldy=c;
                                oldx=a;

#define PCXBASE 0x210  /* ADC base addr. */
                                d=d++;
                                outport(PCXBASE+4,d);

#define PCXBASE 0x220  /* ADC base addr. */

                                }

                fclose(f);
                return 0;

        }
```

```
//* Single Vertical Scan *//

#include <stdio.h>
#include <dos.h>
#include <process.h>
#include <string.h>
#include <time.h>
#include <conio.h>
#include <graphics.h>
#include <dir.h>
#include <stdlib.h>
#include <math.h>
#include <iostream.h>

/*initiating graphics drivers*/
void far detectgraph(int far *graphdriver, int far *graphmode);

/* DAC base address */
#define PCXBASE 0x220

/* Initialising adc board*/
void InitADC(void)
        {

/* select software trigger at base+12 */
        outportb(PCXBASE+11,1);

/* adc gain x1 \=/- 1.25v fsd */
        outportb(PCXBASE+9,3);

/* input channel select */
        outportb(PCXBASE+10,0);
        }

/* Digitise ADC & store result */
unsigned int digit(int channel)
        {
        unsigned int i,hibyte,lobyte,sample;

/* select channel */
        outportb(PCXBASE+10,channel);

/* digitise */
```

```
        outportb(PCXBASE+12,0);
        hibyte= inp(PCXBASE+5);
        lobyte= inp(PCXBASE+4);
        return (hibyte*256)+lobyte;
        }

/*main part of program*/
int main(void)
        {
                int a=0,c=0,j,k;
                char buffer[100];
                outport(PCXBASE+4,c);
                outport(PCXBASE+6,a);
                float e,g;
        long int totala,totalb,zero,one,upper,lower,xgrid,ygrid,oldx=0,oldy=2000;
                FILE *f;
                InitADC();

/* request auto detection */
        int gdriver = DETECT, gmode, errorcode;

/* initialise graphics mode */
        initgraph(&gdriver, &gmode, "C:\\END");
        setlinestyle(0,1,14);

/*open file and prepare to write*/
                        f=fopen("11x_001","w");
                        if (!f) return 1;

/*set limits of scan*/
                        for(k=c;k>0;k--)
                                {
                                c=k;
                                outpw(PCXBASE+4,c);
                                delay(5);
                                }

                while (!kbhit())
                        {

/*set scan resolution*/
                                c=c+2;
                                outpw(PCXBASE+4,c);
```

```
                totala=0;totalb=0;zero=0;

/*averaging factor*/
                for(j=0;j<5000;j++)
                        {
                        totala=totala+digit(0);
                        }
                        zero=totala/5000;

                        fprintf(f,"%u %ld %u\n",a,zero,c);
                        setfillstyle(SOLID_FILL,BLACK);
                        bar(0,436,500,454);
                        sprintf(buffer,"z=%4.0u",c);
                        outtextxy(100,442,buffer);
                        sprintf(buffer,"I=%4.0u",zero);
                        outtextxy(200,442,buffer);

                        line(oldx/7,(oldy/7)*1,c/7,(zero/7)*1);
                        oldx=c;oldy=zero;

                }

        fclose(f);
        return 0;
}
```